RADC-TR-82-225
Final Technical Report
October 1982

ACOSS-16 (ACTIVE CONTROL OF SPACE STRUCTURES)

Honeywell

Sponsored by
Defense Advanced Research Projects Agency (DOD)
ARPA Order No. 3654

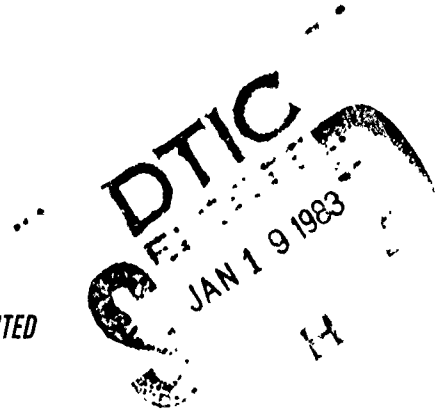

ROME AIR DEVELOPMENT CENTER
Air Force Systems Command
Griffiss Air Force Base, NY 13441

This report has been reviewed by the RADC Public Affairs Office (PA) and is releasable to the National Technical Information Service (NTIS). At NTIS it will be releasable to the general public, including foreign nations.

Some of the machine-produced data are of poor quality reproduction. However, this is insignificant because the relevant data is sufficiently clear to the reader.

RADC-TR-82-225 has been reviewed and is approved for publication.

APPROVED: Richard W. Carman

RICHARD W. CARMAN
Project Engineer

APPROVED: Frank J. Rehm

FRANK J. REHM
Technical Director
Surveillance Division

FOR THE COMMANDER: John P. Huss

JOHN P. HUSS
Acting Chief, Plans Office

If your address has changed or if you wish to be removed from the RADC mailing list, or if the addressee is no longer employed by your organization, please notify RADC (OCSE) Griffiss AFB NY 13441. This will assist us in maintaining a current mailing list.

Do not return copies of this report unless contractual obligations or notices on a specific document requires that it be returned.

UNCLASSIFIED

SECURITY CLASSIFICATION OF THIS PAGE (When Data Entered)

REPORT DOCUMENTATION PAGE	READ INSTRUCTIONS BEFORE COMPLETING FORM
1. REPORT NUMBER: RADC-TR-82-225	2. GOVT ACCESSION NO.: AD-A123 540
	3. RECIPIENT'S CATALOG NUMBER
4. TITLE (and Subtitle): ACOSS-16 (ACTIVE CONTROL OF SPACE STRUCTURES)	5. TYPE OF REPORT & PERIOD COVERED: Final Technical Report, May 81 - July 82
	6. PERFORMING ORG. REPORT NUMBER: 82SRC43
7. AUTHOR(s): Michael F. Barrett, Dave F. Enns	8. CONTRACT OR GRANT NUMBER(s): F30602-81-C-0187
9. PERFORMING ORGANIZATION NAME AND ADDRESS: Honeywell Systems & Research Center, 2600 Ridgway Parkway, PO Box 312, Minneapolis MN 54413	10. PROGRAM ELEMENT, PROJECT, TASK AREA & WORK UNIT NUMBERS: 62301E, C6540116
11. CONTROLLING OFFICE NAME AND ADDRESS: Defense Advanced Research Projects Agency, 1400 Wilson Blvd, Arlington VA 22209	12. REPORT DATE: October 1982
	13. NUMBER OF PAGES: 264
14. MONITORING AGENCY NAME & ADDRESS (if different from Controlling Office): Rome Air Development Center (OCSE), Griffiss AFB NY 13441	15. SECURITY CLASS. (of this report): UNCLASSIFIED
	15a. DECLASSIFICATION/DOWNGRADING SCHEDULE: N/A

16. DISTRIBUTION STATEMENT (of this Report)

Approved for public release; distribution unlimited

17. DISTRIBUTION STATEMENT (of the abstract entered in Block 20, if different from Report)

Same

18. SUPPLEMENTARY NOTES

RADC Project Engineer: Richard W. Carman (OCSE)

19. KEY WORDS (Continue on reverse side if necessary and identify by block number)

Control Theory
Large Space Structures
Structural Dynamics
Flexible Vehicles
Micro Vibration Suppression
Parameter Identification
Modal Parameter Identification
Optimal Regulators
Multivariable Control

20. ABSTRACT (Continue on reverse side if necessary and identify by block number)

The objective of this effort is to develop, design and analyze techniques that can be used to meet future line of sight and jitter control requirements of large space structures that have onboard disturbances. This effort studied parameter identification on a representative large space structure and the impace of on-orbit identification on the design of a disturbance controller for the spacecraft.

DD FORM 1 JAN 73 1473 EDITION OF 1 NOV 65 IS OBSOLETE

UNCLASSIFIED

SECURITY CLASSIFICATION OF THIS PAGE (When Data Entered)

FOREWORD

This work was performed by the Honeywell Systems and Rsearch Center under Contract No. F30602-81-C-0187 for the US Government. The research was sponsored by the Defense Advanced Research Projects Agency (DARPA) of the Department of Defense, and was monitored by the Rome Air Development Center (RADC), Air Force Systems Command. This final technical report covers the period from May 1981 through July 1982. The technical monitors of this program were Lt. Col. A. Herzberg (DARPA) and Mr. R. Carman (RADC).

The program manager at Honeywell was Dr. Thomas B. Cunningham, and the Principal Investigator was Dr. Michael F. Barrett. Mr. Dale F. Enns was Co-Investigator; Dr. Gunter Stein served as Technical Consultant. This report was written by Dr. Barrett and Mr. Enns.

CONTENTS

CONTENTS (continued)

CONTENTS (continued)

CONTENTS (concluded)

LIST OF ILLUSTRATIONS

LIST OF ILLUSTRATIONS (continued)

LIST OF ILLUSTRATIONS (continued)

LIST OF ILLUSTRATIONS (continued)

LIST OF ILLUSTRATIONS (concluded)

LIST OF TABLES

LIST OF TABLES (concluded)

LIST OF ABBREVIATIONS

ACOSS	Active Control of Space Structures
ADOPT	Advanced Optical Technology
ALE	Algebraic Lyapunov equation
CMG	Control moment gyro
HALO	High altitude large optics
ILAS	Identically located activators and sensors
JOSIE	Joint Optics Structures Integrated Experiment
LBET	Large beam expander technology
LODE	Large Optics Demonstration
LOS	Line of sight
LQG	Linear-quadratic-gaussian
LSS	Large space structure
MIMO	Multi-input, multi-output
MLE	Maximum likelihood estimation
NR	Newton-Raphson
PSD	Power spectral density
rms	Root-mean-squared
ROM	Reduced-order model
SCO	Strongly controllable and observable
SISO	Single-input, single-output
SNR	Signal-power-to-noise-power ratio

SECTION 1

INTRODUCTION AND SUMMARY

BACKGROUND

A number of spaceborne surveillance and weapon system concepts of current interest to USAF and DARPA require precision line-of-sight (LOS) control in order to achieve their missions. Each of the four major concepts identified so far--High Altitude Large Optics (HALO), Advanced Optical Technology (ADOPT), Large Beam Expander Technology (LBET), and Large Optics Demonstration (LODE)--call for stringent LOS and figure stability, despite strong environmental and on-board disturbances, which exceeds existing technology. The Active Control of Space Structures (ACOSS) Program sponsored by the Defense Advanced Research Projects Agency (DARPA) has funded a number of studies in support of an overall objective "... to develop and understand a generic, unified, structural dynamics and control technology base for large space structures (LSS) with stringent line-of-sight and figure performance requirements that must be maintained in the presence of on-board and natural disturbances."

This report documents results of the fifteenth such study, ACOSS SIXTEEN, conducted by the Honeywell Systems and Research Center for DARPA and RADC from May 1981 through July 1982. The specific objectives of this effort were:

- To examine the potential for structural characteristics uncertainty reduction using on-orbit identification
- To investigate control design approaches to assess possible performance improvements which reduced uncertainty may allow

SUMMARY AND REPORT OUTLINE

There are four fundamental requirements in the design of high-performance control systems for flexible structures:

- A control problem definition

- o A reliable control design model for the structure to be controlled
- o A control design procedure that exploits this information
- o The necessary hardware to implement this controller

These requirements are addressed in Sections 2 through 6 of the report. Their essential features and results are summarized briefly below.

Control Problem Definition

The control problem addressed in this study is defined in Section 2. Motivated by results of an earlier ACOSS Study (Ref. 1), a control objective and disturbance environment were defined, along with a generic feedback control structure appropriate for attitude and structural vibration control. This feedback structure consists of two feedback control loops--a low-bandwidth LOS pointing loop and a high-bandwidth vibration control loop. Since the "slow" outer loop has little effect on the "fast" inner loop, only the latter vibration control loop was specifically addressed in the remainder of the study. Candidate sensors and actuators were selected and placed to define six concepts. Two of these were selected to span a range of difficulty for identification and control studies--a baseline concept with identically located actuators and sensors (ILAS), and an advanced concept with widely distributed sensors and actuators. Both concepts assume paired shakers on the equipment section for actuators. The baseline concept assumes gyros on the equipment section for sensors, whereas the advanced concept assumes accelerometers on the optical structure. Maximum allowable control bandwidth for both concepts was restricted to less than 100 r/s to remain within the range of model va idity for the ACOSS II structure.

Control Design and Identification Model Requirements

Model requirements for control design are examined in Section 3. Using Honeywell-developed methods for assessing stability and performance robustness to plant uncertainty for multivariable systems, criteria for defining reduced-order models (ROMs) were examined, as were modal-parameter accuracy requirements for modes retained in this model. The resulting stringent accuracy requirements show that identification is virtually unavoidable for the advanced vibration control

concept. Due to the specialized nature of the baseline ILAS concept, these requirements may, however, be relaxed considerably. Ground rules for identification were next established based on a fundamental premise assumed throughout this study: since identification is driven by the control problem, it should impose no fundamental hardware requirements of its own.

Hardware Requirements

Hardware requirements imposed by the vibration control problem are also summarized in Section 3. Required force/mass-stroke capability for actuators is dictated by that required to accommodate the primary vibration disturbance, while allowable sensor errors are dictated by closed vibration-control-loop LOS pointing requirements. The hardware requirements imposed by these constraints are severe. But the driving requirement is for high bandwidth--1000 r/s for actuators and sensors, 200 Hz for computers--which pushes or exceeds the current state of the art.

It was assumed that internal vibration disturbances may be largely eliminated during identification and that the available control actuator capability may then be used to generate test signals to aid in identification. The relative error between delivered and commanded actuator output was assumed to be 10%. Two test signal models were examined--band-limited "white" noise at the force (or torque) level, and the time derivative of this signal. Both concepts favor the latter test signal, which provides greater excitation of high-frequency modes. Three measurement noise models were considered--band-limited white noise at the position, rate, or acceleration levels. Position measurements are recommended for the baseline concept, rate measurements for the advanced concept. All band-limited noise sources were approximated by "equivalent" white noise sources for subsequent analyses.

Identification

The bulk of the study was devoted to examining the feasibility of identifying modal parameters to sufficient accuracy for control design.

General Procedure--Section 4 examines the general maximum likelihood estimation (MLE) identification method, which has been employed at Honeywell in a number of aerospace applications over the past 10 years. Recent developments by Yared (Ref. 7) are exploited to simplify the assessment of basic identification accuracy (i.e., identifiability analysis). The general method, however, has proven to be computationally impractical for the LSS application and is highly susceptible to parameter biases under unavoidable model mismatches between the true system and the identification model.

Simplified Procedures--A number of simplifications to the general MLE method are pursued in Section 5. Elimination of the Kalman filter associated with the MLE method is shown to offer the greatest promise. Results using the associated exact identifiability analysis software show that this achieves a good compromise between bias and stochastic error while yielding enormous computational simplification. This simplification makes the simultaneous identification of frequency, damping, and modal influence coefficients for dozens of modes computationally feasible. Identification of a single mode at a time also appears promising. Since it is restricted to modes for which damping ratio is small compared to relative frequency separation between modes, it is not suitable for all modes (e.g., rigid-body modes and heavily damped isolator modes). Nevertheless, this simplification makes the identification of literally hundreds of modes a practical possibility.

Results--The above assumption of small damping allows analytical solutions for basic identification accuracy, which are also pursued in Section 5. Approximate identifiability analysis software, which evaluates these solutions, provides an inexpensive method to assess approximate identification accuracy even when the small damping assumption fails to hold. Results show that achievable identification accuracy is consistent with that required for control design. The analytical results allow a convenient frequency-domain graphical interpretation, which is useful for obtaining a rough assessment of required identification time for various test signal/measurement combinations. These approximate identifiability analysis results are compared against exact results for the two concepts in Section 6. Discrepancies are generally insignificant for all modes except

rigid-body and heavily damped isolator modes, which were not identified. Identification times of 5 to 10 minutes should suffice for both concepts, assuming recommended test signal/measurement combinations are employed.

Control Design

Control designs for the two concepts are also presented in Section 6.

Baseline Concept--A simple controller was designed for the baseline ILAS concept employing rate-gyro feedback, which allows the excellent "theoretical" robustness properties associated with "positive-real" systems. Even after accounting for the effects of sensor/actuator dynamics, sampling for the digital control law mechanization, and possible use of rate-integrating gyros with a lead-lag compensator, stability margins should be more than adequate. The resulting control design, which has a maximum control-loop gain-crossover frequency of ~100 r/s, fails to meet performance requirements. Ultimate control performance for this concept is not limited by control bandwidth but by the presence of uncontrollable/unobservable modes.

Advanced Concept--A more sophisticated controller for the advanced non-ILAS concept was designed using a Honeywell-developed linear-quadratic-gaussian (LQG) based method with robustness recovery (Ref. 2). Due to the nonminimum phase nature of structural models for the non-ILAS case, control design is far more difficult to accomplish and fundamental limits to control performance are more apparent than for the ILAS case. The final control design, which was based on a 24-mode (48-state) ROM, achieves a maximum control-loop gain-crossover of ~100 r/s, but fails to meet performance requirements. The design has been shown to be closed-loop stable for the 84-mode truth model, but is extremely sensitive to additional design model uncertainty. Higher bandwidth would improve performance, but would require higher order control design (and identification) models. Its sensitivity to model uncertainty could be improved by "tuning up" the design. Ultimate control performance achievable for this concept, however, has not been explored in sufficient depth and therefore is largely unknown at this time. Practical implementation of a 48-state, or larger, LQG compensator remains an open issue.

CONCLUSIONS

The principal conclusions of this study for identification and control may be summarized as follows:

Identification

- MLE identification without the Kalman filter achieves a good compromise between bias and stochastic errors and yields enormous computational savings over general MLE identification.
- Simultaneous identification of all modal parameters associated with dozens of modes is computationally feasible, and achievable parameter accuracy is consistent with control requirements.
- Identification of one mode at a time makes identifying hundreds of modes a practical possibility. This scheme is suboptimal only for modes in which the usual assumption that light damping compared to relative frequency separation fails to hold.
- Rough control design and identification model requirements can be assessed graphically from Bode-like singular value plots of the open-loop plant transfer function (i.e., number of modes, number of parameters, parameter accuracy, identification time, test signals, measurement type).
- Identification times of 5 to 10 minutes should suffice for the two control concepts examined for the recommended test signal/measurement combinations. This implies some 60,000 to 120,000 data samples for a 200 Hz sample frequency.
- However, the stability of modal parameters over time is an open issue. Periodic re-identification and control redesign would probably be necessary for practical applications. Ultimately, an adaptive identification and control scheme would be desirable.

Control

- Vibration control bandwidth requirements on the order of 100 r/s would be required to meet performance requirements for any control concept.

- The maximum practical bandwidth that the 84-mode ACOSS II model will allow is ~100 r/s. Hence, the two control concepts examined were so restricted, and some performance degradation must be expected.
- Required bandwidth for control hardware--1000 r/s for sensors and actuators and 200 Hz for computers--pushes or exceeds the current state of the art.
- A simple rate-gyro-feedback controller for the baseline concept with a maximum gain-crossover frequency of ~100 r/s provides good stability robustness, even after accounting for sensor/actuator dynamics, sampling, and possible implementation with attitude feedback and a lead-lag compensator.
- Ultimate control performance achievable for this concept is not limited by control bandwidth, but by the presence of uncontrollable/unobservable modes. This same limitation applies to the other ILAS concepts considered early in the study, but should not be an inherent limitation with such concepts.
- The nonminimum phase nature of structural models for the non-ILAS case makes control design extremely difficult to accomplish and imposes fundamental limits to control performance.
- An LQG-based control design using a 24-mode ROM, which achieves a maximum control-loop gain-crossover of ~100 r/s, was shown to be closed-loop stable for the 84-mode truth model, but is extremely sensitive to additional design model uncertainty.
- Higher control bandwidth would improve its control performance, but would require higher order control design and identification models. Its sensitivity to modal uncertainty could be improved somewhat by "tuning up" the design.
- Ultimate control performance achievable for this concept, however, has not been explored in any great detail and therefore is largely unknown. Similarly, the practicality of implementing a 48-state, or larger, LQG compensator remains an open issue. Generally, some simplification of this compensator is possible.

RECOMMENDATIONS

Recommendations for further study for identification and control include the following:

Identification

- The capability to identify rigid-body modes, to evaluate stochastic errors due to process noise, and to include test signal shaping should be added to the exact identifiability analysis software.
- An identification simulation should be developed to back up results based on bias and covariance analyses. It should include a high-order truth model, a reduced-order identification model with associated identification software, and all relevant sensor/actuator/structural nonlinearities, test signal/noise/disturbance shaping, sampling, etc.
- Open issues such as the effects of modal-parameter stability over time, nonlinearities, etc. deserve attention.
- The above identification software should be validated in a laboratory setting by applying it to an experimental structure. This would assess the impact of real-world hardware limitations on actual identification performance. The proposed Joint Optics Structures Integrated Experiment (JOSIE) program would provide an ideal vehicle for such validations. Ultimately, on-orbit identification should be demonstrated in space.

Control

- More effective "control design tools" are needed for defining ROMs for control design, as are practical and less conservative representations of associated modeling errors, particularly for the general non-ILAS case.
- Methods for sensor/actuator placement such that nonminimum phase zeros occur beyond the desired control bandwidth should be investigated for the non-ILAS case.
- Development of practical algorithms for designing control laws, which maximize robustness to modal parameter uncertainty, should be addressed.

- Methods proposed for evaluating stability robustness to parameter identification errors for a given control design should be examined further.

- Existing advanced control design techniques, and any refinements available at the time of application, should be validated in a laboratory setting by applying them to an experimental structure to assess the impact of real-world hardware limitations. Here again, the proposed JOSIE program would provide an ideal vehicle for these evaluations. Ultimately, advanced control design techniques should be demonstrated in space.

SECTION 2

CONTROL PROBLEM DEFINITION

This section defines the control problem addressed in the ACOSS SIXTEEN study. We begin by examining the ACOSS II model, which defines the structure, the control system objectives to be met, and the disturbance environment to which this control system will be subjected. Next, we examine a generic feedback control structure appropriate for spacecraft attitude and vibration control and then focus on fundamental vibration control requirements. Finally, we examine candidate sensor and actuator placements appropriate for vibration control and identify the two concepts selected for identification and control studies in the contract.

BASIC CONTROL PROBLEM

ACOSS II Model

The space structure examined in this study was the ACOSS II Model developed by Draper Labs (Ref. 1). As illustrated in Figure 2-1, it consists of two basic sections. The lower equipment section (or "dirty box") houses all control hardware (i.e., reaction jets, control moment gyros--CMGs, cyrogenic coolers, etc.) and serves as the attach point for the flexible solar panels. The upper optical structure (or "clean box") supports the three mirrors and focal plane of the optical mission sensor. The two sections are separated by three isolators, each of which consists of a spring and dashpot damper. These isolators were designed to attenuate the transmission of high-frequency (>0.5 Hz ≈ 3.14 r/s) disturbances from the equipment section to the optical structure.

A finite-element NASTRAN model of the structure was supplied to Honeywell by Draper Labs at the start of the contract. This model consisted of six (1 to 6) rigid-body modes and 78 (7 to 84) flexible-body modes, of which six (7, 8, 11, 12, 13, and 16) correspond to the isolators. The six isolator modes

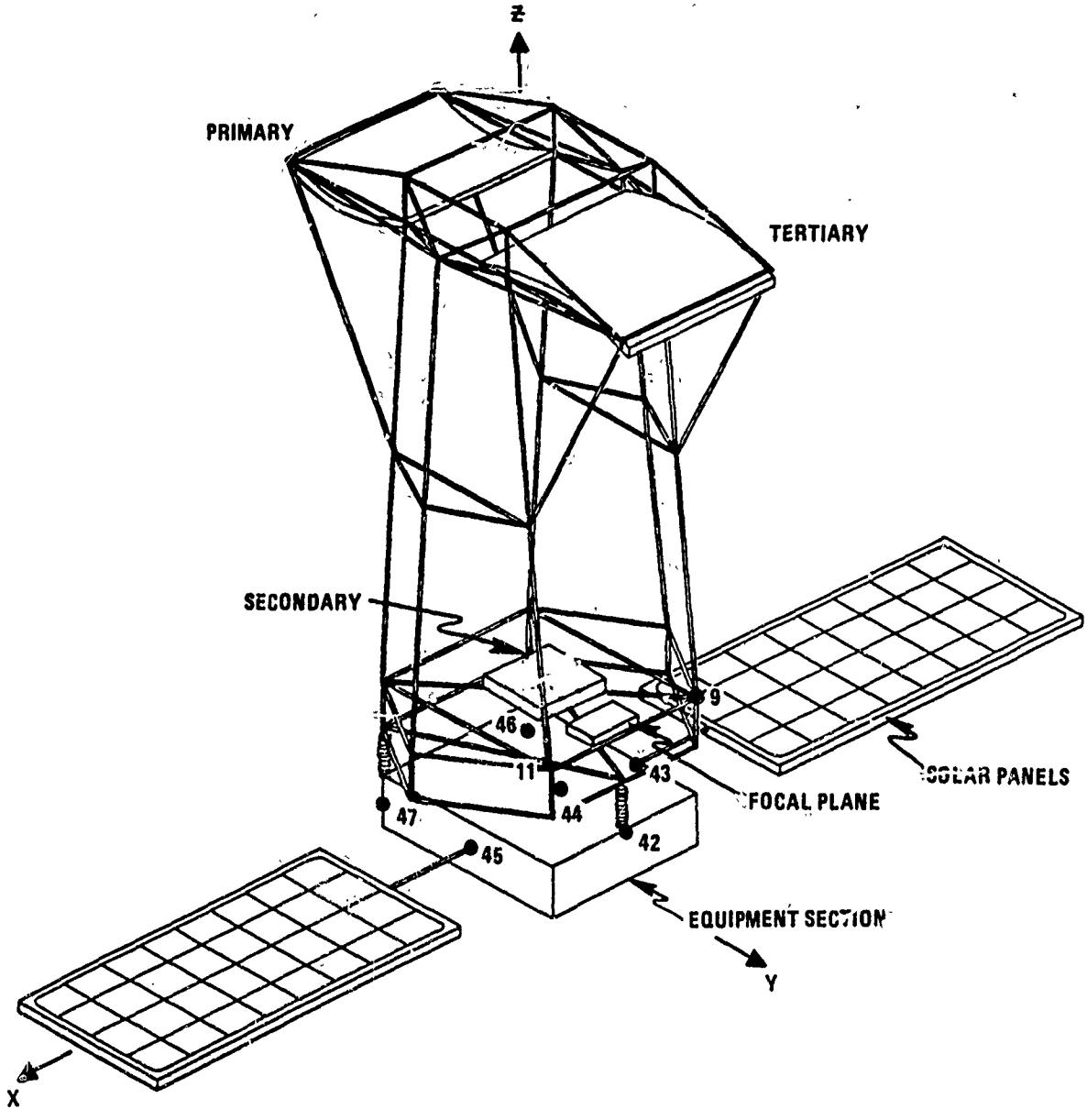

Figure 2-1. ACOSS II Model (from Ref. 1)

assumed a damping ratio of $\zeta = 0.707$ (70.7%) while the remaining 72 flexible modes assumed a damping ratio of $\zeta = 0.005$ (0.5%). Modal influence coefficients (or mode shapes) were defined for 99 nodes for each of the three translational and three rotational degrees of freedom. The locations of several nodes that are relevant in the following discussions are indicated in Figure 2-1. Modal influence coefficients were also supplied to define optical LOS and DEFOCUS errors.

Control Objectives vs Disturbances

Control objectives for this study were also adopted from the Draper study (Ref. 1) and are summarized in Table 2-1. They assume optical LOS pointing error specifications of

$$LOS_x,\ LOS_y < 1\ \mu r \qquad (2\text{-}1)$$
$$DEFOCUS_z < 500\ \mu m$$

TABLE 2-1. CONTROL OBJECTIVES VS DISTURBANCES

- Control Specifications (line of sight errors)
  - --LOS_x, LOS_y < 1 ur
  - --$DEFOCUS_z$ < 500 μm
- Disturbance Environment
  - --Cryo cooler: $F_{z_{46}} = 400 \sin \Omega t$ N, 10 r/s $\Omega \leq$ 100 r/s
  - --Solar, gravity gradient, aerodynamic, thermal: T_d < 0.02 N-m

in the face of both internal and external disturbances. We have also assumed that the primary internal disturbance is a sinusoidal z-axis force at node 46 in Figure 2-1, given by

$$F_{z_{46}} = 400 \sin \Omega t \text{ N} \qquad (2\text{-}2)$$

which is due to mechanical vibrations in the equipment section of the spacecraft, as might be produced by cryo coolers, CMGs, and other rotating machinery. Unlike Ref. 1, we have assumed for this study that this disturbance occurs not at the single frequency Ω = 5 Hz ≃ 31.4 r/s, but at some unknown frequency in the range 10 r/s $\leq \Omega \leq$ 100 r/s. We have also chosen to omit a similar disturbance that is applied to the optical structure at node 37.

The motivation for the first choice was to allow for possible disturbance excitation at any of several mode frequencies. Another possible choice, however, would have been to assume a power spectral density (PSD) description, such as a flat PSD over some frequency range. This latter choice, for example, would be more appropriate if the dominant disturbance were due to coolant flow in the lines rather than to discrete-frequency vibrations produced by mass unbalances in the cryo pump itself. The disturbance at node 37 was eliminated because it appeared to be somewhat at odds with the clean-box/dirty-box spacecraft design principle. Even if some disturbance does bypass the isolator, it was felt that the 200 N amplitude assumed by Draper was too severe to allow a practical control solution.

In addition to the primary internal disturbance, various sources for external disturbances were examined--solar, gravity gradient, aerodynamic, and thermal. Rough calculations showed that the largest external disturbance, solar torque, was bounded by

$$T_d < 2\, q\, A\, c$$

where

q = near-earth solar pressure constant ≃ 4.5×10^{-6} N/m^2

A = solar-panel area ≃ 2 x (7 x 20) = 280 m^2

c = center of pressure offset from cg ≃ 7.6m

Substituting these values gives roughly $T_d = 0.02$ N-m at frequencies of orbit rate or less. This disturbance torque is 10^5 times smaller than the sinusoidal torque of 2000 N-m induced by the primary internal disturbance force applied at a moment arm of 5m.

Although the effect of constant external disturbances on LOS pointing errors is negligible over the short term, it will ultimately dominate the effect of sinusoidal internal disturbances over the long term, that is, for periods greater than

$$T_{crit} \triangleq \frac{1}{\omega_i}\sqrt{2\,\frac{T_i}{T_e}} \simeq \frac{1}{31.4}\sqrt{2(10^5)} = 14 \text{ sec} \qquad (2\text{-}3)$$

since $\omega_{crit} \triangleq 1/T_{crit}$ is well below the frequency of the first flexible mode ($\omega_7 \simeq 1$ r/s), external disturbances are critical only for control and identification of rigid-body modes.

Disturbance to LOS Transmissions

To illustrate the severity of the control problem, frequency responses for the transmissions from a z-axis force disturbance at node 46 to LOS_x, LOS_y, and $DEFOCUS_z$ are shown in Figures 2-2a through 2-2c. Mode numbers associated with all significant flexure modes are indicated on each of these plots. Note that modes 1 to 6 corresponding to the rigid body are not indicated, nor are modes 77 to 84, which occur above $\omega = 1000$ r/s. Damping ratio for the isolator modes, which are indicated by an x over the mode number, was taken to be $\zeta = 0.005$ for most of the frequency-response plots in this section in order to show the location of mode frequencies. For the prescribed damping of $\zeta = 0.707$ these modes are nearly "invisible," and can usually be neglected.

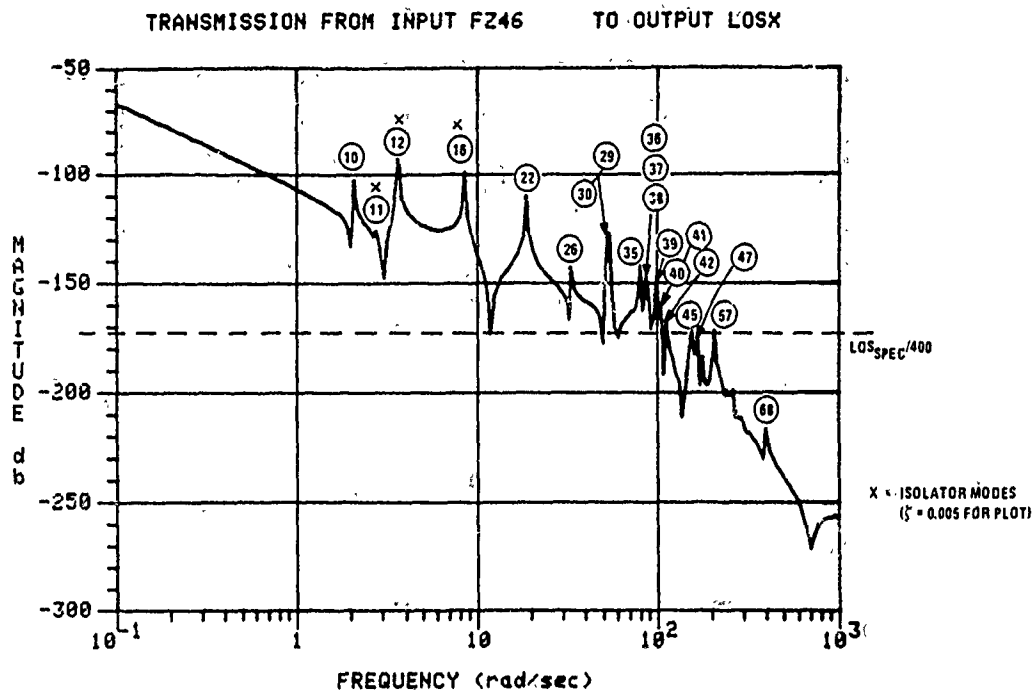

Figure 2-2a. Disturbance to LOS_x Transmission: Open-Loop

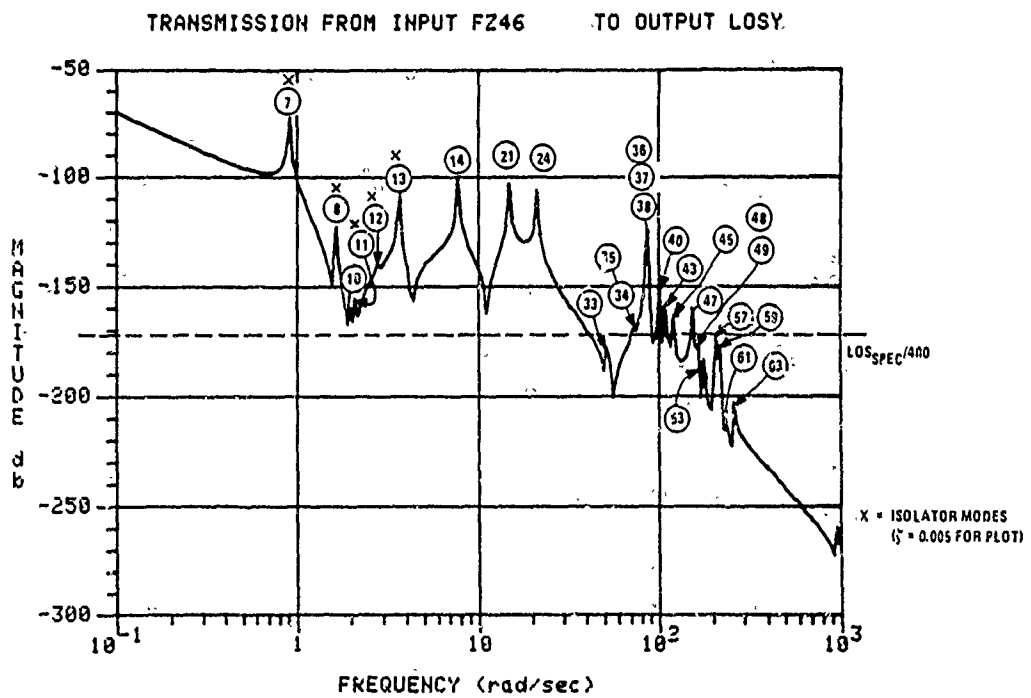

Figure 2-2b. Disturbance to LOS_y Transmission: Open-Loop

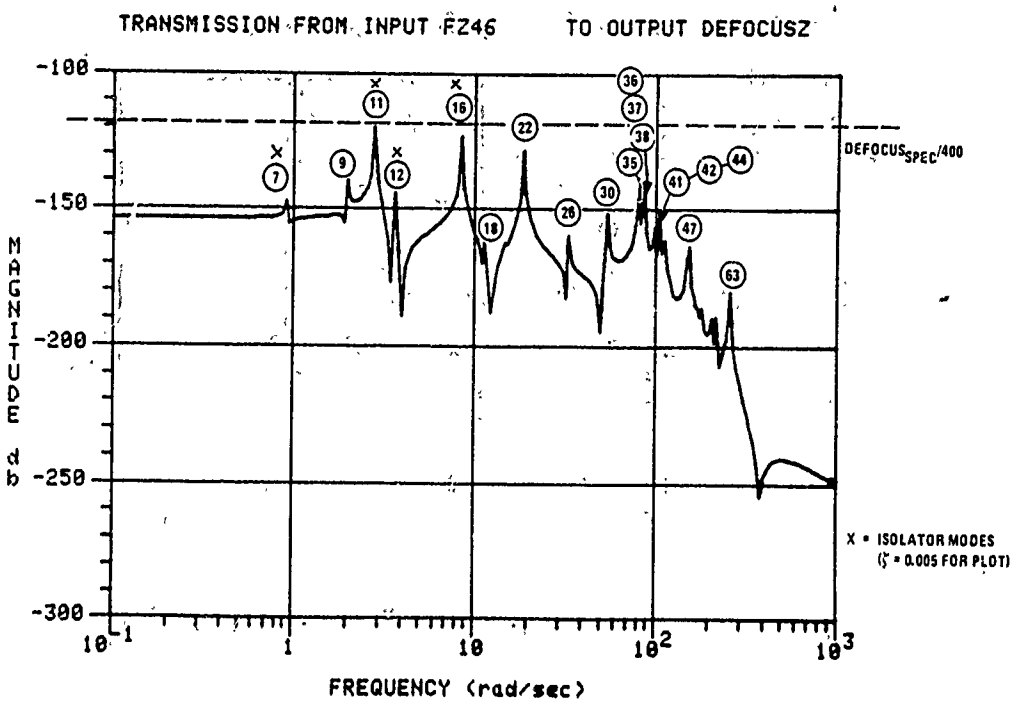

Figure 2-2c. Disturbance to $DEFOCUS_z$ Transmission: Open-Loop

Also shown in these figures are the appropriate specifications on LOS and DEFOCUS errors, normalized by the assumed 400 N internal disturbance force level. Note that the DEFOCUS specification is met even without active control for all disturbance frequencies $\Omega > 0$. Neither LOS specification is met open-loop in the critical frequency range, 10 r/s $\leq \Omega \leq$ 100 r/s, except at certain zeros of the transfer functions. The worst-case specification violation is $\simeq$ 70 dB at mode 21 for LOS_y. Thus the LOS control problem is a difficult one.

FEEDBACK CONTROL SOLUTION

Overall Control Structure

A suitable feedback control structure for controlling LOS is illustrated in Figure 2-3. It consists of two multivariable feedback control loops. The outer loop feeds back sensed or inferred LOS through the primary CMG actuators. This is a low-bandwidth loop designed to maintain the LOS within pointing specifications in the face of low-frequency external disturbances--primarily solar, gravity gradient, aerodynamic, and thermal.

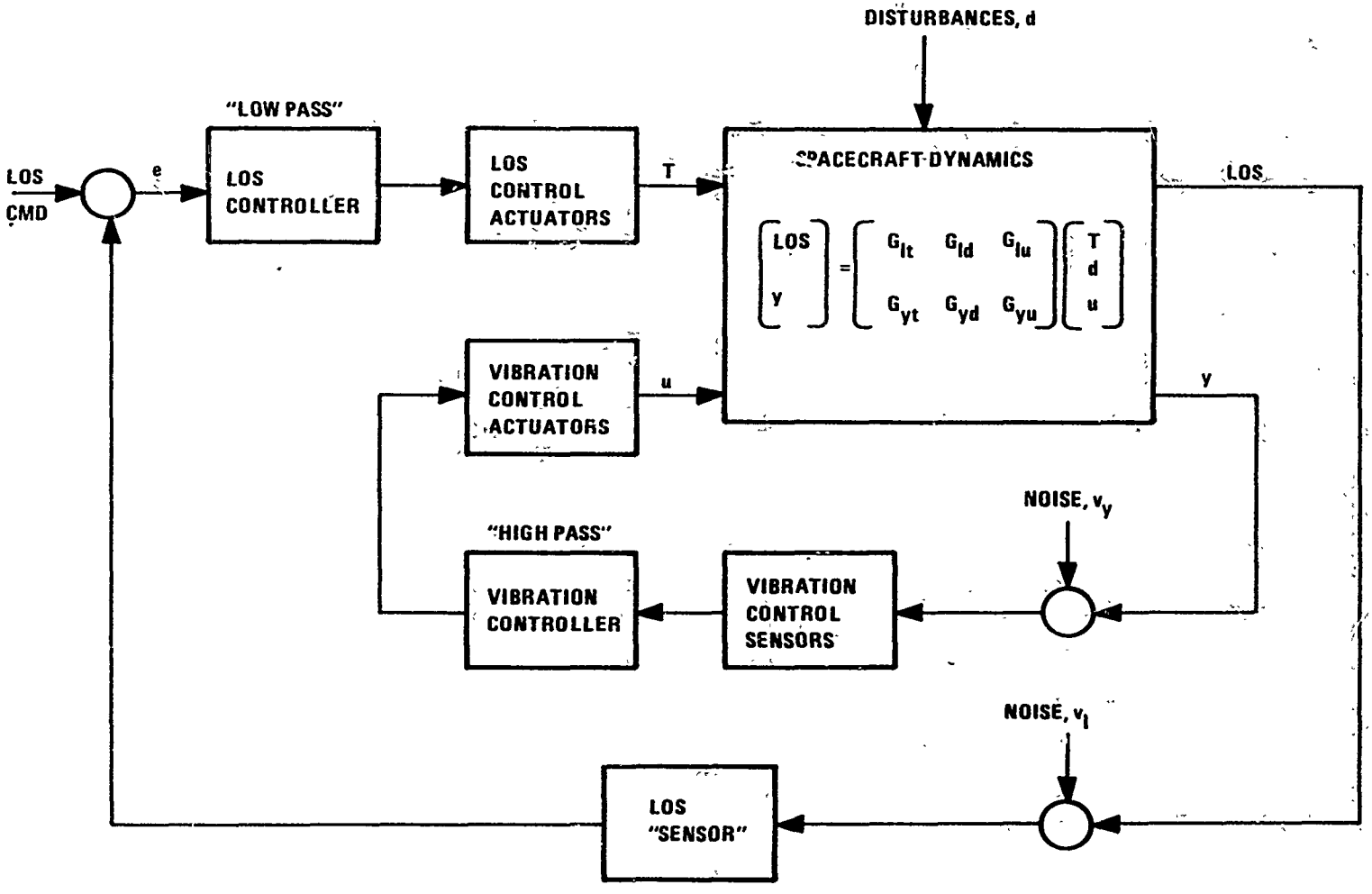

Figure 2-3. Feedback Control Structure

The inner loop in Figure 2-3 is a high-bandwidth loop designed to attenuate LOS errors due to high-frequency internal disturbances--forces and torques caused by rotating and vibrating machinery in the equipment section. Sensors and actuators for this loop must have much higher bandwidth than those for the outer LOS loop. But low-frequency accuracy of these instruments is not critical since the vibration controller may be designed to high-pass low frequencies where the LOS controller operates. The primary CMG actuators may serve also as the vibration control actuators if bandwidth is sufficient for control.

Control design for the outer LOS loop may be accomplished based on simple rigid-body models of the spacecraft and is not of primary concern for this study. Rather, we concentrate here on the inner vibration control loop, which calls for more sophisticated models, control hardware, and control design techniques.

Based on LOS pointing accuracy requirements and the disturbance environment, rough order-of-magnitude requirements for vibration-control-loop sensors and actuators may now be established. To meet pointing accuracy requirements, sensors must have resolutions of at least 1 μr for angular measurements or 1 μm for position measurements, assuming the smallest spacecraft dimensions that affect angular errors are on the order of 1m. To accommodate disturbances, actuators must be capable of delivering forces of at least 400 N or torques of at least 2000 N-m, assuming they are mounted on the equipment section. Smaller actuators might well suffice if they were mounted on the optical structure to take advantage of the isolator's natural attenuation of internal disturbances. It was further assumed that the force or torque delivered by actuators could be resolved to within 10% of the commanded level. We note finally that these resolutions must hold over the frequency bandpass of the vibration control loop.

Vibration Control Fundamentals

As illustrated in Figure 2-3, active vibration control requires the placement of sensors and actuators on the structure to form the inner feedback loop. The function of this loop is to remove vibration energy due to high-frequency

disturbances from the structure and thereby permit a simpler low-bandwidth control loop to point the LOS. The control design objective, then, is to reduce the LOS to disturbance transmission at high frequencies using a feedback control law of the form

$$u = -K(s)y \tag{2-4}$$

Neglecting sensor and actuator dynamics, this closed-loop transmission is given by

$$LOS_{CL} \triangleq \left[G_{\ell d} - G_{\ell u}K(I + G_{yu}K)^{-1}G_{yd}\right] d \tag{2-5}$$

This expression may be further simplified by assuming a modal expansion for each element of G, that is,

$$G_{pq} = \sum_{i-1}^{\infty} g_i c_{pi} b_{qi}^T \qquad p = \ell, y;\ q = d, u \tag{2-6a}$$

where b_{qi} and c_{pi} are modal (position) input and output influence coefficients for the i^{th} mode and

$$g_i(s) = \frac{1}{s^2 + 2\zeta_i\omega_i s + \omega_i^2} \tag{2-6b}$$

is a scalar transfer function describing the dynamic characteristics of the i^{th} mode where, ω_i and ζ_i denote modal frequency and damping. When these transfer functions are dominated by the i^{th} mode near the resonance frequency ω_i, that is,

$$G_{pq} \simeq g_i c_{pi} b_{qi}^T \qquad s \simeq j\omega_i \tag{2-6a}'$$

then closed-loop LOS to disturbance transmission may be approximated by (using the Matrix Inversion Lemma)

$$LOS_{CL} \simeq \left[g_i c_{\ell i} b_{di}^T - g_i c_{\ell i} b_{ui}^T K(I + g_i c_{yi} b_{ui}^T K)^{-1} g_i c_{yi} b_{di}^T\right] d \tag{2-7a}$$

$$= \frac{1}{1 + g_i b_{ui}^T K\, c_{yi}}\ LOS_{OL}$$

where

$$LOS_{OL} = G_{\ell d} d \simeq g_i c_{\ell i} b_{di}^T d \qquad (2\text{-}7b)$$

is the open-loop LOS response to disturbance.

Loop-Gain Requirements

This simple equation shows that LOS response to disturbance near each structural resonance is attenuated by the action of a scalar feedback loop with loop transfer function

$$\ell_i(s) = g_i(s)\, b_{ui}^T K(s)\, c_{yi} \qquad i = 1,2,3,\ldots \qquad (2\text{-}8)$$

To meet LOS pointing specifications in the face of disturbances, our design objective for vibration control is then to choose $K(j\omega)$ so that

$$\left|\ell_i(j\omega)\right| \simeq \left|1 + \ell_i(j\omega)\right| > \left|LOS_{OL}(j\omega)\right| / LOS_{spec} \qquad (2\text{-}9)$$

near mode frequencies within the passband of the disturbance. For stability, we require that the phase angle of $\ell_i(j\omega)$ be maintained in a limited range whenever the magnitude of $\ell_i(j\omega)$ crosses over from large values ($|\ell| > 1$) to small values ($|\ell| < 1$) (i.e., phase stabilization). If $|\ell_i(j\omega)|$ never exceeds unity, on the other hand, phase may remain arbitrary (i.e., gain stabilization). Since little attenuation of disturbances occurs in the latter case, phase stabilization is unavoidable at critical modes for effective vibration control.

Sidestepping the stability issue for now, it is clear that good disturbance attenuation at the i^{th} mode can be achieved if $K(j\omega)$ for frequencies near $\omega = \omega_i$ is chosen so that:

1. Its magnitude is large,
2. Its direction serves to align the vectors b_{ui} and $P_R(Kc_{yi})$ (or equivalently c_{yi} and $P_R(K^T b_{ui})$), where $P_R(.)$ denotes the projection of a vector in the complex vectors space C^n onto the real vector space R^n, and

3. The phase angle of $\ell_i(j\omega)$ is close to zero so as to maximize $|1 + \ell_i|$.

These attributes can be achieved using an ideal control structure of the form (for $s \simeq j\omega_i$)

$$K(s) \triangleq \begin{cases} k(s)\, b_{ui} c_{yi}^T \Big/ \left|b_{ui}\right| \left|c_{yi}\right| & c_{yi} \neq b_{ui} \quad (2\text{-}10a) \\ k(s)\, I & c_{yi} = b_{ui} \quad (2\text{-}10b) \end{cases}$$

where $k(s)$ is a scalar transfer function chosen such that $\angle g_i(j\omega) k(j\omega) \simeq 0$ for $\omega \simeq \omega_i$. The second case (2-10b) assumes identical location of actuators and sensors (ILAS). More general statements for condition 2 will allow more general control structures, but are unnecessary for our purposes. By substitution of (2-10a) into (2-8) it is easily shown that

$$\begin{aligned} \left|\ell_i(s)\right| &= \left|g_i(s)\right| \left|k(s)\right| \left|c_{yi}\right| \left|b_{ui}\right| \quad (2\text{-}11) \\ &= \left[\left|g_i(s)\right| \left|c_{yi}\right| \left|b_{ui}\right|\right] \left[\left|k(s)\right|\right] \\ &= \bar{\sigma}\left(g_i(s) c_{yi} b_{ui}^T\right) \bar{\sigma}\left(k(s) b_{ui} c_{yi}^T \Big/ \left|b_{ui}\right| \left|c_{yi}\right|\right) \\ &\simeq \bar{\sigma}(G_{yu}(s))\, \bar{\sigma}(K(s)) \end{aligned}$$

where

$$\bar{\sigma}(A) \triangleq \max_{|x|_2=1} |Ax|_2 = \sqrt{\max_k \{\lambda_k(A^* A)\}} \quad (2\text{-}12)$$

$$\underline{\sigma}(A) \triangleq \min_{|x|_2=1} |Ax|_2 = \sqrt{\min_k \{g_k(A^* A)\}}$$

define, respectively, the maximum and minimum singular values of the matrix A. These quantities represent the maximum and minimum amplification of the unit vector x by the matrix A, as measured by the Euclidean norm, $|\cdot|_2$.

Given vibration control loop gain requirements imposed by equation (2-9) and the LOS to disturbance transmissions of Figures 2-2, equation (2-11) allows us to directly relate these requirements to Bode-like plots of the singular values of the transfer function matrix $G_{yu}(s)$ for various input/output pairs. Thus for the worst-case open-loop specification violation of ~70 dB at mode 21, $\sigma(G_{yu}(j\omega))$ must exceed the effective 0 dB line by ~70 dB. Thus rough bandwidth requirements for vibration control may be established graphically.

It should be recognized that these analyses are technically valid only over a limited range for control gain. Although disturbance to LOS transmissions is attenuated at the mode frequencies of controllable/observable modes, for sufficiently high gain the exact expression (2-5) gives (assuming the appropriate inverses exist)

$$LOS_{CL} \simeq \left[I - G_{\ell u} G_{yu}^{-1} G_{yd} G_{\ell d}^{-1}\right] LOS_{CL}$$

for all frequencies except near uncontrollable or unobservable modes. Thus disturbance to LOS transmissions need not be attenuated, and may in fact be amplified, at frequencies away from the mode frequency, unless $G_{yu} \simeq G_{\ell u}$ and $G_{yd} \simeq G_{\ell d}$ or $G_{yu} \simeq G_{yd}$ and $G_{\ell u} \simeq G_{\ell d}$. For this reason, it is desirable to place actuators near the source of the disturbance, or to use sensors whose measurements closely approximate the LOS, or both. To the extent that these desirable features are unachievable, potential vibration control performance is largely limited to damping of controllable/observable modes.

SENSOR/ACTUATOR PLACEMENT FOR VIBRATION CONTROL

Given the primary set of actuators for the low-bandwidth LOS control loop, we now examine candidate sensor/actuator placements for vibration control. In view of equation (2-9) it is clear that sensors should be placed to maximize the observability (i.e., maximize $|c_{yi}|$) of modes that are critical to the LOS in the critical frequency band of the disturbance. Similarly, actuators should be placed to maximize controllability (i.e., maximize $|b_{ui}|$) of modes excited by the disturbance.

Generally, strong controllability favors placing actuators on the (rigid) equipment section near the source of the primary disturbance, while strong observability favors distributing sensors about the (flexible) optical structure near nodes that strongly affect LOS. On the other hand, control design and implementation favor identical location of actuators and sensors (ILAS) for which simple control laws suffice and robustness to model uncertainty is large. Thus, there are tradeoffs to be made.

Candidate Concepts

A number of candidate sensor/actuator placement concepts are identified in Table 2-2, along with advantages and disadvantages of each. Each concept is discussed in greater detail below. In all cases, Bode magnitude and phase plots are presented for selected input/output pairs (usually diagonal elements of the transfer function matrix $G(j\omega)$). These plots are followed by a Bode-like plot of the singular values of $G(j\omega)$, which bound the gain of $G(j\omega)$.

Concept 1: Accelerometers and Shakers at Node 46--Concept 1 in Table 2-2 is an ILAS concept using translational-motion sensors and actuators located at the source of the disturbance, node 46. Note that ILAS concepts require that both sensors and actuators sense and actuate either translational motion, rotational motion, or some linear combination of the two. Although a single actuator that supplies a z-axis force at node 46 would, in theory, suffice for the assumed disturbance, actuators in three axes allow for the more realistic case in which disturbances are not confined to a single axis. Clearly, reaction jets are inappropriate for the high-frequency, continuous operation required for vibration control. Proof-mass thrusters or shakers, however, are ideally suited here since their mass-stroke product can be sized to absorb oscillatory disturbances.

Accelerometers in three axes also located at node 46 provide a suitable sensor complement to measure translational motion at this node. Bode loop transmission from force inputs to position outputs at node 46 are shown in Figure 2-4. Only the diagonal elements of the symmetric 3 x 3 matrix transfer function are shown

TABLE 2-2. POTENTIAL SENSOR/ACTUATOR PLACEMENTS FOR VIBRATION CONTROL

Concept Number	Sensors	Actuators	Advantages	Disadvantages
1	Accels at 46x,y,z	Shakers at 46x,y,z	ILAS	Not all critical modes are SCO* Strongly coupled dynamics (translational and rotational)
2	Accels at 42z, 43z, and 42x	Shakers at 42z, 43z, and 42x	ILAS	Not all critical modes are SCO* Strongly coupled dynamics (translational and rotational)
3	Gyros at 44x,y,z	CMGs at 44x,y,z	ILAS Uncoupled dynamics (approx) No translational dynamics	Not all critical modes are SCO CMG torques too small CMG bandwidth too low
Baseline 4	Gyros at 44x,y,z	Paired shakers to give torque about 44x,y,z	ILAS Uncoupled dynamics (approx) No translational dynamics	Not all critical modes are SCO
Advanced 5	Accels at 11x,y,z	Paired shakers to give torque about 44x,y,z	All critical modes are SCO	Strongly coupled dynamics Not ILAS
6	Accels at 11x,y,z	Shakers at 11x,y,z	ILAS Requires low control authority	Not all critical modes are SCO Strongly coupled dynamics (translational and rotational)

*SCO - strongly controllable and observable

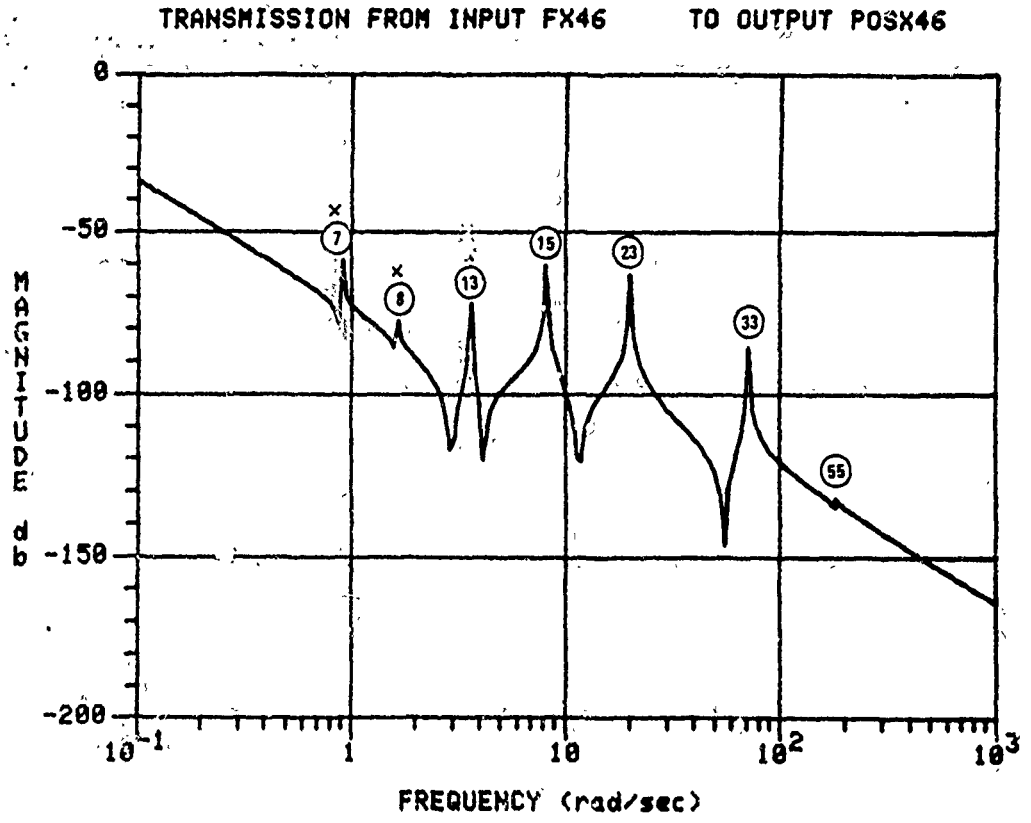

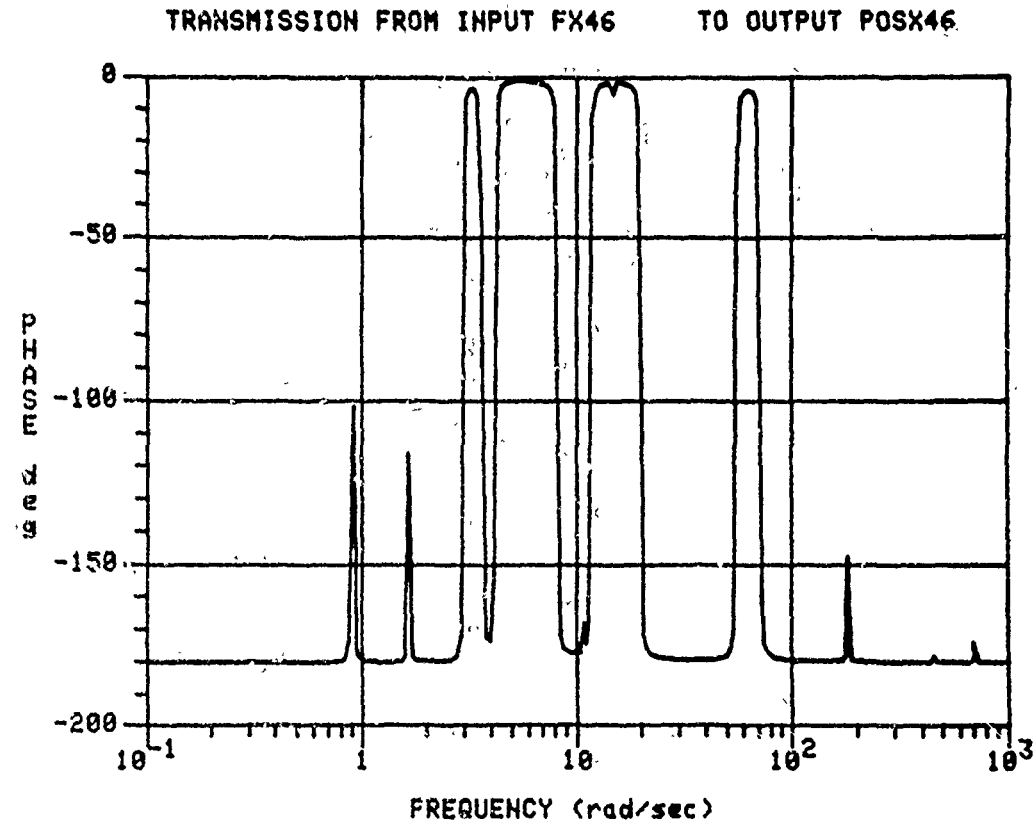

Figure 2-4a. Loop Transmission for Concept 1: $F_{x_{46}}$ to $P_{x_{46}}$

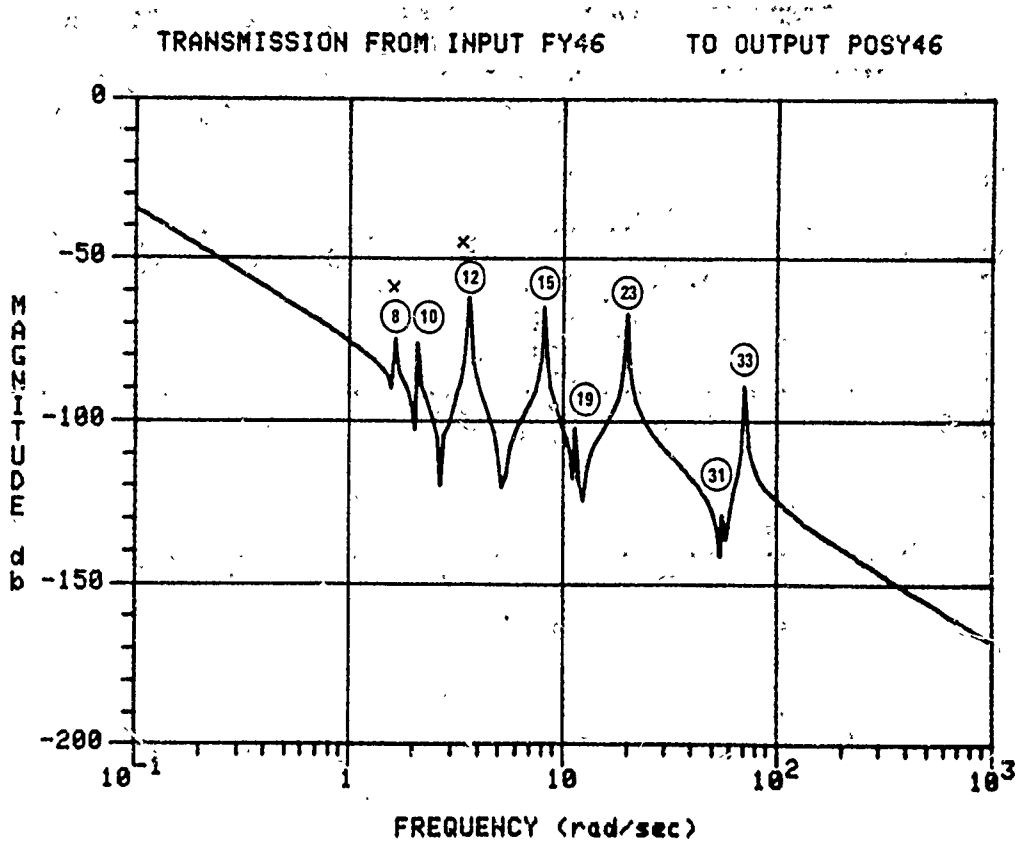

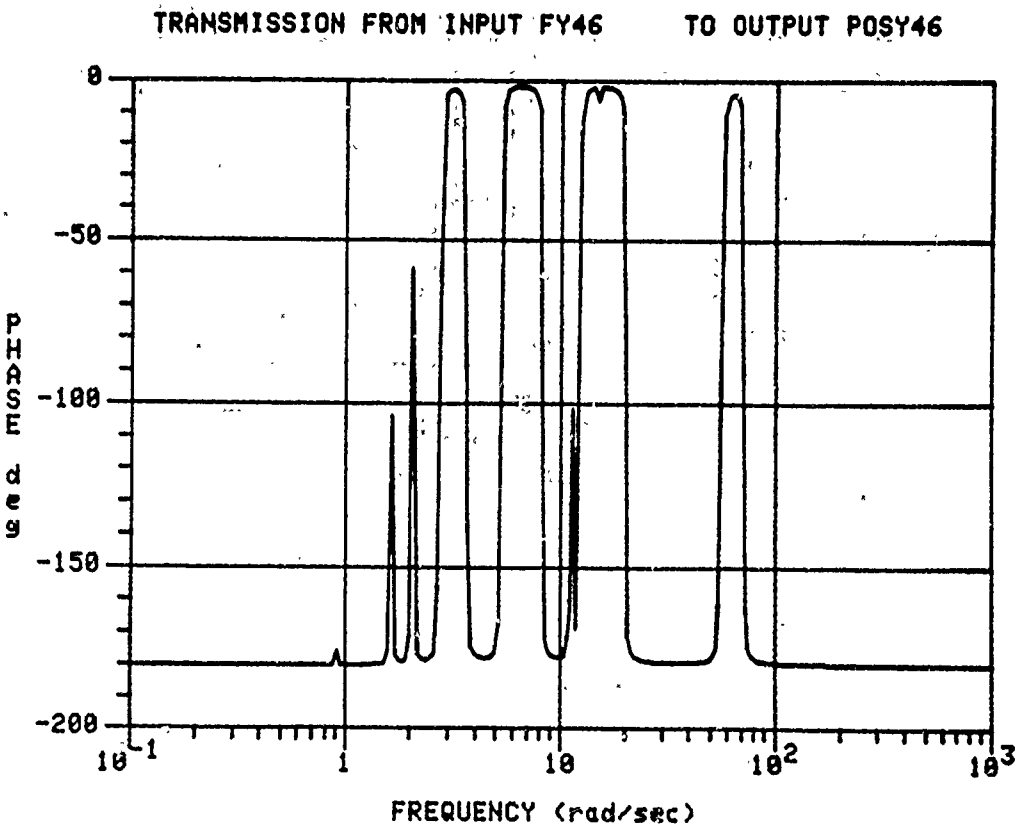

Figure 2-4b. Loop Transmission for Concept 1: $F_{y_{46}}$ to $P_{y_{46}}$

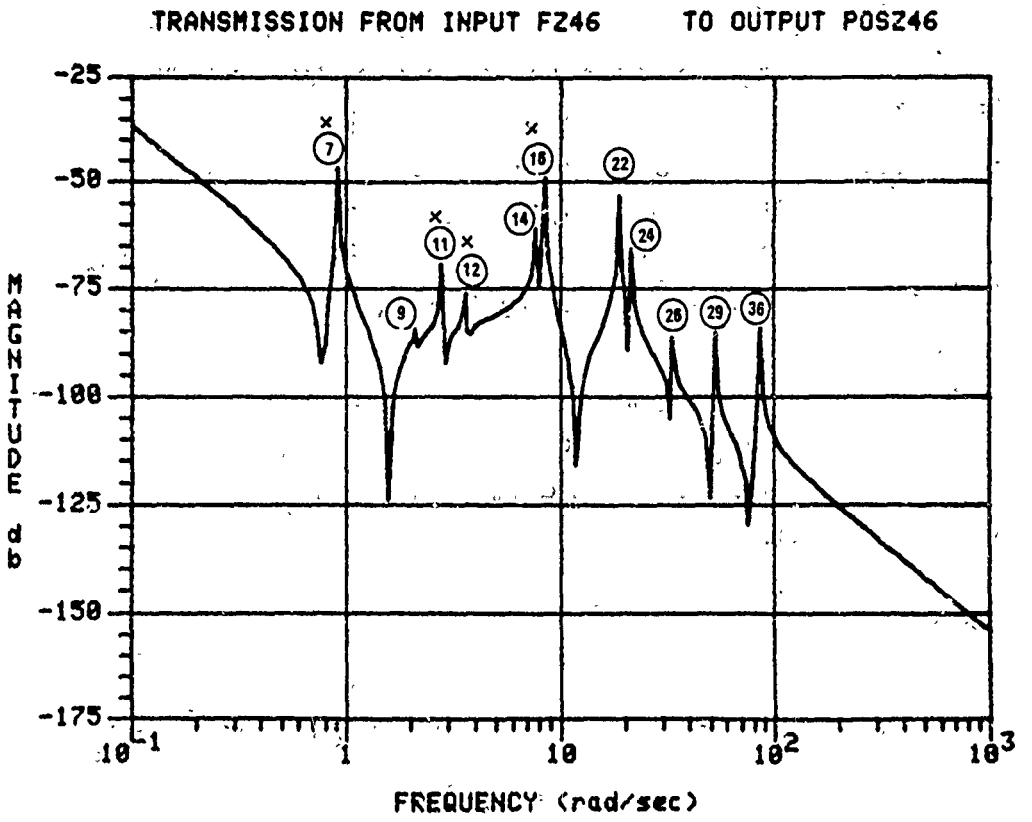

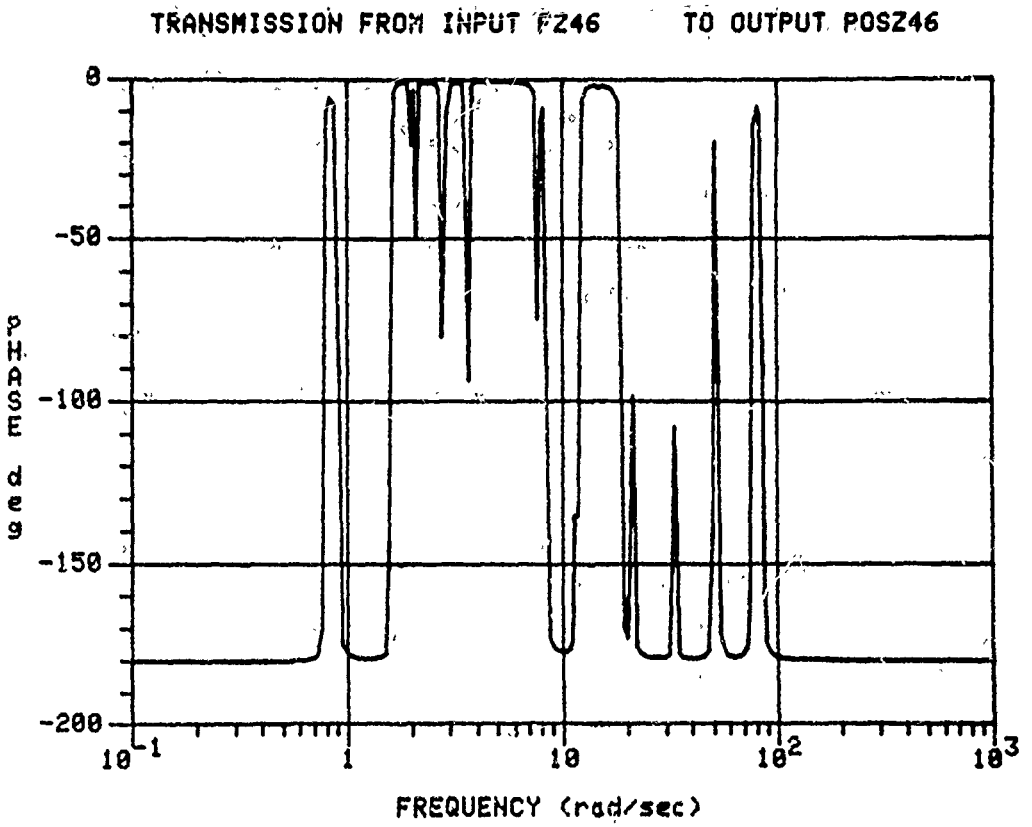

Figure 2-4c. Loop Transmission for Concept 1: $F_{z_{46}}$ to $P_{z_{46}}$

since off-diagonal elements, while nonzero, convey no additional information. Note that phase plots for the ILAS case are confined to the range -180 deg $\leq \phi \leq$ 0 deg. Singular value plots that bound the magnitude of the transfer function matrix are shown in Figure 2-5. While all plots shown here are for position output, those for velocity (acceleration) output differ only by the addition of +20 dB/decade (+40 dB/decade) to the magnitude and +90 deg (+180 deg) to the phase of $G(j\omega)$.

The most obvious disadvantage of this concept is that not all critical modes are strongly controllable and observable from node 46. Mode 21, for example, is critical to LOS_y performance, but appears in none of the transmission of Figures 2-4 or 2-5 and hence will not be attenuated by the vibration controller. This occurs because the influence coefficient for mode 21 is small at node 46, ($|b_{21}| \simeq 10^{-3}$) while that at the LOS is large ($|c_{21}| \simeq 10^{-2}$). Thus the controllability/observability product is small ($|b_{21}|^2 \simeq 10^{-6}$) for transmissions from node 46 to node 46, but of moderate size ($|c_{21}||b_{21}| \simeq 10^{-5}$) for transmissions from node 46 to the LOS. Similar comments apply for modes 30, 35, 37, and 38. As indicated in Figure 2-4, loop gain requirements imposed by modes 24 and 36 imply a control gain requirement of k = 145 dB with loop crossover around ω = 600 r/s.

Another disadvantage of this concept is strong coupling between axes and between rotational and translational modes. Modes 15, 23, and 33, in particular, are strongly coupled between at least two axes. This coupling increases the order of the model necessary for control design. Neglecting isolator modes, a multi-input, multi-output (MIMO) control design with three, four, and seven flexible modes for the x, y, and z axes, respectively, would most likely be necessary to achieve a reasonable fit with the truth model.

Concept 2: Accelerometers and Shakers at Nodes 42z, 43z, and 42x--Concept 2 in Table 2-2 alleviates coupling between axes of concept 1 to some extent by moving accelerometers and shakers to nodes 42 and 43, which lie in the y-z and x-z planes, respectively. Bode loop transmissions from force inputs to position outputs for diagonal elements shown in Figure 2-6 indicate somewhat less coupling

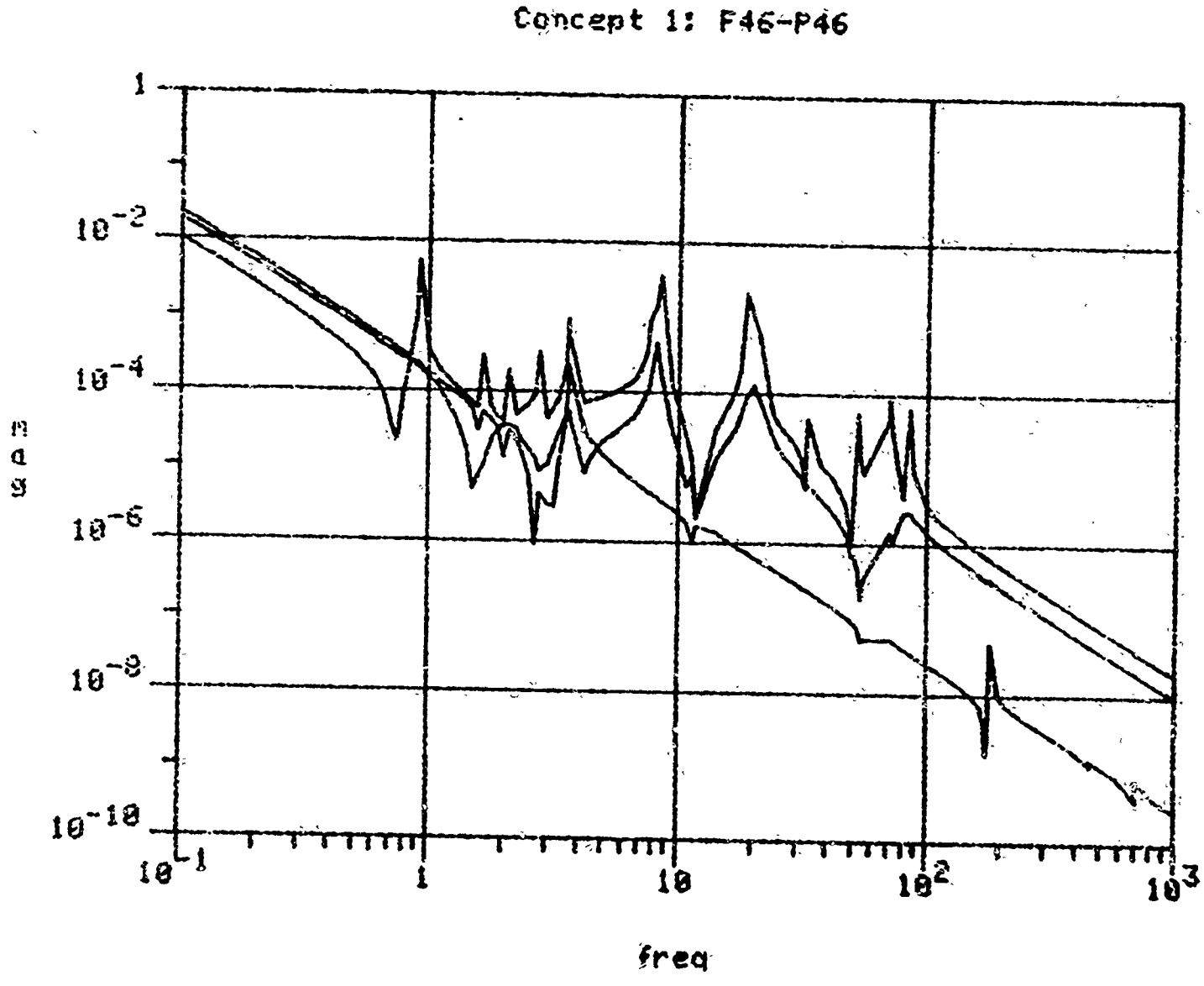

Figure 2-5. Singular Values of G(jω): Concept 1

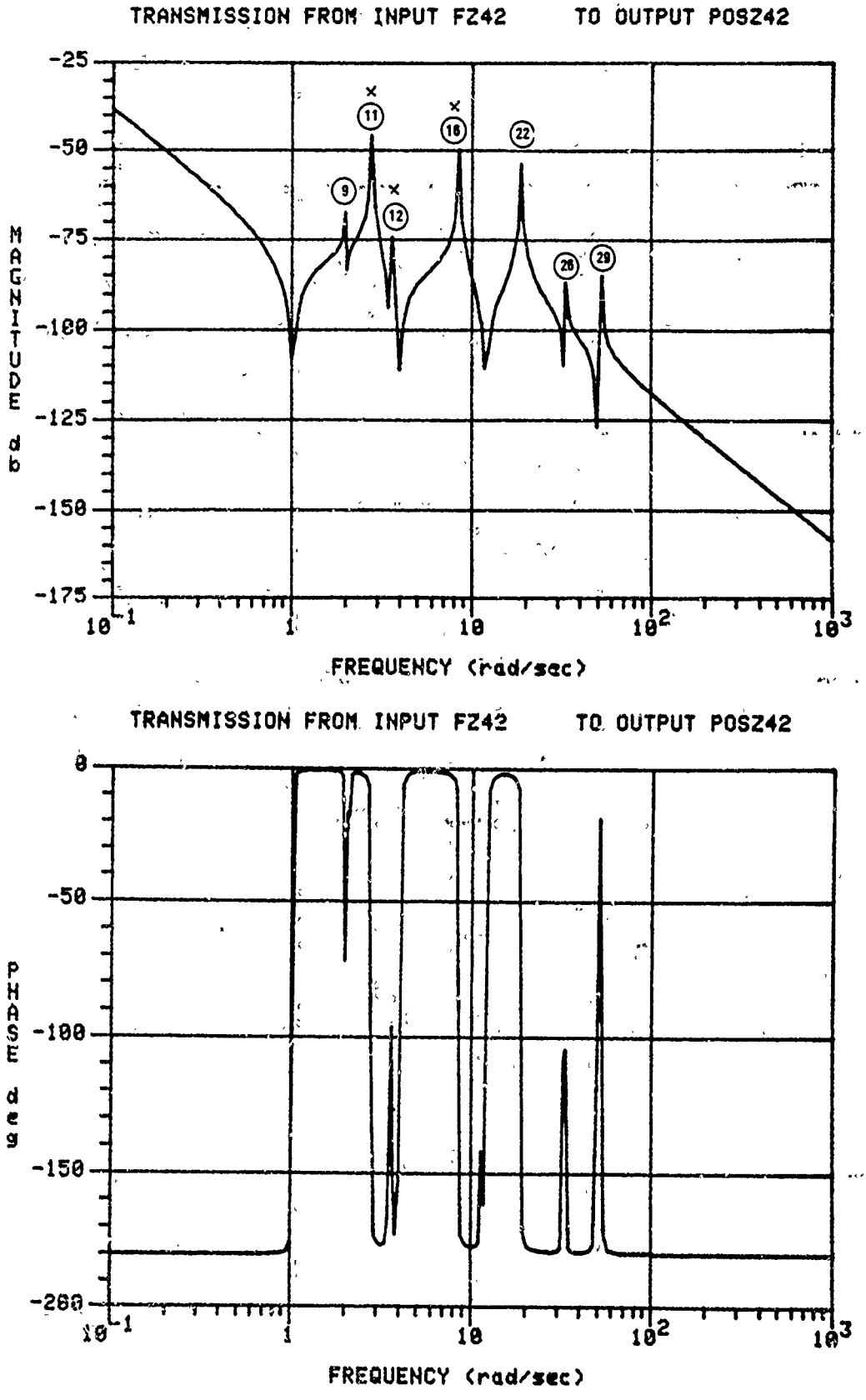

Figure 2-6a. Loop Transmission for Concept 2: $F_{z_{42}}$ to $P_{z_{42}}$

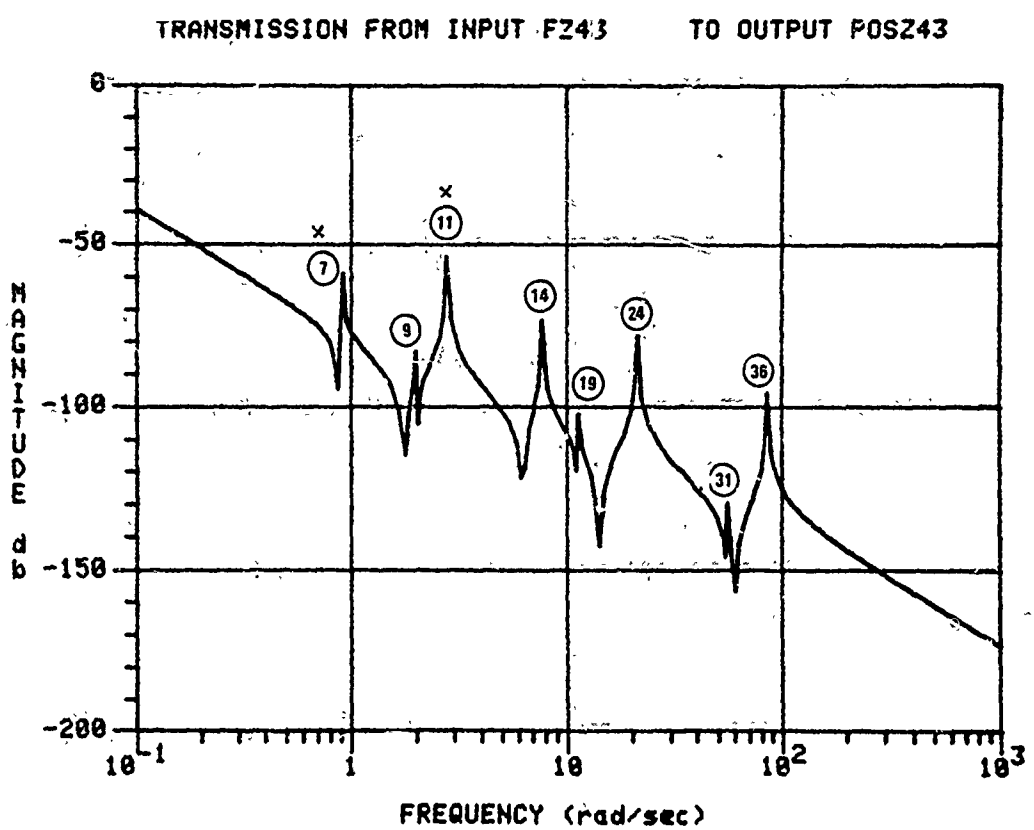

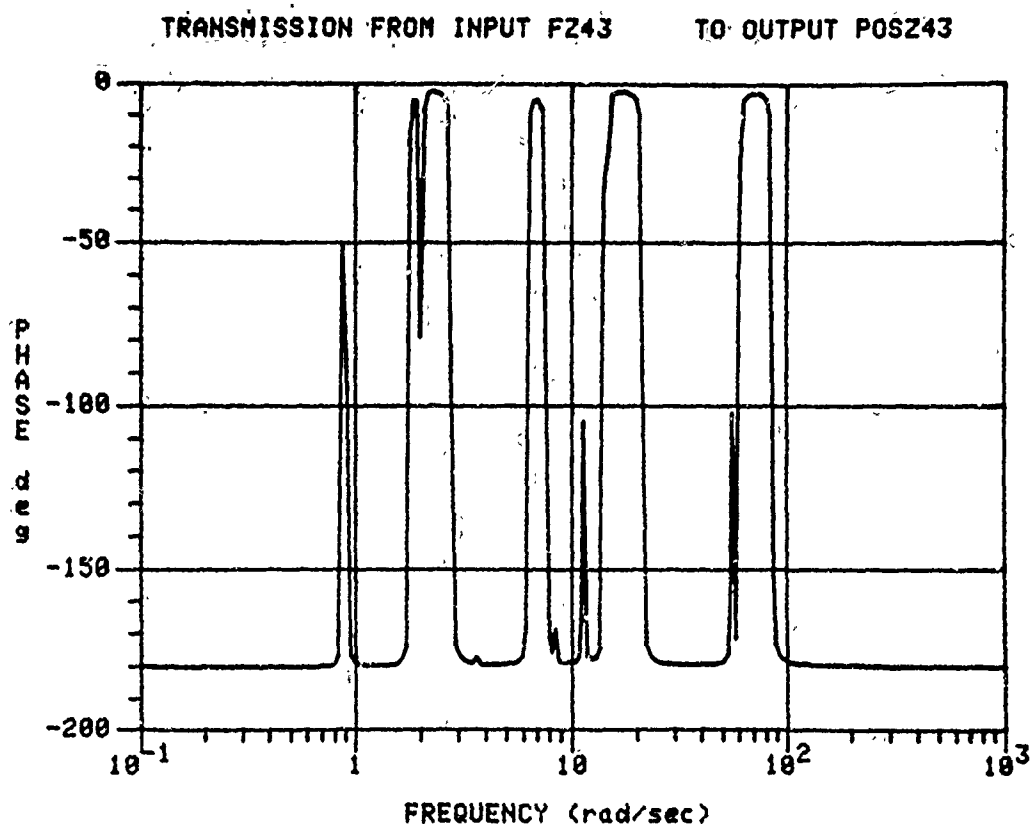

Figure 2-6b. Loop Transmission for Concept 2: $F_{z_{43}}$ to $P_{z_{43}}$

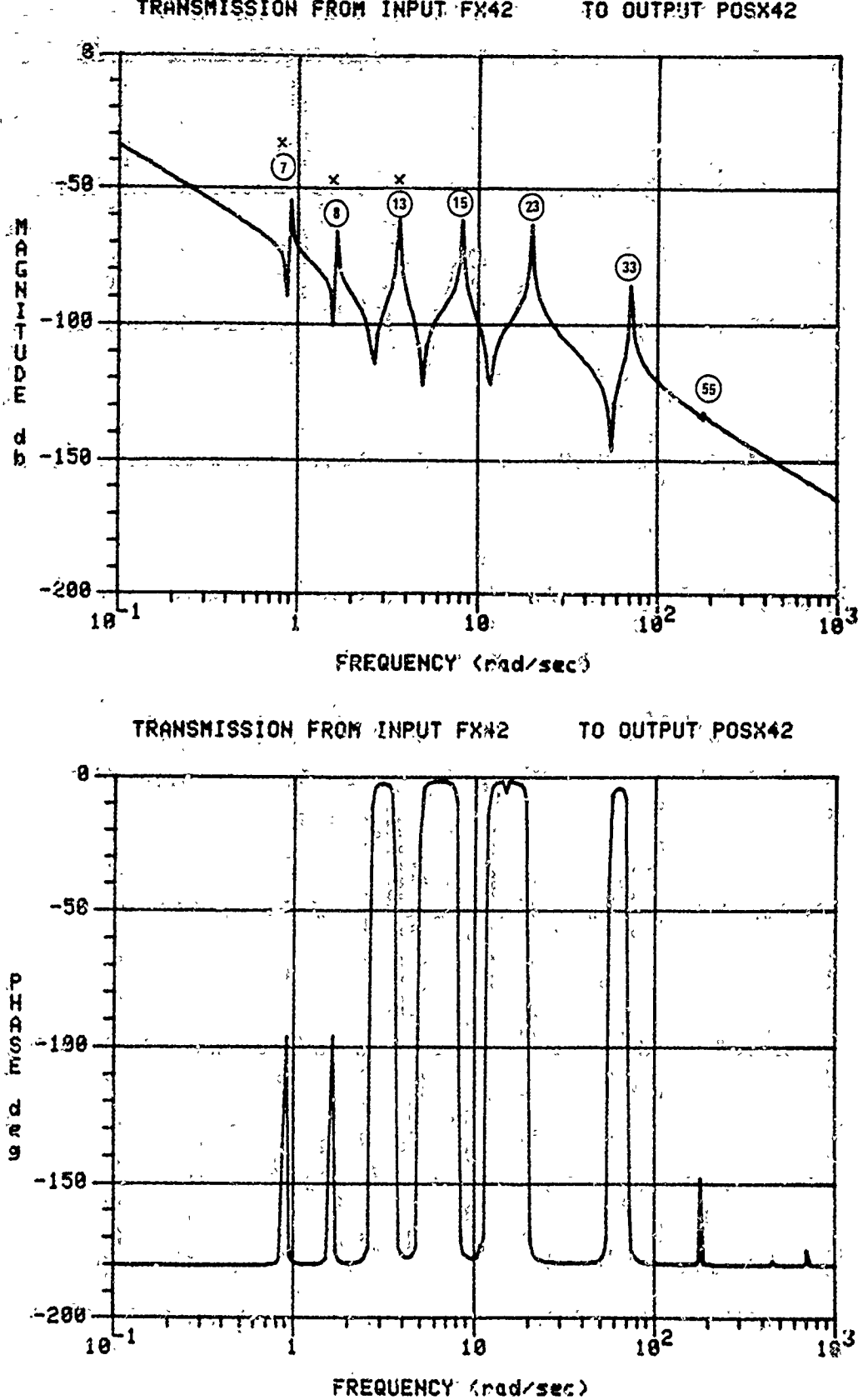

Figure 2-6c. Loop Transmission for Concept 2: $F_{x_{42}}$ to $P_{x_{42}}$

than before. Only mode 7 is strongly coupled between two axes. Even so, a MIMO control design model with four, five, and three flexible modes for the three axes, respectively, would most likely be necessary. Here again, modes 21, 30, 35, 37, and 38 are absent in all transmissions and hence will not be attenuated by the vibration controller. As is evident from Figure 2-7, control gain requirements of ~180 dB imply a control loop crossover beyond 1000 r/s. Thus, this concept offers little if any advantage over concept 1.

Concept 3: Gyros and CMGs at Node 44--Concept 3 is another ILAS concept that uses rotational-motion sensors and actuators located at the center of the equipment section. This choice produces essentially uncoupled dynamics between axes and little excitation of translational modes. Bode loop transmissions from force inputs to attitude outputs at node 44 for diagonal elements shown in Figure 2-8 indicate that three single-input, single-output (SISO) design models with four, three, and three flexible modes for the x, y, and z axes, respectively, would give a nearly perfect fit with the truth model. Once again, however, modes 21, 30, 35, 37, and 38 fail to appear in any of these transmissions and hence will not be attenuated by the vibration controller. This concept offers essentially the same vibration control performance potential as concept 1 because z-axis disturbance at node 46 can be decomposed into torques about the x and y axes, and a negligible force along the z axis at node 44. Figure 2-9 shows that control gain requirements of ~165 dB imposed by modes 24 and 36 imply a loop crossover beyond 300 r/s.

Two fundamental limitations with this concept are a serious lack of control torque capability to handle disturbance torques of $T_d \simeq (5m)\ (400\ N) = 2000\ N\text{-}m$ and the need for very high bandwidth CMGs. Bandwidth requirements of roughly ω = 1000 r/s are necessary to control vibrations out to 100 r/s in order to ensure adequate control loop rolloff. Similar bandwidth requirements, of course, apply to vibration control sensors and actuators for all concepts. These requirements eliminate CMGs as practical vibration control actuators.

Concept 4: Gyros and Paired Shakers at Node 44--The above torque and bandwidth requirements, however, could conceivably be met using three pairs of shakers mounted symmetrically about node 44 on the equipment section to produce net torques about each axis. Concept 4, then, is just a practical means of

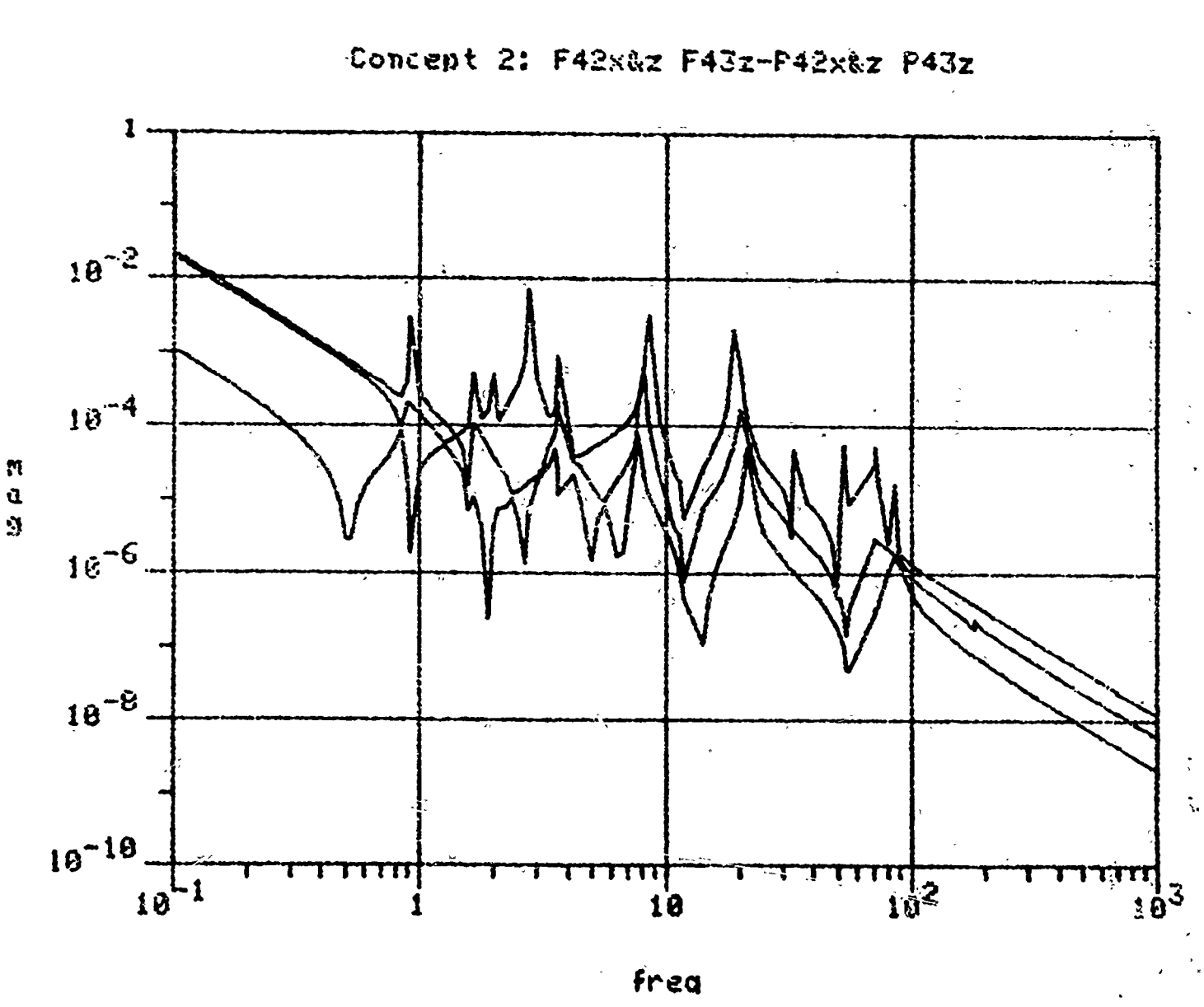

Figure 2-7. Singular Values of G(jω): Concept 2

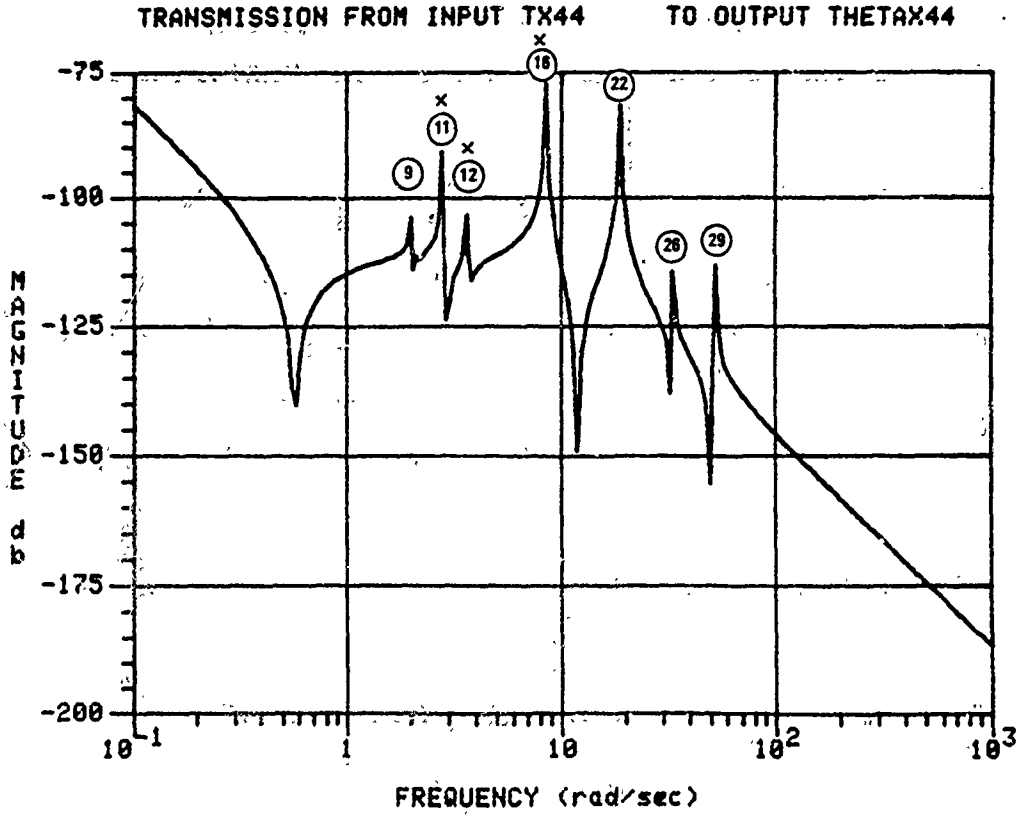

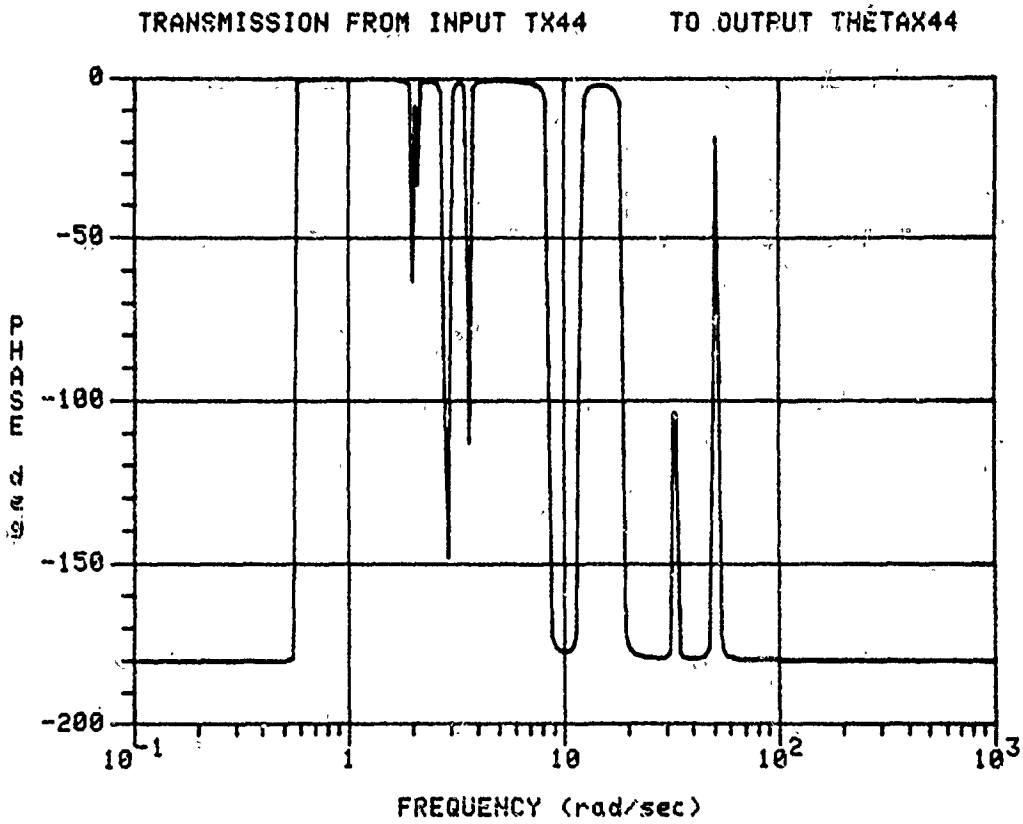

Figure 2-8a. Loop Transmission for Concepts 3 and 4: $T_{x_{44}}$ to $\theta_{x_{44}}$

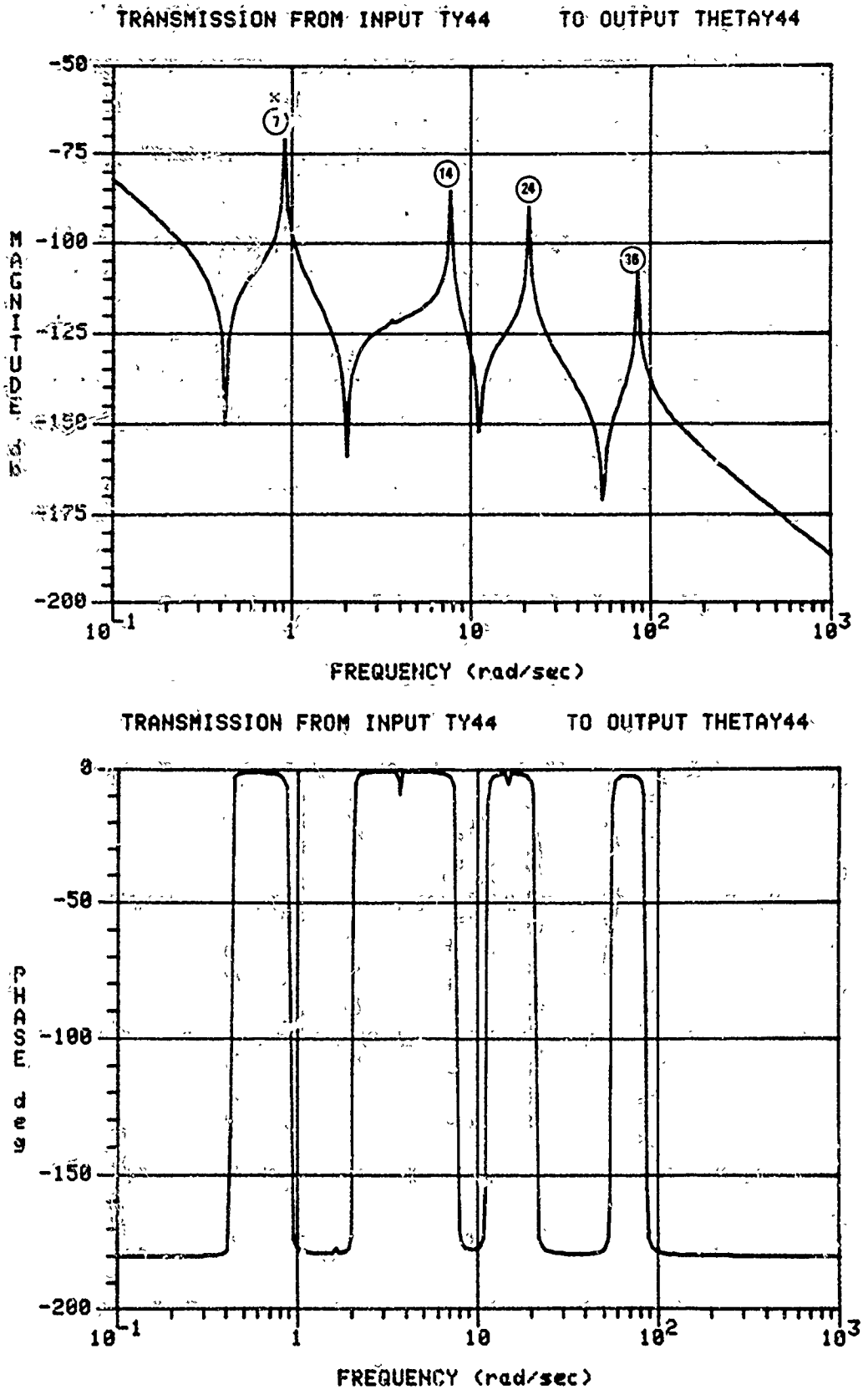

Figure 2-8b. Loop Transmission for Concepts 3 and 4: $T_{y_{44}}$ to $\theta_{y_{44}}$

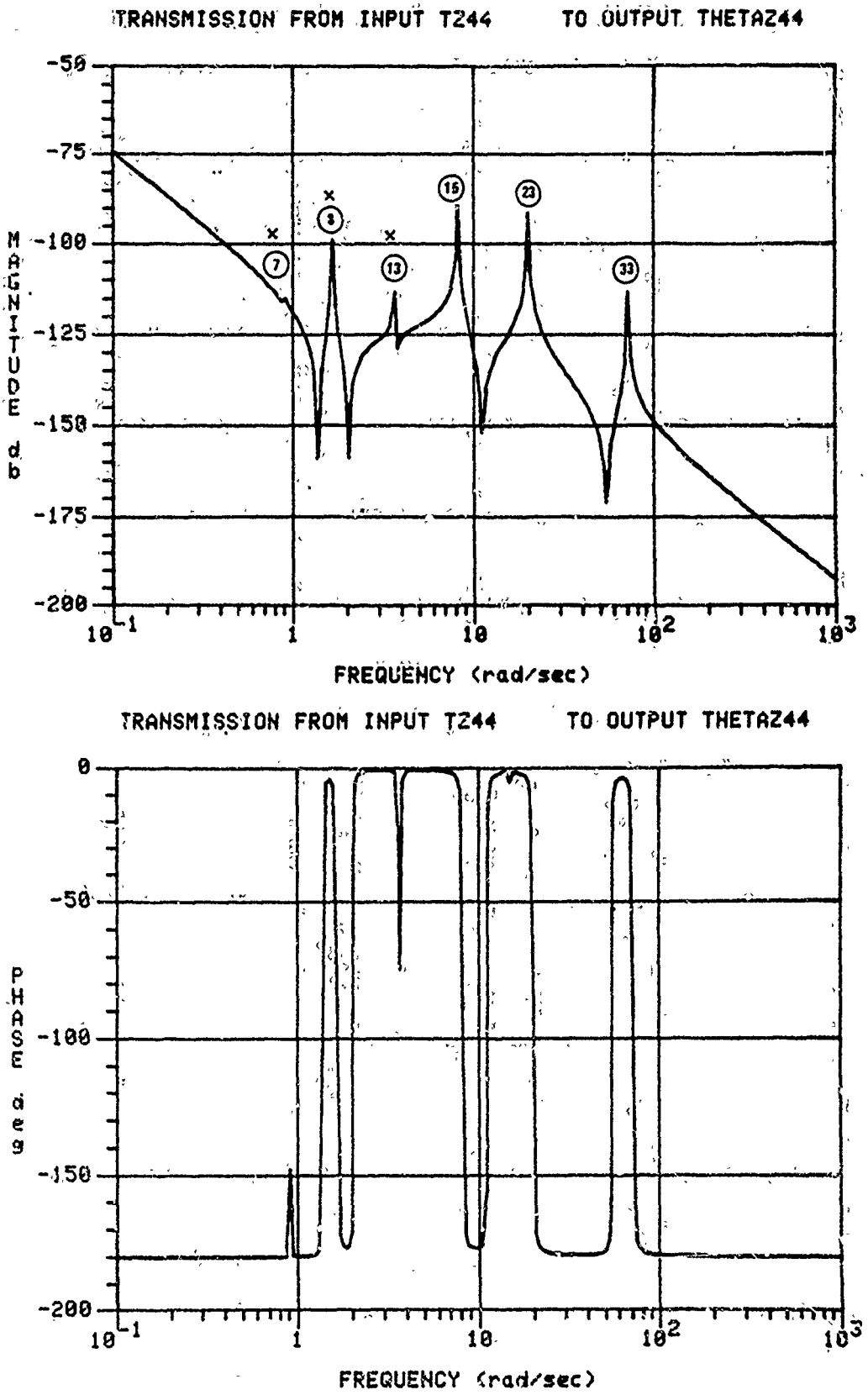

Figure 2-8c. Loop Transmission for Concepts 3 and 4: $T_{z_{44}}$ to $\theta_{z_{44}}$

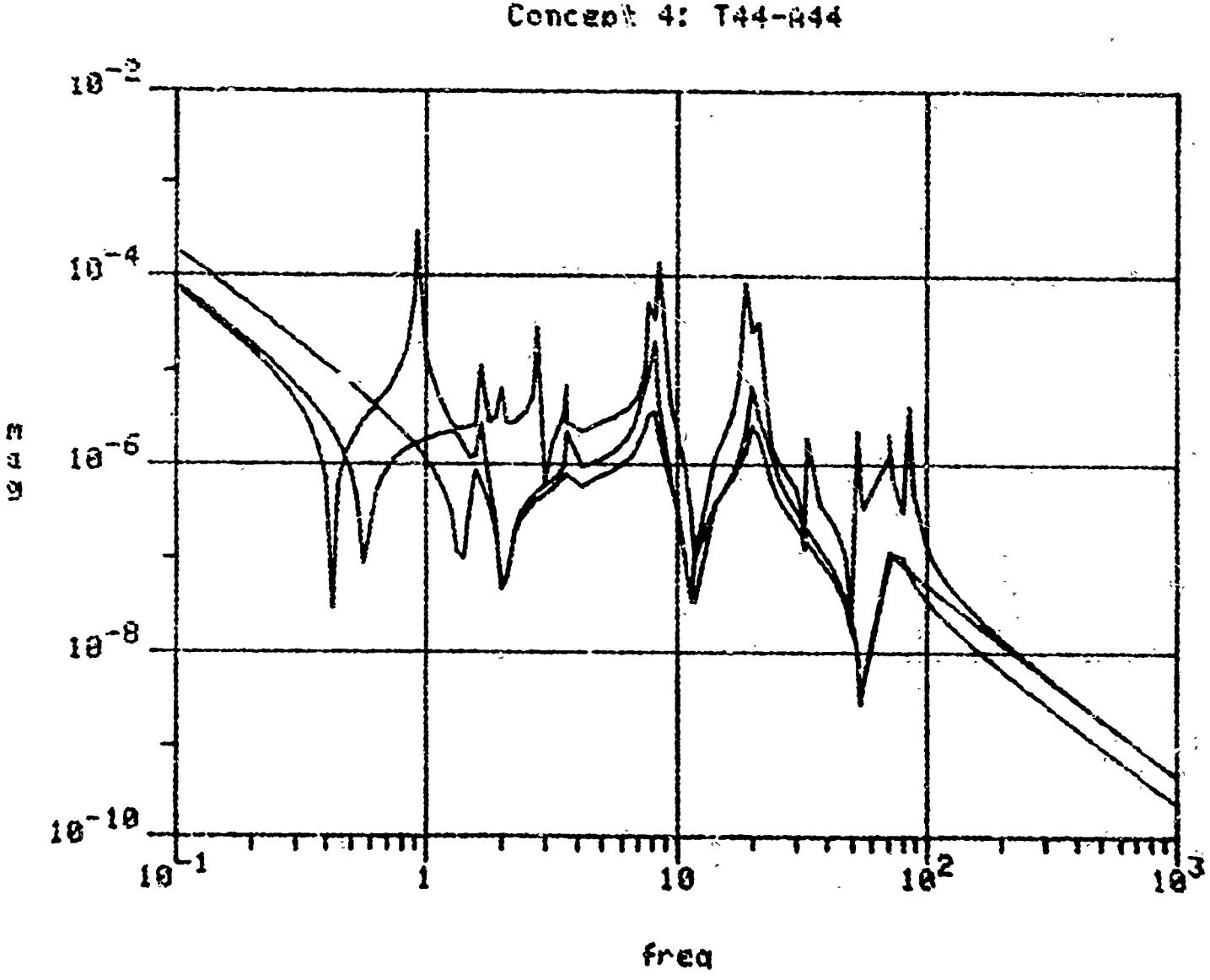

Figure 2-9. Singular Values of G(jω): Concepts 3 and 4

implementing concept 3. Should, as is likely, sensor bandwidth requirements prove impossible to meet with gyros, a similar scheme using paired accelerometers, which have greater bandwidth capabilities than gyros, could be used to sense angular accelerations and thereby eliminate the gyros. In any case the basic loop transmission characteristics of Figures 2-8 and 2-9 still apply, subject to obvious ω or ω^2 corrections to produce angular rate or acceleration outputs.

Concept 5: Accelerometers at Node 11 and Paired Shakers at Node 44--Concept 5 is the first (and only) non-ILAS concept. It uses paired shakers to produce torques on the equipment section and accelerometers on the optical structure. The accelerometers were placed at node 11 near the focal plane since all modes critical to LOS pointing are observable from this node. Bode loop transmissions for the three torque inputs to z-position output in Figure 2-10 show that all critical modes are controllable and observable. In practice, x- and y-axis accelerometers would also be included to complete the triad.

Since this is a non-ILAS concept, phase for the three loop transmissions of Figure 2-10 is no longer confined to the range -180 deg $\leq \phi \leq$ 0 deg. Thus control design for this concept is considerably more difficult and requires a more accurate model than for the ILAS concepts. This places more stringent requirements on the control design model. The stronger coupling between axes further increases model complexity. Neglecting isolator modes, some 21 flexible modes below 100 r/s appear in Figure 2-11, many of which would likely be required for this model. Figure 2-11 shows that control gain requirements of ~200 dB imply a loop crossover beyond 200 r/s.

Concept 6: Accelerometers and Shakers at Node 11--The last concept in Table 2-2 uses three-axis accelerometers and shakers, all mounted on the optical structure at node 11. Bode loop transmissions for diagonal elements in Figure 2-12 show at least eight flexible modes below 100 r/s that are significant. Six flexible modes above 100 r/s also appear critical for control. Some modes critical to LOS performance, however, such as modes 22, 24, and 29, are absent and hence will not be attenuated by the vibration control loop. A significant

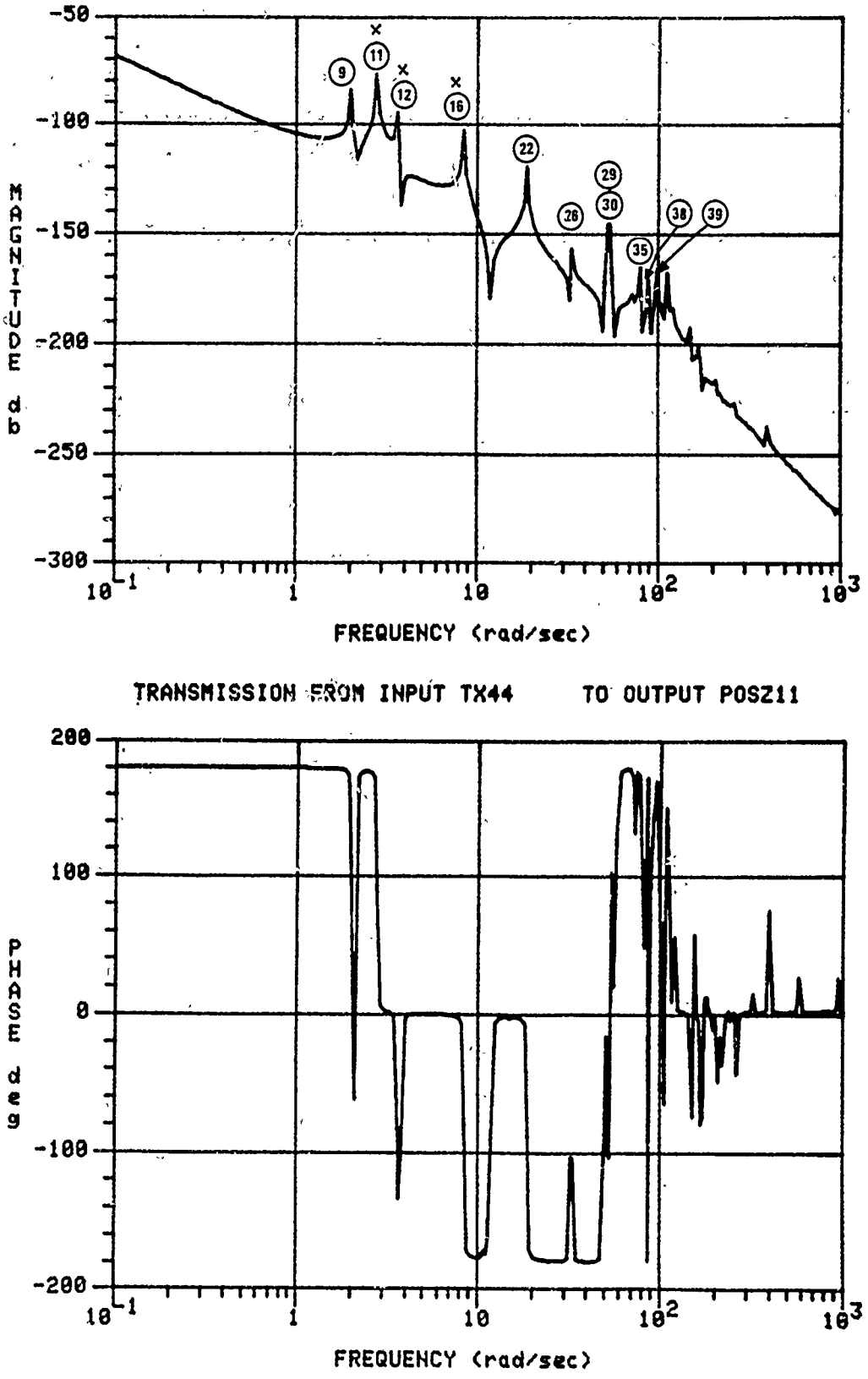

Figure 2-10a. Loop Transmission for Concept 5: $T_{x_{44}}$ to $P_{z_{11}}$

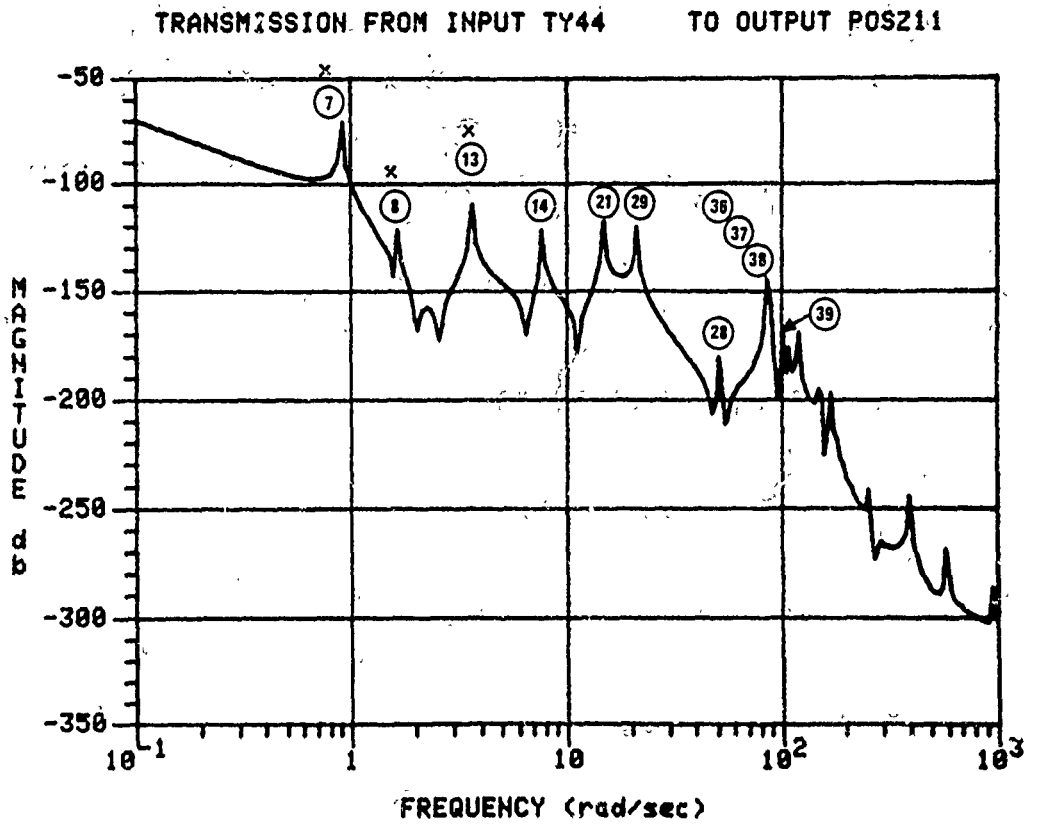

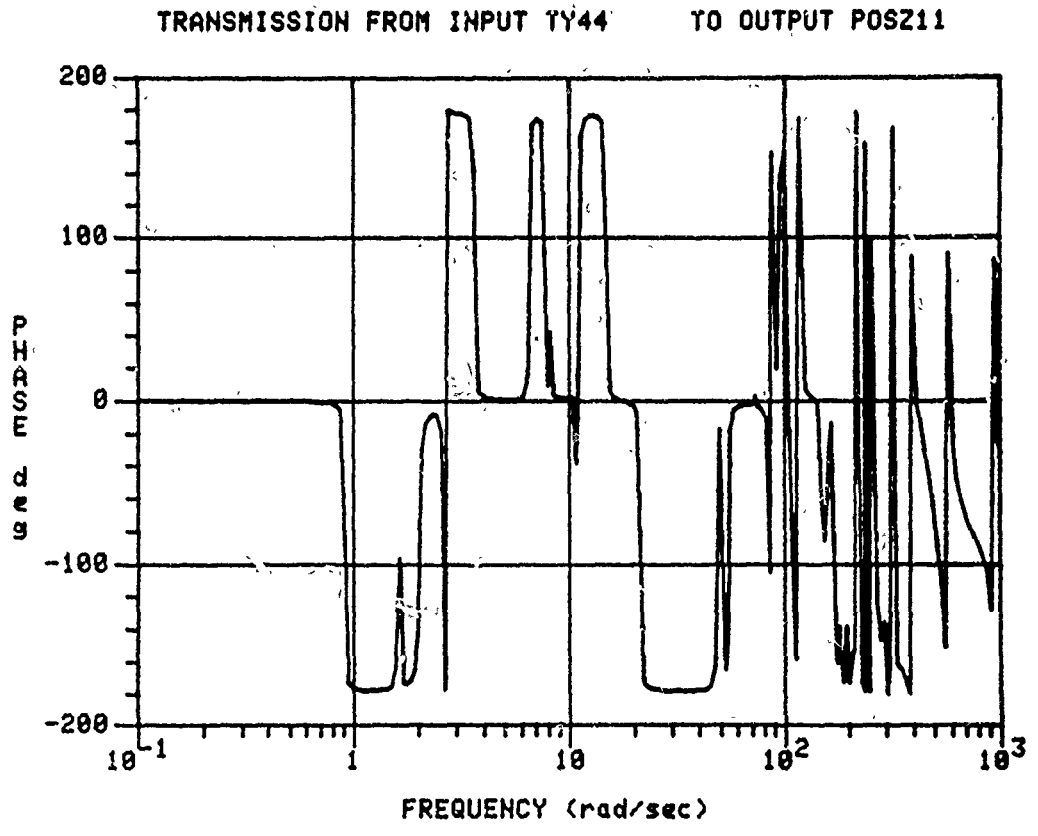

Figure 2-10b. Loop Transmission for Concept 5: $T_{y_{44}}$ to $P_{z_{11}}$

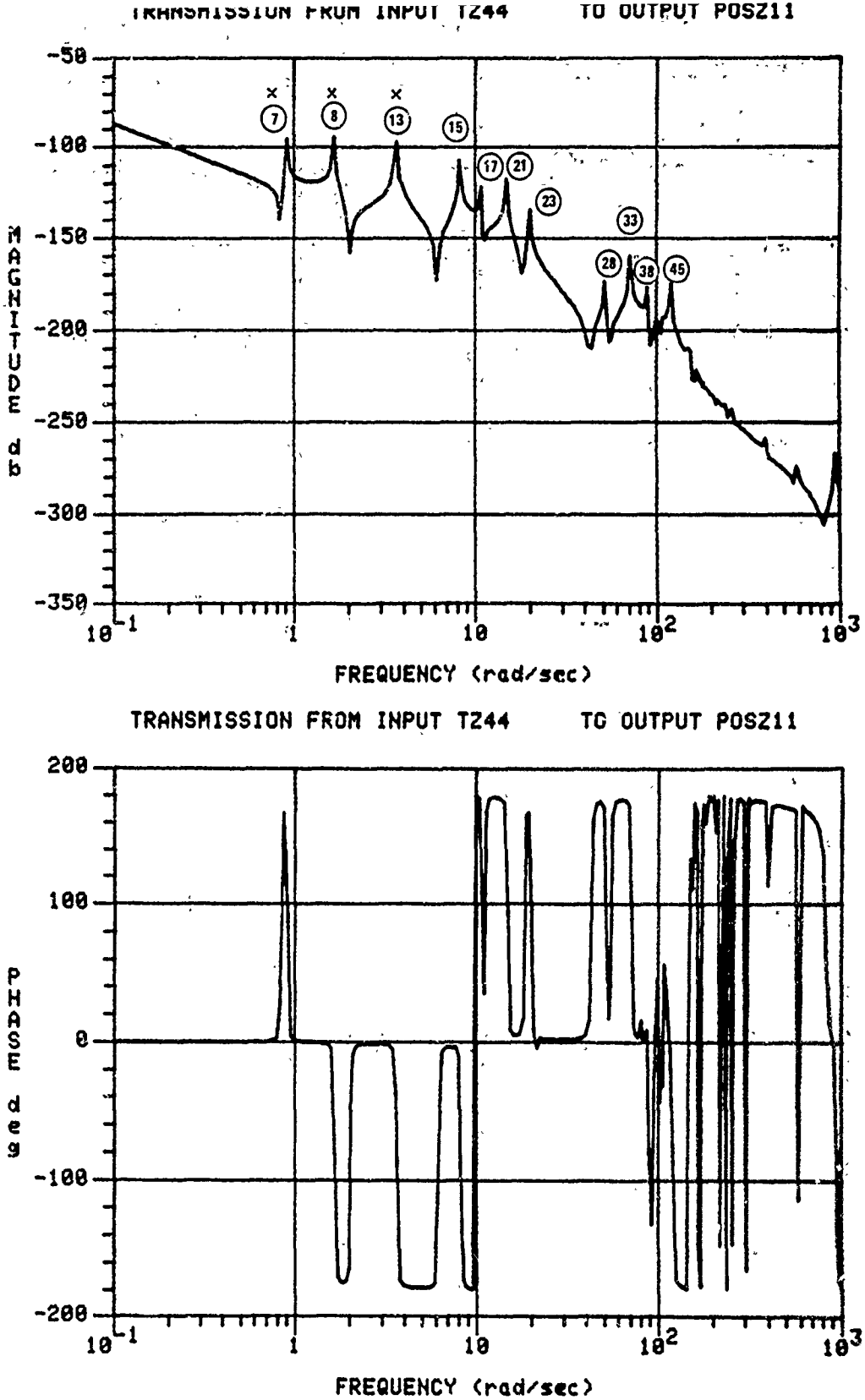

Figure 2-10c. Loop Transmission for Concept 5: $T_{z_{44}}$ to $P_{z_{11}}$

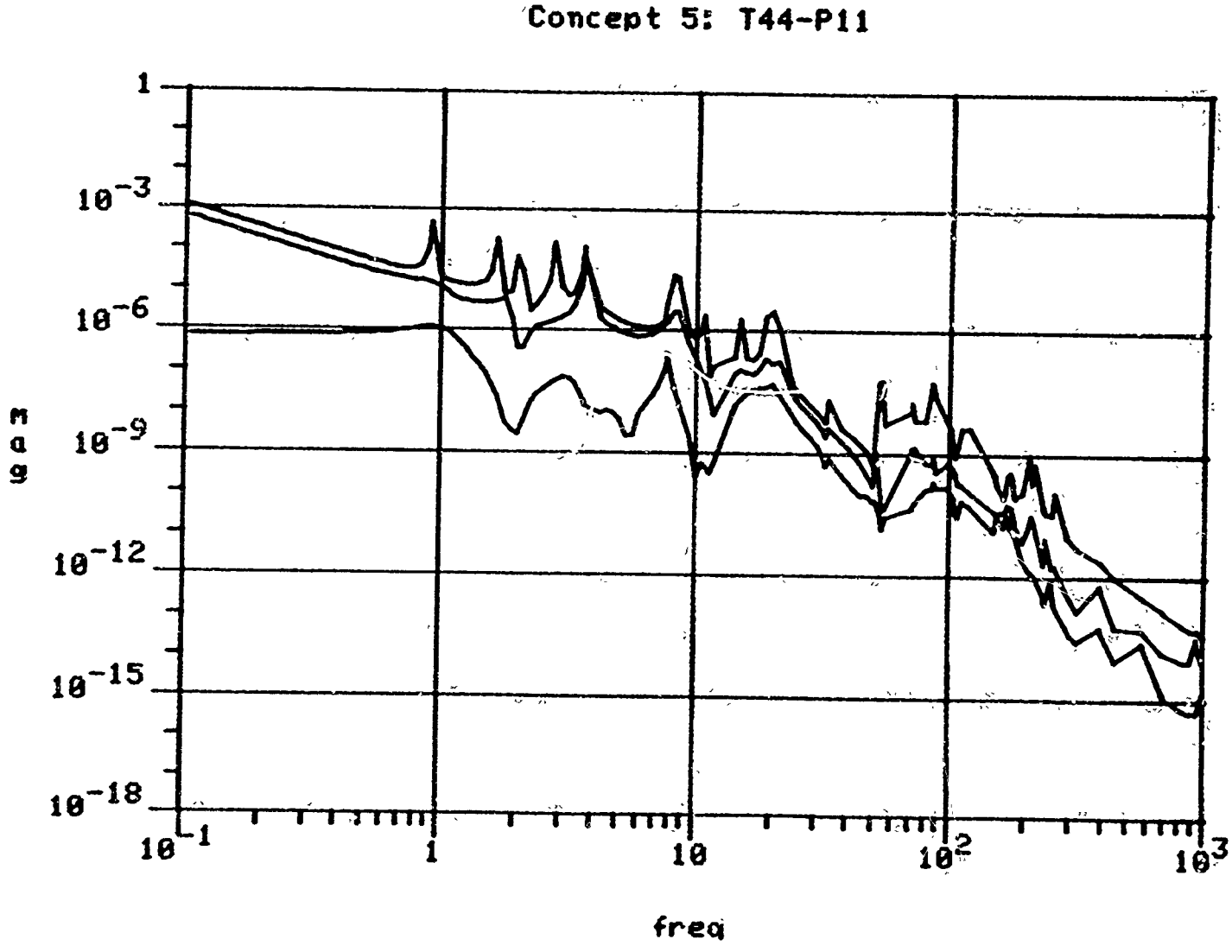

Figure 2-11. Singular Values of G(jω): Concept 5

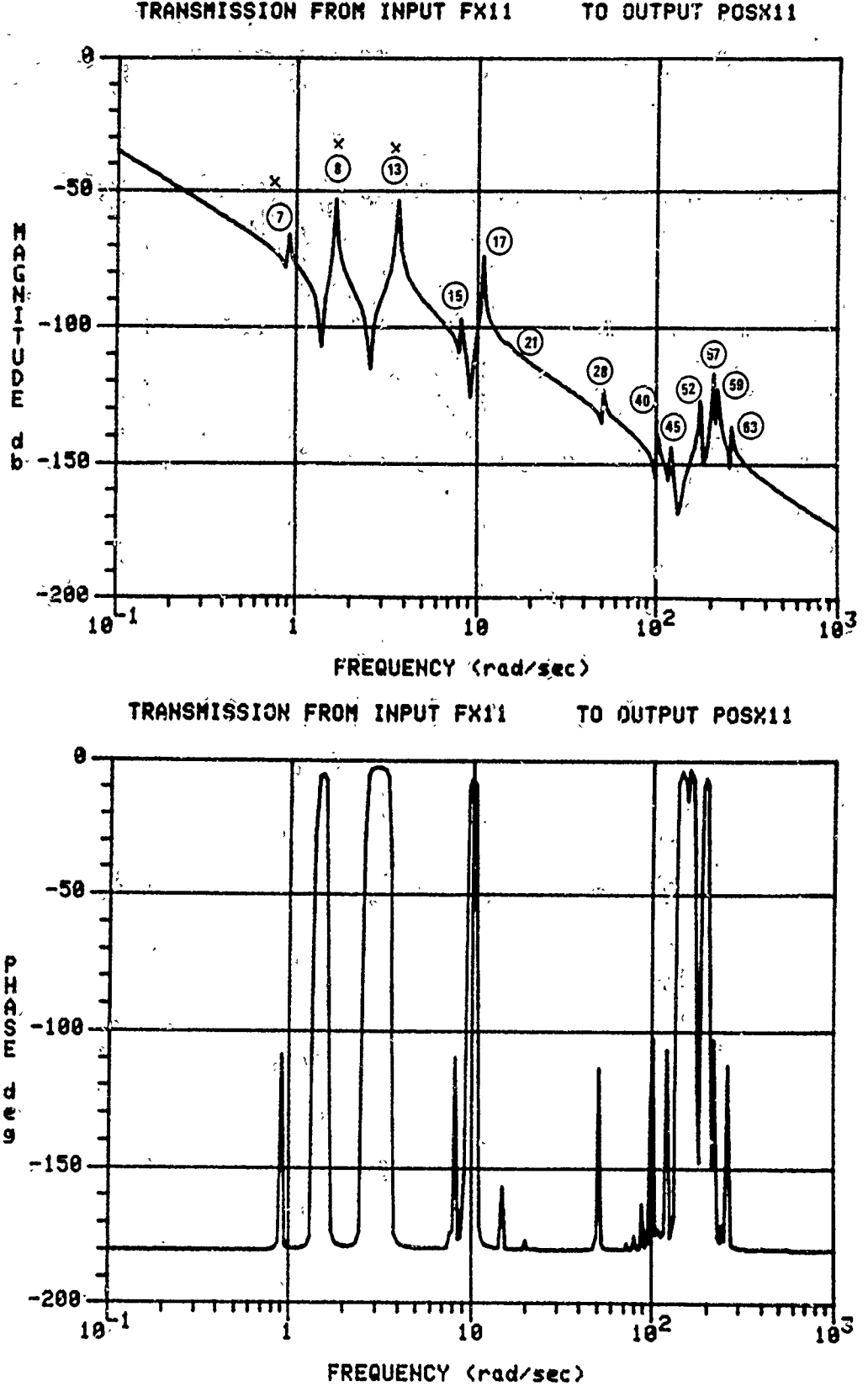

Figure 2-12a. Loop Transmission for Concept 6: $F_{x_{11}}$ to $P_{x_{11}}$

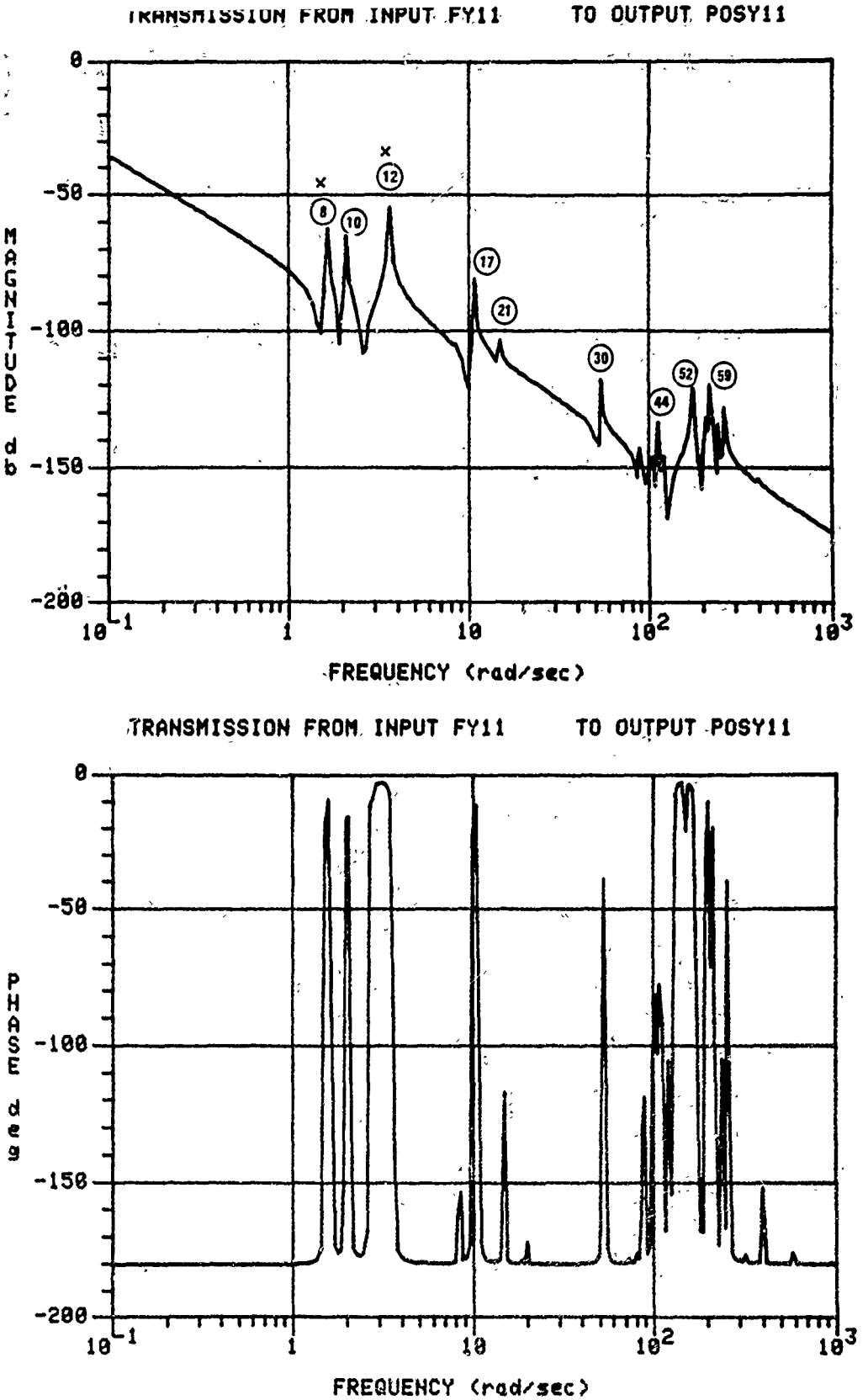

Figure 2-12b. Loop Transmission for Concept 6: $F_{y_{11}}$ to $P_{y_{11}}$

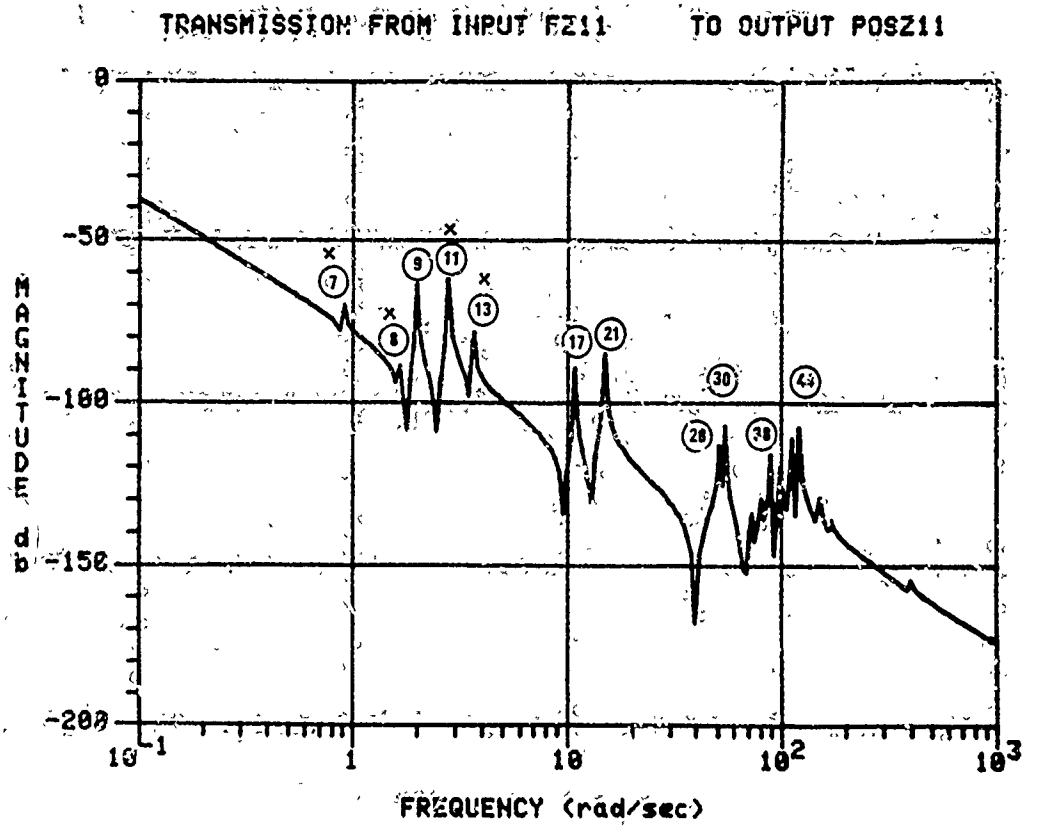

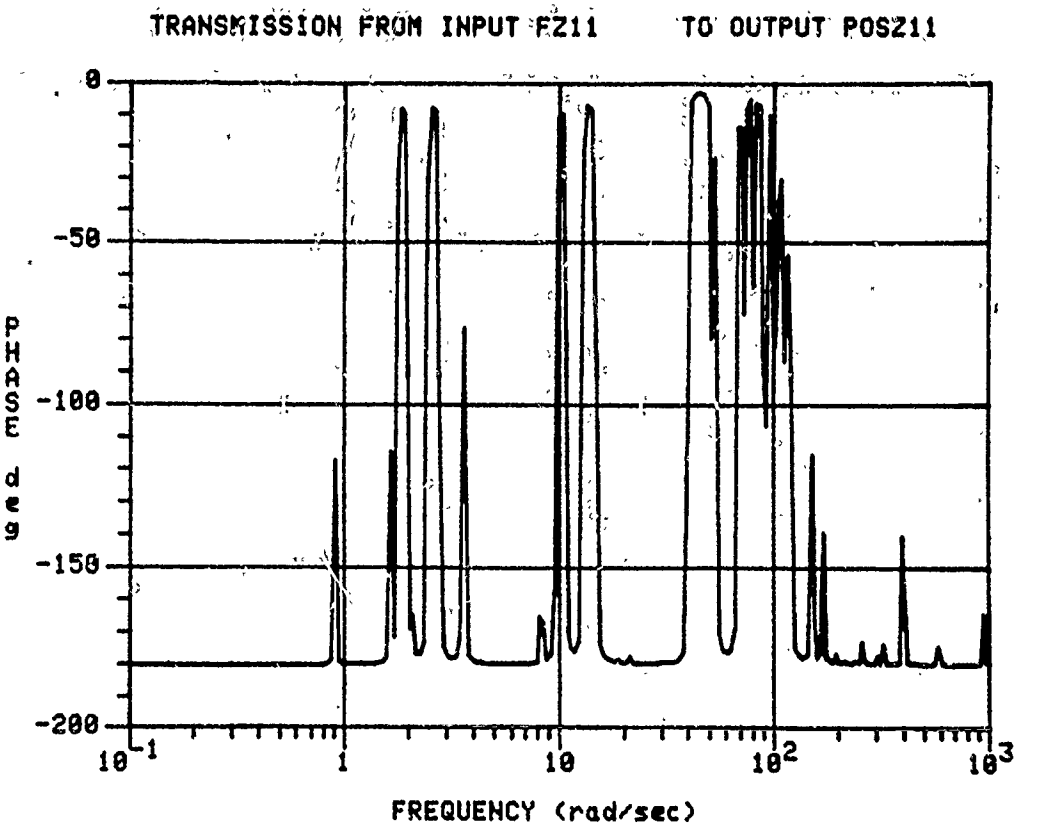

Figure 2-12c. Loop Transmission for Concept 6: $F_{z_{11}}$ to $P_{z_{11}}$

advantage of this concept is that actuators mounted on the optical structure require considerably less control authority to attenuate disturbances at the LOS than when they are mounted on the equipment section, since much of the work is accomplished by the passive isolator. Thus it is conceivable that careful placement of additional sensors and actuators could make this concept viable. As evident from Figure 2-13, control gain requirements of ~165 dB imply a loop crossover beyond 500 r/s.

Concept Selection

Because some critical modes are not both controllable and observable, none of the ILAS concepts of Table 2-2 are suitable for disturbance attenuation over the entire disturbance frequency range 10 r/s < Ω < 100 r/s. Rather, most are limited to a frequency range of about 15 r/s < Ω < 50 r/s. Nevertheless, the simplicity of control and identification for the ILAS case favored the selection of one of these concepts for identifiability and control analyses studies. Of the ILAS concepts, concept 4 was selected as the baseline concept due to its lack of inter-axis coupling, its relatively small control bandwidth requirements, and its potential for simple low-order control design model representations. Concept 5, on the other hand, was selected as the advanced concept because it was the only concept examined that could, in theory, meet control requirements over the entire disturbance frequency passband. Moreover, it offered a significant practical challenge to our identification and control design capabilities.

It should be observed that all of the vibration control concepts examined, including the two selected for further analyses, call for control loop gain crossover frequencies in excess of ω = 100 r/s. It is generally recognized, however, that finite-element models are unreliable for frequencies beyond those of the first half of the modes included in the model. Thus the ACOSS II model, and hence the frequency responses presented in this section, are probably good out to frequencies no larger than $\omega \approx$ 200 r/s. Good engineering judgment, therefore, dictates that we must relax control requirements somewhat to ensure that loop gains do not exceed one for frequencies above 100 r/s, and accept the fact that stringent pointing specifications in the face of severe disturbance levels call for more reliable models. Even this control design philosophy pushes the validity

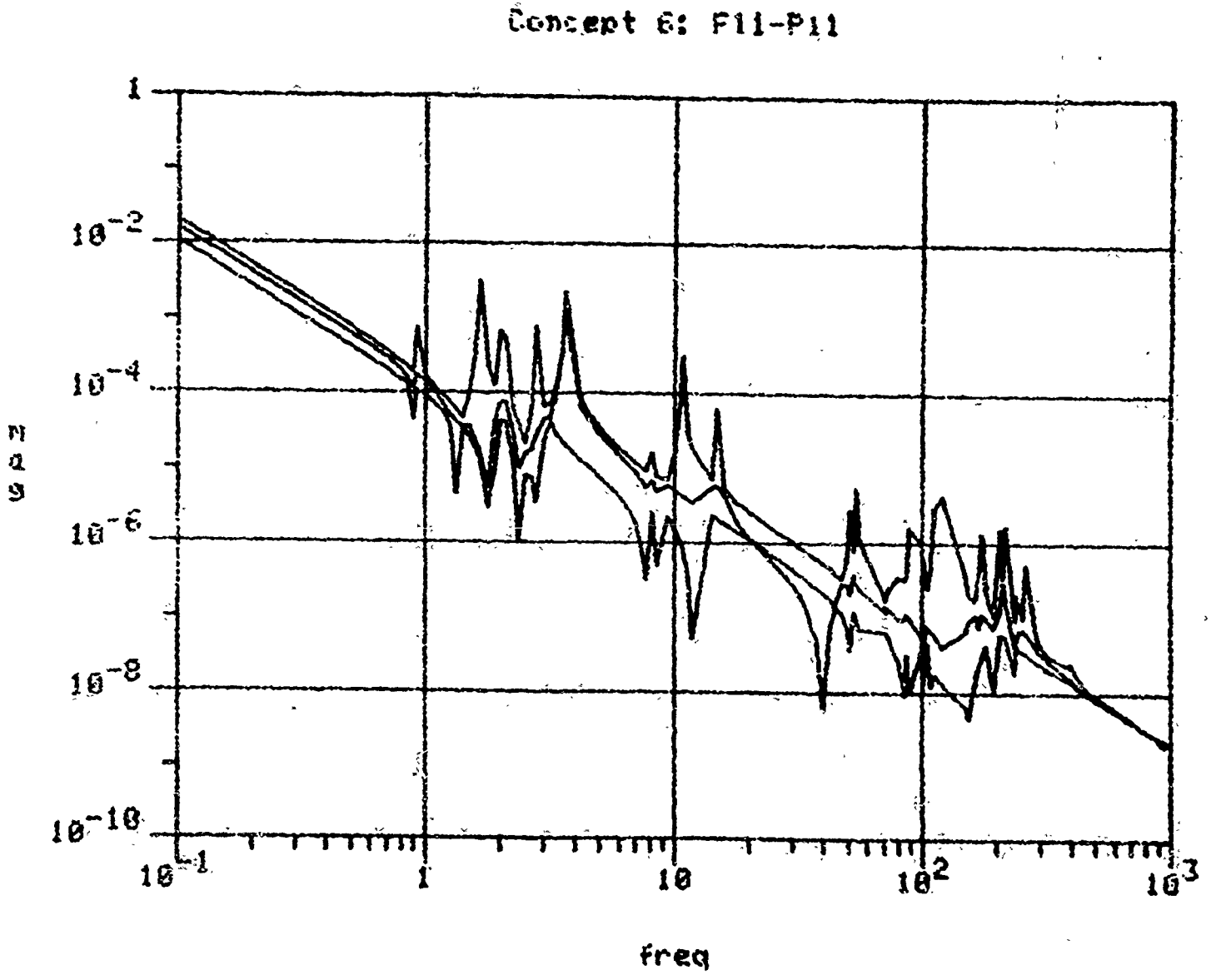

Figure 2-13. Singular Values of G(jω): Concept 6

of the ACOSS II Model in that certain high-frequency modes above 100 r/s are clearly unaccounted for, even in the 84-mode finite-element approximation. The true vehicle, for example, would almost certainly contain several solar panel modes above 100 r/s if a finer finite-element approximation were used for the solar array. Even for these relaxed requirements, bandwidth for all control hardware--sensors, actuators, computers, etc.--must be nearly 1000 r/s to ensure phase stability throughout the control-loop gain crossover region.

SECTION 3

IDENTIFICATION PROBLEM DEFINITION

This section defines the identification problem addressed in the ACOSS SIXTEEN study. We begin by examining model requirements imposed by control requirements. Using Honeywell-developed methods for assessing stability and performance robustness to plant uncertainty for multivariable systems, we develop criteria for defining reduced-order models (ROMs) for control design and modal-parameter accuracy requirements for modes that are retained in this model. The resulting stringent accuracy requirements show that identification is in general virtually unavoidable for vibration control. Next we examine the identification problem, establishing ground rules and specific requirements for the two selected identification and control concepts. Finally we address the subjects of test signal selection and measurement noise definition for identification studies. These results along with other hardware requirements for identification and control are summarized for the two concepts.

CONTROL REQUIREMENTS DRIVE IDENTIFICATION

In Section 2 we examined a generic two-MIMO-loop feedback control structure suitable for both low-frequency attitude and high-frequency vibration control. We then focused on the inner vibration control loop and examined control performance requirements imposed by LOS pointing specifications in the face of disturbances. We now re-examine this inner loop, which we have redrawn in the standard MIMO form of Figure 3-1, from the broader perspective of performance and stability. Here c denotes the command inputs, u the input to the structure together with the sensors and actuators, G(s), y the output, and e the error input to the controller K(s).

In addition, w denotes the disturbances, v the sensor measurement error, and P(s) a possible command shaping network. Regardless of the technique used to generate the feedback law, the fundamental requirements for control, model fidelity, and sensors and actuators are most easily specified in the frequency domain.

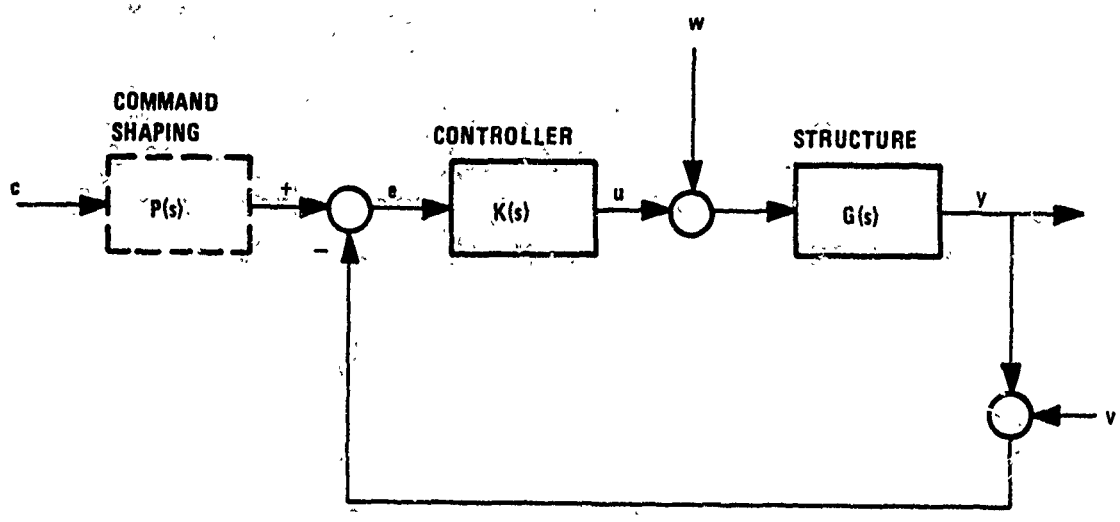

Figure 3-1. Standard Feedback Configuration

Control Requirements

Given the control objective and appropriate descriptions for the disturbance environment and desired response to commands, control requirements may typically be specified for three frequency regions. These are illustrated on a Nyquist plot for the SISO case in Figure 3-2. Magnitudes of scalar quantities in the SISO case are replaced by maximum and minimum singular values ($\bar{\sigma}$ and $\underline{\sigma}$) of matrix quantities in the MIMO case.

Low Frequency--At low frequencies, control requirements are dominated by performance constraints of the form

$$\underline{\sigma}(I + GK(j\omega)) \cong \underline{\sigma}(GK(j\omega)) > R(\omega) \qquad \omega_0 < \omega < \omega_1 \qquad (3\text{-}1)$$

where (ω_0, ω_1) defines the passband of the disturbance and/or command-input spectra and R relates these characteristics to control accuracy specifications.

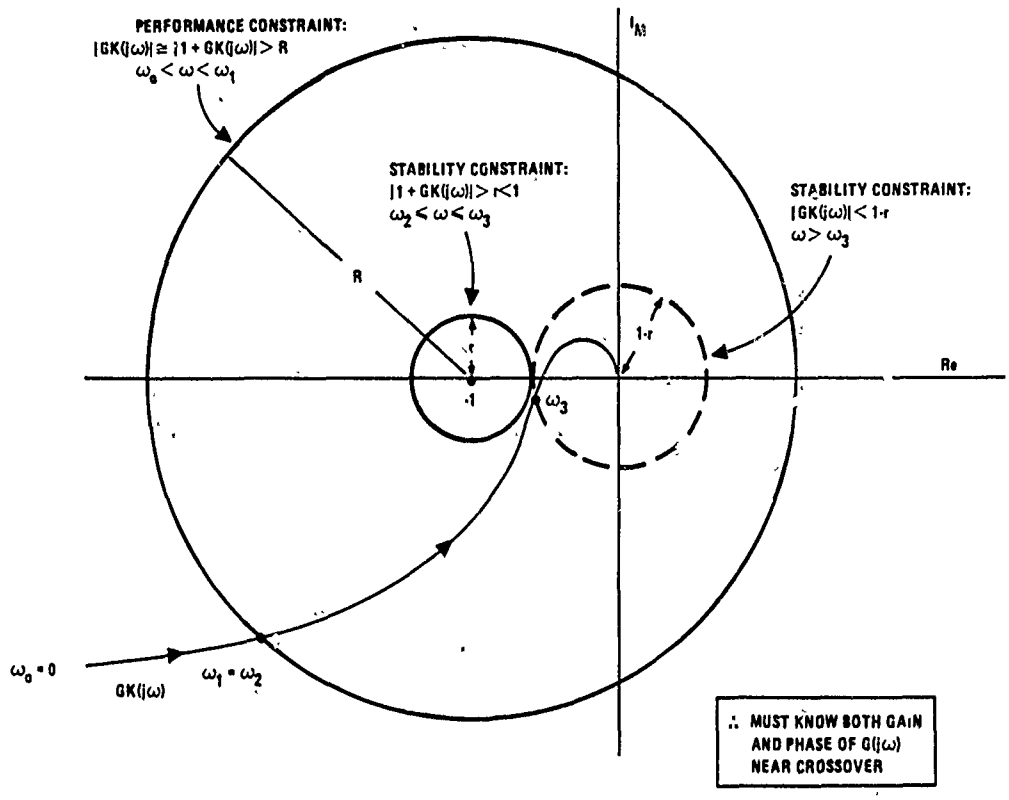

Figure 3-2. Control Design Requirements Drive Identification: Typical Control Problem

This is a MIMO generalization, familiar to classical control engineers, of the requirement for high loop-gain at low frequencies to achieve performance. In most applications ω_0 is taken to be zero; for the vibration control problem it is not since very low frequency disturbances are controlled by the outer vibration control loop.

Mid Frequency--At mid frequencies, control requirements are dictated largely by stability robustness constraints of the form

$$\underline{\sigma}(I + GK(j\omega)) > r, \qquad \omega_2 < \omega < \omega_3 \tag{3-2}$$

where $0 < r < 1$. This is a MIMO generalization of the classical control requirement to avoid the critical point. Equation (3-2) ensures "adequate" stability margins to gain and phase variation uncertainties in the plant $G(j\omega)$. In most applications $R(\omega) >> 1 \geq r$ for $\omega_0 < \omega < \omega_1$ so that (3-2) is automatically satisfied for low frequencies. Here we may take $\omega_2 \geq \omega_1$.

For the vibration control problem, however, $R(\omega)$ must be large only for frequencies near poles (or mode frequencies ω_i) and may well approach zero near zeros of the disturbance to LOS transmissions. Thus, low-frequency performance constraints and mid-frequency stability robustness constraints overlap. For all practical purposes we may assume that $\omega_2 = \omega_0$.

High Frequency--At high frequencies, control requirements are again dictated by stability robustness constraints of the form

$$\bar{\sigma}(GK(j\omega)) < 1 - r, \qquad \omega > \omega_3 \tag{3-3}$$

This is a MIMO generalization of the classical requirement for small loop-gain at high frequency. Equation (3-3) ensures gain stability in the face of phase variations, which invariably exceed ± 180 deg at high frequencies in any practical system.

Model Requirements

From the above discussion, and Figure 3-2 in particular, it is clear that detailed knowledge of plant characteristics is unnecessary for either the low ($\omega < \omega_2$) or high ($\omega > \omega_3$) frequency regions. Here simple magnitude, or norm, bounds on $G(j\omega)$ are usually sufficient to ensure that closed-loop performance and stability constraints are met.* It is only for the mid-frequency region ($\omega_2 \leq \omega \leq \omega_3$) that more detailed knowledge of both gain and phase for $G(j\omega)$ is necessary to ensure closed-loop stability. This critical mid-frequency band is illustrated, for example, on a Bode plot for a hypothetical SISO flexible loop-transfer-function magnitude, $|GK(j\omega)|$, shown in Figure 3-3, where seven flexible modes fall within this region. A suitable model for design of a controller for the corresponding open-loop transfer function $G(j\omega)$, illustrated in Figure 3-4, would require no more than seven flexible modes plus the rigid-body mode.

*There are two important exceptions to this rule--open-loop unstable systems and nonminimum phase systems--which are characterized by right half-plane poles and zeros, respectively. The first is not relevant for spacecraft applications but the second is.

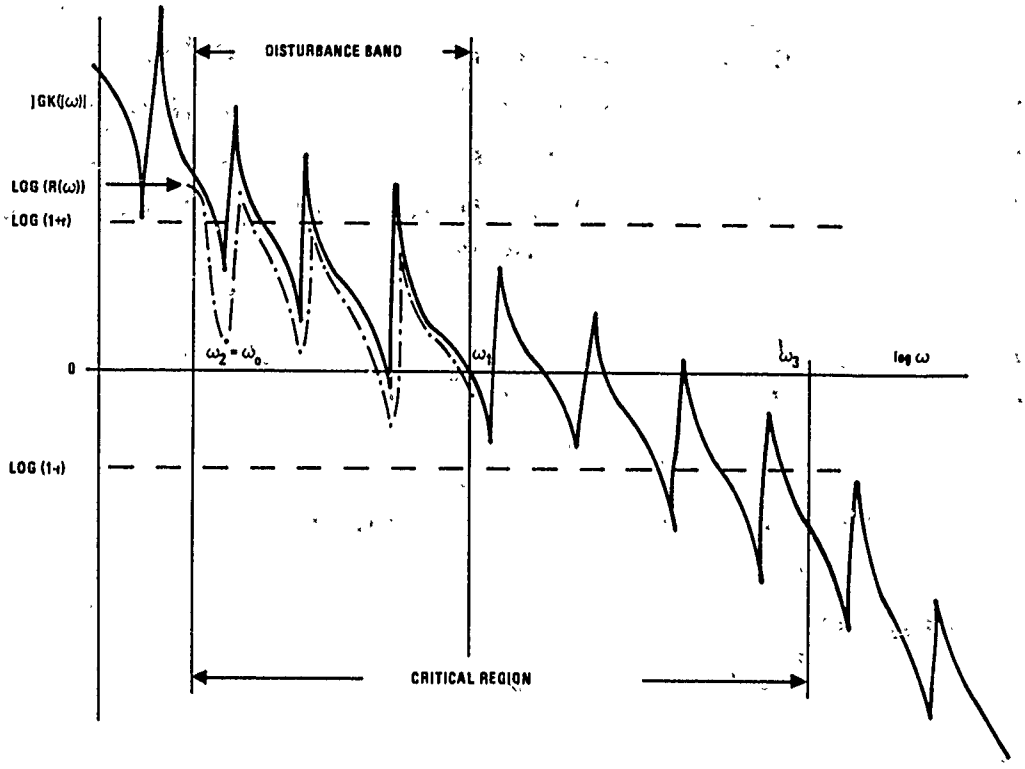

Figure 3-3. Control Requirements Drive Identification: Vibration Control Problem

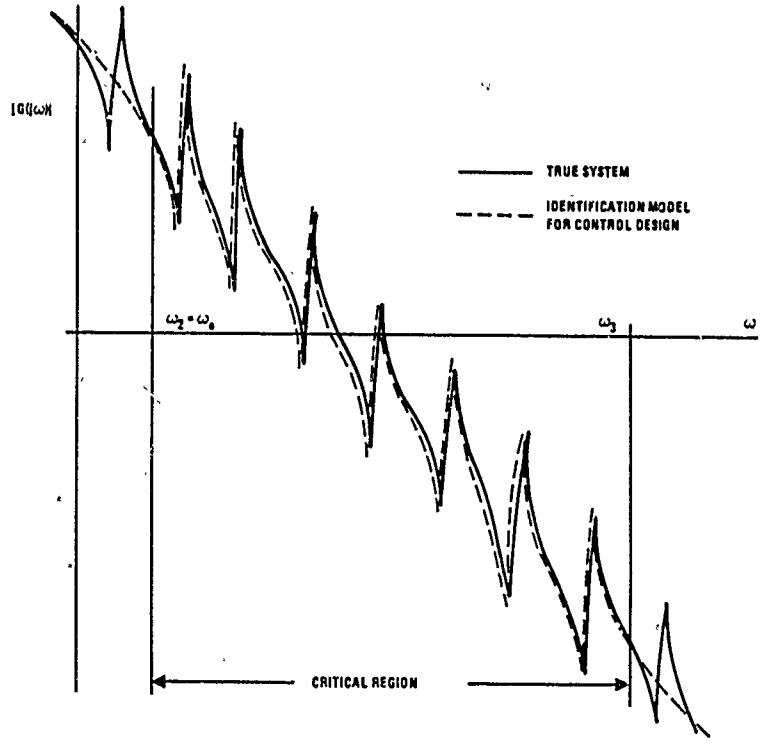

Figure 3-4. Model Requirements for Open-Loop System

Stability and Performance Robustness--These arguments, however, only establish upper bounds on model complexity. Lower bounds, unfortunately, are not as easily established in general. Ultimately, they depend on specific characteristics of both the structure and controller in question. To be more specific about model requirements, we consider the following problem in multivariable robustness.

> MIMO Robustness Problem: Let $G(s)$ be the true system to be controlled, let $G_o(s)$ be a model for the true system, and let $\Delta G(s) = G(s) - G_o(s)$ define the error between them. Given a controller $K_o(s)$, for which the model closed-loop system
>
> $$T_o \triangleq G_oK_o(I + G_oK_o)^{-1} \triangleq G_o(I + K_oG_o)^{-1}K_o \tag{3-4a}$$
>
> is stable and meets performance requirements, under what conditions does the true closed-loop system
>
> $$T = G K_o(I + GK_o)^{-1} \triangleq G(I + K_oG)^{-1}K_o \tag{3-4b}$$
>
> remain stable and meet performance requirements?

This problem has been examined by many investigators (Ref. 2,3,4). The most useful results are due to Doyle and Stein (Ref. 2), who derive sufficient conditions for robustness to model uncertainty starting from the Multivariable Nyquist Theorem. Assuming loops are broken at the output (y), the conditions for stability robustness may take either of two forms:

$$\ell_a(\omega) \triangleq \bar{\sigma}[\Delta G K_o(j\omega)] < \underline{\sigma}[I + G_oK_o(j\omega)], \ \omega \geq 0 \tag{3-5a}$$

or

$$\ell_m(\omega) \triangleq \bar{\sigma}\left[\Delta G K_o(j\omega)\,(G_oK_o(j\omega))^{-1}\right] \tag{3-5b}*$$

$$< \underline{\sigma}\left[I + (G_oK_o(j\omega))^{-1}\right] = 1/\bar{\sigma}\left[G_oK_o(I + G_oK_o)^{-1}\right], \ \omega > 0$$

---

*In most applications, the multiplicative perturbation in G_o is defined via $G(s) \triangleq (I + L(s))\,G_o(s)$ so that the lefthand side of (3-5b) becomes $\ell_m(\omega) \triangleq \sigma(L(j\omega))$.

That for performance robustness is given by

$$\underline{\sigma}[G_o K_o(j\omega)] > R(\omega)/(1 - \ell_m(\omega)), \quad \omega_o \leq \omega \leq \omega_1, \quad \ell_m(1) < 1 \tag{3-6}$$

These conditions provide practical means for testing robustness. The lefthand sides of stability conditions (3-5a) and (3-5b), respectively, define measures of so-called additive and multiplicative uncertainty for G_o, while the righthand sides define lower bounds for the return difference and inverse return difference. The latter is also the inverse magnitude of the model closed-loop transfer function (T_o). Good control loop design demands that the inverse return difference be approximately equal to 1 for low frequencies, much greater than 1 at high frequencies, and only slightly less than 1 for mid frequencies near control-loop gain crossover. Performance condition (3-6) differs from (3-1) in that the righthand side is divided by $1 - \ell_m(\omega)$ to account for model uncertainty. Note that performance constraints can only be met for frequencies in which $\ell_m(\omega) < 1$.

Stability conditions (3-5) are particularly well suited to so-called unstructured uncertainty, for which only an additive or multiplicative bound $\ell(\omega)$ is known. For structured uncertainties of the type we shall consider shortly, these conditions can be very conservative because they represent sufficient conditions only. That is, they fail to hold and thereby predict potential instabilities where none actually exist. Less conservative conditions for closed-loop stability in this case may be derived directly from a related, but stronger, stability condition (Ref. 3,4) originally used to prove (3-5a), that is,

$$\det [I + G_o(j\omega)\ K_o(j\omega) + \varepsilon \Delta G(j\omega)\ K_o(j\omega)] \neq 0 \tag{3-7}$$

for all $\omega \geq 0$ and $0 \leq \varepsilon \leq 1$. Condition (3-7) is sometimes also stated in either of two other equivalent forms--as a condition for nonsingularity of the matrix $[\cdot]$, or as a singular-value inequality, $\sigma[\cdot] > 0$.

For the space structure application, the true system can be represented by an infinite-dimensional transfer function of the form

$$G(s) \triangleq \sum_{i=1}^{\infty} G_i(s) \triangleq \sum_{i=1}^{\infty} g_i(s) c_i b_i^T \tag{3-8a}$$

where

$$g_i(s) \triangleq \frac{1}{s^2 + 2\zeta_i\omega_i s + \omega_i^2} \qquad i = 1,2,\ldots \tag{3-8b}$$

Here ω_i and ζ_i denote frequency and damping ratio for the i^{th} mode while b_i and c_i denote input and output influence coefficient vectors. Suppose now that a finite-dimensional n-mode model for the true system is given by

$$G_o(s) \triangleq \sum_{1}^{n} G_{oi}(s) = \sum_{i=1}^{n} g_{oi}(s)\, c_{oi} b_{oi}^T \tag{3-9a}$$

where

$$g_{oi}(s) = \frac{1}{s^2 + 2\zeta_{oi}\omega_{oi} s + \omega_{oi}^2} \qquad i = 1,2,\ldots,n \tag{3-9b}$$

Then the error between the true system and the model is given by

$$\Delta G(s) \triangleq G(s) - G_o(s) \tag{3-10a}$$

$$\triangleq \sum_{i=1}^{n} \Delta G_i(s) + \sum_{i=n+1}^{\infty} G_i(s)$$

The first term represents the error in the retained modes; the second represents the error due to neglected modes. To first order, the error due to the i^{th} retained mode is given by the linearized expression

$$\Delta G_i(s) \triangleq -g_{oi}^2\left(\Delta\omega_i^2 + s\Delta 2\zeta_i\omega_i\right) c_{oi} b_{oi}^T \tag{3-10b}$$

$$+ g_{oi}\left(c_{oi}\Delta b_i^T + \Delta c_i b_{oi}^T\right) \qquad i \leq n$$

where $\Delta(\cdot)$ denote errors between the true and model parameters. We now examine the impact of each of the two classes of errors identified above.

Model Errors Due to Neglected Modes--Assuming for the moment that errors due to retained modes in $G_o(s)$ are zero, that G_o and K_o are both square and nonsingular (i.e., $\Delta G_i = 0$, $i \leq n$), and that

$$\Delta G = \sum_{i=n+1}^{\infty} G_i \simeq G_i \triangleq g_i c_i b_i^T \tag{3-10a}$$

at the mode frequency ω_i for the i^{th} mode, conditions (3-5) for closed-loop stability in the face of errors due to neglected modes reduce to the following:

$$\ell_a(\omega) \triangleq \left|g_i(j\omega)\right| \left|c_i\right| \left|K_o^T(j\omega) b_i\right| < \underline{\sigma}[I + G_o K_o(j\omega)] \tag{3-11a}$$

$$\ell_m(\omega) \triangleq \left|g_i(j\omega)\right| \left|c_i\right| \left|\tilde{G}_o^T(j\omega) b_i\right| < \underline{\sigma}\left[I + (G_o K_o(j\omega))^{-1}\right] \tag{3-11b}$$

Conditions (3-11) provide a practical means for testing stability robustness to neglected modes. The former is best suited for mode frequencies above crossover, while the latter is best suited for mode frequencies below crossover because the righthand sides approach 1 in this case. Modes that satisfy either condition may safely be neglected in the model for G_o without compromising closed-loop stability. Modes that fail to satisfy either condition should be retained in the model. Analogous stability conditions for loops broken at the input (u) may be obtained from (3-11) by interchanging the roles of b_i and c_i and replacing G_o with G_o^T and K_o with K_o^T. Unfortunately, few modes will satisfy these conditions.

Somewhat stronger stability results can, however, be obtained directly from (3-7) as follows:

$$\det\left[I + G_o K_o + \varepsilon g_i c_i b_i^T K_o\right] \neq 0 \tag{3-12a}$$

$$\longleftrightarrow \det\left[I + \varepsilon g_i c_i b_i^T K_o (I + G_o K_o)^{-1}\right] \neq 0 \tag{3-12b}$$

$$\longleftrightarrow 1 + \varepsilon g_i^T b_i K_o (I + G_o K_o)^{-1} c_i \neq 0 \tag{3-12c}$$

$$\longleftrightarrow g_i b_i^T K_o (I + G_o K_o)^{-1} c_i \neq -\varepsilon^{-1} \tag{3-12d}$$

$$\longleftrightarrow g_i b_i^T G_o^{-1}\left(I + (G_o K_o)^{-1}\right)^{-1} c_i \neq -\varepsilon^{-1} \tag{3-12e}$$

for $\omega \geq 0$ and $0 \leq \varepsilon \leq 1$. These five conditions are all equivalent. Condition (3-12b) follows from the fact that $I + G_o K_o$ is nonsingular, while (3-12c) follows from the standard determinant identity,

$$\det[I + cb^T] = 1 + b^T c \tag{3-13}$$

The fourth condition is obvious. Condition (3-12e) assumes that G_o and K_o are both square and nonsingular. When these conditions fail to hold G_o^{-1} can be replaced by its pseudo-inverse, $G_o^{\#} = (G_o^T G_o)^{-1} G_o^T$, provided G_o and K_o are of full rank. It is easily shown using the identity

$$|y^T A x| \leq |y||Ax| \leq |x||y|\bar{\sigma}(A) \tag{3-14}$$

and minor manipulation that condition (3-12d) is implied by (3-11a), while (3-12e) is implied by (3-11b). Thus, conditions (3-12d) and (3-12e) are stronger (or less conservative) conditions for stability. Unfortunately, it is impossible to apply them unless the controller is explicitly defined. Thus conditions (3-11) are to be preferred for frequencies near control-loop gain crossover.

For frequencies well after and well before crossover we have, respectively,

$$I + G_o K_o \simeq I, \qquad \omega >> \omega_c \tag{3-15a}$$

$$I + (G_o K_o)^{-1} \simeq I, \qquad \omega << \omega_c \tag{3-15b}$$

so that (3-12d) and (3-12e) reduce to

$$g_i(j\omega) b_i^T K_o(j\omega) c_i \neq -\varepsilon^{-1}, \qquad 0 < \varepsilon \leq 1, \ \omega >> \omega_c \tag{3-16a}$$

$$g_i(j\omega) b_i^T G_o^{-1}(j\omega) c_i \neq -\varepsilon^{-1}, \qquad 0 < \varepsilon \leq 1, \ \omega << \omega_c \tag{3-16b}$$

These last conditions are the strongest (or least conservative) ones available for defining ROMs for identification and control in the frequency ranges indicated. Unfortunately both condition (3-16a) and its singular value version (3-11a) depend explicitly on the controller $K_o(j\omega)$. Since the controller is not normally explicitly defined at the model definition phase, it is necessary to replace the matrix K_o by its magnitude, $\bar{\sigma}(K_o)$, which presumably is known, to define a more practical condition for high frequencies. In this case, these stability conditions for high frequency reduce to

$$\bar{\sigma}(G_i(j\omega)) = |g_i(j\omega)||c_i||b_i| < 1/\bar{\sigma}(K_o(j\omega)),\ \omega >> \omega_c \qquad (3\text{-}17a)$$

This more conservative stability condition also allows for the possibility that only the magnitude $\bar{\sigma}(G_i)$, but not the "direction," $c_i b_i^T/|c_i||b_i|$, of the i^{th} mode is known, which becomes more and more likely for high-frequency modes. Should this same "direction" information also be unavailable for modes below crossover, then conditions (3-16b) and (3-11b) must be reduced to

$$\bar{\sigma}(G_i(j\omega)) \triangleq |g_i(j\omega)||c_i||b_i| < \underline{\sigma}(G_o(j\omega)),\ \omega << \omega_c \qquad (3\text{-}17b)$$

Conditions (3-17) are the weakest (or most conservative) ones for defining ROMs. For most applications, conditions (3-16b) and (3-17a) should be most appropriate.

Model Errors Due to Retained Modes--Assuming now that errors due to neglected modes are indeed negligible, we next examine conditions for closed-loop stability in the face of errors in the retained modes. For retained modes we can safely assume that the i^{th} mode dominates for frequencies near its mode frequency ω_i,

$$G_o \simeq g_{oi} c_{oi} b_{oi}^T \qquad (3\text{-}18a)$$

$$\Delta G \simeq \Delta G_i = -g_{oi}^2 \left(\Delta\omega_i^2 + j\omega\Delta 2\zeta_i\omega_i\right) c_{oi} b_{oi}^T + g_{oi}\left(c_{oi}\Delta b_i^T + \Delta c_i b_{oi}^T\right) \qquad (3\text{-}18b)$$

Because G_o is singular and ΔG is highly structured, the stability robustness conditions (3-5) are not appropriate here. We turn instead to the more fundamental condition (3-7). Substituting (3-18) into (3-7) and using the determinant identity

$$\det[I + cb^T + c\Delta b^T + \Delta c b^T] = 1 + b^T c + \Delta b^T c + b^T \Delta c \qquad (3\text{-}19)$$

$$+ c^T \Delta b \Delta c^T b - b^T c \Delta b^T$$

Δc

we get (retaining only terms to first order in parameter errors)

$$1 + g_{oi} b_{oi}^T K_o c_{oi} - \varepsilon\, g_{oi}^2 (\Delta\omega_i^2 + j\omega\,\Delta 2\zeta_i\omega_i) b_{oi}^T K_o c_{oi} \qquad (3\text{-}20)$$

$$+ \varepsilon\, g_{oi}\left(\Delta b_i^T K_o c_{oi} + b_{oi}^T K_o \Delta c_i\right) \neq 0$$

Now dividing (3-20) by $g_{oi} b_{oi}^T K_o c_{oi}$, taking the magnitude of each term, and recognizing that

$$|g_{oi}^2(j\omega)| \leq |g_{oi}(j\omega)|/2\zeta_{oi}\omega_{oi}^2,$$

we find that (3-20) is implied by

$$TF_{re} \triangleq \frac{1}{2\zeta_{oi}} \frac{|\Delta\omega_i^2|}{\omega_{oi}^2} + \frac{|\Delta 2\zeta_i\omega_i|}{2\zeta_{oi}\omega_{oi}} + \frac{1}{|\cos\theta_{1i}(\omega)|} \frac{|\Delta b_i|}{|b_{oi}|} \tag{3-21}$$

$$+ \frac{1}{|\cos\theta_{2i}(\omega)|} \frac{|\Delta c_i|}{|c_{oi}|} < 1 + \frac{1}{g_{oi}(j\omega) b_{oi}^T K_o(j\omega) c_{oi}} > r'$$

where

$$\cos\theta_{1i}(\omega) \triangleq b_{oi}^T K_o(j\omega) c_{oi} \Big/ |K_o(j\omega) c_{oi}| |b_{oi}| \tag{3-22a}$$

$$\cos\theta_{2i}(\omega) \triangleq b_{oi}^T K_o(j\omega) c_{oi} \Big/ |K_o^T(j\omega) b_{oi}| |c_{oi}| \tag{3-22b}$$

define complex direction cosines between the appropriate vectors. Note that, except for these direction cosines, all terms on the lefthand side in (3-21) are independent of frequency.

It can be shown that the term on the right above is closely related to one over the maximum singular value of the model closed-loop transfer function (T_o). As noted earlier, this term near crossover must be greater than some constant $0 < r' \leq 1$ in order that the scalar loop-transfer-function avoids the critical $-1 + j0$ point in the Nyquist plane. For good stability robustness, it is desirable that r' be as close to 1 as possible and that $K_o(j\omega) c_{oi}$ and b_{oi}, or $K_o^T(j\omega) b_{oi}$ and c_{oi}, be nearly parallel for ω near ω_{oi}, so that

$$|\cos\theta_{1i}(\omega_{oi})| \simeq |\cos\theta_{2i}(\omega_{oi})| \simeq 1$$

The "ideal" control structure given earlier in (2-10) meets these objectives precisely. In this case (3-21) can be approximated by

$$TF_{re} \simeq \frac{1}{2\zeta_{oi}} \frac{|\Delta\omega_i^2|}{\omega_{oi}^2} + \frac{|\Delta 2\zeta_i\omega_i|}{2\zeta_{oi}\omega_{oi}} + \frac{|\Delta b_i|}{|b_{oi}|} + \frac{|\Delta c_i|}{|c_{oi}|} < 1 \tag{3-21}$$

Thus rough model accuracy requirements for control design can be stated in terms of relative errors as (assuming $\zeta_{oi} << 1$)

$$\frac{1}{2}\frac{|\Delta\omega_i^2|}{\omega_{oi}^2} \simeq \frac{|\Delta\omega_i|}{\omega_{oi}} << \zeta_{oi} \qquad (3\text{-}23a)$$

$$\frac{|\Delta 2\zeta_i\omega_i|}{2\zeta_{oi}\omega_{oi}} \simeq \frac{|\Delta\zeta_i|}{\zeta_{oi}} << 1 \qquad (3\text{-}23b)$$

$$\frac{|\Delta b_i|}{|b_{oi}|} << 1 \qquad (3\text{-}23c)$$

$$\frac{|\Delta c_i|}{|c_{oi}|} << 1 \qquad (3\text{-}23d)$$

Note that model accuracy requirements are most stringent for modal frequency (i.e., relative errors must be of order damping (ζ_{oi})). This is not surprising in view of the fact that small errors in mode frequency, which move the resonance peak in the transfer function, produce large errors in ΔG near resonance. All other requirements call for relative parameter errors of order 1. When, as will generally be the case, these model accuracy requirements cannot be met for retained modes by ground-based testing, then on-orbit identification will be required. These general requirements may, however, be relaxed in certain special cases, such as ILAS, which exhibit inherent robustness to parameter uncertainty.

IDENTIFICATION PROBLEM

Having established that identification requirements are driven by control requirements, we now examine the identification problem. We begin by establishing general ground rules for identification. Next we present specific identification requirements in terms of the number of modes, the number of parameters per mode, identification accuracy, etc. for both the baseline and advanced concepts. We then address the use of test signals to provide persistent excitation of modes during identification. Two test signal models are developed: (1) band-limited "white" noise, which produces a flat power spectrum over the identification frequency passband, and (2) the time derivative of this signal, which produces a

spectrum that grows as ω^2. Finally, we define measurement noise models for the various types of measurements--positions, rates, and accelerations (both angular and linear). These results are tabulated and recommendations are made for the two identification and control concepts.

Identification Ground Rules

A number of ground rules were established to define a meaningful identification problem. First, it was assumed that internal disturbances generated on-board the spacecraft could be largely eliminated during identification. In particular, cryo-cooler and other vibrational disturbances were assumed absent during identification. This assumes, of course, that the spacecraft's payload is not operational during the identification interval. Second, it was assumed that the same sensors and actuators used for vibration control would be available to excite the structure via test signals and to measure its response to those inputs. Though additional sensors and actuators might possibly improve the identification of modal frequency and damping, these instruments would obviously not improve identification of input/output influence coefficients for the primary vibration control loop. Thus there appeared to be no fundamental reason for including additional control hardware for identification. Finally, it was assumed that identification itself could be accomplished off-line. The only real-time capability assumed necessary for identification was that necessary to excite the structure and sample its measurements at sufficiently high rates (100 Hz or so). Presumably real-time capability for control would dominate these requirements for identification. Sampled data could either be processed on-board, or relayed to the ground periodically through telemetry links for ground processing.

Specific Identification Problem

Using the general criteria for control design model requirements developed earlier, we now define the specific identification problems addressed in this study for the two concepts selected in Section 2.

Baseline Concept (ILAS)--Recall that this concept assumes the identical location of actuators and sensors and is therefore characterized by a transfer function in which output and input modal influence coefficients are identical for each mode

(i.e., $c_i = b_i$). This produces the familiar alternating pole-zero pattern that was illustrated in the Bode plots of Figure 2-8. Because phase is confined to -180 deg to 0 deg for this case, robust control solutions (Ref. 15) employing simple lead networks with carefully controlled rolloff in each channel suffice to stabilize such systems. Control structure (2-10b) meets this requirement.

Thus when robust control solutions are employed, detailed knowledge of frequency (ω_i) and influence coefficients (b_i) for each mode is unnecessary for control design. Given that desired modes are strongly controllable and observable and given sufficient gain to meet performance requirements, only a bound for the open-loop frequency response envelope, which implies a lower bound on damping ratio (ζ_i) for each mode near the desired control-loop crossover, is necessary to ensure stability of the corresponding closed-loop system. When this information can be determined from ground tests, no on-orbit identification is necessary. Only when such bounds are unavailable is on-orbit identification necessary for the ILAS case. Even here, identification requirements are critical only for damping, where relative errors in identified damping subtract directly from available gain margins (e.g., a worst-case relative error of 1 implies a possible 6 dB loss in gain margin). As a practical matter, however, it is difficult to identify damping without also identifying frequency and influence coefficients.

When less robust control solutions are employed, identification requirements become more demanding and ultimately must approach the more general requirements called for in (3-23) as the controller exploits more and more information about the model. Because of the difficulty in identifying damping alone, we opted to impose the same stringent identification requirements on ILAS as well as non-ILAS concepts.

The final selection of modes for identification was based on a graphical procedure analogous to that suggested earlier in Figure 3-3. In Figure 3-5, we have replotted the singular values of the transfer function $G(j\omega)$, shown earlier in Figure 2-9, with damping on the isolator modes now increased to $\zeta = 0.7$. Superimposed on this plot is a representative inverse control gain characteristic ($1/k$), which is designed to achieve a final gain crossover near the maximum

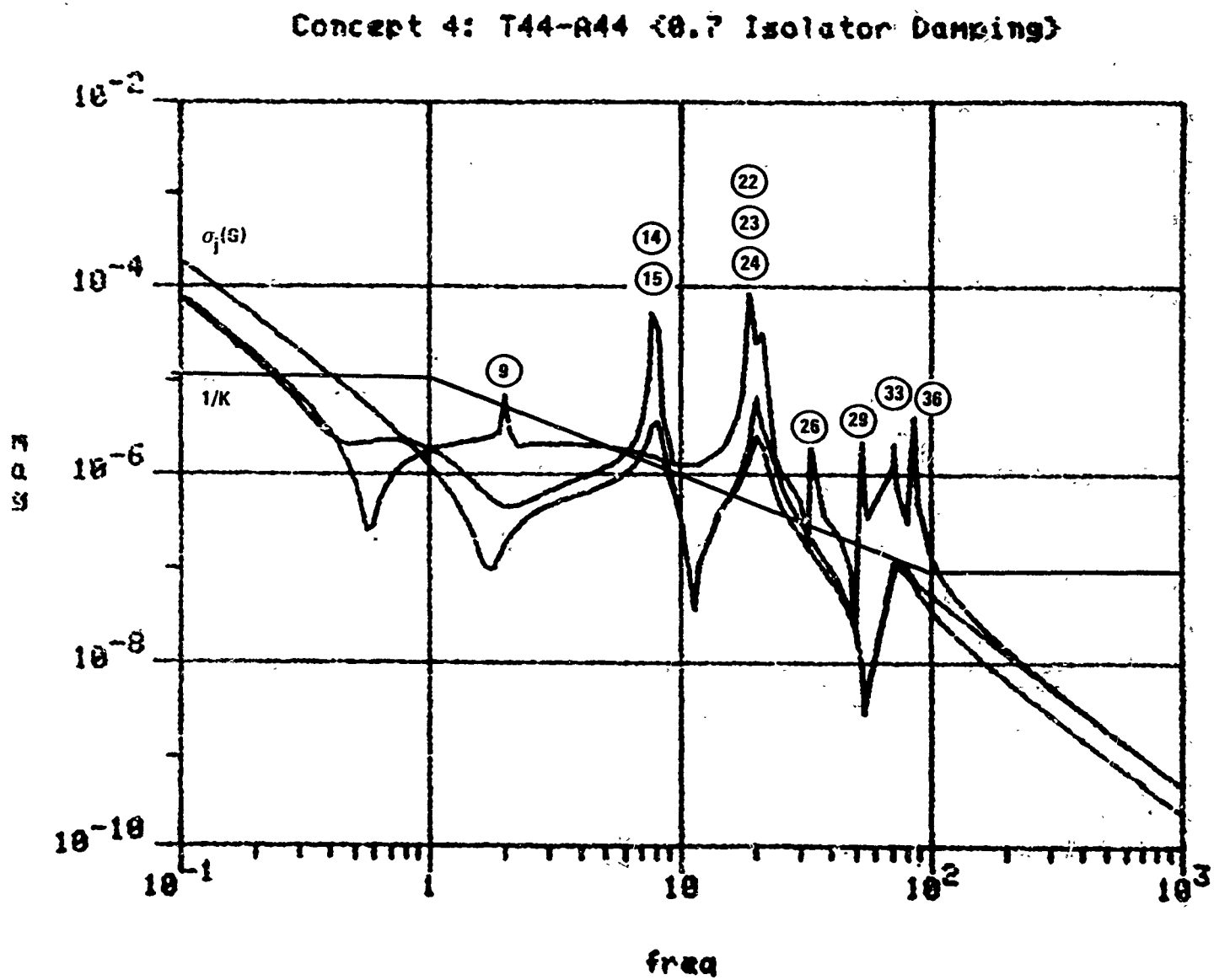

Figure 3-5. Identification Problem for Baseline Concept

allowable frequency of ω_c = 100 r/s. This controller develops lead over a two-decade-wide frequency band (1 to 100 r/s), and should provide roughly 45 deg of phase margin at the extremes of this band and nearly 90 deg at the center (10 r/s). Since all 10 of the lightly damped flexible modes apparent in this figure intersect 1/k, in view of condition (3-17a) all should be included in the control design (and identification) model.

Since the transfer function $G(j\omega)$ for this concept is essentially diagonal, model identification may be carried out for a single axis at a time. With reference to Figure 2-8, the number of modes (n) to be identified for each axis assumes the ranges indicated in Table 3-1, depending on whether isolator modes are included. Since there are three parameters per mode for each axis (ω_i, ζ_i, b_i), the total number of parameters is 3n. Thus, at most a total of 21 parameters (corresponding to seven modes) would have to be identified simultaneously. If modes for all three axes were identified simultaneously, still assuming a diagonal structure, a total of some 30 to 48 parameters would be required. For an assumed nondiagonal structure, this would increase to some 50 to 80 parameters since b_i is a 3 x 1 vector for this case.

TABLE 3-1. COMPLEXITY OF IDENTIFICATION PROBLEM

Concept/Axis	Number of Modes (N)	Number of Parameters Per Mode	Total Number of Parameters (N_p)
Baseline: ILAS			
--Roll (x)	4-7	3	12-21
--Pitch (y)	3-4	3	9-12
--Yaw (z)	3-5	3	9-15
	10-16	3	30-48 (diagonal)
		5	50-80 (nondiagonal)
Advanced: Non-ILAS			
--All axes (x,y,z)	15-21	7	105-147

Note: $N_p = \begin{cases} N[n_i + 2] & \text{ILAS} \\ N[n_i + n_o + 2 - 1] & \text{Non-ILAS} \end{cases}$ where $n_i \triangleq$ number of inputs; $n_i \triangleq$ number of outputs

Advanced Concept (Non-ILAS)--Since this concept assumes distributed actuators and sensors, it is characterized by a transfer function in which output and input modal influence coefficients are different for each mode (i.e., $c_i \neq b_i$). This produces the more general irregular pole-zero pattern that was illustrated in the Bode plots of Figure 2-10. Because phase is no longer confined to -180 deg to 0 deg, robust control solutions no longer apply. Here detailed knowledge of frequency (ω_i), damping (ζ_i), and output and input influence coefficients (c_i and b_i) for each mode near crossover is necessary for control design.

Regardless of the control structure assumed, non-ILAS concepts are inherently more sensitive to parameter variation than ILAS concepts. The stringent model accuracy requirements called for in (3-23) are most relevant for this case. Because these requirements call for relative errors in modal frequency for critical modes of less than ζ(= 0.5%), it is unlikely that they can be met by any means short of on-orbit identification. The final selection of modes for identification for this concept is illustrated in Figure 3-6. Here again, we have replotted the singular values of $G(j\omega)$ for heavily damped isolator modes and have postulated an inverse control gain characteristic designed to achieve a final gain crossover near ω_c = 100 r/s. For the non-ILAS case, design of a stabilizing controller is a nontrivial problem. In theory, there is no guarantee that a stabilizing controller with the asymptotic characteristic shown even exists. However, because the general plant rolloff characteristic is roughly $1/s^2$, the controller characteristic shown appears reasonable. Here again, all of the lightly damped flexible modes apparent in this figure (except modes 26, 28, and 35) intersect $1/k$, and according to (3-17a) should be included in the control design (and identification) model.

It should be noted that transfer functions for the general non-ILAS case are nonminimum phase (i.e., they contain right half-plane transmission zeros). When these zeros occur at frequencies beyond the control passband, they cause no difficulties. Recent analyses (Section 6) for the advanced concept, however, show that several right half-plane zeros occur within the desired control passband. The presence of these near-in unstable zeros imposes fundamental limitations on control system performance and places greater demands on model fidelity. Thus, the heavily damped isolator modes and a few more lightly damped modes were included in the control design model and should have been included for identification.

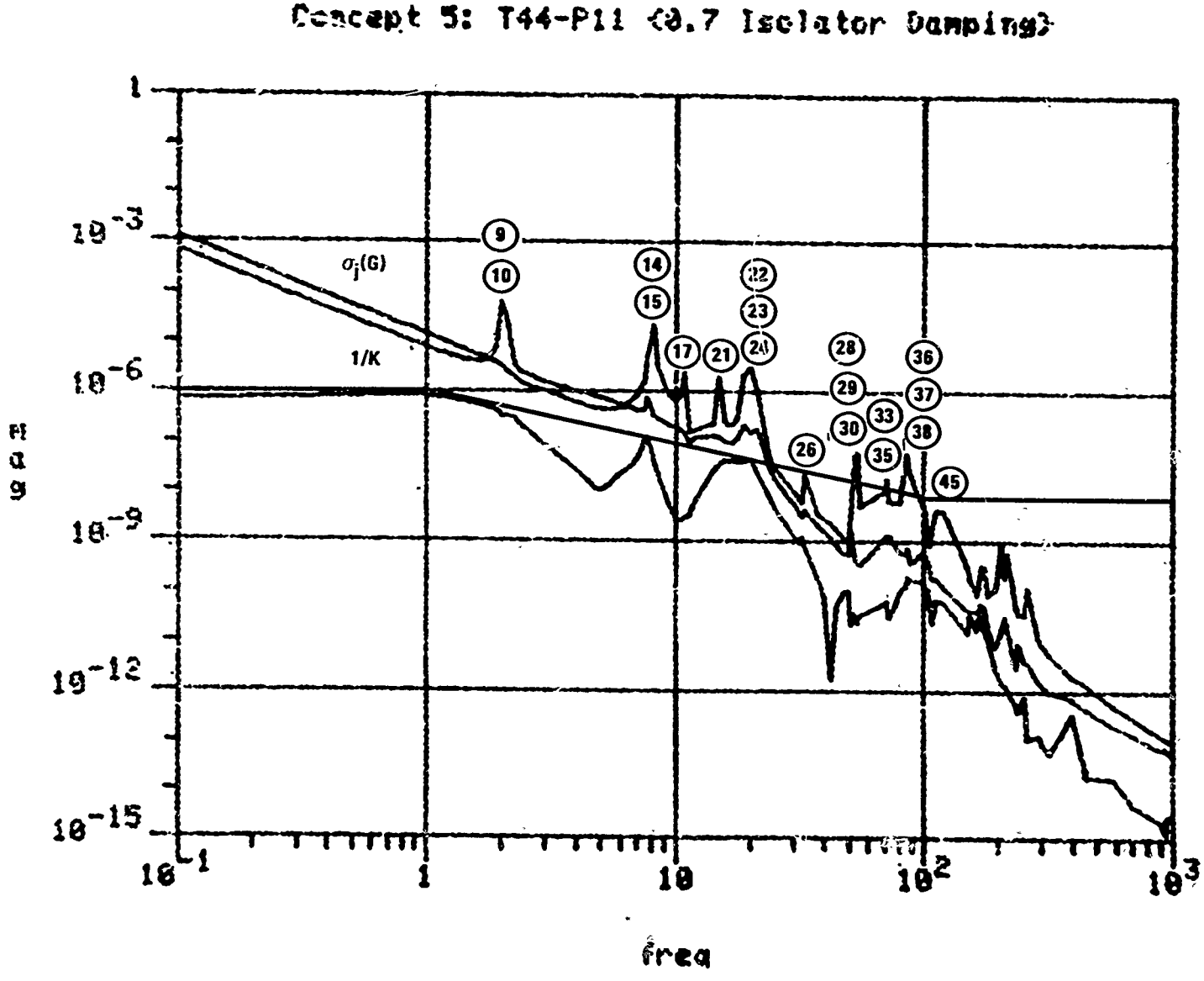

Figure 3-6. Identification Problem for Advanced Concept

As shown in Table 3-1, some 14 to 21 flexible modes may require identification (not counting the isolator modes). Since there is no diagonal structure to take advantage of here, all three axes must be identified simultaneously. Since one element of either the b_i's or the c_i's is redundant and may thus be eliminated, there remain seven parameters per mode to be identified. This is true because either the b_i or c_i vector for each mode may be normalized to have unit magnitude, so that the resulting scale factor may be absorbed by the other vector. This leaves a grand total of some 105 to 147 parameters for possible simultaneous identification. This would appear to be a formidable problem, even for super computers. Thus, suboptimal schemes and various other simplifications are essential in our approach to identification.

Test Signal Selection

To aid in identification it is advantageous to use test signals to excite mode frequencies of interest. For ground-based vibration testing it is common practice to employ impulsive test signals using a calibrated hammer-like device. Since the power spectral density (PSD) of an "ideal" impulse is flat, such test signals do excite modes over a wide frequency range. But conventional control actuators designed to accommodate sinusoidal disturbances are not ideally suited to generating impulses for on-orbit testing.

Although reaction control jets would seem to be an exception to this claim, the actual impulse they deliver is not highly predictable. Moreover, the long identification intervals that are required for structural model identification favor the use of persistent test signals which continue to excite the structure long after transients due to impulsive inputs have died out. Thus we are forced to consider other alternatives.

Our analyses in Section 2 showed that control actuators mounted on the equipment section must be sized to accommodate sinusoidal internal disturbance forces of 400 N or torques of 2000 N-m. Assuming paired shakers are used to generate this control force, this implies that a mass-stroke product of

$$mx = \frac{|F_d|}{\Omega^2} \qquad (3\text{-}24)$$

$$= \frac{400}{31.4^2}$$

$$\simeq 0.4 \text{ kg-m}$$

is necessary to buck sinusoidal disturbances at the frequency assumed by Draper (Ref. 1). For a disturbance frequency of Ω = 10 r/s, which is at the low end of the desired frequency range for vibration control, this requirement would increase to 4 kg-m. Assuming internal disturbances are absent during identification, this control capability is available to generate test signals to aid in structural identification. We would now like to bound the magnitude of this test signal and show that external disturbances are dominated by inaccuracies in our knowledge of the actual test signal delivered by the actuators.

Test Signal 1--A natural choice for a test signal is a white-noise sequence since its PSD, like that for the impulse, is also flat. Unfortunately a white-noise test signal cannot be generated in practice since the actuator's mass-stroke product has an infinite root-mean-squared (rms) value. As we will see shortly, to bound this rms a low-frequency attenuation of at least fourth order at the PSD level is required. This can be implemented by passing white noise through a second-order high-pass filter at $\omega = \omega_L$. A second-order low-pass filter at $\omega = \omega_H$ can also be used to provide high-frequency attenuation, although no high-frequency attenuation is necessary to bound the mass-stroke product rms. In practice, the actuator's natural rolloff characteristics would likely provide sufficient high-frequency attenuation. A wide-bandwidth test signal with a power spectral density characteristic like that shown in Figure 3-7a, for example, closely approximates the flat PSD for frequencies in the range $\omega_L << \omega << \omega_H$ and should be well-suited for identifying modal frequencies in this range. Once we have established the appropriate intensity levels, the actual test signal may be approximated by an "equivalent" flat PSD of the same intensity.

In order to meet mass-stroke limitations, we must relate control forces to mass-stroke product. Since the latter is just the double integral of applied force, the mass-stroke product PSD of Figure 3-7b is obtained by multiplying the force PSD by $1/\omega^4$. This follows from the well-known formula

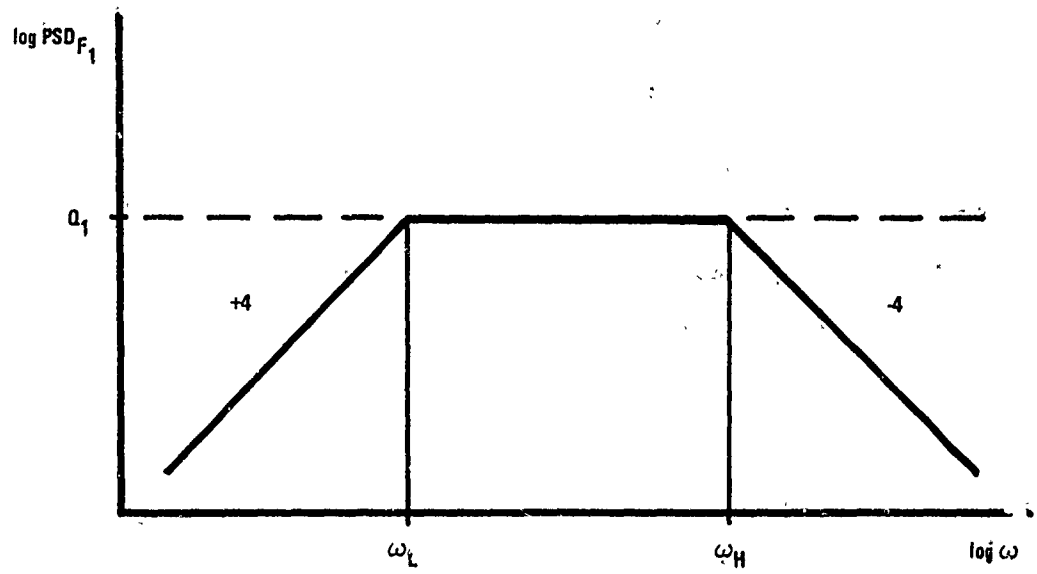

a. Force

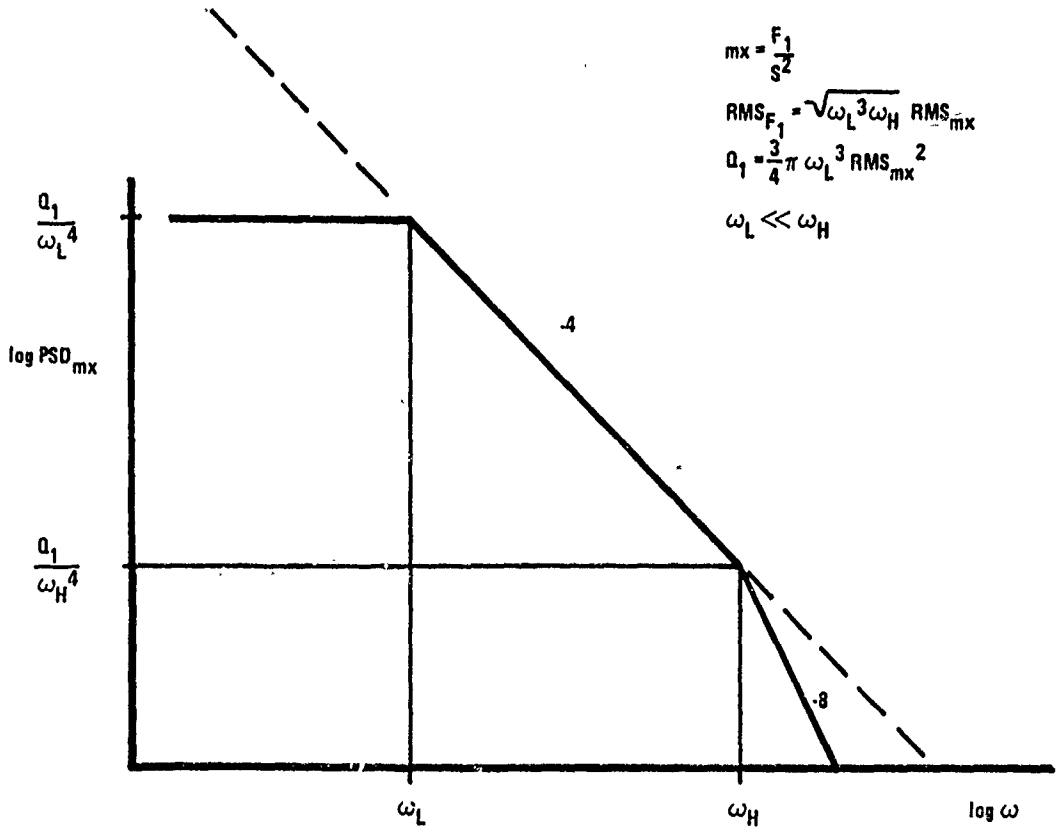

b. Mass-stroke

Figure 3-7. Test Signal 1 Power Spectral Densities (at force input)

$$PSD_y(\omega) = |H(j\omega)|^2 \, PSD_u(\omega) \tag{3-25}$$

where y and u are related through

$$y(s) \triangleq mx(s) = \frac{1}{s^2} F(s) = H(s)\, u(s) \tag{3-26}$$

The mean-squared value for each signal in Figure 3-7 is obtained by integrating the corresponding PSD over all frequencies. Performing these integrations for the asymptotic approximations of Figure 3-7 and exploiting the fact that $\omega_L << \omega_H$ gives

$$RMS_{F_1}^2 = \frac{1}{\pi}\int_0^\infty PSD_F(\omega)\, d\omega \tag{3-27a}$$

$$\simeq \frac{Q_i}{\pi}\left\{\int_0^{\omega_H} d\omega + \int_{\omega_H}^\infty \left(\frac{\omega_H}{\omega}\right)^4 d\omega\right\} = \frac{4}{3}\frac{Q}{\pi}\frac{1}{\omega_H}$$

$$RMS_{mx}^2 = \frac{1}{\pi}\int_0^\infty PSD_{mx}(\omega)\, d\omega \tag{3-27b}$$

$$\simeq \frac{Q_1}{\pi\omega_L^4}\left\{\int_0^{\omega_L} d\omega + \int_{\omega_L}^\infty \left(\frac{\omega_L}{\omega}\right)^4 d\omega\right\} = \frac{4}{3}\frac{Q_1}{\pi}\frac{1}{\omega_L^3}$$

Eliminating the force spectral intensity Q_1 from (3-27), assuming that ω_L = 0.1 r/s and ω_H = 1000 r/s bracket the frequency range of interest, and substituting for RMS_{mx} from (3-24) implies test signal force constraints of

$$RMS_{F_1} = \sqrt{\omega_L^3 \omega_H}\; RMS_{mx} \tag{3-28a}$$

$$\leq \sqrt{(0.1)^3\,(1000)}\;\;(0.4)$$

$$= 0.4 \text{ N}$$

and

$$Q_1 = \frac{3}{4}\pi\omega_L^3 \, RMS_{mx}^2 \simeq 4 \times 10^{-4} \ N^2/Hz \tag{3-28b}$$

For paired thrusters located near the edges of the equipment section, the corresponding moment arm of d ≃ 5m implies test signal torque constraints of

$$\begin{aligned} RMS_{T_1} &\simeq 2d \, RMS_{F_1} \\ &\leq 2(5)(0.4) \\ &= 4.0 \ N\text{-m} \end{aligned} \tag{3-29a}$$

and

$$U_1 = (2d)^2 Q_1 \simeq 4 \times 10^{-2} \ (N\text{-m})^2/Hz \tag{3-29b}$$

It is reasonable to assume that control actuator characteristics will be known (via ground testing) to within 10% of their true values over the above frequency passband. Constant (bias) errors are not critical here since the vibration controller and the test signal used for identification are both high-passed. Thus, disturbance torques arising from actuators used to generate the test signal should be no larger than 10% of the test signal level, that is,

$$\begin{aligned} RMS_{T_{d_1}} &\leq 0.1 \, RMS_{T_1} \\ &\simeq 0.4 \ N\text{-m} \end{aligned} \tag{3-30a}$$

and

$$W_1 = (0.1)^2 U_1 = 4 \times 10^{-4} \ (N\text{-m})^2/Hz \tag{3-30b}$$

This disturbance due to inaccuracies between the torque commanded and that actually delivered by the actuators clearly dominates external disturbances of $T_d \simeq 0.02$ N-m. Thus we can safely neglect external disturbances during identification.

One drawback associated with generating a wide-bandwidth flat PSD test signal with the control actuators is that it severely limits test signal amplitude. This is evident when we compare the large assumed 400 N force capability of the actuators

at a single frequency (ω = 31.4 r/s) with 0.4 N rms level associated with the PSD of Figure 3-7a. The impact of test signal limitations on the two identification concepts is illustrated in the singular-value plots of $G(j\omega)$ in Figures 3-8 and 3-9. Superimposed on $\sigma_i(G)$ in each case we show the square root of the ratio of measurement noise power (R_1) to test signal power (U_1), assuming angular and linear position measurements, respectively (indicated by the dashed line). Measurement noise power was assumed to be flat, with intensities to be defined shortly. We have tacitly assumed that test signal and measurement noise statistics are independent and identically distributed for each axis (i.e., $W = W_1 I$, $R = R_1 I$). The extent to which the magnitude of $G(\omega)$ exceeds $\sqrt{R_1/U_1}$ defines the square root of the signal-power-to-noise-power ratio (SNR) for signals reflected to the output. For the baseline concept this quantity ranges from roughly 1 to 2.5 orders of magnitude for all mode peaks, so that identification of these modes appears feasible. For the advanced concept, this quantity is less than 1 for roughly half the modes. Thus, identification for this case would appear to be next to hopeless. Therefore, we are obliged to examine other possible test signals.

Test Signal 2--An alternative to the "flat" PSD of Figure 3-7a is illustrated in Figure 3-10a, which corresponds to the first derivative of white noise over the frequency band (ω_L, ω_H). It too may be implemented by passing white noise through two second-order filters--a high-pass at ω_L cascaded with a lead (s x low-pass) at ω_H. As before, noise intensity Q_2 is constrained by RMS_{mx} = 0.4 kg-m. Using an approach analogous to that developed for Test Signal 1, we find that noise rms and intensity are given by

$$RMS_{F_2} = (\omega_H/\omega_L)\ RMS_{F_1} \tag{3-31a}$$

$$Q_2\omega^2 = (\omega/\omega_L)^2\ Q_1 \qquad \omega_L \leq \omega_H \leq \omega \tag{3-31b}$$

Note that noise intensity for Test Signal 2 is equal to that for Test Signal 1 at $\omega = \omega_L$ and increases to a factor of $(\omega_H/\omega_L)^2 = 10^8$ larger at $\omega = \omega_H$. At the rms level this amounts to an increase of $(\omega_H/\omega_L) = 10^4$.

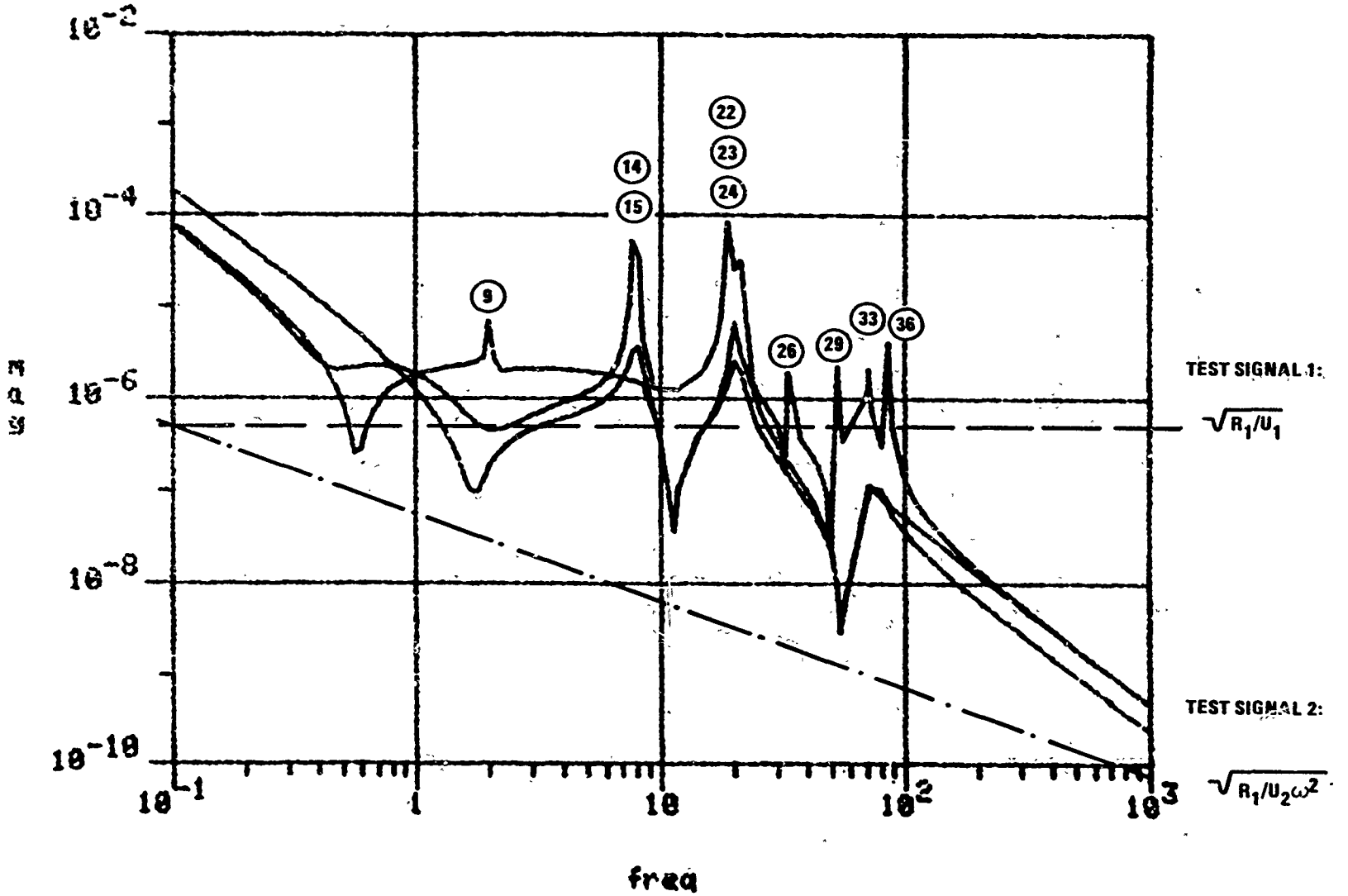

Figure 3-8. Test Signal Limitations for Baseline Concept: Position Measurements

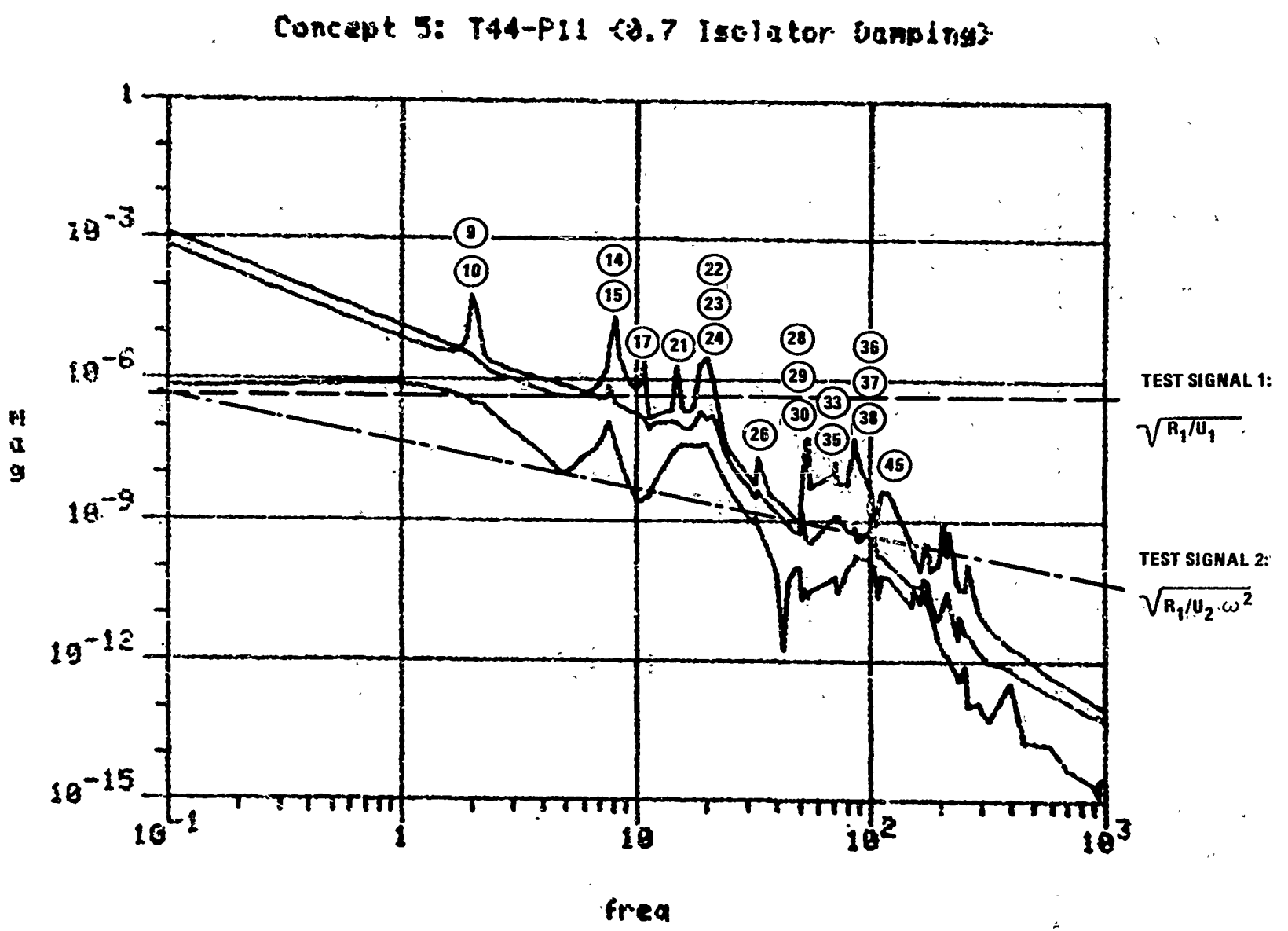

Figure 3-9. Test Signal Limitations for Advanced Concept: Position Measurements

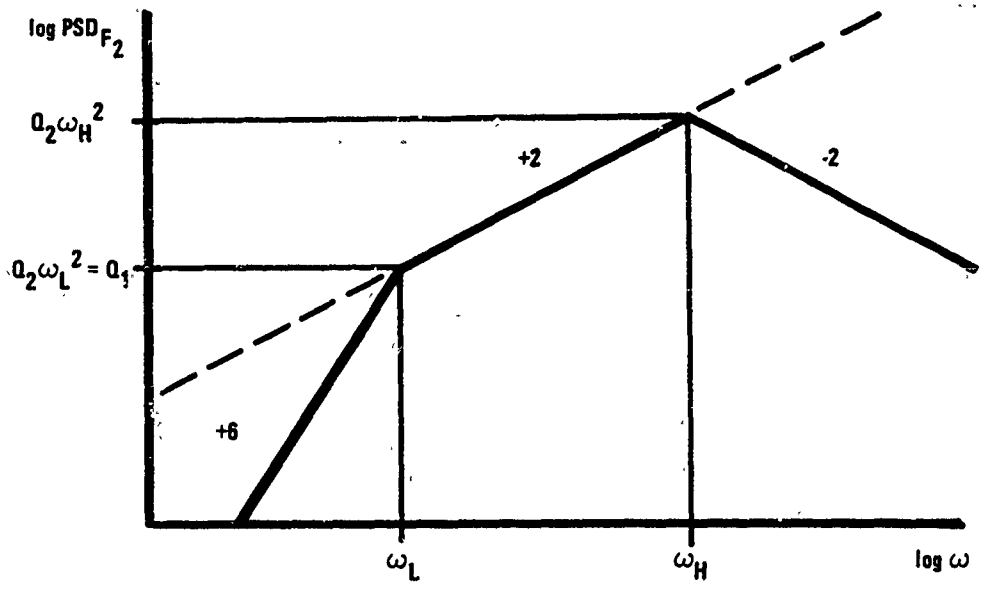

a. Force

$$mx = \frac{F_2}{S^2}$$

$$RMS_{F_2} = \sqrt{\omega_L \omega_H^3}\ RMS_{mx}$$

$$Q_2 = \frac{3}{4}\pi\,\omega_L\,RMS_{mx}^2$$

$$= Q_1/\omega_L^2$$

$$\omega_L \ll \omega_H$$

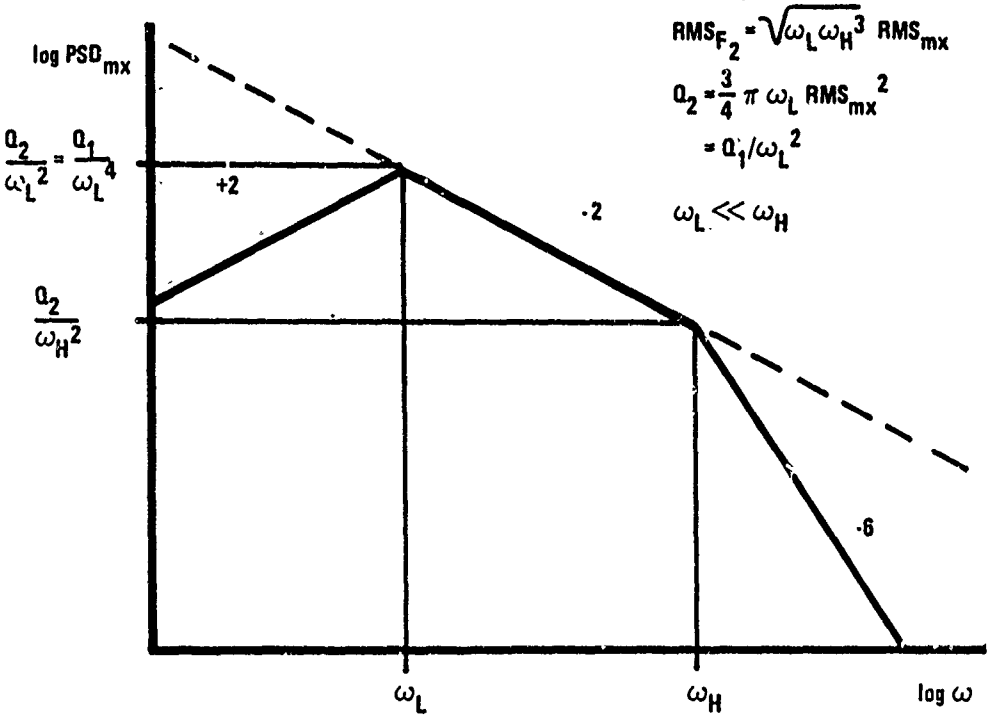

b. Mass-stroke

Figure 3-10. Test Signal 2 Power Spectral Densities (at force input)

These results for Test Signal 2, after converting to torques using the expressions (3-29a) and (3-29b), are displayed in Figures 3-8 and 3-9 for comparison against results for Test Signal 1. The improvement in both cases is dramatic. Square root SNRs for the baseline case now range from roughly 2.5 to 4.5 orders of magnitude, so the ease of identification should be greatly improved. For the advanced concept, all indicated modes should, in principle, be identifiable.

It should be recognized, of course, that mass-stroke constraints are not the only actuator limitations. The rms force level, which works out to $RMS_{F2} = 4000$ N for this case, would undoubtedly exceed the actuator's force capability. Thus, in practice the high-frequency bandwidth limit (ω_H) would have to be relaxed somewhat. As evident from the equation for RMS_{F2} in Figure 3-10, a reduction to $\omega_H \simeq 200$ r/s would limit rms force to 400 N, which is necessarily within the actuator's capability and is still more than adequate to excite all modes critical for vibration control.

Measurement Noise Definition

Early in Section 2, we established that resolution requirements for vibration control sensors must be of order 1 μr for angular position and 1 μm for linear position. These requirements should be interpreted as rms requirements over the control passband which extends from ω_L to ω_c, the desired crossover frequency of the control loop. This is true because measurement noise power below ω_L will be attenuated by the high-pass in Figure 2-3, while that above ω_c will be attenuated by the vibration control loop feedback. It is assumed, however, that sensors, just like actuators, must provide "intelligence" bandwidth out to some frequency (ω_H) well beyond control-loop crossover in order to ensure phase stability throughout the gain crossover region.

Three types of measurements were considered for both the linear and angular cases--position, rate, and acceleration. Selection of the appropriate spectral noise intensity for position measurements is straightforward. We simply assume a flat noise spectrum (R_1) over the passband ω_L to ω_H, such that its rms level (RMS_y) over the narrower control passband ω_L to ω_c is equal to the specified 1 μr or 1 μm values. Noise intensity selection for the rate and

acceleration levels is less obvious. The approach used in our early analyses was to allow the noise spectrum for rate and acceleration measurements to grow with frequency (i.e., $R_2 = R_1\omega^2$ for rates and $R_3 = R_1\omega^4$ for accelerations). Thus, the corresponding noise spectrum at the position level would remain the same for all three types of measurements, so identification performance would be insensitive to the type of measurement.

Although the above approach would seem to allow a fair comparison between different types of sensors, it is not consistent with physical characteristics of rate and acceleration instruments. That is, their noise power does not, in general, grow with ω^2 and ω^4, respectively. While actual noise spectrums are seldom flat over wide bandwidths, this choice is certainly more realistic than our earlier assumptions. Thus, for more recent analyses we have assumed a flat noise spectrum over the passband ω_L to ω_H for position, rate, or acceleration measurements with intensities R_1, R_2, and R_3, respectively. These intensities were chosen to give a constant rms position error (RMS_y) over the control passband. Thus, errors for each type of measurement still have the same impact on closed-loop control performance.

The corresponding noise spectrum at the position level is illustrated for all three types in Figure 3-11. Relationships between noise parameters for each type were derived using procedures analogous to those used for test signals. Assuming again that $\omega_L = 0.1$ r/s and $\omega_H = 1000$ r/s, choosing an "ideal" control-loop crossover frequency of $\omega_c = 250$ r/s, and letting $RMS_y = 1$ μr for angular and 1 μm for position measurements, gives noise intensities of

$$R_1 = \frac{3}{4}\frac{\pi}{\omega_c} RMS_y^2 = 1 \times 10^{-14} \text{ r}^2/\text{Hz (or m}^2/\text{Hz)} \qquad (3\text{-}32a)$$

$$R_2 = \omega_L\omega_c R_1 = 2.5 \times 10^{-13} (\text{r/s})^2/\text{Hz (or (m/s)}^2/\text{Hz)} \qquad (3\text{-}32b)$$

$$R_3 = \omega_L^3\omega_c R_1 = 2.5 \times 10^{-15} (\text{r/s}^2)^2/\text{Hz (or (m/s}^2)^2/\text{Hz)} \qquad (3\text{-}32c)$$

Comparison of noise power at the position level for the three cases shows that for $\omega_L < \omega < \omega_H$

acceleration levels is less obvious. The approach used in our early analyses was to allow the noise spectrum for rate and acceleration measurements to grow with frequency (i.e., $R_2 = R_1\omega^2$ for rates and $R_3 = R_1\omega^4$ for accelerations). Thus, the corresponding noise spectrum at the position level would remain the same for all three types of measurements, so identification performance would be insensitive to the type of measurement.

Although the above approach would seem to allow a fair comparison between different types of sensors, it is not consistent with physical characteristics of rate and acceleration instruments. That is, their noise power does not, in general, grow with ω^2 and ω^4, respectively. While actual noise spectrums are seldom flat over wide bandwidths, this choice is certainly more realistic than our earlier assumptions. Thus, for more recent analyses we have assumed a flat noise spectrum over the passband ω_L to ω_H for position, rate, or acceleration measurements with intensities R_1, R_2, and R_3, respectively. These intensities were chosen to give a constant rms position error (RMS_y) over the control passband. Thus, errors for each type of measurement still have the same impact on closed-loop control performance.

The corresponding noise spectrum at the position level is illustrated for all three types in Figure 3-11. Relationships between noise parameters for each type were derived using procedures analogous to those used for test signals. Assuming again that $\omega_L = 0.1$ r/s and $\omega_H = 1000$ r/s, choosing an "ideal" control-loop crossover frequency of $\omega_c = 250$ r/s, and letting $RMS_y = 1$ μr for angular and 1 μm for position measurements, gives noise intensities of

$$R_1 = \frac{3}{4}\frac{\pi}{\omega_c} RMS_y^2 = 1 \times 10^{-14} \text{ r}^2/\text{Hz (or m}^2/\text{Hz)} \qquad (3\text{-}32a)$$

$$R_2 = \omega_L\omega_c R_1 = 2.5 \times 10^{-13} (\text{r/s})^2/\text{Hz (or (m/s)}^2/\text{Hz)} \qquad (3\text{-}32b)$$

$$R_3 = \omega_L^3\omega_c R_1 = 2.5 \times 10^{-15} (\text{r/s}^2)^2/\text{Hz (or (m/s}^2)^2/\text{Hz)} \qquad (3\text{-}32c)$$

Comparison of noise power at the position level for the three cases shows that for $\omega_L < \omega < \omega_H$

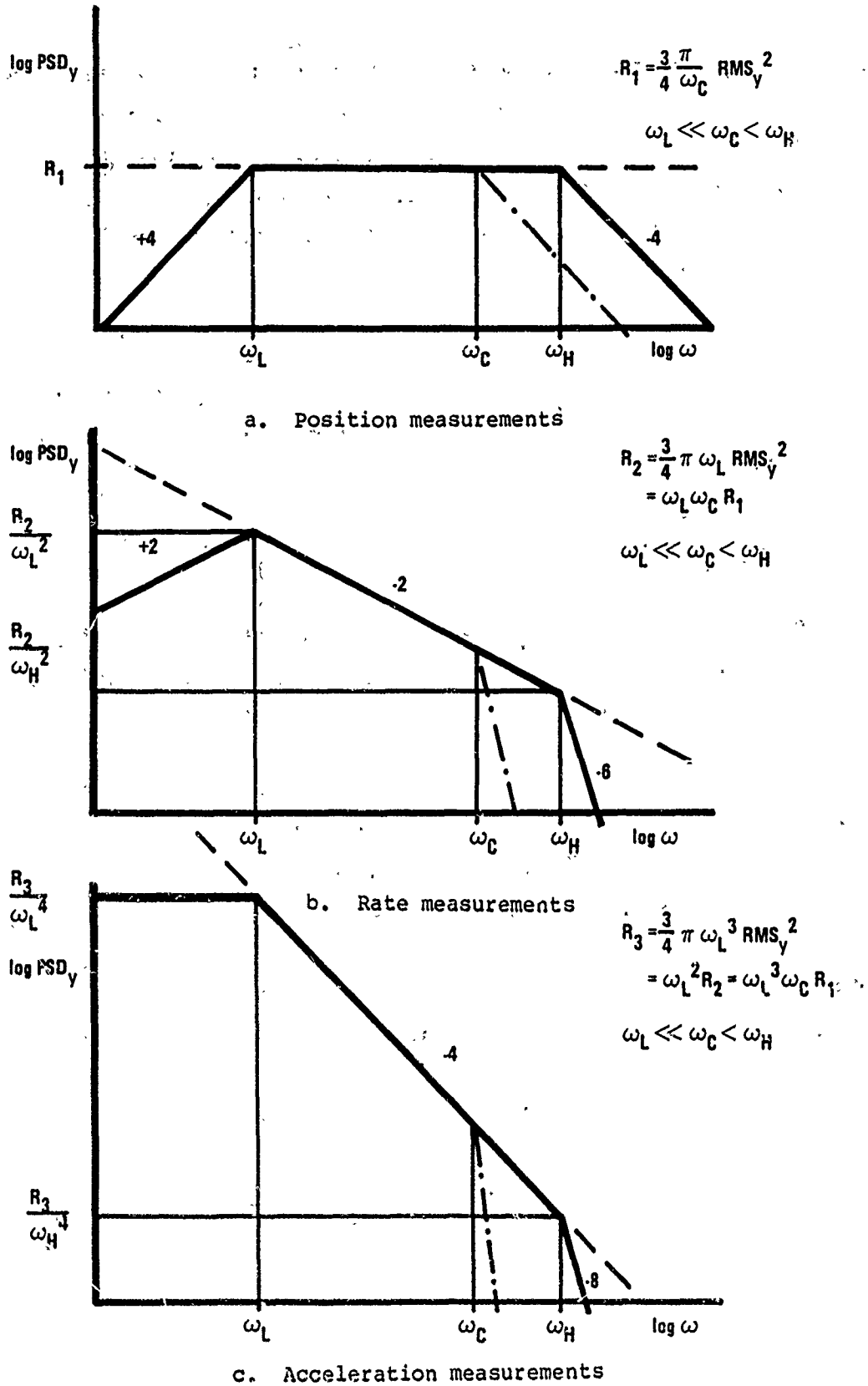

Figure 3-11. Measurement-Noise Power Spectral Densities (at position output)

$$\frac{R_2}{\omega^2} = \left(\frac{\omega_L}{\omega}\right)\left(\frac{\omega_c}{\omega}\right) R_1 \qquad (3\text{-}33a)$$

$$\frac{R_3}{\omega^4} = \left(\frac{\omega_L}{\omega}\right)^2 \left(\frac{R_2}{\omega^2}\right) = \left(\frac{\omega_L}{\omega}\right)^3 \left(\frac{\omega_c}{\omega}\right) R_1 \qquad (3\text{-}33b)$$

Thus, noise power for rate or acceleration measurements is larger than that for position measurements at low frequencies but smaller at high frequencies. Also, noise power for acceleration measurements is smaller than that for rate measurements over the entire passband. The frequencies at which these PSDs intersect are given by

$\omega_{12} = \sqrt{\omega_L \omega_c} = 5$ r/s for position and rate measurements

$\omega_{13} = \sqrt[4]{\omega_L^3 \omega_c} = 0.707$ r/s for position and acceleration measurements

$\omega_{23} = \omega_L = 0.1$ r/s for rate and acceleration measurements

The impact of test signal limitations on the two identification concepts when rate measurements are used is illustrated in Figures 3-12 and 3-13. As expected, Test Signal 2 yields much higher SNRs at the output than Test Signal 1. Comparing these figures with those for position measurements in Figures 3-8 and 3-9, we find that rate measurements yield larger SNRs for frequencies above $\omega_{12} = 5$ r/s, but smaller SNRs below that frequency. Corresponding results for acceleration measurements in Figures 3-14 and 3-15 follow similar trends. SNRs for the acceleration cases are smaller than those for the corresponding rate cases for all frequencies above $\omega_{23} = 0.1$ r/s, and exceed those for the corresponding position cases only for frequencies below $\omega_{13} = 0.707$ r/s. Note that results for Test Signal 1 and acceleration measurements are identical to those for Test Signal 2 and rate measurements.

Hardware Requirements Summary

Hardware requirements for control and identification are summarized for both the baseline (ILAS) concept and the advanced (non-ILAS) concept in Table 3-2. In both cases, vibration control of modes in the 10 to 100 r/s bandpass demands sensor and actuator bandwidths that span 0.1 to 1000 r/s, and computer sample rates of

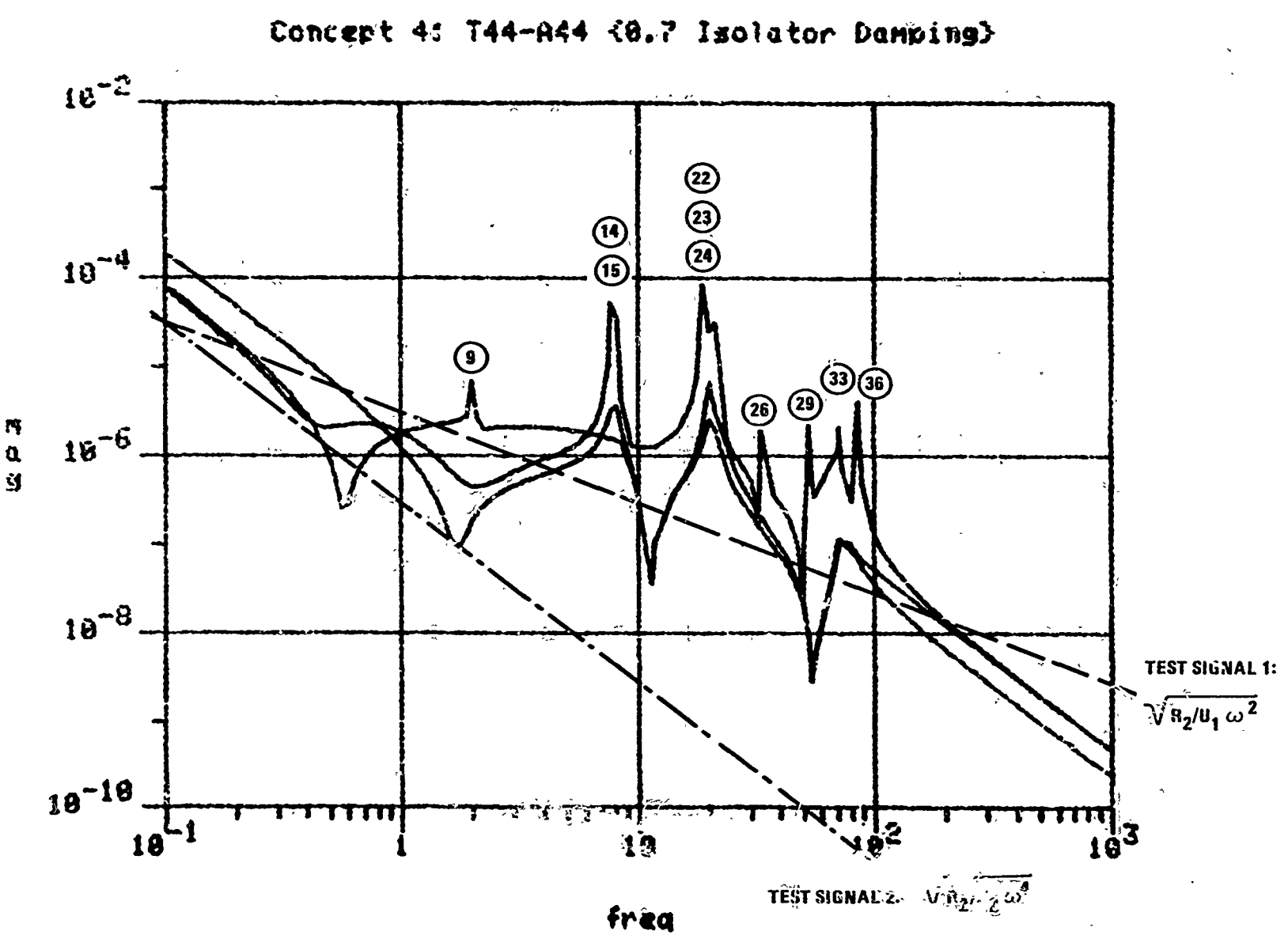

Figure 3-12. Test Signal Limitations for Baseline Concept: Rate Measurements

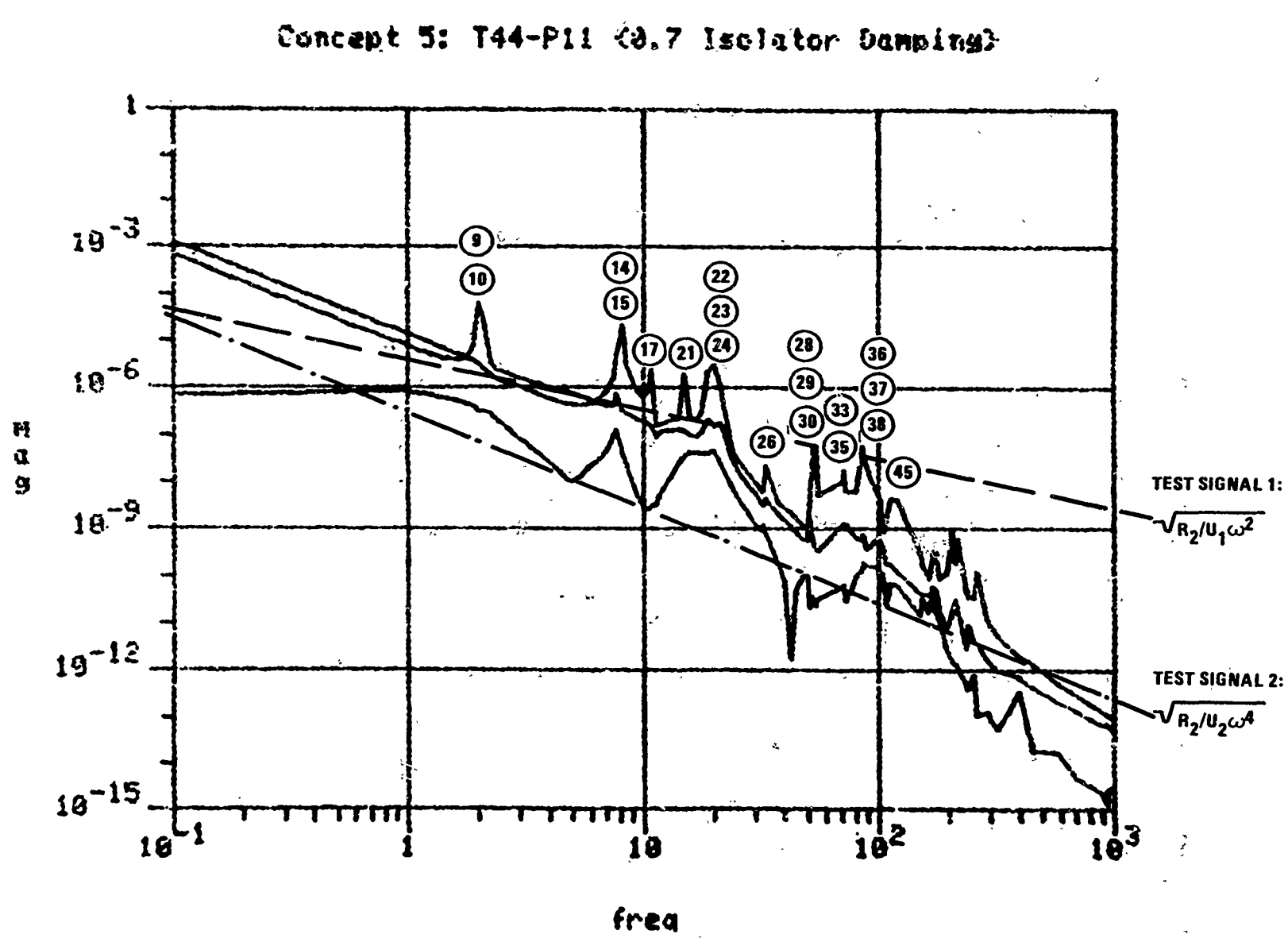

Figure 3-13. Test Signal Limitations for Advanced Concept: Rate Measurements

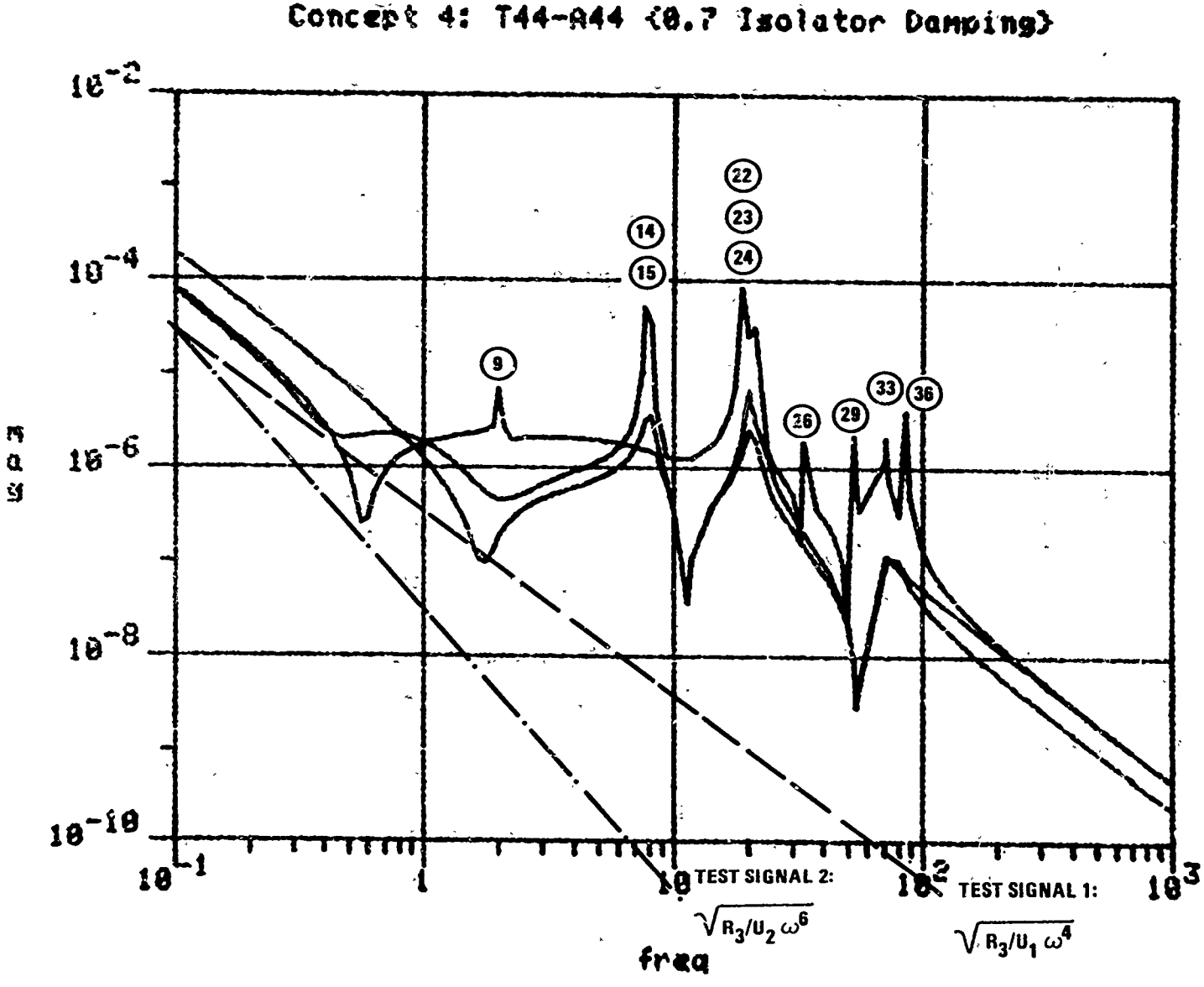

Figure 3-14. Test Signal Limitations for Baseline Concept: Acceleration Measurements

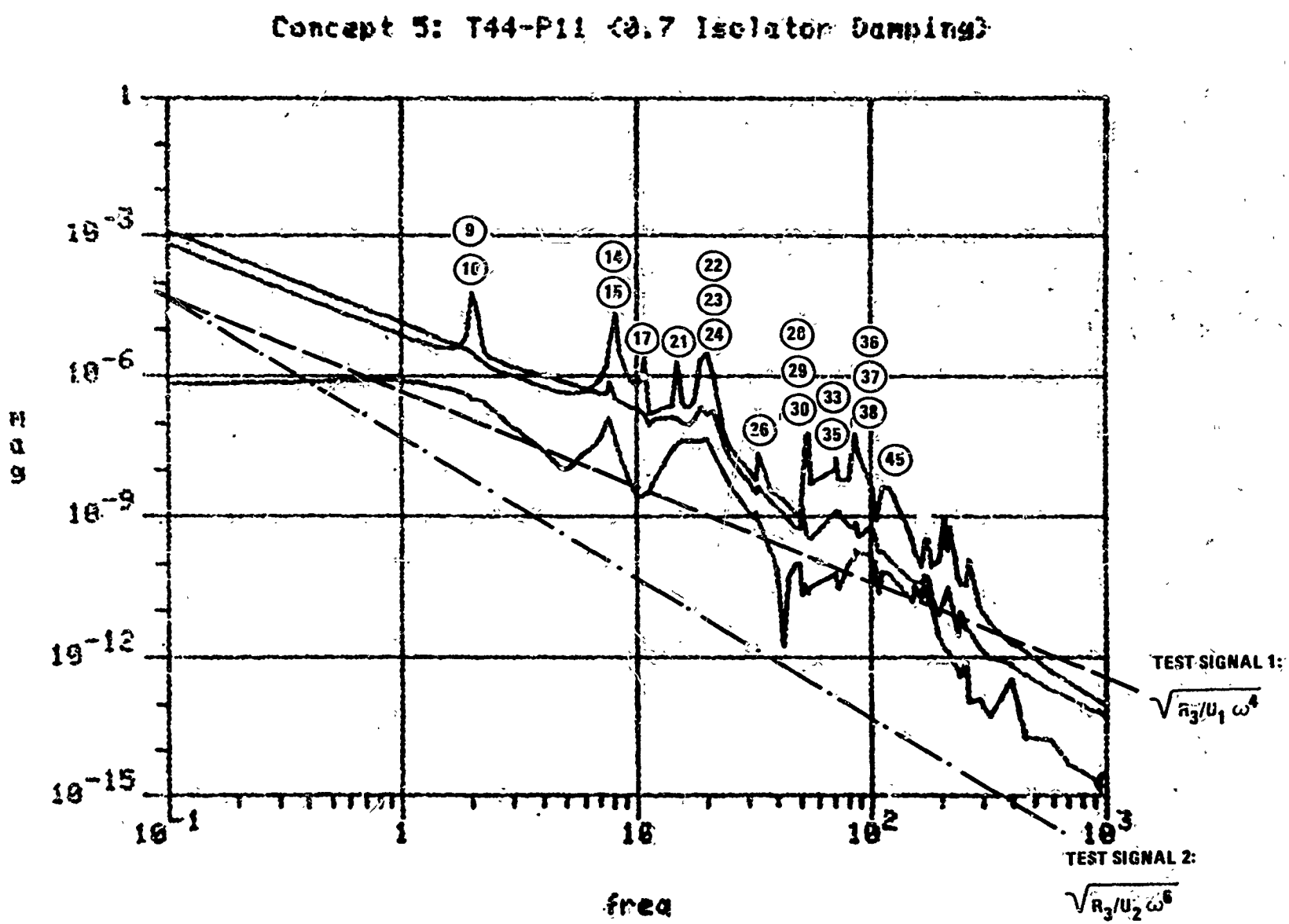

Figure 3-15. Test Signal Limitations for Advanced Concept: Acceleration Measurements

roughly 200 Hz (≈ 1250 r/s) to ensure phase stability throughout the vibration control loop gain crossover region. Actuator test signal and associated noise characteristics over this same passband are shown for the two types of test signals just described, along with the control design constraints used to define these characteristics. Sensor noise PSDs are given for measurements at the position, rate, or acceleration level, as constrained by the allowable position noise over the control passband (ω_L - ω_c). Note that low-frequency accuracy below ω_L = 0.1 r/s is not critical either for sensors or actuators.

Computer requirements in Table 3-2 indicate that sample frequency must be on the order of f_s = 200 Hz to meet stability and performance requirements, while throughput must be roughly 100,000 "operations"/sec. The latter requirement is driven by computational requirements to implement a steady-state LQG controller with as many as 40 states, 3 inputs, and 3 outputs at the 200 Hz sample rate.

The high sensor resolution required for both concepts favors the use of rate-integrating gyros for the baseline concept and rate-integrating accelerometers for the advanced concept. These instruments use pulse-rebalanced loops to generate quantized measurements of angular position ($\Delta\theta$) and linear velocity (Δv), respectively. Since quantization errors will likely dominate measurement errors over the passband 0.1 to 1000 r/s, the effective measurements are angular position for the baseline concept and linear velocity (or rate) for the advanced concept. In view of Figures 3-8 and 3-13, and the need to generate sufficient excitation for all modes near control-loop crossover, Test Signal 2 is the recommended choice for both concepts. Test signal, disturbance, and sensor noise characteristics corresponding to the above choices are enclosed in boxes in Table 3-2.

It should be noted that the combination of high bandwidth and high resolution pushes or exceeds the state of the art for most control hardware. Whereas bandwidth requirements could be relaxed by perhaps a factor of two for the ACOSS II Model as defined, the probable existence of significant unmodeled flexural modes for the solar panels above 100 r/s actually favors increasing hardware bandwidth by a factor of 2 to 5.

TABLE 3-2. HARDWARE REQUIREMENTS FOR VIBRATION CONTROL AND IDENTIFICATION

Source	Actuators (3 paired shakers to give torque about 44x,y,z)	Sensors	
		Baseline Concept (3 gyros at 44x,y,z)	Advanced Concept (3 accel at 11x,y,z)
Bandwidth, $\omega_L - \omega_H$	0.1 - 1000 r/s	0.1 - 1000 r/s	0.1 - 1000 r/s
Test Signal Capability			
TS 1 PSD ($\omega_L - \omega_H$)	$U_1 = 4 \times 10^{-2}$ (N-m)^2/Hz		
TS 2 PSD ($\omega_L - \omega_H$)	$U_2 = 4$ (N-m-s)^2/Hz		
Design Constraint	$RMS_{mx} \leq 0.4$ kg-m		
Mid-Frequency Noise (Resolution)			
Actuators			
TS 1 Dist. PSD ($\omega_L - \omega_H$)	$W_1 = 4 \times 10^{-4}$ (N-m)^2/Hz		
TS 2 Dist. PSD ($\omega_L - \omega_H$)	$W_2 = 4 \times 10^{-2}$ (N-m-s)^2/Hz		
Design Constraint	10% RMS errors		
Sensors			
Position error PSD ($\omega_L - \omega_H$)		$R_1 = 1 \times 10^{-14}$ r^2/Hz	$R_1 = 1 \times 10^{-14}$ m^2/Hz
Rate Error PSD ($\omega_L - \omega_H$)		$R_2 = 2.5 \times 10^{-13}$ (r/s)^2/Hz	$R_2 = 2.5 \times 10^{-13}$ (m/s^2)^2/Hz
Accel. Error PSD ($\omega_L - \omega_H$)		$R_3 = 2.5 \times 10^{-15}$ (r/s^2)^2/Hz	$R_3 = 2.5 \times 10^{-15}$ (m/s^2)^2/Hz
Design Constraint ($\omega_C = 250$ r/s)		RMS_y ($\omega_L - \omega_C$) ≤ 1 µr	RMS_y ($\omega_L - \omega_C$) ≤ 1 µm
Low-Frequency Noise (Accuracy)			
PSD($\omega < \omega_L$)	$< W_j(\omega_L/\omega)^4$	$< R_j(\omega_L/\omega)^4$	$< R_j(\omega_L/\omega)^4$

Computer Requirements

Sample frequency: $f_s = 200$ Hz ($\omega_s = 1250$ r/s).

Throughput: 500 "operations"/cycle x 200 Hz = 100,000 "operations"/sec where:

1 "operation" $\triangleq$ 3 LOADS + 1 STORE + 1 MULTIPLY + 1 ADD

SECTION 4

MAXIMUM LIKELIHOOD ESTIMATION IDENTIFICATION

Identification is the process of determining a mathematical model for an unknown system's response to (possibly known) inputs in the face of unknown disturbances. Parametric identification, which generates a parameterized mathematical model, is particularly convenient (often imperative) when this model is also required for control design. The general procedure, as applied to large flexible space structures (LSS), is illustrated generically in Figure 4-1. Here a wide-bandwidth test signal (u) is used to excite both the true structure, through its control actuators, and a parameterized (computer) model for this structure. The response of the true structure, as measured by its control sensors, and the response of the model are differenced to form a residual error (r). This error is then processed by an identification algorithm that periodically updates the unknown parameter vector (α) to minimize some function of the residual error. The true structure's response is, of course, corrupted by disturbances, which include both process errors (w) and measurement errors (v).

Although simpler identification methods suffice for certain applications, none can match the power of maximum likelihood estimation (Ref. 5,6), which employs a Kalman filter within the identification algorithm. Honeywell has used this technique extensively over the past 10 years (Ref. 8 through 13) and has developed a number of variations on the basic method to improve its speed and make it more economical and/or make it feasible for on-line use. Recent developments by Yared (Ref. 7) greatly simplify the evaluation of theoretical identification accuracy. The general method, however, is extremely complicated for the LSS application due to the large number of potential parameters needed to describe highly flexible structures.

MLE METHOD

Maximum likelihood estimation addresses the problem of finding unknown parameters in the model of a noisy dynamic system from observations of the system outputs in

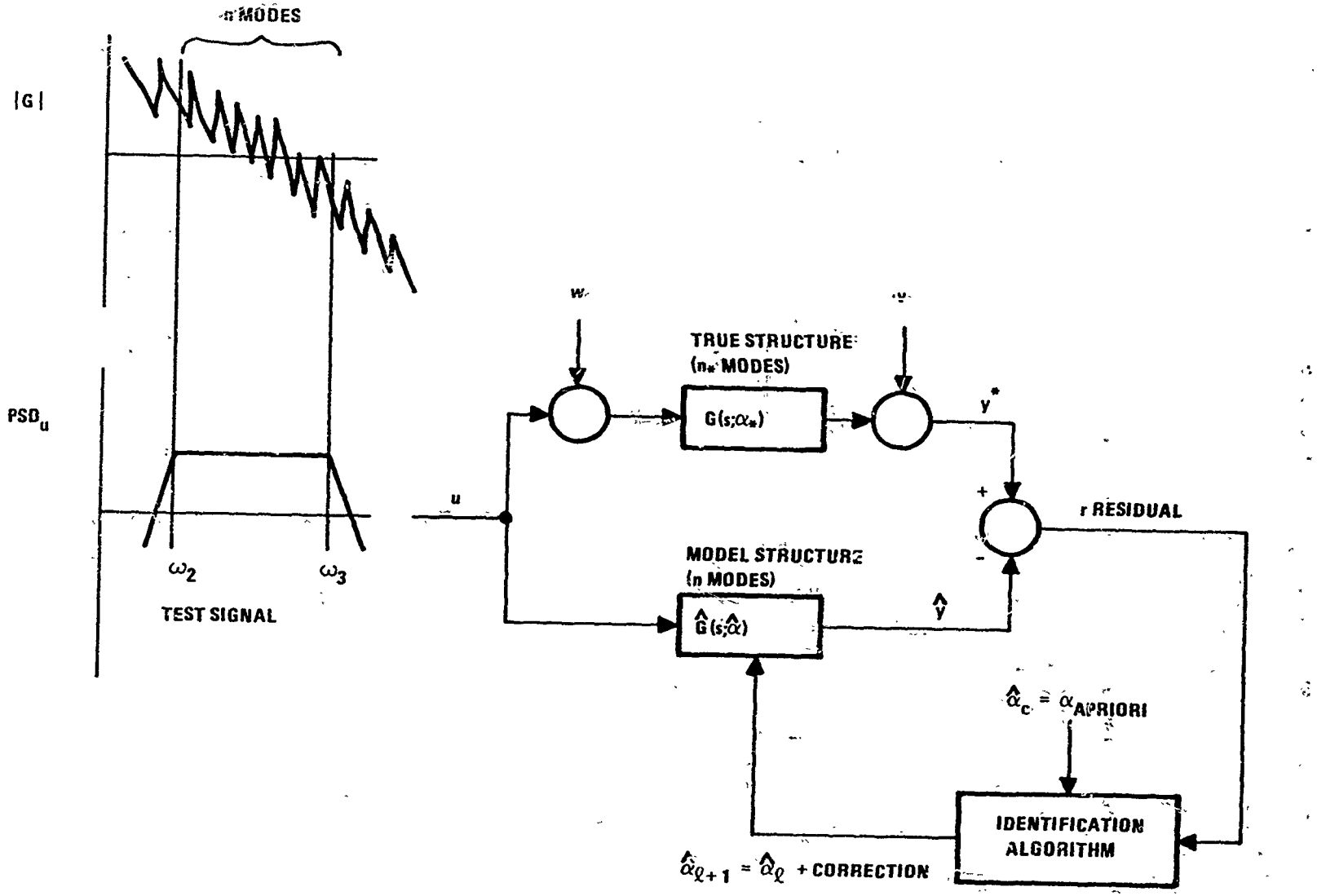

Figure 4-1. Large Space Structure Identification

response to (possibly known) inputs. This problem can be stated in mathematical terms as follows.

Model Forms

Consider the linear discrete-time system of the form

Discrete-Time Model:

$$x^*_{k+1} = A_* x^*_k + B_* u_k + B_* w_k \tag{4-1a}$$

$$y^*_k = C_* x_k + v_k \tag{4-1b}$$

where k is the discrete-time index, x^*_k is the $2n_*$-dimensional state vector, u_k is the n_i-dimensional input vector, y^*_k is the n_o-dimensional output vector, and w_k and v_k are (white) process and measurement noise vectors, all of appropriate dimensions. Assume that noises w_k and v_k are zero-mean and uncorrelated with covariances

$$E\left\{w_k w_\ell^T\right\} = W_d * \delta_{k\ell} \tag{4-2a}$$

$$E\left\{v_k v_\ell^T\right\} = R_d * \delta_{k\ell} \tag{4-2b}$$

where $\delta_{k\ell}$ is the Kronecker delta function.

Assume further that the known test signal u_k is also zero-mean and uncorrelated with either v_k or w_k and has known variance

$$E\left\{u_k u_\ell^T\right\} = U_d \delta_{k\ell} \tag{4-2c}$$

For future reference, it is further assumed that the above discrete-time representation has an equivalent continuous-time representation in block-diagonal modal-coordinate form, that is,

Continuous-Time Model:

$$\dot{x}^* = F_* x_* + G_* u + G_* w \tag{4-3a}$$

$$y^* = C_* x^* + v \tag{4-3b}$$

where

$$F_* \triangleq \text{diag}\left\{\begin{bmatrix} 0 & 1 \\ -\omega_i^{*2} & -2\zeta_i^* \omega_i^* \end{bmatrix}\right\} \tag{4-3c}$$

$$G_* \triangleq \text{col}\left\{\begin{bmatrix} 0 \\ b_i^{*T} \end{bmatrix}\right\} \tag{4-3d}$$

$$C_* \triangleq \text{row}\{[c_i^* \quad 0]\}$$

Here n_* corresponds to the number of modes, while $2n_*$ again corresponds to the number of states. The vectors u, w, and v now represent continuous-time uncorrelated white (or wide bandwidth) noise processes with spectral intensities

$$E\{w(t)w^T(\tau)\} = W_* \delta(t - \tau) \tag{4-4a}$$

$$E\{v(t)v^T(\tau)\} = R_* \delta(t - \tau) \tag{4-4b}$$

$$E\{u(t)u^T(\tau)\} = U\delta(t - \tau) \tag{4-4c}$$

where $\delta(\cdot)$ is the dirac delta function. The above state-space model also has the transfer function equivalent

$$G_*(s) = \sum_{i=1}^{n_*} \frac{c_i^* b_i^{*T}}{s^2 + 2\zeta_i^* \omega_i^* s + \omega_i^{*2}}$$

It well known that these models are related via

$$A_* = e^{F_* T} \simeq I + F_* T \tag{4-5a}$$

$$B_* = F_*^{-1}(I - e^{F_* T})G_* \simeq G_* T \tag{4-5b}$$

$$W_d^* = W_*/T \tag{4-5c}$$

$$R_d^* = R_*/T \tag{4-5d}$$

$$U_d = U/T \tag{4-5e}$$

where T is the sample interval for the discrete system. The above approximations for A_* and B_* hold for sufficiently high sample rates, such that $|\omega_i{}_* T| << 1$ for each mode.

Let the true system (4-1) be designated by

$$M_* = \{A_*, B_*, C_*, W_d^*, R_d^*\}$$

where the matrices in M_* depend on the true parameter vector α_*.

Likewise let

$$M_\alpha = \{A, B, C, W_d, R_d\}$$

denote a model set with the same structure as (4-1), but with state vector of dimension 2n (possibly different from $2n_*$), where the matrices in M_α depend on the unknown parameter (vector) α.

The problem then is to find the parameter value, $\hat{\alpha}$, which maximizes the probability of occurrence of the observed sequence of measurements. In order to evaluate α, functional forms for the probability density functions of process noise (w) and observation noise (v) must be known or assumed. If all noise processes are assumed gaussian the solution is obtained as follows.

Likelihood Functions

Let $r_k(\alpha) \triangleq y_k - \hat{y}_k(\alpha)$ denote the residual sequence of the Kalman filter corresponding to M_α. It can then be shown that the maximum likelihood estimate $\hat{\alpha}$ for α at time NT is the value of α that <u>minimizes</u> the negative log likelihood function

$$L^N(y^N; \alpha) \triangleq \sum_{k=0}^{N} L_k(\alpha) \tag{4-6a}$$

where

$$L_k(\alpha) \triangleq L(y_k | Y^{k-1}; \alpha) \tag{4-6b}$$

$$\triangleq \frac{1}{2} \log \det S_k + \frac{1}{2} r_k^T(\alpha) S_k^{-1} r_k(\alpha)$$

is the conditional negative log likelihood function, and

$$S_k \triangleq E_\alpha \{[y_k - \hat{y}_\kappa(\alpha)][y_k - \hat{y}_k(\alpha)]^T\} \tag{4-6c}$$

is the predicted residual error covariance for the Kalman filter based on the parameter α. Here

$$Y^k \triangleq \{y_0, y_1, \ldots, y_k\} \tag{4-6d}$$

denotes the collection of measurements up to time kT.

It is well known that the above quantities can be obtained from the Kalman filter corresponding to M_α:

$$\hat{x}_{k+1}(\alpha) = A\hat{x}_k(\alpha) + Bu_k + A_k r_k(\alpha) \tag{4-7a}$$

$$r_k(\alpha) \triangleq y_k - \hat{y}_k(\alpha) \triangleq y_k - C\hat{x}_k(\alpha) \tag{4-7b}$$

where

$$K_k = \Sigma_k C^T S_k^{-1} \tag{4-7c}$$

$$S_k = C\Sigma_k C^T + R_d \tag{4-7d}$$

$$\Sigma_{k+1} = A\Sigma_k A^T + BW_d B^T - AK_k S_k K_k^T A^T \tag{4-7e}$$

define the filter gain, residual covariance, and state covariance, respectively.

The parameter estimate α, which minimizes (4-6a),

$$\hat{\alpha} \triangleq \text{Arg}\{\min_\alpha L^N(\alpha)\} \tag{4-8}$$

cannot, in general, be solved for explicitly. In practice, it is necessary to use iterative numerical methods to accomplish this minimization.

Iterative Algorithms

Two iterative, numerical minimization techniques are commonly used for this purpose.

Gradient Method: This method uses a parameter update iteration of the form:

$$\hat{\alpha}^{j+1} = \hat{\alpha}^{j} - \varepsilon^{j} \nabla L^{N}(\hat{\alpha}^{j}) \tag{4-9a}$$

where the superscript j refers to the j^{th} iteration of the algorithm and $\varepsilon^{j} > 0$ is a step size parameter that is usually adjusted in some ad hoc manner to improve convergence.

Newton-Rhapson (NR) Method: This method employs a parameter update iteration of the form:

$$\hat{\alpha}^{j+1} = \hat{\alpha}^{j} - [\nabla^2 L^{N}(\hat{\alpha}^{j})]^{-1} \nabla L^{N}(\hat{\alpha}^{j}) \tag{4-9b}$$

The distinguishing feature of this algorithm is that the ad hoc (scalar) step size parameter ε^{j} is replaced by the inverse of the Hessian matrix.

Here

$$\nabla L^{N}(\alpha) \triangleq \left.\frac{\partial L^{N}(\alpha)}{\partial \alpha}\right|_{\alpha=\hat{\alpha}} \triangleq \sum_{k=0}^{N} \left.\frac{\partial L_k(\alpha)}{\partial \alpha}\right|_{\alpha=\hat{\alpha}} \tag{4-10a}$$

$$\nabla^2 L^{N}(\alpha) \triangleq \left.\frac{\partial^2 L^{N}(\alpha)}{\partial \alpha^2}\right|_{\alpha=\hat{\alpha}} \triangleq \sum_{k=0}^{N} \left.\frac{\partial^2 L_k(\alpha)}{\partial \alpha^2}\right|_{\alpha=\hat{\alpha}} \tag{4-10b}$$

denote, respectively, the first and second partial derivatives of the likelihood function with respect to the unknown parameter vector, α, evaluated at $\alpha = \hat{\alpha}$. These quantities will sometimes be referred to respectively as the gradient vector and Hessian matrix of the likelihood function. The general procedure is illustrated in Figure 4-2.

In general, the computational effort required to evaluate these partials is enormous. For a vector of N_p unknown parameters, evaluating ∇L^{N} is roughly equivalent to propagating N_p 2n-dimensional Kalman filters of the form (4-7). Likewise, evaluating $\nabla^2 L^{N}$ is roughly equivalent (due to symmetry) to propagating $(1/2)N_p^2$ Kalman filters. Thus the computational effort required to perform a single iteration of (4-9) is of order $NN_p n^3$ multiplies for the gradient method and $NN_p^2 n^3$ multiplies for the NR method. Clearly some

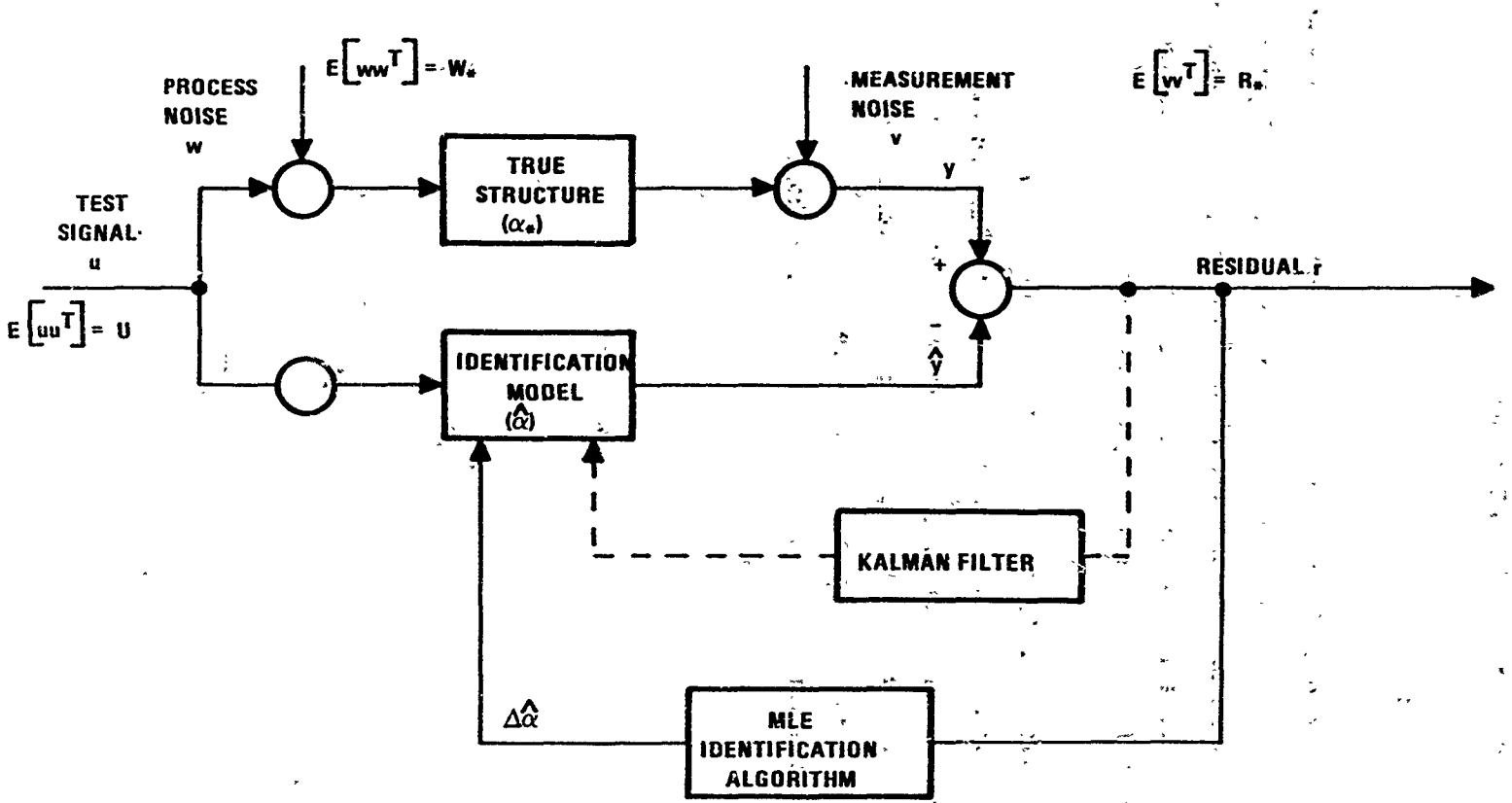

Figure 4-2. Maximum Likelihood Estimation (MLE) Identification

simplifications are desirable to reduce MLE identification to a tractable problem for space structures. Before pursuing such simplifications, however, we first examine potential accuracy of the MLE method.

IDENTIFICATION ACCURACY

Given that data has been collected for a time interval NT, and that the likelihood function and its partials have been accumulated and associated parameter updates (4-9) have been carried out for a "sufficient" number of iterations, we now address two related questions--what is the accuracy of the resulting parameter estimates, and what factors influence this accuracy?

It is well known that the MLE identification procedure of Figure 4-2 commits two types of errors--systematic and stochastic. Each of these is illustrated for a two-dimensional parameter space in Figure 4-3. Without loss of generality, the true parameter is taken to be the origin of the parameter space. Systematic error or bias is indicated as the distance from the center of the 1-sigma ellipse to the origin. Stochastic error is indicated by the size and shape of the 1-sigma ellipse.

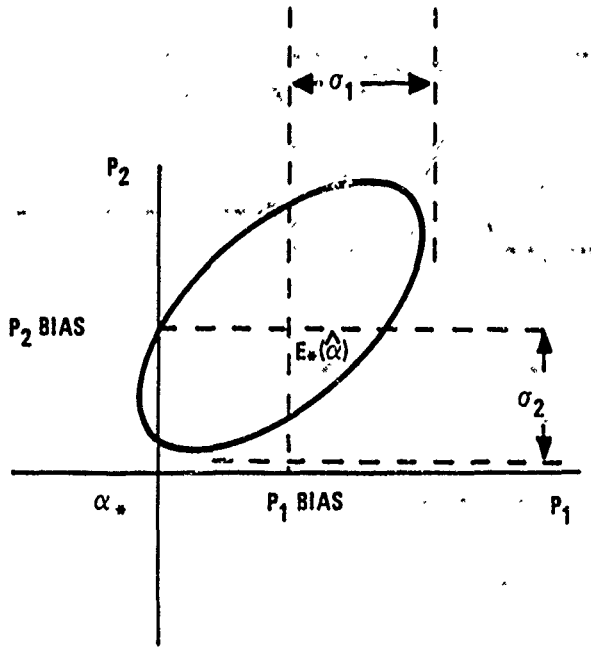

Figure 4-3. Parameter Identification Errors: Systematic and Stochastic

Systematic Errors

Systematic errors (or biases) are defined as the expected error between the converged parameter estimate and the true parameter, that is, $\alpha_{BIAS} = E_*\{\alpha\} - \alpha_* = \hat{\alpha}_* - \alpha_*$. (In theory, this comparison cannot be made unless $\dim(\alpha_*) = \dim(\alpha)$. In practice, however, it is usually possible to pair each element in α with a corresponding element in α_*.) These arise from (1) model-order mismatches between the theoretically infinite-dimensional representation for the true structure and its finite-dimensional representation used for the identification model, (2) similar mismatches between true actuator and sensor dynamics and the simplified models used to represent them, and (3) systematic disturbances such as constant or slowly varying solar torques, gravity gradients, etc., as well as sensor and actuator biases. The first two can be greatly minimized by using band-passed test signals (u) that emphasize the desired frequency band of interest for the identification model, as opposed to the white (or wide bandwidth) test signals assumed earlier.

Stochastic Errors

Similarly, stochastic (or random) errors are defined as the covariance of the parameter estimation error, that is, $Cov\{\alpha\} = E_*\{(\hat{\alpha} - \hat{\alpha}_*)(\hat{\alpha} - \hat{\alpha}_*)^T\}$. These arise from random disturbances, as well as sensor and actuator noise. Stochastic parameter errors are normally proportional to these disturbance and noise covariances, but inversely proportional to both test signal intensity and the identification time interval. For the LSS application, errors between the commanded test signal and that actually delivered to the structure by the actuators constitute the primary disturbance source during identification. Thus, the assumption of identical input matrices for test signal u and disturbance w in equations (4-1) and (4-3) and in Figures 4-1 and 4-2 is justified.

Identifiability Analysis

Identifiability analysis provides a theoretical prediction for parameter errors that would remain after MLE identification. Following the approach developed by

Yared (Ref. 7), the expected parameter estimate is obtained formally by taking expectations in (4-8) with respect to the true parameter set M_* to give

$$\hat{\alpha}_* \triangleq E_*\{\alpha\} \triangleq \text{Arg}\{\min_{\alpha} E_*[L^N(\alpha)]\} \triangleq \text{Arg}\{\min_{\alpha} I_*^N(\alpha)\} \tag{4-11a}$$

where

$$I_*^N(\alpha) \triangleq E_*[L^N(\alpha)] = \sum_{k=0}^{N} I_k^*(\alpha) \tag{4-11b}$$

and

$$I_k^*(\alpha) \triangleq E_*[L_k(\alpha)] = \frac{1}{2}\log \det S_k + \frac{1}{2}\text{Tr}(S_k^{-1} S_k^*) \tag{4-11c}$$

are, respectively, the expected values of the total and conditional log likelihood functions, both with respect to the true parameter set M_*, and

$$S_k^* = E_*\{[y_k^* - \hat{y}_k(\alpha)][y_k^* - \hat{y}_k(\alpha)]^T\} \tag{4-11d}$$

is the actual residual error covariance based on the true parameter set M*.

Letting

$$\bar{X}_k \triangleq E\left\{\begin{bmatrix} x^*_k \\ x_k \end{bmatrix}\begin{bmatrix} x^{*T}_k & x^T_k \end{bmatrix}\right\} \tag{4-12a}$$

denote the covariance for the augmented $2(n_* + n)$-dimensional state vector $\bar{x}_k^T = (x_k^{*T}\ x_k^T)$, the actual residual error covariance (4-11c) can be evaluated using

$$S_k^* = \bar{C}\bar{X}_k\bar{C}^T + R_d^* \tag{4-12b}$$

$$\bar{X}_{k+1} = \bar{A}_k\bar{X}_k\bar{A}_k^T + \bar{B}U_d\bar{B}^T + \bar{Q}_k \tag{4-12c}$$

where

$$\underline{\underline{A}}_k \triangleq \begin{bmatrix} A_* & 0 \\ AK_kC & A(I - K_kC) \end{bmatrix}, \qquad \underline{\underline{B}} \triangleq \begin{bmatrix} B_* \\ B \end{bmatrix} \tag{4-12d}$$

$$\underline{\underline{C}} \triangleq \begin{bmatrix} C_* & -C \end{bmatrix}, \qquad Q_k \triangleq \begin{bmatrix} B_* W_d B_*^T & 0 \\ 0 & * \\ & AK_k R_d K_k^T A^T \end{bmatrix} \tag{4-12e}$$

Here K_k, S_k, and Σ_k are as given in (4-7c) to (4-7e).

We observe once again that the minimization in (4-11a) cannot be performed explicitly, but must be accomplished by iterative numerical techniques. For the gradient and NR schemes employed earlier in (4-9), the corresponding parameter updates now take the form

$$\hat{\alpha}_*^{j+1} = \hat{\alpha}_*^j - \varepsilon^j \nabla I_*^N(\hat{\alpha}_*^j) \tag{4-13a}$$

and

$$\hat{\alpha}_*^{j+1} = \hat{\alpha}_*^j - [\nabla^2 I_*^N(\hat{\alpha}_*^j)]^{-1} \nabla I_*^N(\hat{\alpha}_*^j) \tag{4-13b}$$

where

$$\nabla I_*^N(\alpha) \triangleq \sum_{k=0}^{N} \nabla I_k^*(\alpha) \tag{4-14a}$$

$$\nabla^2 I_*^N(\alpha) \triangleq \sum_{k=0}^{N} \nabla^2 I_k^*(\alpha) \tag{4-14b}$$

denote, respectively, the first and second partials of the expected log likelihood function with respect to the parameter vector α.

Computational requirements to assess identification accuracy are comparable to those required for identification alone. Evaluating ∇I_*^N and $\nabla^2 I_*^N$ requires propagating, respectively, N_p and $(1/2)N_p^2$ $2(n_* + n)$-dimensional Lyapunov equations

for each measurement update. Thus the total computational effort required to perform a single iteration of (4-13a) and (4-13b) is, respectively, of order $NN_p(n_* + n)^3$ multiplies for the gradient method and $NN_p^2(n_* + n)^3$ multiplies for the NR method. Thus simplifications for accuracy analysis are also highly desirable.

Note that the evaluation of $\hat{\alpha}_*$ assumes that the true system is known. Though this assumption will never hold in practice, it is nevertheless useful for analysis and experiment design purposes. When the true system is known, the bias in the parameter estimate can be directly determined by comparing the true parameter α_* with the estimate $\hat{\alpha}_*$.

Similarly, knowledge of the true system allows us to bound the stochastic error in parameters. Asymptotic normality of maximum likelihood estimators, when the model set contains the true parameter set, implies the following classical result.

Matched Models: Let $\hat{\alpha}_N$ be the maximum likelihood estimate of α at time NT and let $\hat{\alpha}_* = \alpha_*$ be the value of α that minimizes (4-11a). Then as $N \to \infty$, $(\hat{\alpha}_N - \hat{\alpha}_*)$ is asymptotically normally distributed with zero mean and covariance matrix

$$\text{Cov}[\hat{\alpha}_N] = E_*\left[(\hat{\alpha}_N - \hat{\alpha}_*)(\hat{\alpha}_N - \hat{\alpha}_*)^T\right] = \left[\nabla^2 I_*^N(\hat{\alpha}_*)\right]^{-1} \tag{4-15a}$$

On the other hand, when the true system is not contained in the model set, the following result can be shown to hold.

Mismatched Models: Let $\hat{\alpha}_N$ be the maximum likelihood estimate of α at time NT and let $\hat{\alpha}_* \neq \alpha_*$ be the value of α that minimizes (4-11a). Then as $N \to \infty$, $(\hat{\alpha}_N - \hat{\alpha}_*)$ is asymptotically normally distributed with zero mean and covariance matrix

$$\begin{aligned}\text{Cov}[\hat{\alpha}_N] &= E_*\left[(\hat{\alpha}_N - \hat{\alpha}_*)(\hat{\alpha}_N - \hat{\alpha}_*)^T\right] \\ &= \left[\nabla^2 I_*^N(\hat{\alpha}_*)\right]^{-1} E_*\left[\nabla L^N(\hat{\alpha}_*)\nabla L^N(\hat{\alpha}_*)^T\right]\left[\nabla^2 I_*^N(\hat{\alpha}_*)\right]^{-1}\end{aligned} \tag{4-15b}$$

It is easily verified that when $\alpha_* = \hat{\alpha}_*$,

$$E_*\left[\nabla L^N(\hat{\alpha}_*)\nabla L(\hat{\alpha}_*)^T\right] = E_*\left[\nabla^2 L^N(\hat{\alpha}_*)\right] = \nabla^2 I_*^N(\hat{\alpha}_*) \qquad (4\text{-}15c)$$

in which case (4-15a) and (4-15b) are equivalent. In general, however, (4-15b) is considerably more complicated to evaluate than (4-15a).

Steady-State Identifiability Analysis

A commonly used approximation in Kalman filter applications is to use the (constant) steady-state filter gain in place of the optimal time-varying gain. This approximation greatly reduces computational requirements for both state estimation and parameter identification in that the dominant filter gain computation need be performed only once, rather than at every measurement update. Once initial transients have subsided after a few time constants for the slowest flexible mode ($\tau_{max} = 1/(\zeta\omega)_{min} \simeq 100$ sec for the first non-isolator mode for the ACOSS II model), state estimates in either case will be the same. Assuming the identification time interval is much longer than this initial transient period, identification accuracy predictions based on steady-state analysis will closely match time-varying predictions.

The computational savings realized for steady-state identification accuracy (or identifiability) analysis is even more dramatic. Here the expected parameter estimate (4-11a) becomes

$$\hat{\alpha}_* \triangleq E_*\{\alpha\} \simeq \text{Arg}\left\{\min_{\alpha}(N+1)I^*(\alpha)\right\} = \text{Arg}\left\{\min_{\alpha} I^*(\alpha)\right\} \qquad (4\text{-}11a)'$$

where

$$I^*(\alpha) \triangleq \frac{1}{2}\log\det S + \frac{1}{2}\text{Tr}(S^{-1}S^*) \qquad (4\text{-}11b)'$$

is the (time-invariant) expected conditional log likelihood function. Thus in steady-state it suffices to minimize the conditional rather than the total expected log likelihood function, so that a factor of N savings in computational effort is realized. Note that both residual covariances in (4-11b)' are now time-invariant. That predicted by the filter (S) is obtained from the steady-state version of the Kalman filter corresponding to M_α (4-7):

$$\hat{x}_{k+1}(\alpha) = A\hat{x}_k(\alpha) + Bu_k + AKr_k(\alpha) \qquad (4\text{-}7a)'$$

$$r_k(\alpha) \triangleq y_k - \hat{y}_k \triangleq y_k - C\hat{x}_k(\alpha) \qquad (4\text{-}7b)'$$

where

$$K = \Sigma C^T S^{-1} \qquad (4\text{-}7c)'$$

$$S = C\Sigma C^T + R_d \qquad (4\text{-}7d)'$$

$$\Sigma = A\Sigma A^T + BW_dB^T - AKSK^TA^T \qquad (4\text{-}7e)'$$

Actual residual covariance (S*) is given by the steady-state version of (4-12):

$$S^* = \bar{C}\bar{X}\bar{C}^T + R_d^* \qquad (4\text{-}12b)'$$

$$\bar{X} = \bar{A}\bar{X}\bar{A}^T + \bar{B}U_d\bar{B}^T + \bar{Q} \qquad (4\text{-}12c)'$$

where

$$\bar{A} \triangleq \begin{bmatrix} A_* & 0 \\ AKC & A(I - KC) \end{bmatrix}, \quad \bar{B} \triangleq \begin{bmatrix} B_* \\ B \end{bmatrix} \qquad (4\text{-}12d)'$$

$$\bar{C} \triangleq \begin{bmatrix} C_* & -C \end{bmatrix}, \quad \bar{Q} \triangleq \begin{bmatrix} B_*W_dB_*^T & 0 \\ 0 & AKR_d^*K^TA^T \end{bmatrix} \qquad (4\text{-}12e)'$$

The minimization in (4-11a)' is now accomplished using, respectively, the gradient and NR iterations

$$\hat{\alpha}_*^{j+1} = \hat{\alpha}_*^j - \varepsilon^j \nabla I^*(\hat{\alpha}_*^j) \qquad (4\text{-}13a)'$$

and

$$\hat{\alpha}_*^{j+1} = \hat{\alpha}_*^j - [\nabla^2 I^*(\hat{\alpha}_*^j)]^{-1} \nabla I^*(\hat{\alpha}_*^j) \qquad (4\text{-}13b)'$$

while parameter error covariances for, respectively, the matched and mismatched models cases become

$$\mathrm{Cov}[\hat{\alpha}_N] \simeq \frac{1}{N+1} [\nabla^2 I^*(\hat{\alpha}_*)]^{-1} \qquad (4\text{-}15a)'$$

and

$$\text{Cov}[\alpha_N] \simeq \frac{1}{(N+1)^2}\,[\nabla^2 I^*(\hat{\alpha}_*)]^{-1} E_*[\nabla L^N(\hat{\alpha}_*)\nabla L^N(\hat{\alpha}_*)^T]\,[\nabla^2 I^*(\hat{\alpha}_*)]^{-1} \qquad (4\text{-}15b)'$$

Note that the center term of (4-15b)' involves the expected value of a product of summations. Though this term is exceedingly difficult to evaluate for the mismatched models case, it can be shown that its growth is linear in N for large N. Thus, parameter error covariance is in both cases inversely proportional to the number of measurements taken.

PRELIMINARY IDENTIFIABILITY ANALYSIS STUDIES (NASA Langley Study)

Early in this program, and in a parallel LSS identification study for NASA Langley (Ref. 14), it was recognized that, because of the large number of potential parameters, full-blown MLE identification and associated accuracy analyses, with gradient and NR parameter update loops, was not a practical possibility for LSS. Clearly some simplifications beyond the already mentioned steady-state filter gain approximation were necessary to reduce the computational load to manageable levels.

Expected Likelihood Program

In order to get some feeling for the scope of the identification problem and to test out various simplification schemes, a computer program was developed under the NASA Langley contract to evaluate the expected likelihood function $I^*(\alpha)$ as a function of modal frequency (ω_i) and damping (ζ_i) for each mode of an n-mode truth model. Modal influence coefficients (b_i and c_i) were assumed fixed for these analyses. By evaluating $I^*(\alpha)$ for a sufficiently fine sweep of the 2n-dimensional parameter vector, and locating local minima, a relatively simple procedure could be provided for steady-state identifiability analysis which avoided the formidable task of evaluating first and second partials of $I^*(\alpha)$.

The steps that this program was designed to carry out are:

1. Define continuous state-space representations (4-3) for the truth model and the identification model, parameterized by the known and unknown parameter vector α_* and α, respectively.
2. Discretize these models for some specified sample time (T).

3. Compute the discrete steady-state Kalman filter gain (K) and predicted residual covariance (S) using (4-7)'.

4. Compute the actual steady-state covariance (S*) using (4-12)'.

5. Evaluate $I^*(\alpha)$ using (4-11b)'.

These steps are repeated* for each combination of frequency (ω_i) and damping (ζ_i) for $i = 1,\ldots,n$:

$$\omega_i = \omega_{Si} + \ell_i \Delta\omega_i,\ \ell_i = 0,1,\ldots,(\omega_{Fi} - \omega_{Si})/\Delta\omega_i$$

$$\zeta_i = \zeta_{Si} + m_i \Delta\zeta_i,\ m_i = 0,1,\ldots,(\zeta_{Fi} - \zeta_{Si})/\Delta\zeta_i$$

where S and F subscripts define the range limits for the parameter sweep and $\Delta(.)$ defines the increment.

Computational Simplifications

The block-diagonal structure of truth and identification models was exploited wherever possible to minimize computational effort. Discretization of continuous state-space models was reduced to explicit evaluation of 2 x 2 matrix exponentials for each mode. One-time state-covariance evaluation for the truth model was reduced to solving $(1/2)n_*^2$ 2 x 2 algebraic Lyapunov equations (ALEs), which amounts to a factor of n_* computational savings over the general $2n_* \times 2n_*$ problem. No significant computational savings due to model structure was possible for the filter gain or 2n x 2n identification model state-covariance evaluations because the Kalman filter couples the dynamics for all states together. However, cross-covariance between the truth and identification model states was reduced to solving n_* 2 x 2n ALEs, which amounts to a factor of n_* savings for each parameter combination. When the number of modes to be identified is much less than the number present in the true system (i.e., $n << n_*$), these computational savings can be substantial.

---

*Technically, only the identification-model-dependent part is repeated. Truth model definition, discretization, and state and output covariance evaluations are performed only one time.)

Preliminary Identification Results

For purposes of illustration the program was exercised on a 14-mode truth model, which was used to represent the Shuttle orbiter, together with a payload attached to the flexible remote manipulator system arm and a one-mode identification model. Influence coefficients (b_i and c_i) for the identification model were set equal to the truth model coefficients for the first flexible mode, which occurs at $\omega^* = 0.5692$ r/s with $\zeta^* = 0.005$. For this two-parameter identification problem it is possible to plot the expected likelihood function surface versus identification model frequency and damping and examine local minima graphically. This is illustrated in Figures 4-4 through 4-6 for three cases. The first case, in Figure 4-4, is a coarse parameter sweep that reveals a local minimum (determined from numerical output) at $\omega = 0.55$ r/s and $\zeta = 0.005$, which is as close to the true values as can be expected for the coarse parameter increments used here. Although not shown here, a broader sweep in frequency reveals that local minima occur at frequencies near several of the modes of the truth model. Such minima do not occur, however, when the influence coefficients for these modes are nearly orthogonal to those assumed for the first mode.

The second case, illustrated in Figure 4-5, uses a finer sweep over a narrower parameter range than that used for the first case. It reveals a local minimum in $I^*(\alpha)$ at $\omega = 0.558$ r/s and $\zeta = 0.005$? These errors between the truth and identification model parameters are much larger than the corresponding parameter increments and correspond to relative errors of 2% in frequency and 4% in damping. Although the damping error is acceptable, the frequency error is large enough to cause potential closed-loop instabilities for control design based on the identification model. Recall that from Section 3, relative errors for critical modes should be much less than ζ(= 0.5%) for frequency and 1(= 100%) for damping to ensure closed-loop stability. The only possible explanation for these errors is the model-order mismatch between the truth and identification models, since all noise and test signal statistics for the identification model were assumed equal to those for the truth model. Evidently, the Kalman filter attempts to compensate for this mismatch by producing biases in parameters.

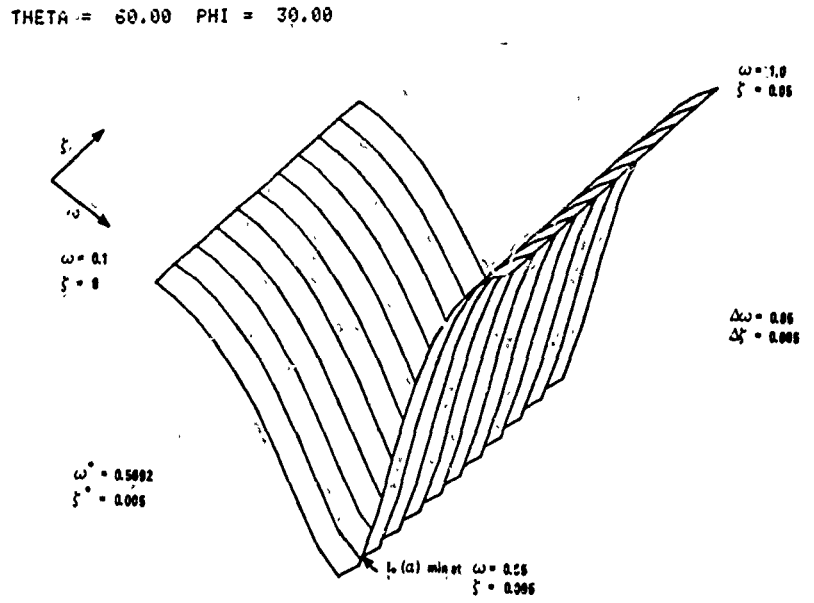

Figure 4-4. Expected Likelihood Function: Coarse Sweep

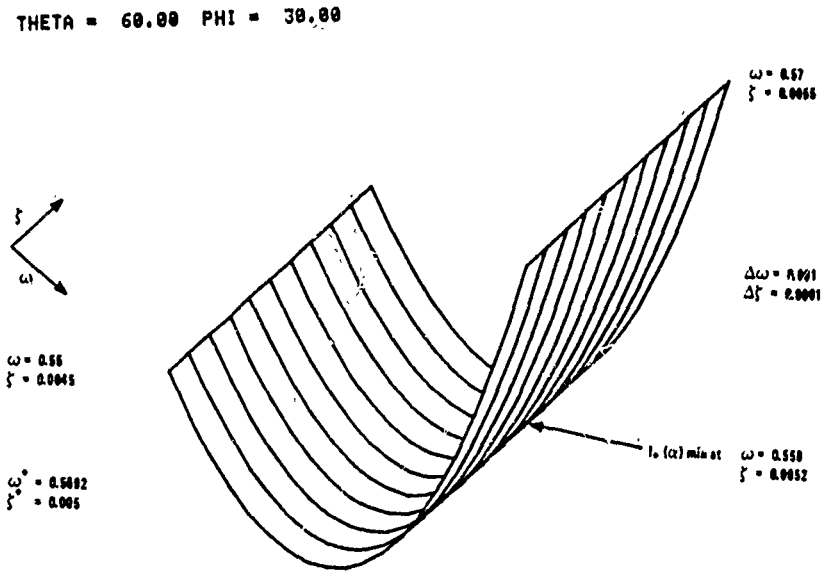

Figure 4-5. Expected Likelihood Function: Fine Sweep

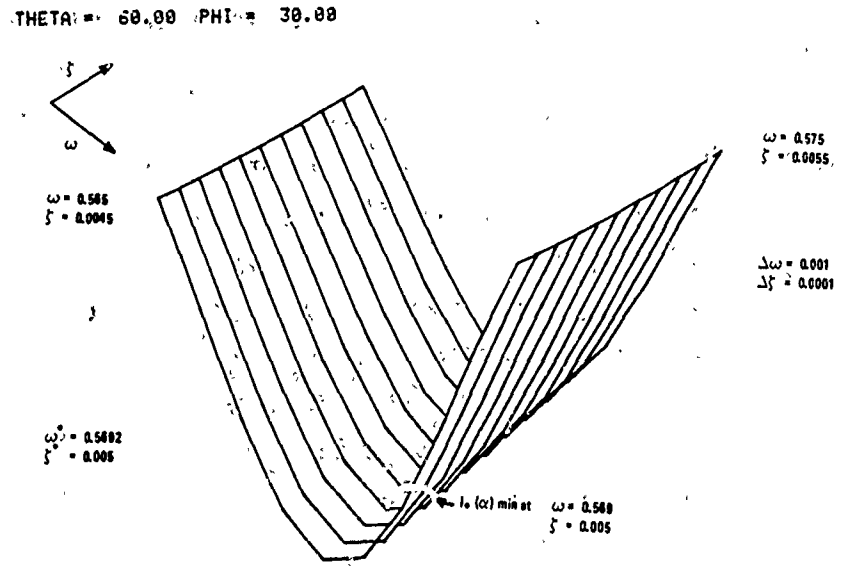

Figure 4-6. Expected Likelihood Function: Fine Sweep, No Process Noise (W = 0)

When process noise is reduced, so that filter gains approach zero, these biases disappear. The limiting case for no process noise ($W_d = 0$) is illustrated in Figure 4-6. The identification model frequency and damping which minimize $I^*(\alpha)$ for this case match the true values to within the assumed parameter increments. That is, no biases occur when the Kalman filter is absent. Furthermore, this fortuitous result has been shown to hold even under process and measurement noise mismatches, provided the Kalman filter is absent (i.e., W_d is assumed to be zero for filter design) and no correlations between the test signal and these noise sources exist.

Bias, of course, represents only one component of the identification error. The other component, stochastic error, is largely determined by the second partials matrix of $I^*(\alpha)$, which is just the "curvature" of the $I^*(\alpha)$ surface. As evident from Figures 4-4 through 4-6, the curvature in the ω-dimension is much larger than in the ζ-dimension, relative to the nominal parameter values. That is, a 10% variation in frequency produces a much larger variation in $I^*(\alpha)$ than does a 10% variation in damping. Since stochastic error is inversely proportional to this curvature, the relative error in damping after identification can be expected to be much larger than that in frequency. As might be expected

curvature increases, and thus stochastic error decreases, as process noise decreases. The same observation also applies as measurement noise decreases.

Elimination of the Kalman filter when process noise exists, however, does incur a cost in identification accuracy--an increase in stochastic error. This cannot be predicted by the curvature in $I^*(\alpha)$, because of the inherent noise mismatch between the truth model and the identification model (i.e., $W_d^* = W_d = 0$). This can only be assessed using the more general expression for stochastic error (4-15b)'. Technically this same qualification also applies to model order mismatch. Model order mismatch is, however, believed to be much less critical than noise mismatch in stochastic error evaluations. We examine the quantitative effect on identification accuracy of eliminating the Kalman filter and other simplifications in the next section.

SECTION 5

IDENTIFIABILITY ANALYSIS SIMPLIFICATIONS

Thus far, we have examined the general Kalman-filter-based MLE identification procedure and discussed appropriate methods for assessing identification accuracy for both transient and steady-state analysis. Based on the insight gained on the NASA Langley contract with the expected likelihood computer program just described, we now discuss various means of simplification for the general MLE identification method that were investigated in the current ACOSS SIXTEEN identification and control study for DARPA.

We begin by examining asymptotic characteristics of a Kalman filter for a MIMO system with only one flexible mode as the process-to-measurement-noise ratio approaches either zero or infinity. Next we examine the impact of eliminating the Kalman filter on identification and identifiability analysis. We then explore the potential for computational simplifications, which are possible once the filter is absent, due to the block-diagonal structure associated with systems in modal coordinate form. Characteristics of the "exact" identifiability analysis software, which incorporates these simplifications, are described next. Further analytical results are then presented that summarize findings on parameter convergence analyses, and the impact of various types of model mismatch on parameter biases for MLE identification with and without the Kalman filter. Next, we exploit the light damping common to flexible large space structures (LSS) to show that MLE identification can be accomplished one mode at a time with a negligible loss in identification accuracy. An approximate identification accuracy analysis program, which exploits these simplifications, is described, and a frequency domain interpretation is presented that allows a graphical assessment of approximate identifiability analysis. Finally, procedures are examined to verify closed-loop stability in the face of parameter identification errors for controllers designed for the identification model, but implemented on the true system.

ELIMINATION OF KALMAN FILTER

In order to determine conditions under which the Kalman filter can be eliminated, we examine the filter gain and estimation error for a model with a single mode, but several inputs and outputs. For simplicity we work with the continuous case, recognizing that conclusions drawn for this case will carry over to the discrete case for sufficiently high sample rates. Thus we assume a model of the form

$$\dot{x} = \frac{d}{dt}\begin{bmatrix} x_1 \\ x_2 \end{bmatrix} = \begin{bmatrix} 0 & 1 \\ -\omega_o^2 & -2\zeta_o\omega_o \end{bmatrix}\begin{bmatrix} x_1 \\ x_2 \end{bmatrix} + \begin{bmatrix} 0 \\ b^T \end{bmatrix}(u + w) \triangleq Fx + G(u + w) \tag{5-1a}$$

$$y = [c \quad 0]\begin{bmatrix} x_1 \\ x_2 \end{bmatrix} + v \triangleq Cx + v \tag{5-1b}$$

with corresponding transfer function,

$$G_i(j\omega) = \frac{cb^T}{\omega_o^2 - \omega^2 + j2\zeta_o\omega_o\omega} \tag{5-1c}$$

The vectors u, v, and w are assumed to be uncorrelated white noise processes with zero mean and spectral intensities U, R, and W, respectively.

The continuous Kalman filter for this system is given by

$$\dot{\hat{x}} = F\hat{x} + Gu + K(y - C\hat{x}) \tag{5-2a}$$

where

$$K \triangleq PC^TR^{-1} = \frac{p}{c^TR^{-1}c}\begin{bmatrix} 1 \\ \frac{1}{2}p \end{bmatrix} c^TR^{-1} \tag{5-2b}$$

$$P = \frac{p}{c^TR^{-1}c}\begin{bmatrix} 1 & \frac{1}{2}p \\ \frac{1}{2}p & \frac{1}{2}\left(p^2 + 2\zeta_o\omega_o p + 2\omega_o^2\right) \end{bmatrix} \tag{5-2c}$$

with

$$p = -2\zeta_o\omega_o + \sqrt{(2\zeta_o\omega_o)^2 + 2\left(\sqrt{\omega_o^4 + b^TWbc^TR^{-1}c} - \omega_o^2\right)} \tag{5-2d}$$

We now examine this filter under two extreme noise assumptions. The noise conditions that define these cases can be stated in terms of a weighted singular-value test applied to the transfer function evaluated at some frequency.

Small Process-to-Measurement-Noise Ratio

The general condition that defines this case,

$$\bar{\sigma}\left[R^{-1/2}G_i(j\omega_o)W^{1/2}\right] = \frac{\sqrt{b^T W b c^T R^{-1} c}}{2\zeta_o\omega_o^2} << 1 \qquad (5\text{-}3)$$

may be simplified when $W = W_o I$ and $R = R_o I$ to give

$$\bar{\sigma}(G_i(j\omega_o)) << \sqrt{R_o/W_o} \qquad (5\text{-}3)'$$

which says that the magnitude of the transfer function evaluated at the mode frequency is much less than the square root ratio of measurement to process noise. For this case it is readily shown that the following approximations hold (to first order in p):

$$p \simeq \frac{b^T W b\ c^T R^{-1} c}{4\zeta_o\omega_o^3} << \zeta_o\omega_o \qquad (5\text{-}4a)$$

$$P \simeq \frac{b^T W b}{4\zeta_o\omega_o^3}\begin{bmatrix} 1 & 0 \\ 0 & \omega_o^2 \end{bmatrix} \to 0 \text{ as } W \to 0 \qquad (5\text{-}4b)$$

$$K \simeq \frac{b^T W b}{4\zeta_o\omega_o^3}\begin{bmatrix} c^T R^{-1} \\ 0 \end{bmatrix} \to 0 \text{ as } W \to 0 \text{ (or } R \to \infty) \qquad (5\text{-}4c)$$

Large Process-to-Measurement-Noise Ratio

The condition that defines this case,

$$\bar{\sigma}\left[R^{-1/2}G_i(j\omega_o)W^{1/2}\right] = \frac{\sqrt{b^T W b c^T R^{-1} c}}{2\zeta_o\omega_o^2} \gg 1/2\zeta_o \qquad (5\text{-}5)$$

may be simplified when $W = W_o I$ and $R = R_o I$ to give

$$\bar{\sigma}(G_i(j\omega_o)) \gg \sqrt{R_o/W_o}\,/2\zeta_o \qquad (5\text{-}5)$$

which says that the magnitude of the transfer function evaluated at the mode frequency is much greater than the square-root ratio of measurement to process noise divided by $2\zeta_o$.* For this case we have

$$p \simeq \sqrt{2}\ \sqrt[4]{b^T W b c^T R^{-1} c} \gg \sqrt{2\,\omega_o} \qquad (5\text{-}6a)$$

$$p \simeq \frac{1}{c^T R^{-1} c}\begin{bmatrix} p & \frac{1}{2}p^2 \\ \frac{1}{2}p^2 & \frac{1}{2}p^3 \end{bmatrix} \begin{matrix} \to \infty & \text{as } W \to \infty \\ \to 0 & \text{as } R \to 0 \end{matrix} \qquad (5\text{-}6b)$$

$$K \simeq \frac{1}{c^T R^{-1} c}\begin{bmatrix} \sqrt{2}\ \sqrt[4]{b^T W b c^T R^{-1} c} \\ \sqrt{b^T W b c^T R^{-1} c} \end{bmatrix} \quad c^T R^{-1} \to \infty \text{ as } W \to \infty \text{ (or } R \to 0) \qquad (5\text{-}6c)$$

These two cases illustrate the asymptotic properties of the Kalman filter under two important noise assumptions. The first case shows that both filter gains and the estimation error approach zero as $W \to 0$. More important, it is apparent that the estimation error for this low-gain filter is to first order in p the same as that for a zero-gain filter. Thus the Kalman filter may safely be eliminated for this case with no apparent degradation in estimation or identification performance. The second case yields a high-gain Kalman filter. In the limit as $W \to \infty$ (or $R \to 0$) the filter may (ideally) be eliminated and the measurements differentiated repeatedly to generate estimates for position and rate states, and accelerations as well. Parameters may then be estimated using the classical least-squares method. There is also a third case, intermediate to these two extreme cases, but of no particular interest here. It can be shown further that conditions for the first case also apply for rate measurements if we replace

*The above conditions may also be defined in terms of the magnitude of G_i at zero frequency, but the definitions here are easier to verify graphically.

R_o by R_1/ω^2 or for process noise due to Test Signal 2 if we replace W_o by $W_2\omega^2$. Similar results are expected to hold for other process/measurement noise combinations.

Applicability to ACOSS II Model

To establish which, if either, of the limiting cases apply for this problem, we re-examine the singular-value plots for $G(j\omega)$ for the two identification concepts in Figures 5-1 and 5-2, assuming position measurements and Test Signal 1. Superimposed on each of these plots we have shown $\sqrt{R_1/U_1}$, $\sqrt{R_1/W_1}$, and $\sqrt{R_1/W_1}$ / $2\zeta_o$ for $W_1 = 0.01U_1$, $2\zeta_o = 0.01$. For the baseline concept we find that only the last four modes satisfy the first condition (5-3)', while none satisfy the second condition (5-5)'. The first six modes lie intermediate to the two conditions. Thus identification without the Kalman filter is "optimal" only for the last four modes. For the advanced concept, all but four modes satisfy the first condition, so that identification without the Kalman filter is "optimal" for all but these modes.

These comparisons, however, point up a fundamental conflict between the desire for large test signals for which

$$\bar{\sigma}(G(j\omega)) >> \sqrt{R_1/U_1}$$

and small process noise for which

$$\bar{\sigma}(G(j\omega)) << \sqrt{R_1/W_1} = 10\sqrt{R_1/U_1}$$

This conflict becomes even more severe for the smaller high-frequency measurement noise associated with rate and acceleration measurements, as well as for the larger high-frequency process noise associated with Test Signal 2. For the recommended test signal/measurement combinations given earlier in Table 3-2 for the two concepts, these analyses tend to favor the use of the Kalman filter for identification (or least-squares estimation when $R/W \to 0$). Thus, there will be a stochastic error performance penalty associated with identification without the Kalman filter. But this penalty must be balanced against the increased susceptibility of Kalman-filter-based identification to bias errors under model order

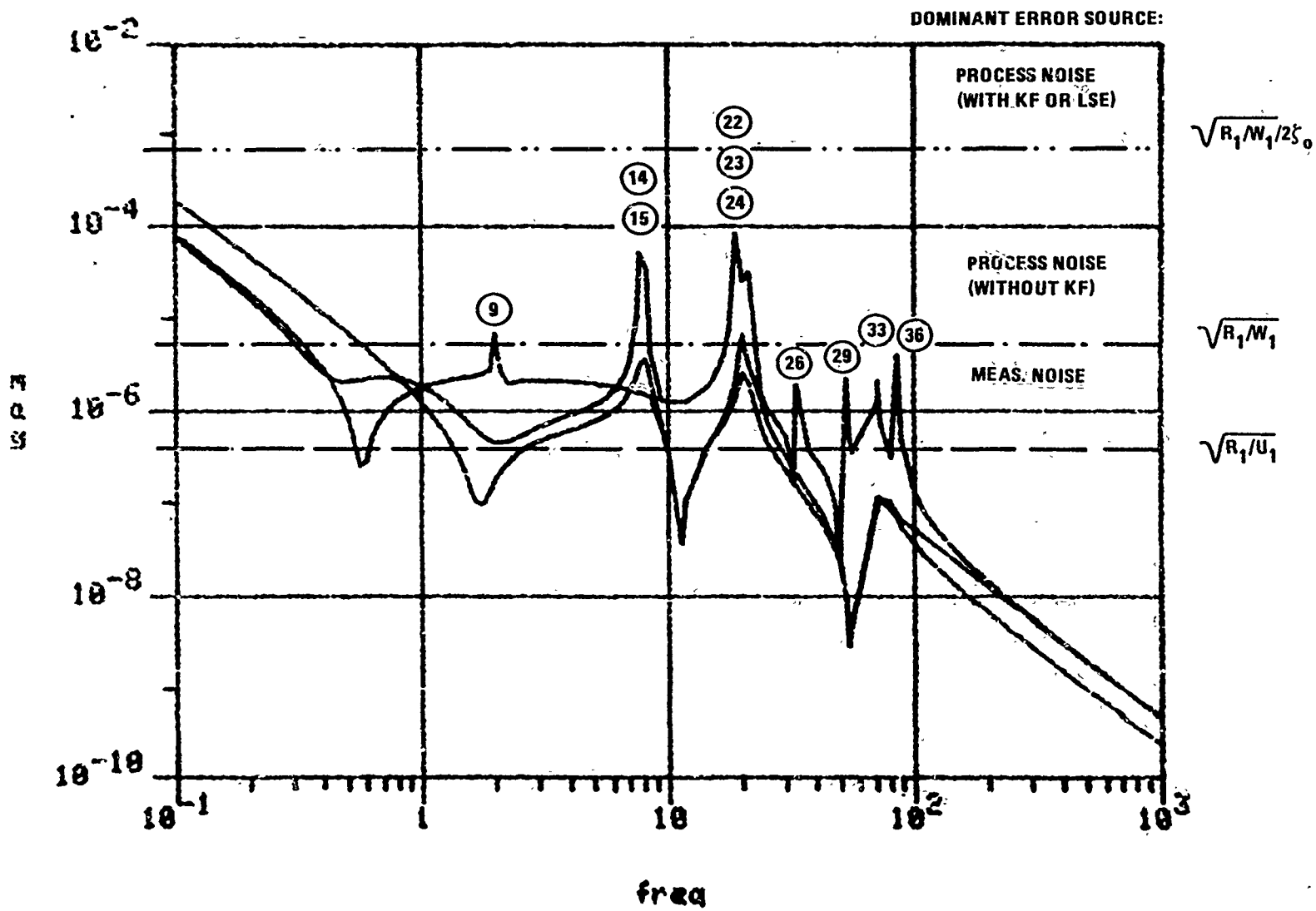

Figure 5-1. Process Noise Limitations for Baseline Concept: Position Measurements, Test Signal 1

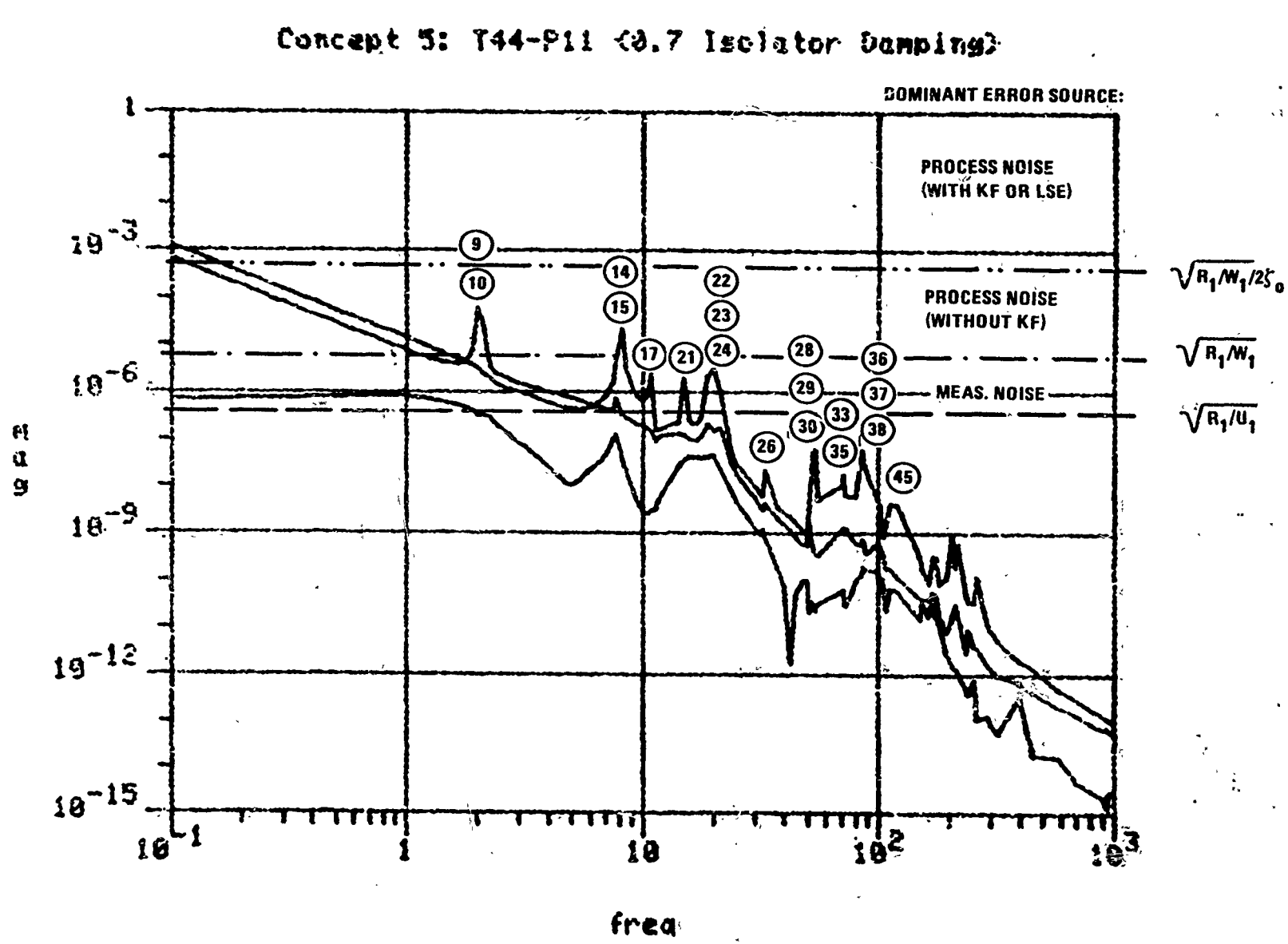

Figure 5-2. Process Noise Limitations for Advanced Concept: Position Measurements, Test Signal 1

mismatch observed in Section 4 and examined analytically later in this section. More detailed analyses have shown that the stochastic error penalty is the lesser of the two evils. Therefore, the Kalman filter was eliminated.

IDENTIFIABILITY ANALYSIS WITHOUT KALMAN FILTER

When the Kalman filter is eliminated, evaluation of the expected likelihood function and its partials is greatly simplified.

Expected Likelihood Function

Since $K = \Sigma = 0$ implies $S = R_d$, the general equations for the expected likelihood function simplify to

$$I^*(\alpha) \triangleq \frac{1}{2}\log \det R_d + \frac{1}{2}\mathrm{Tr}\ (R_d^{-1}S^*) \tag{5-7a}$$

where

$$S^* = C_*X_*C_*^T + CXC^T - CMC_*^T - C_*M^TC^T + R_d^* \tag{5-7b}$$

is the actual residual-error covariance, and

$$X_* = A_*X_*A_*^T + B_*U_dB_*^T + B_*W_d^*B_*^T \tag{5-8a}$$

$$X = AXA^T + BU_dB^T \tag{5-8b}$$

$$M = A_*MA^T + B_*U_dB^T \tag{5-8c}$$

are the now uncoupled state covariance equations for the partitioned system, where

$$\bar{X} \triangleq E_*\left\{\begin{bmatrix} x_k^* \\ x_k \end{bmatrix}\begin{bmatrix} x_k^{*T} & x_k^T \end{bmatrix}\right\} \triangleq \begin{bmatrix} X_* & M \\ M^T & X \end{bmatrix}$$

defines the partitioned covariance matrix. Note that we have dropped the $\hat{}$ symbol in $\hat{x}_k$ for $K = 0$. Note also that the original $2(n_* + n) \times 2(n_* + n)$ ALE for state covariance has been reduced to three independent ALEs of dimensions $2n_* \times 2n_*$, $2n \times 2n$, and $2n_* \times 2n$, for a net computational savings of as much as a factor of 2.

For sufficiently high sample rates, such that $|\omega_i T| << 1$ for each mode, and consequently

$$A_* \simeq I + F_* T, \quad B_* \simeq G_* T, \quad W_d^* = W_*/T, \quad R_d^* = R^*/T \tag{5-9a}$$

$$A \simeq I + FT, \quad B \simeq GT, \quad W_d = W/T, \quad R_d = R/T, \quad U_d = U/T \tag{5-9b}$$

we can replace discrete-time ALEs by their continuous-time equivalents,

$$F_* X_* + X_* F_*^T + G_* U G_*^T + G_* W G_*^T = 0 \tag{5-10a}$$

$$FX + XF^T + GUG^T = 0 \tag{5-10b}$$

$$F_* M + M F^T + G_* U G^T = 0 \tag{5-10c}$$

The main advantage of these continuous-time equations is that partials of F and G with respect to the parameters ω_i, ζ_i, and b_i are much easier to compute (analytically) than are partials of their exact discrete-time counterparts,

$$A = e^{FT}, \quad B = F^{-1}(I - e^{FT})G$$

Partials of C with respect to c_i are the same in either case. The requirement $|\omega_i T| << 1$ is not a severe one, since identification of modal frequency and damping must ultimately require several samples per cycle. Moreover, this requirement is consistent with sample-rate requirements for digital control of flexible modes.

First and Second Partials

Partials of the expected likelihood function $I^*(\alpha)$ with respect to the parameters can now be taken with relative ease. For the first partial with respect to the p^{th} element of α, we have (from 5-7a) assuming R_d is constant:

$$\nabla_p I^*(\alpha) = \frac{1}{2} \mathrm{Tr}\left[R_d^{-1} \nabla_p S^*\right] \tag{5-11a}$$

while the second partial with respect to the p^{th} and q^{th} element is given by

$$\nabla_{pq}^2 I^*(\alpha) = \frac{1}{2} \mathrm{Tr}\left[R^{-1} \nabla_{pq}^2 S^*\right] \tag{5-11b}$$

Partials of S^* and, in turn, M and X in (5-7), and expected parameter update iterations (4-13)' are now relatively straightforward, albeit tedious, to carry out. But the computational requirements to do so are still of order $N_p(n_* + n)^3$ for each gradient parameter update and $N_p^2(n_* + n)^3$ for each NR parameter update. Thus simplifications to reduce computational requirements are still desirable.

Parameter Error Covariance

Similarly, parameter error covariance evaluations for the mismatched models case simplify somewhat when $S = R_d$ is constant. The difficult center term in (4-15b)' now becomes

$$\tilde{I}^*_{pq} = E_* \left\{ \nabla_p L^N(\alpha_*) \nabla_q L^N(\alpha_*) \right\} \tag{5-12a}$$

$$= \sum_{k=0}^{N} \sum_{\ell=0}^{N} E_* \left\{ r_k^T R_d^{-1} \nabla_p r_k r_\ell^T R_d^{-1} \nabla_q r_\ell \right\}$$

$$= \sum_{k=0}^{N} \sum_{\ell=0}^{N} \mathrm{Tr}\left[R_d^{-1} S^*_{rr}(\ell - k) \right] \mathrm{Tr}\left[R_d^{-1} S^*_{\nabla_p r \nabla_q r}(\ell - k) \right]$$

$$\approx (N+1) \sum_{\ell-k=-\infty}^{\infty} \mathrm{Tr}\left[R_d^{-1} S^*_{rr}(\ell - k) \right] \mathrm{Tr}\left[R_d^{-1} S^*_{\nabla_p r \nabla_q r}(\ell - k) \right]$$

where

$$S^*_{rr}(\ell - k) \triangleq E_* \left\{ r_\ell r_k^T \right\} \tag{5-12b}$$

$$S^*_{\nabla_p r \nabla_q r}(P - k) \triangleq E_* \left\{ \nabla_p r_\ell \nabla_q r_k^T \right\} \tag{5-12c}$$

are, respectively, the auto-correlation function of the residual r and the cross-correlation function of its partials $\nabla_p r$ and $\nabla_q r$. Note that the third equality in (5-12a) holds only when $\alpha = \hat{\alpha}_*$, where $I^*(\alpha)$ is minimized and $\nabla_* I(\hat{\alpha}_*) = 0$. The approximate equality, which applies only for $N >> 1$, exploits the fact that for stable A_* and A the correlation functions approach zero (exponentially) as $|\ell - k| \to \infty$, so that the doubly infinite summation has a

limit. Note also that, in general, the order of differentiation and expectation is important in (5-12c) since

$$\nabla^2_{pq} S^*_{rr}(\ell - k) \triangleq \nabla^2_{pq} E_*\left\{r_\ell r_k^T\right\} \tag{5-13}$$

$$= E_*\left\{\nabla^2_{pq}\left[r_\ell r_k^T\right]\right\}$$

$$= S^*_{\nabla_p r \nabla_q r}(\ell - k) + S^*_{\nabla_q r \nabla_p r}(\ell - k)$$

$$+ S^*_{r \nabla^2_{pq} r}(\ell - k) + S^*_{\nabla^2_{pq} rr}(\ell - k)$$

Thus, the direct approach for evaluating $\nabla_p I^*$ and $\nabla^2_{pq} I^*$ is not compatible with that required to evaluate $\tilde{I}^*_{pq}$.

The correlation functions in (5-12) can be generated from the cross-covariance matrix for two $2(n_* + 2n)$-dimensional augmented-state vectors $x_p^T = (x^{*T}, x^T, \nabla_p x^T)$, and $x_q^T = (x^{*T}, x^T, \nabla_q x^T)$ to give

$$S^*_{rr}(\ell - k) = C_o X_o(\ell - k) C_o^T + R^*_d \delta_{k\ell} \tag{5-14a}$$

$$S^*_{\nabla_p r \nabla_q r}(\ell - k) \triangleq C_p X_o(\ell - k) C_q^T \tag{5-14b}$$

where

$$X_o(\ell - k) \triangleq E_*\left\{x_{p\ell} x_{qk}^T\right\} = \begin{cases} e^{F_p(\ell - k)T} X_o & \ell \geq k \\ X_o e^{F_q^T(k - \ell)T} & \ell \leq k \end{cases} \tag{5-14c}$$

is the cross-correlation function for the states, and

$$F_p X_o + X_o F_q^T + G_p U G_q^T + G_o W G_o^T = 0 \tag{5-14d}$$

defines the cross-covariance $X_o = E_*\left\{x_{pk} x_{qk}^T\right\}$. Here

$$F_p \triangleq \begin{bmatrix} F_* & 0 & 0 \\ 0 & F & 0 \\ 0 & \nabla_p F & F \end{bmatrix}, \quad F_q \triangleq \begin{bmatrix} F_* & 0 & 0 \\ 0 & F & 0 \\ 0 & \nabla_q F & F \end{bmatrix} \tag{5-15}$$

$$G_o \triangleq \begin{bmatrix} G_* \\ 0 \\ 0 \end{bmatrix}, \quad G_p \triangleq \begin{bmatrix} G_* \\ G \\ \nabla_p G \end{bmatrix}, \quad G_q \triangleq \begin{bmatrix} G_* \\ G \\ \nabla_q G \end{bmatrix}$$

$$C_o \triangleq [C_* \quad -C \quad 0]$$

$$C_p \triangleq [0 \quad -\nabla_p C \quad -C]$$

$$C_q \triangleq [0 \quad -\nabla_q C \quad -C]$$

For the SISO case $\tilde{I}^*_{pq}$ may, when $|\omega_i T| << 1$ for all modes, be approximated further to give

$$\tilde{I}^*_{pq} = \frac{N+1}{R_d^2} \sum_{\ell-k=-\infty}^{\infty} {}^*S_{rr}(\ell-k)\, {}^*S_{\nabla_p r \nabla_q r}(\ell-k) \tag{5-16a}$$

$$\approx (N+1)\frac{R_d^*}{R_d^2} S^*_{\nabla_p r \nabla_q r}(0)$$

$$+ (N+1)\frac{2}{R^2 T}\int_0^\infty C_o X_o e^{F_q^T t} C_o^T C_p e^{F_p t} X_o C_q^T dt$$

$$= (N+1)\frac{R_d^*}{R_d^2} S^*_{\nabla_p r \nabla_q r}(0) + (N+1)\frac{2}{R_d^2 T} C_o X_o H_o X_o C_q^T$$

where H_o is the solution to the $2(n_* + 2n)$-dimensional adjoint Lyapunov equation

$$F_q^T H_o + H_o F_p^T + C_o^T C_p = 0 \tag{5-16b}$$

A similar but more complicated approximation for $\tilde{I}^*_{pq}$ holds for the MIMO case as well. When the only mismatch between the truth and identification models is due to process noise, the first term in (5-16a) becomes

$$(N+1)\nabla^2_{pq} I(\hat{\alpha}_*)$$

Thus when $\tilde{I}^*$ is substituted into (4-15b)', this first term gives the usual stochastic error due to measurement noise R predicted for the matched models case (4-15a)', while the second term gives the correction due to process noise W_*.

SIMPLIFICATIONS DUE TO DIAGONAL STRUCTURE

Now that the Kalman filter is absent, the block-diagonal nature of both the truth and identification models may be used to full advantage.

Expected Likelihood Function

The expected likelihood function for this case can be simplified to give (in view of (4-3))

$$I^*(\alpha) = \frac{1}{2}\left\{\log\det(R/T) + \mathrm{Tr}(R^{-1}R_*)\right\} \qquad (5\text{-}17)$$

$$+ \frac{T}{2}\sum_{i,j\in J^*}\left(\beta^*_{ij} + \gamma^*_{ij}\right)e_1^T X^*_{ij} e_1 + \frac{T}{2}\sum_{i,j\in J}\beta_{ij}e_1^T X_{ij} e_1$$

$$-T\sum_{\substack{i\in J^*\\ j\in J}}\beta^c_{ij}e_1^T M_{ij} e_1$$

where

$$F_i^* X_{ij}^* + X_{ij}^* F_j^{*T} + e_2 e_2^T = 0, \qquad i,j\in J^* \qquad (5\text{-}18a)$$

$$F_i X_{ij} + X_{ij} F_j^T + e_2 e_2^T = 0, \qquad i,j\in J \qquad (5\text{-}18b)$$

$$F_i^* M_{ij} + M_{ij} F_j^T + e_2 e_2^T = 0, \qquad i\in J^*, j\in J \qquad (5\text{-}18c)$$

are "normalized" 2 x 2 covariance equations relating the i^{th} and j^{th} modes of the truth and identification models, with the definitions

$$E_*\left\{\begin{bmatrix} x_i^* \\ x_i \end{bmatrix}\begin{bmatrix} x_j^{*T} & x_j^T \end{bmatrix}\right\} \triangleq \begin{bmatrix} b_i^{*T}(U + W_*)b_j^* X_{ij}^* & b_i^{*T}Ub_j M_{ij} \\ b_i^T Ub_j^* M_{ij}^T & b_i^T Ub_j X_{ij} \end{bmatrix} \tag{5-19}$$

$$F_i^* \triangleq \begin{bmatrix} 0 & 1 \\ -\omega_i^{*2} & -2\zeta_i^*\omega_i^* \end{bmatrix} \quad i\in J^*$$

$$F_i \triangleq \begin{bmatrix} 0 & 1 \\ -\omega_i^2 & -2\zeta_i\omega_i \end{bmatrix} \quad i\in J$$

$$\gamma_{ij}^* \triangleq c_i^{*T}R^{-1}c_j^* b_i^{*T}W_* b_j^* \qquad i,j\in J^*$$

$$\beta_{ij}^* \triangleq c_i^{*T}R^{-1}c_j^* b_i^{*T}Ub_j^* \qquad i,j\in J^*$$

$$\beta_{ij} \triangleq c_i^T R^{-1}c_j b_i^T Ub_j \qquad i,j\in J$$

$$\beta_{ij}^c \triangleq c_i^{*T}R^{-1}c_j b_i^{*T}Ub_j \qquad i\in J^*, j\in J$$

$$e_1^T \triangleq (1 \;\; 0), \; e_2^T \triangleq (0 \;\; 1)$$

$$J^* \triangleq \{1,2,\ldots,n_*\}, \; J \triangleq \{1,2,\ldots,n\}$$

These equations follow from (5-7) and (5-10) by inspection. Normalized covariance equations (5-18) are employed for convenience, to eliminate the dependence of M_{ij} and X_{ij} on the parameters b_i and b_j, thus simplifying subsequent evaluation of partials with respect to the parameters. By exploiting the diagonal structure of F_* and F we have reduced computational effort in evaluating $I^*(\alpha)$ to that of solving $(1/2)(n_* + n)^2$ 2 x 2 ALEs, for a net savings of $(n_* + n)$ over the general nondiagonal case. Moreover, exact analytical solutions for these 2 x 2 ALEs are readily derived, so that numerical evaluation of $I^*(\alpha)$ can be reduced to summing up a series of exact Lyapunov-equation solutions that are each evaluated numerically at the current parameter values.

First and Second Partials

Partial derivatives of the expected likelihood function are now trivial to evaluate. For the first partial with respect to the p^{th} element of the parameter vector α, we have (since R and R_* are constant;)

$$\nabla_p I^*(\alpha) = \frac{T}{2} \sum_{i,j\in J} \left\{ \beta_{ij} e_1^T \nabla_p X_{ij} e_1 + \nabla_p \beta_{ij} e_1^T X_{ij} e_1 \right\} \tag{5-20}$$

$$-T \sum_{\substack{i\in J^* \\ j\in J}} \left\{ \beta^c_{ij} e_1^T \nabla_p M_{ij} e_1 + \nabla_p \beta^c_{ij} e_1^T M_{ij} e_1 \right\}$$

where

$$F_i \nabla_p X_{ij} + \nabla_p X_{ij} F_j^T + X_{ij} \nabla_p F_j^T + \nabla_p F_i X_{ij} = 0 \tag{5-21a}$$

$$F_i^* \nabla_p M_{ij} + \nabla_p M_{ij} F_j^T + M_{ij} \nabla_p F_j^T = 0 \tag{5-21b}$$

Similarly, for the second partial with respect to the p^{th} and q^{th} element of α, we have

$$\nabla^2_{pq} I^*(\alpha) = \frac{T}{2} \sum_{i,j\in J} \left\{ \beta_{ij} e_1^T \nabla^2_{pq} X_{ij} e_1 + \nabla^2_{pq} \beta_{ij} e_1^T X_{ij} e_1 \right. \tag{5-22}$$

$$\left. + \nabla_p \beta_{ij} e_1^T \nabla_q X_{ij} e_1 + \nabla_q \beta_{ij} e_1^T \nabla_p X_{ij} e_1 \right\}$$

$$- T \sum_{\substack{i\in J^* \\ j\in J}} \left\{ \beta^c_{ij} e_1^T \nabla^2_{pq} M_{ij} e_1 + \nabla^2_{pq} \beta^c_{ij} e_1^T X_{ij} e_1 \right.$$

$$\left. + \nabla_p \beta^c_{ij} e_1^T \nabla_q M_{ij} e_1 + \nabla_q \beta^c_{ij} e_1^T \nabla_p M_{ij} e_1 \right\}$$

where

$$F_i \nabla^2_{pq} X_{ij} + \nabla^2_{pq} X_{ij} F_j^T + \nabla_p X_{ij} \nabla_q F_j^T + \nabla_q F_i \nabla_p X_{ij} \tag{5-23a}$$

$$+ \nabla_q X_{ij} \nabla_p F_j^T + \nabla_p F_i \nabla_q X_{ij} = 0$$

$$F_i^* \nabla^2_{pq} M_{ij} + \nabla^2_{pq} M_{ij} F_j^T + \nabla_p M_{ij} \nabla_q F_j^T + \nabla_q M_{ij} \nabla_p^T F_j = 0 \tag{5-23b}$$

These equations assume that $\nabla^2_{pq} F_i = 0$, which will be true if we choose ω_i^2 and $2\zeta_i\omega_i$ as parameters rather than ω_i and ζ_i. This choice also simplifies the structure of the partial derivative equations for M_{ij} and X_{ij}. Though these partials still appear formidable, it should be noted that the driving terms in $\nabla_p I^*$ are nonzero only when the p^{th} parameter corresponds to either the i^{th} or j^{th} mode. Similarly, the driving terms in $\nabla^2_{pq} I^*$ are nonzero only when either the p^{th} or q^{th} parameter corresponds to either the i^{th} or j^{th} mode. Thus it is possible to

sum up the contributions to I^*, $\nabla_p I^*$, and $\nabla^2_{pq} I^*$ all within the same i,j double loop. Moreover, outside of that required for a few 2 x 2 matrices, the only storage required is the $N_p^2 + N_p + 1$ elements needed to store the final results--I^*, ∇I^*, and $\nabla^2 I^*$.

Computational Requirements

Computational requirements necessary to make one parameter update iteration, in terms of both the number of 2 x 2 ALEs and the number of multiplies, can be summarized as shown in Table 5-1 (assuming 16 multiplies per 2 x 2 ALE).

TABLE 5-1. COMPUTATIONAL REQUIREMENTS FOR EXACT IDENTIFIABILITY ANALYSIS

Evaluation	Number of 2 x 2 ALEs	Approximate Number of Multiplies
Likelihood: I^*	$(1/2)(n_* + n)^2$	$8(n_* + n)^2$
Gradient: ∇I^*	$2n(n_* + n)$	$32n(n_* + n)$
Hessian: $\nabla^2 I^*$	$4n(n_* + n)$	$64n(n_* + n)$
NR: $(\nabla^2 I^*)^{-1}\nabla^* I$	---	$(1/3)[(n_o + n_i + 1)n]^3$
Total/Iteration	$(1/2)(n_* + n)(n_* + 13n)$	$8(n_* + n)(n_* + 13n)$ $+ (1/3)(n_o + n_i + 1)^3 n^3$

Thus, not counting the NR update itself, computational requirements for identifiability analysis without the Kalman filter for systems in block-diagonal modal form is of order $n(n_* + n)$ per iteration, which represents an $n(n_* + n)^2$

savings over the general nondiagonal case. Note that identification of influence coefficients (b_i and c_i) for each mode does not increase the number of ALEs to be solved since these parameters appear only in the coefficents β_{ij} and β^c_{ij} of $I^*(\alpha)$. Therefore, they have negligible impact on computational requirements, assuming the number of system inputs and outputs is small compared to the number of modes. When the NR update is included, however, total computational requirements are dominated by the Hessian matrix inversion, which is of order n^3.

The diagonal structure of F^* and F can also be used to simplify expressions of (5-14d) and (5-16) for $\tilde{I}^*$, which is needed for parameter error covariance evaluations in the mismatched models case. Unfortunately, these simplifications do not lead to as simple results for $\tilde{I}^*$ as they do for I^* and its partials. Thus, we will pursue them no further here.

Rate and Acceleration Measurements and Test Signal 2

The setup just described applies only for position measurements with Test Signal 1. For rate measurements we need only replace e_1 by e_2 in (5-17) through (5-23) to select the second state as the output and replace $R_o = R_1$ by $R_o = R_2$. Results for acceleration measurements, however, are a bit more involved.

For this case we must replace $R_o = R_1$ by $R_o = R_3$ and make the following substitutions in (5-17):

$$e_1^T X^*_{ij} e_1 \leftarrow d_i^{*T} X^*_{ij} d_j^* + 1/T \tag{5-24a}$$

$$e_1^T X_{ij} e_1 \leftarrow d_i^T X_{ij} d_j + 1/T \tag{5-24b}$$

$$e_1^T M_{ij} e_i \leftarrow d_i^{*T} M_{ij} d_j + 1/T \tag{5-24c}$$

where

$$d_i^{*T} \triangleq \begin{bmatrix} -\omega_i^{*2} & -2\zeta_i^*\omega_i^* \end{bmatrix} \tag{5-25a}$$

$$d_i^T \triangleq \begin{bmatrix} -\omega_i^2 & -2\zeta_i\omega_i \end{bmatrix} \tag{5-25b}$$

define the second rows of F_i^* and F_i, respectively. Because d_i is a function of the parameters, additional terms arise when the gradient vector and Hessian matrix are evaluated in (5-20) and (5-22). Although these steps would be relatively straightforward to carry out, they have not been implemented in the current version of the software.

Since Test Signal 2 implies another level of differentiation, the setup for position and rate measurements with Test Signal 2 is identical to that for, respectively, rate and acceleration measurements with Test Signal 1, except that $U_o = U_1$ and $W_o = W_1$ are replaced by $U_o = U_2$ and $W_o = W_2$. Test Signal 2 with acceleration measurements, however, cannot be accommodated in the current version of the software.

Exact Identification Analysis Software

A computer program was developed to compute identification systematic and stochastic errors for the parameters of an $n_o \times n_i$ transfer function matrix G(s) of the following form

$$G(s) = \sum_{i=1}^{n} \frac{c_i b_i^T}{s^2 + 2\zeta_i \omega_i s + \omega_i^2} \qquad (5\text{-}26a)$$

where the true system is

$$G_*(s) = \sum_{i=1}^{n_*} \frac{c_{i*} b_i^T}{s_*^2 + 2\zeta_i^* \omega_i^* s + \omega_i^{*2}} \qquad (5\text{-}26b)$$

The parameters are the natural frequency, ω_i, damping ratio, ζ_i, the n_o elements of the output influence vector, c_i, and the n_i elements of the input influence vector, b_i, for each of the n (n need not equal n_*) modes. These parameters are not all independent, as illustrated in the following cases:

Case 1: SISO ($n_i = n_o = 1$)
Only the product $c_i b_i$ is an independent parameter.

Case 2: ILAS ($b_i = c_i$)

Only the elements of one of the vectors are independent.

Case 3: Non-ILAS ($b_i \neq c_i$)

Only the directions of b_i and c_i and the product of their magnitudes are independent parameters, hence only $n_i + n_o - 1$ of the $n_i + n_o$ elements of the b_i and c_i vectors are independent.

The appropriate independent parameters are arranged into a parameter vector α as follows for these three cases.

Case 1: $\alpha^T = \left[\omega_1^2, 2\zeta_1\omega_1, c_1 b_1, \omega_2^2, 2\zeta_2\omega_2, c_2 b_2, \ldots, \omega_n^2, 2\zeta_n\omega_n, c_n b_n\right]$

where α is a $3n \times 1$ vector

Case 2: $a^T = \left[\omega_1^2, 2\zeta_1\omega_1, b_1^T, \omega_2^2, 2\zeta_2\omega_2, b_2^T, \ldots, \omega_n^2, 2\zeta_n\omega_n, b_n^T\right]$

where $c_i = b_i$ and α is a $(2 + n_i)n \times 1$ vector

Case 3: $\alpha^T = \left[\omega_1^2, 2\zeta_1\omega_1, \tilde{b}_1^T, \tilde{c}_1^T, \omega_2^2, 2\zeta_2\omega_2, \tilde{b}_2^T, \tilde{c}_2^T, \ldots, \omega_n^2, 2\zeta_n\omega_n, \tilde{b}_n^T, \tilde{c}_2^T\right]$

where either: $\tilde{b}_i = b_i$ and $\tilde{c}_i = c_i$ without the M^{th} element (i.e., eliminate the M^{th} element of c_i)

or: $\tilde{b}_i = b_i$ without the L^{th} element (i.e., eliminate the L^{th} element of b_i), and $\tilde{c}_i = c_i$

The rule for eliminating an element is discussed later in this section.

The parameter vector may be chosen to include any subset of the above parameters. Similarly, let α_* denote the parameter vector containing the true parameter values. The n modes included in the parameter vector must all have $\zeta_i\omega_i > 0$. That is, the model must be asymptotically stable or the residual covariance of the MLE identification method grows without bound. This condition precludes the identification of rigid-body input and output influence vectors. This is not a

severe limitation since these vectors can be predicted very accurately on the ground from mass, inertia, and geometry properties of the LSS. The program could, however, be adapted to accommodate these rigid-body modes.

The exact identification analysis software is only exact for zero process noise. This condition leads to a tremendous simplification of the computations required. An exact treatment of the finite process noise case was beyond the scope of this study. An approximate treatment is examined in a later section. Both test signal and measurement noise for this computer program were assumed to be white.

The errors computed are

- Systematic errors (or biases) due to model mismatch (e.g., $n \neq n_*$)
- Stochastic errors due to measurement noise

To evaluate these parameter errors the computer program must perform the following steps:

Step 1: $\min_{\alpha} I^*(\alpha)$

Let $\hat{\alpha} = \text{Arg}\left\{\min_{\alpha} I^*(\alpha)\right\}$

Step 2: $\alpha_{bias} = E\alpha_* - \hat{\alpha}$

where E is an identity matrix without the columns corresponding to parameters of the true system not included in the model, and therefore is not estimated. Note that when $n = n_*$, $E = I$ and $\hat{\alpha} = \alpha_*$ (i.e., systematic errors are zero when there is no model order mismatch).

Step 3: $E\left[(\hat{\alpha} - \alpha_*)(\hat{\alpha} - \alpha_*)^T\right] = \left[\nabla^2 I^*\right]^{-1}$

where $\nabla^2 I^* = \dfrac{\partial^2 I^*}{\partial\alpha\partial\alpha^T}(\hat{\alpha})$

When $n = n_*$, step 1 is trivial because $\hat{\alpha} = \alpha_*$. When $n \neq n_*$, one (or both) of the following minimization algorithms are used.

Gradient Method: This method uses a parameter update iteration of the form

$$\hat{\alpha}^{j+1} = \hat{\alpha}^j - \varepsilon^j \nabla I^*(\hat{\alpha}^j) \tag{5-27}$$

where $\nabla I^*(\alpha) = \dfrac{\partial I^*}{\partial \alpha^T}(\alpha)$,

the superscript j refers to the j^{th} iteration of the algorithm, and $\varepsilon^j > 0$ is a step size parameter that is usually adjusted in some ad hoc manner to improve convergence. One method of adjusting ε^j that was useful for minimizing I^* over one of the frequencies is the following. Let $\alpha = \omega_i$ (a scalar) and let

$$\varepsilon^j = \begin{cases} 1.3\varepsilon^{j-1} & \nabla I^*(\hat{\alpha}^j)\nabla I^*(\hat{\alpha}^{j-1}) > 0 \qquad (5\text{-}28a) \\ 0.2\varepsilon^{j-1} & \nabla I^*(\hat{\alpha}^j)\nabla I^*(\hat{\alpha}^{j-1}) < 0 \qquad (5\text{-}28b) \end{cases}$$

This method will be referred to as the modified gradient method in the following.

Newton-Rhapson Method: This method employs a parameter update iteration of the form

$$\hat{\alpha}^{j+1} = \hat{\alpha}^j - \left[\nabla^2 I^*(\hat{\alpha}^j)\right]^{-1} \nabla I^*(\hat{\alpha}^j) \tag{5-29}$$

The distinguishing feature of this algorithm is that the ad hoc (scalar) step size parameter ε_j is replaced by the inverse of the Hessian matrix.

Parameter Convergence Analysis

The MLE method is an iterative minimization algorithm and hence its success depends on the convergence of this algorithm. When the quantity being minimized is highly nonlinear, as is the negative log likelihood function, this convergence is dependent on being "close enough" to the minimum at the start of the minimization algorithm. Another issue is that of reaching a local minimum rather

than the global minimum. Only in the simplest cases can any analytical results be derived for how close is "close enough," and whether a global minimum will be found. Two of these simple cases will be described and then some general statements will be made based on these results and numerical results obtained using the exact identification analysis software.

Convergence of the MLE identification algorithm may be described in terms of an identifiability region, which is defined as the subset of the parameter space containing the true parameter, such that $\nabla^2 I^*$ is positive definite.

Identifiability Region for ω^2 Parameter--Let the true system be given by

$$G_*(s) = \frac{b^2}{s^2 + 2\zeta\omega s + \omega_*^2} \tag{5-30a}$$

and the model system be given by

$$G(s) = \frac{b^2}{s^2 + 2\zeta\omega s + \omega^2} \tag{5-30b}$$

Expressions for I^*, $\frac{\partial I^*}{\partial \omega^2}$, and $\frac{\partial^2 I^*}{\partial (\omega^2)^2}$ can be derived and used to determine the region of convergence for the parameter ω^2. A sketch of I^* vs ω^2/ω_*^2 is shown in Figure 5-3.

Region of convergence for NR method:

$$\frac{\partial^2 I^*}{\partial (\omega^2)^2} > 0 \rightarrow \left| \frac{\omega^2_{start}}{\omega_*^2} - 1 \right| < 2\zeta \tag{5-31}$$

Region of convergence for gradient method:

$$\omega^2 < \omega_*^2 \text{ and } \frac{\partial I^*}{\partial \omega^2} < 0 \rightarrow \frac{\omega^2_{start}}{\omega_*^2} < 1 \tag{5-32a}$$

$$\omega^2 > \omega_*^2 \text{ and } \frac{\partial I^*}{\partial \omega^2} > 0 \rightarrow \frac{\omega^2_{start}}{\omega_*^2} - 1 < 4\zeta^{2/3} \tag{5-32b}$$

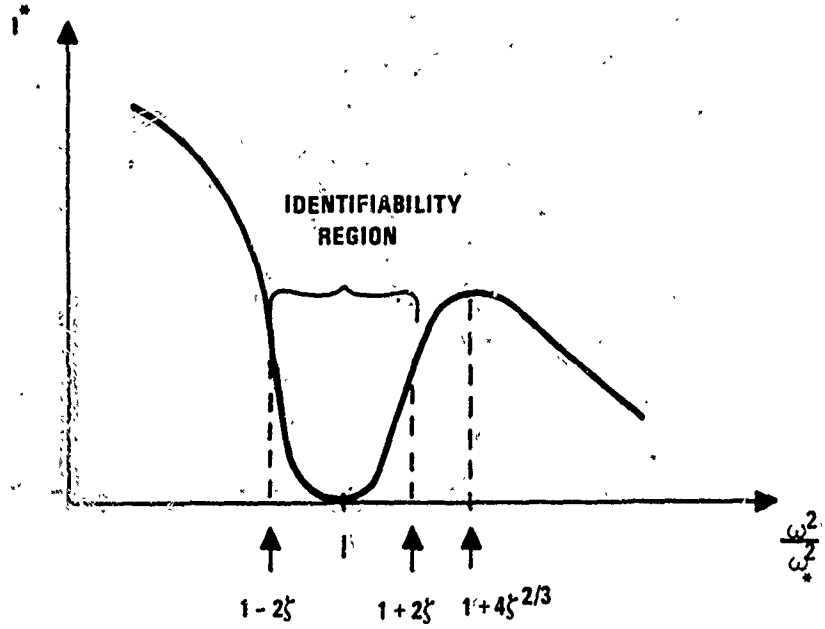

Figure 5-3. Identifiability Region for ω^2 Parameter

The global minimum corresponds to the true ω^2 value; however, it can be seen that if ω^2 becomes too large both NR and gradient methods will diverge.

Identifiability Region for $2\zeta\omega$ and b Parameter--Let the true system be given by

$$G_*(s) = \frac{c_* b_*}{s^2 + (2\zeta\omega)_* s + \omega_*^2} \tag{5-33a}$$

and the model system be given by

$$G(s) = \frac{c_* b}{s^2 + (2\zeta\omega) s + \omega_*^2} \tag{5-33b}$$

Again expressions for I^*, $\partial I^*/\partial 2\zeta\omega$, $\partial I^*/\partial b$, $\partial I/\partial(2\zeta\omega)^2$, $\partial I^*/\partial(2\zeta\omega)\,\partial b$, $\partial^2 I^*/\partial b^2$ can be derived and used to determine the region of convergence for these two parameters. A sketch of the region of convergence is shown in Figure 5-4.

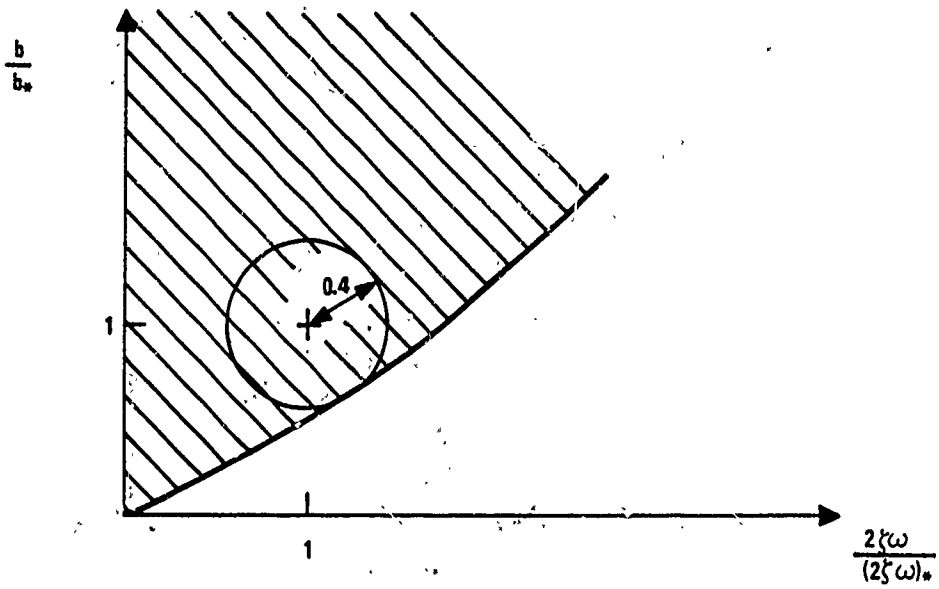

Figure 5-4. Identifiability Region for $2\zeta\omega$ and b Parameters

The shaded region corresponds to the region such that the Hessian matrix is positive definite. The circle of radius 0.4 is the practical region of convergence since the direction of the initial error will not be known in practice.

The gradient method's region of convergence would correspond to the whole plane. There is only the global minimum in this case. Hence the gradient method would converge for any starting parameter. From these two examples and numerical results obtained using the exact identification analysis software, the valleys in I^* for damping and the b's and c's were found to be very broad, and are hence easy to find and follow to the bottom. However, the valleys in I^* for frequency are very localized and steep, and are thus hard to find. Frequency updates thus required special handling.

Satisfactory convergence was obtained with the following procedure:

Step 1: Update each of the frequency parameters one at a time with the modified gradient method.

Step 2: Update the entire parameter vector, including the frequencies, with the NR method.

By using this combination of modified gradient and NR methods, convergence is obtained for starting values from 1/2 to 2 times the true parameter. In some cases a much larger range is possible.

Analytical Predictions for Systematic Errors

The exact identification analysis software was used to generate numerical results for the general case. Here, we examine analytical results for some special cases. Parameter bias in general is determined by comparing the parameter value that minimizes I^* to the true parameter. The parameter value that minimizes I^* is obtained by setting the gradient of I^* to zero. This was done for the following special cases.

Parameter Bias Due to Measurement Noise--If the MLE method is applied without using a Kalman filter, as is done in the exact identification analysis software, measurement noise can be factored out of the gradient. In this case measurement noise cannot introduce a parameter bias. This is not true, however, when a Kalman filter is used. The measurement noise covariance will impact the Kalman filter gains. Thus it has the potential of introducing a parameter bias if the value of measurement noise covariance used to design the filter is in error.

Parameter Bias Due to Process Noise-- here are four special cases to be discussed with respect to parameter biases due to process noise.

Case 1: MLE without the Kalman filter and no correlation between test signal and process noise.

In this case the process noise covariance can be factored out of the gradient and hence it cannot introduce parameter biases.

Case 2: MLE without Kalman filter and finite correlation between test signal and process noise.

In this case parameter biases are possible; an example will be discussed. Consider the situation of a SISO one-mode true system and model, that is, $n = n_* = n_i = n_o = 1$ and $b = c$. Let the correlation between test signal, u, and process noise, w, be of the form

$$E[uw] = \varepsilon E[u^2] \tag{5-34}$$

This is representative of correlation due to a scale factor error in the actuator for the test signal input. The results for this case are shown in Table 5-2 and are good approximations for the conditions listed. As evident from the table, the MLE method tries to compensate for process noise by making the damping ratio slightly smaller, or the b parameter slightly larger. The frequency bias is negligible for light damping. For the case of estimating all three parameters, only the b parameter is biased.

TABLE 5-2. PARAMETER BIASES DUE TO PROCESS NOISE (correlated with test signal) USING MLE WITHOUT THE KALMAN FILTER

Parameter(s) Estimated			
ζ	b	ω	ζ, b, ω
$\hat{\zeta} = (1 - \varepsilon)\zeta_*$ $\lvert \varepsilon \rvert << 1$	$\hat{b} = \sqrt{1 + \varepsilon}\ b_*$	$\lvert\hat{\omega} - \omega_*\rvert < 3\zeta_*^2\omega_*$ $\zeta_* << 1$ $\lvert \varepsilon \rvert < 1/2$	$\hat{\zeta} = \zeta_*$ $\hat{b} = \sqrt{1 + \varepsilon}\ b_*$ $\hat{\omega} = \omega_*$

Cases 3 & 4: MLE with the Kalman filter with and without correlation between test signal and process noise.

In these two cases an error in the value of the process noise covariance used to design the filter has the potential of introducing parameter biases.

Frequency Bias Due to Model Order Mismatch Using MLE Without the Kalman Filter--An approximation for frequency bias was obtained for the SISO n_*-mode true system and one-mode model system with $\zeta_{k*} = \zeta$ and $b_{k*} = c_{k*}$ for all n_* modes of the true system. A sketch of I^* vs frequency is shown in Figure 5-5.

The true system's frequencies are indicated by the ω_*'s and the local minimums of I^* by ω's. The difference between the two is the frequency bias. Since the damping ratio was assumed to be known, the only parameters to be estimated are ω and b of the model. The following approximate expressions were derived.

$$\frac{\hat{b}_k^2 - b_{k*}^2}{b_{k*}^2} \simeq 8\zeta^2 \sum_{\substack{i=1 \\ i\neq k}}^{n_*} \frac{\beta_i}{(1+\phi_i)(1-\phi_i)^2} \tag{5-35a}$$

$$\frac{\hat{\omega}_k^2 - \omega_{k*}^2}{1_{k*}^2} \simeq -8\zeta^4 \sum_{\substack{i=1 \\ i\neq k}}^{n_*} \frac{\beta_i\left(3\phi_i^2 + 2\phi_i + 3\right)}{1-\phi_i^2\,{}^2(1-\phi_i)} \tag{5-35b}$$

where

$$\beta_i \triangleq \left(\frac{b_i}{b_k}\right)^2 \tag{5-35c}$$

and

$$\phi_i \triangleq \frac{\omega_i}{\omega_k} \tag{5-35d}$$

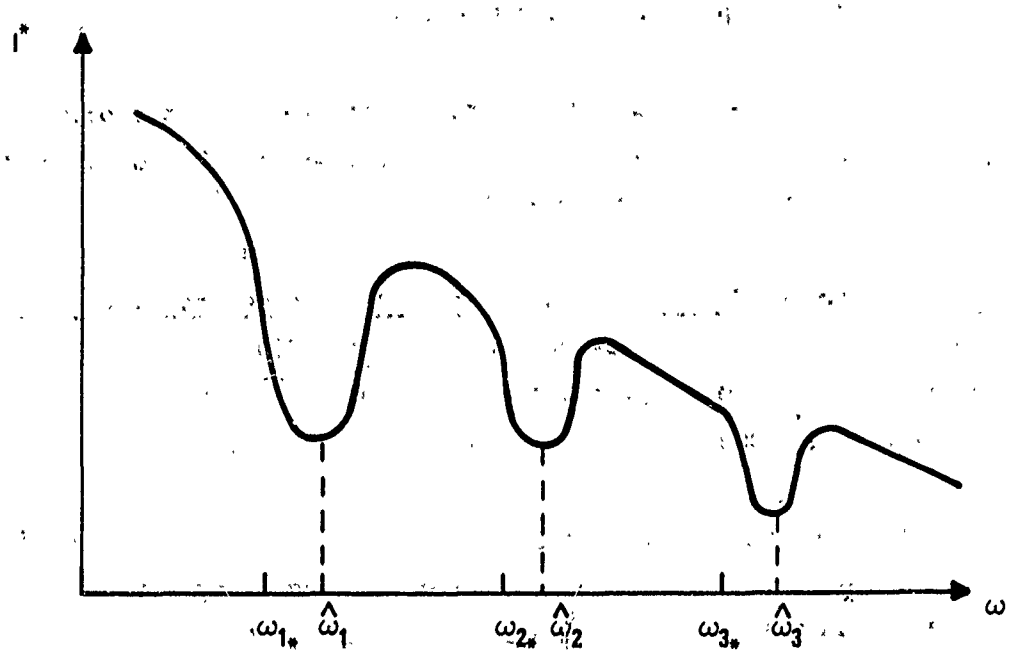

Figure 5-5. Frequency Bias Due to Model Order Mismatch

These parameter biases are seen to be proportional to either damping ratio squared or raised to the fourth power. For lightly damped structures these parameter biases are negligible.

The results for parameter bias are summarized in Table 5-3. These results show that MLE identification without the Kalman filter is less likely to give parameter biases than its counterpart with the filter. Specifically, MLE identification without the Kalman filter (which is itself a model mismatch when process noise is present) gives unbiased estimates under process and measurement noise mismatches, assuming no correlation with the test signal. Biases are, however, possible if noise correlations exist or if model order mismatches occur. For MLE identification with the Kalman filter, on the other hand, biases in parameter estimates are unavoidable under any model mismatch conditions. This evidence points up the need for accurate disturbance/noise models for Kalman-filter-based identification methods.

TABLE 5-3. PARAMETER ESTIMATE BIAS

MLE Implementation	Process Noise Mismatch		Measurement Noise Mismatch	Model Order Mismatch
	Correlated With	Uncorrelated With		
Without Kalman Filter	bias $\neq 0$	bias = 0	bias = 0	bias $\neq 0$
With Kalman Filter	bias $\neq 0$	bias $\neq 0$	bias $\neq 0$	bias $\neq 0$

SIMPLIFICATIONS DUE TO LIGHT DAMPING

Thus far, simplifications to the general MLE identification procedure have exploited general properties that may be expected to hold for most (if not all) LSS identification problems--small sample times, long identification intervals, small process-to-measurement-noise ratios, and the block-diagonal structure of systems in modal form. We now examine one final simplification that exploits a more specialized property also common to LSS's--lightly damped modes.

Hessian Matrix for Expected Likelihood Function

We have already noted that the expected likelihood function and its partials can be formed by using the computer to sum the exact contributions of individual mode pairs. When these quantities are evaluated at the parameter value $\hat{\alpha}_*$, which minimizes $I^*(\alpha)$ as is appropriate for identifiability analysis, further simplifications apply. Since MLE identification without the Kalman filter yields essentially unbiased parameter estimates, we can assume that after identification,

$$F_i(\hat{\alpha}_*) \simeq F_i^* \tag{5-36}$$

$$b_i(\hat{\alpha}_*) \simeq b_i^*$$

$$c_i(\hat{\alpha}_*) \simeq c_i^*$$

for each mode identified, which implies

$$\beta_{ij}(\hat{\alpha}_*) \simeq \beta_{ij}^c(\hat{\alpha}_*) \simeq \beta_{ij}^* \tag{5-37}$$

$$X_{ij}(\hat{\alpha}_*) \simeq M_{ij}(\hat{\alpha}_*) \simeq X_{ij}^*$$

By solving a 2 x 2 ALE it can be shown that terms in $I^*(\alpha_*)$ in (5-17a) are of the general form (assuming position measurements)

$$\beta_{ij} e_1^T X_{ij} e_1 = \beta_{ij} \frac{2(\zeta_i\omega_i + \zeta_j\omega_j)}{\left(\omega_i^2 - \omega_j^2\right)^2 + 4\omega_i\omega_j(\zeta_i\omega_i + \zeta_j\omega_j)(\zeta_i\omega_j + \zeta_j\omega_i)} \tag{5-38}$$

Since (5-38) exhibits a sharp resonance when $\omega_j = \omega_i$ and $\zeta_i, \zeta_j << 1$, it can be shown that off-diagonal ($j \neq i$) terms in the summation (5-17a) will be small relative to the corresponding diagonal terms whenever

$$\sqrt{\beta_{ij}/\beta_{ii}}\, 2\zeta_i << \frac{\left|(\omega_j/\omega_i)^2 - 1\right|}{\sqrt{2(1 + \zeta_j\omega_j/\zeta_i\omega_i)}} \qquad \text{for all } i,j \tag{5-39}$$

When $U = U_o I$, $W = W_o I$, and $R = R_o I$, a slightly weaker but easier to interpret condition is given by

$$\sqrt{\left|\cos\theta_{ij}^c \cos\theta_{ij}^b\right|}\ \max\{2\zeta_i, 2\zeta_j\} \tag{5-40a}$$

$$<< \frac{1}{\sqrt{2}} \min\left\{\sqrt{\gamma_i/\gamma_j}\left|\omega_j/\omega_i - 1\right|, \sqrt{\gamma_j/\gamma_i}\left|\omega_i/\omega_j - 1\right|\right\}$$

where

$$\cos\theta_{ij}^c \triangleq c_i^T c_j / |c_i|\,|c_j| \tag{5-40b}$$

$$\cos\theta_{ij}^b \triangleq b_i^T b_j / |b_i|\,|b_j| \tag{5-40b}$$

define the direction cosines between the vectors c_i, c_j and b_i, b_j, respectively and

$$\gamma_i \triangleq \bar{\sigma}\left(c_i b_i^T\right) = |c_i|\,|b_i| \qquad (5\text{-}40c)$$

$$\gamma_j \triangleq \bar{\sigma}\left(c_j b_j^T\right) = |c_j|\,|b_j| \qquad (5\text{-}40c)$$

define the magnitudes of the residues for the i^{th} and j^{th} modes, respectively. When $\gamma_i = \gamma_j$, condition (5-40) essentially ensures that off-diagonal terms in (5-17) will be negligible whenever damping is small relative to frequency separation, or when either c_i and c_j or b_i and b_j are nearly orthogonal. When $\zeta_j = \zeta_i = \zeta$, $\gamma_j \simeq \gamma_i$, and $\omega_j \simeq \omega_i$, condition (5-39) can be reduced to the much simpler condition

$$2\zeta << |\Delta\omega_{ij}|/\omega_i \qquad (5\text{-}40)'$$

which says essentially that modal damping must be small relative to frequency separation, where $\Delta\omega_{ij} \triangleq \omega_j - \omega_i$. This condition is satisfied for virtually all critical flexible modes for the ACOSS II structure, except for the six heavily damped isolator modes.

Conditions (5-40) or (5-40)' also ensure that off-diagonal terms in $\nabla_p I^*(\hat{\alpha}_*)$ and $\nabla^2_{pq} I^*(\hat{\alpha}_*)$ are negligible relative to diagonal terms. Thus the double summations over $i,j \in J^*$ in (5-17) can be reduced to a single summation over $i \in J^*$. Double summations over $i,j \in J$ in (5-17), (5-20), and (5-22) reduce to a single summation over $i \in J$, while double summations over $i \in J^*, j \in J$ reduce to a single summation over $i \in J^* \cap J$. Under these assumptions, the Hessian matrix $\nabla^2_{pq} I^*(\hat{\alpha}_*)$ reduces to a block-diagonal matrix, with nonzero elements only where the p^{th} and q^{th} element of α both correspond to some parameter associated with the i^{th} mode. Thus, the inverse of this matrix is also block-diagonal, so that parameter updates using the NR method and error covariances are uncoupled between modes. For all practical purposes, MLE parameter identification and associated accuracy analysis for lightly damped modes may be accomplished one mode at a time.

Under this assumption of lightly damped modes, it is possible to develop analytical expressions for the Hessian matrix $\nabla^2 I^*(\hat{\alpha}_*)$ by successively solving 2 x 2 ALEs and substituting into (5-22). Results for a single mode are summarized in Figures 5-6a and 5-6b for two cases--ILAS and non-ILAS. In both

$$\nabla^2 \ell_i^* = T \cdot SNR_R$$

$$\begin{bmatrix} \dfrac{1+4\zeta_i^2}{8\zeta_i^2\omega_i^4} & 0 & \dfrac{-b_i^T}{\omega_i^2 |b_i|^2} \\ 0 & \dfrac{1}{8\zeta_i^2\omega_i^2} & \dfrac{-b_i^T}{2\zeta_i\omega_i |b_i|^2} \\ \dfrac{-b_i}{\omega_i^2 |b_i|^2} & \dfrac{-b_i}{2\zeta_i\omega_i |b_i|^2} & 2\dfrac{|b_i|^2 I + b_i b_i^T}{|b_i|^4} \end{bmatrix}$$

$$U \triangleq U_0 I,\ R \triangleq R_0 I,\ SNR_R \triangleq \frac{|b_i|^4}{4\zeta_i\omega_i^3}\ \frac{U_0}{R_0}$$

$$\alpha_i \triangleq \left\{\omega_i^2,\ 2\zeta_i\omega_i \,|\, b_{i1},\ b_{i2},\ \ldots,\ b_{in_i}\right\}$$

Figure 5-6a. Hessian Matrix for a Single Mode: ILAS Case ($c_i = b_i$)

$$\nabla^2 \ell_i^* = T \cdot SNR_R$$

$$\begin{bmatrix} \dfrac{1+4\zeta_i^2}{8\zeta_i^2\omega_i^4} & 0 & \dfrac{-b_i^T}{2\omega_i^2 |b_i|^2} & \dfrac{-c_i^T}{2\omega_i^2 |c_i|^2} \\ 0 & \dfrac{1}{8\zeta_i^2\omega_i^2} & \dfrac{-b_i^T}{4\zeta_i\omega_i |b_i|^2} & \dfrac{-c_i^T}{4\zeta_i\omega_i |c_i|^2} \\ \dfrac{-b_i}{2\omega_i^2 |b_i|^2} & \dfrac{-b_i}{4\zeta_i\omega_i |b_i|^2} & |b_i|^{-2} I & \dfrac{b_i c_i^T}{|c_i|^2 |b_i|^2} \\ \dfrac{-c_i}{2\omega_i^2 |c_i|^2} & \dfrac{-c_i}{4\zeta_i\omega_i |c_i|^2} & \dfrac{c_i b_i^T}{|c_i|^2 |b_i|^2} & |c_i|^{-2} I \end{bmatrix}$$

$$U \triangleq U_0 I,\ R \triangleq R_0 I,\ SNR_R \triangleq \frac{|c_i|^2 |b_i|^2}{4\zeta_i\omega_i^3}\ \frac{U_0}{R_0}$$

$$\alpha_i \triangleq \left\{\omega_i^2,\ 2\zeta_i\omega_i \,|\, b_{i1}, b_{i2}, \ldots, b_{in_i} | c_{i1}, c_{i2}, \ldots, c_{in_0}\right\}$$

Figure 5-6b. Hessian Matrix for a Single Mode: Non-ILAS Case ($c_i \neq b_i$)

cases, ω_i and ζ_i denote mode frequency and damping ratio, while b_i and c_i denote input and output influence coefficient vectors. For simplicity, test signal covariance, U, and measurement noise covariance, R, have been assumed to be a scalar times the identity. Process noise covariance W is assumed to be zero for this analysis. The scalar SNR_R is just the SNR of test signal variance at the output to measurement noise intensity for the i^{th} mode. Note that T now multiplies SNR_R in the expression for $\nabla^2 I^*$, so that it can be lumped with $(N + 1)$ factors that appear in (4-15a)' and (4-15b)'. For the ILAS case, the parameter vector includes frequency squared (ω_i^2), the damping factor $(2\zeta_i\omega_i)$, and the input vector b_i. For the non-ILAS case, the parameter vector includes, in addition to the above, the output vector c_i.

Stochastic Errors Due to Measurement Noise

In view of these structural simplifications, parameter error covariance due to measurement noise for any lightly damped mode is given approximately by the inverse of the Hessian matrix $\nabla^2 I^*$ for that mode.

TABLE 5-4a. APPROXIMATE STOCHASTIC ERROR FOR MLE PARAMETER IDENTIFICATION: ILAS CASE ($c_i = b_i$)

Parameter	Stochastic Error Due to Measurement/Process Noise	
	Absolute	Relative
α_i	$\sigma_{\alpha_i}^2 \times SNR_T(N + 1)T$	$\frac{\sigma_{\alpha_i}^2}{\alpha_i^2} \times SNR_T(N + 1)T$
ω_i^2	$8\zeta_i^2\omega_i^4$	$8\zeta_i^2$
$2\zeta_i\omega_i$	$16\zeta_i^2\omega_i^2\left(1 + 2\zeta_i^2\right)$	$4\left(1 + 2\zeta_i^2\right)$
$b_{i\ell}$	$\frac{1}{2}\left(\lvert b_i\rvert^2 + 4\zeta_i^2 b_{i\ell}^2\right)$	$\frac{1}{2}\left(1 + 4\zeta_i^2 \frac{b_{i\ell}^2}{\lvert b_i\rvert^2}\right)$
$SNR_T^{-1} \triangleq SNR_R^{-1} = \frac{4\zeta_i\omega_i^3}{\lvert b_i\rvert^4}\frac{R_o}{U_o} + \frac{1}{\zeta_i\omega_i}\frac{W_o}{U_o}$		

ILAS Case--For the ILAS case of Figure 5-6a, the inverse of the partitioned matrix may be computed analytically by block manipulations. The diagonal elements of this inverse correspond to the theoretical residual error variances for each element of the parameter vector α_i that would remain after MLE identification based on a single sample. Both absolute and relative errors are summarized for this case in Table 5-4a. Note that relative error variance for $b_{i\ell}$ is defined as the rms absolute error variance divided by the vector magnitude $|b_i|^2$, as opposed to the scalar magnitude $|b_{i\ell}|^2$, to avoid possible division by zero. All entries should be divided by a composite SNR, SNR_T, and by the number of data samples taken times the sample time, $(N + 1)T$, to give error variance after time NT. Note that SNR_T^{-1} consists of the already defined inverse signal-to-measurement-noise ratio, SNR_R^{-1}, plus an inverse signal-to-process-noise ratio, SNR_W^{-1}, which will be discussed shortly. It should be noted that relative errors for ω_i^2 are of order ζ_i^2 smaller than those for $2\zeta_i\omega_i$ and the elements of b_i (at the variance level). These achievable accuracies are in general agreement with required accuracies called for in (3-23).

Non-ILAS Case--For the non-ILAS case of Figure 5-6b, the lower $(n_i + n_o) \times (n_i + n_o)$ block of the given Hessian matrix is singular and thus its inverse cannot be computed. This is because one element of the b_i or c_i vector is redundant and cannot be identified. Eliminating any nonzero element of either b_i or c_i from the parameter vector and fixing its value at some constant makes the Hessian matrix invertible and parameter identification possible.

In practice, the parameter eliminated would be assigned some convenient value (such as 1) and identification of the remaining parameters would proceed in the usual manner. For identifiability analysis studies it has proven more convenient to fix the eliminated parameter at its nominal value in the truth model so that identification model parameters match those of the truth model, as opposed to some arbitrary scalar multiple of the truth model parameters.

Given that either the L^{th} element of b_i or the M^{th} element of c_i is eliminated, the inverse of the resulting partitioned Hessian matrix may again be computed by block manipulations. The corresponding parameter error variances are summarized in Table 5-4b. Note that errors for ω_i^2 and $2\zeta_i\omega_i$ are unchanged from the

TABLE 5-4b. APPROXIMATE STOCHASTIC ERROR FOR MLE PARAMETER IDENTIFICATION: NON-ILAS CASE ($c_i \neq b_i$)

Parameter	Stochastic Error Due to Measurement/Process Noise	
	Absolute	Relative
α_i	$\sigma^2_{\alpha_i} \times SNR_T(N+1)T$	$\frac{\sigma^2_{\alpha_i}}{\alpha_i^2} \times SNR_T(N+1)T$
ω_i^2	$8\zeta_i^2\omega_i^4$	$8\zeta_i^2$
$2\zeta_i\omega_i$	$16\zeta_i^2\omega_i^2\left(1+2\zeta_i^2\right)$	$4\left(1+2\zeta_i^2\right)$
$b_{i\ell}$	$\lvert b_i\rvert^2 + \left[\rho^{-1} + 1 - \delta\, 4\zeta_i^2\right]b_{i\ell}^2$	$1 + \left[\rho^{-1} + 1 - \delta\, 4\zeta_i^2\right]\frac{b_{i\ell}^2}{\lvert b_i\rvert^2}$
c_{im}	$\lvert c_i\rvert^2 + \left[\rho^{-1} + 1 + \delta\, 4\zeta_i^2\right]c_{im}^2$	$1 + \left[\rho^{-1} + \left(1+\delta\right)4\zeta_i^2\right]\frac{c_{im}^2}{\lvert c_i\rvert^2}$

$\rho_b \triangleq \max_{\ell}\left\{\frac{b_{i\ell}^2}{\lvert b_i\rvert^2}\right\}$, $\rho_c \triangleq \max_{m}\left\{\frac{c_{im}^2}{\lvert c_i\rvert^2}\right\}$, $\rho \triangleq \max\{\rho_b, \rho_c\}$, $\delta \triangleq \begin{cases} +1 & \rho = \rho_b,\ b_L \text{ eliminated} \\ -1 & \rho = \rho_c,\ c_M \text{ eliminated} \end{cases}$

$$SNR_T^{-1} \triangleq SNR_R^{-1} + SNR_W^{-1} = \frac{4\zeta_i\omega_i^3}{\lvert c_i\rvert^2\lvert b_i\rvert^2}\frac{R_o}{U_o} + \frac{1}{\zeta_i\omega_i}\frac{W_o}{U_o}$$

ILAS case, while those for $b_{i\ell}$ for $\ell \neq L$ are a factor of 4 or more larger. Note further that, depending on which parameter is eliminated from α_i, we have

$$\rho \triangleq \begin{cases} \rho_b = \dfrac{b_{iL}^2}{\lvert b_i\rvert^2}, \quad \delta = +1 \ (b_{iL} \text{ eliminated}) & (5\text{-}41a) \\ \rho_c = \dfrac{c_{iM}^2}{\lvert c_i\rvert^2}, \quad \delta = -1 \ (c_{iM} \text{ eliminated}) & (5\text{-}41b) \end{cases}$$

Since $\rho \leq 1$ and normally $8\zeta_i^2 << 1 \leq \rho^{-1}$, to minimize error covariance we must choose L or M to maximize ρ. The choice given at the bottom of Table 5-4b meets this objective. The achievable accuracies in this table are again generally consistent with required accuracies stated in (3-23).

It is interesting to note that this same choice for ρ also minimizes the condition number with respect to inversion of the lower $(n_i + n_o - 1) \times (n_i + n_o - 1)$ block of $\nabla^2 I^*$, which may be demonstrated by taking the ratio of the maximum eigenvalue to the minimum eigenvalue of this (symmetric) matrix. If we further assume that appropriate scaling is used to reduce $\nabla^2 I^*$ to a matrix with ones along the diagonal, as is presently done in the general MLE algorithm NR update loop, the condition number of the scaled $\nabla^2 I^*$ matrix can be shown to be given by

$$K = \frac{1 + \sqrt{1 - \rho}}{1 - \sqrt{1 - \rho}} \tag{5-42}$$

When, as is often the case, <u>either</u> the b_j or c_i vector contains one element that dominates the remaining elements, this dominant element may be eliminated from the parameter vector, in which case $\rho \to 1$ and $K \to 1$. This corresponds to an ideal situation from a numerical analysis standpoint and thus ensures maximum numerical accuracy of the inverse. At worst, for n_i inputs and n_o outputs we have

$$\rho \geq \frac{1}{\max\{n_i, n_o\}} \triangleq \frac{1}{n_{io}} \tag{5-43a}$$

$$K = \frac{1 + \sqrt{1 - 1/n_{io}}}{1 - \sqrt{1 - 1/n_{io}}} \simeq 4n_{io}, \quad n_{io} >> 1 \tag{5-43b}$$

Thus, even for systems with many inputs and outputs, the above scheme for eliminating the redundant parameter guarantees good numerical accuracy for the inverse of the Hessian matrix. Due to the excellent conditioning of the Hessian matrix under the above-described scaling and redundant parameter elimination schemes, exact identifiability analyses and associated NR update iterations have been carried for systems with as many as 147 parameters using a single-precision 36-bit word length.

Stochastic Errors Due to Process Noise

To assess the effect of process noise W_* on identification accuracy, we must evaluate $\tilde{I}^*$ using (5-16) and the definitions (5-15) for a single mode, and then substitute this result into (4-15b)'. Even for a single mode, however, these

steps are tedious to carry out analytically, and have therefore been carried out only for a few terms in the covariance matrix. These analyses indicate that the resulting parameter-error covariances due to process noise W_* have essentially the same form as that given in Tables 5-4a and 5-4b, with an effective SNR bounded by

$$\zeta_i\omega_i \frac{U_o}{W_o} \leq SNR_W \leq 2\zeta_i\omega_i \frac{U_o}{W_o} \tag{5-44}$$

where process noise covariance $W_* = W_o I$ has also been taken to be a scalar multiple of the identity.

These bounds also have a certain intuitive appeal since

$$S^*_{rr}(\ell - k),\ S^*_{\nabla_p r \nabla_q r}(\ell - k)$$

in (5-16a), or more generally (5-12a), contain exponentially decaying sinusoids of the form

$$e^{-\zeta_i\omega_i t} \cos\left(\omega_i\sqrt{1 - \zeta_i^2}\, t + \phi\right)$$

Now, since

$$Tr\left[R_d^{-1}(S^*_{rr}(0) - R_d)\right] = \frac{|c_i|^2|b_i|^2}{4\zeta_i\omega_i^3} \frac{W_o}{R_o}$$

$$Tr\left[R_d^{-1} S^*_{\nabla_p r \nabla_q r}(0)\right] = \nabla^2_{pq} I^*$$

an upper bound for $(SNR_W)^{-1}$ for parameter error covariance due to process noise is given by

$$(SNR_W)^{-1}_{UB} = \frac{W_o}{U_o}\int_0^\infty 2e^{-\zeta_i\omega_i t}dt = \frac{W_o}{\zeta_i\omega_i U_o} \tag{5-45a}$$

while a lower bound is given by

$$(SNR_W)^{-1}_{LB} \doteq \frac{W_o}{U_o}\int_0^\infty 2e^{-\zeta_i\omega_i t}\cos^2\left(\omega_i\sqrt{1-\zeta_i^2}\,t+\phi\right)dt \qquad (5\text{-}45b)$$

$$= \frac{W_o}{2\zeta_i\omega_i U_o}$$

in agreement with (5-44).

The upper bound (5-45a) may also be deduced from an upper bound for the process noise (PSD) reflected to the output, which is given by

$$S_{yy}(\omega) = G_i(j\omega)S_{uu}(\omega)G_i^T(-j\omega) \qquad (5\text{-}46)$$

Letting $S_{uu}(\omega) = W_o I$ and recognizing that $G_i(j\omega)$ reaches a maximum at $\omega = \omega_i$, an upper bound for process noise reflected to the output is given by the flat noise spectrum

$$R_{W_{max}} = \bar{\sigma}^2(G_i(j\omega_i))W_o = \frac{|c_i|^2|b_i|^2}{4\zeta_i^2\omega_i^4}W_o$$

Now, substituting for R_o in SNR_R (defined in Figure 5-6b) gives

$$SNR_W = \zeta_i\omega_i\,\frac{U_o}{W_o} \qquad (5\text{-}47)$$

which again agrees with (5-45a).

Thus, an inverse composite SNR that includes the effects of both process and measurement noise is given by

$$SNR_T^{-1} = SNR_R^{-1} + SNR_W^{-1} \qquad (5\text{-}48)$$

$$= SNR_R^{-1}\left(1+\frac{SNR_R}{SNR_W}\right)$$

$$= \frac{4\zeta_i\omega_i^3}{|c_i|^2|b_i|^2}\,\frac{R_o}{U_o}\left(1+\bar{\sigma}^2(G(j\omega_i))\frac{W_o}{R_o}\right)$$

$$= \frac{4\zeta_i\omega_i^3}{|c_i|^2|b_i|^2}\frac{R_o}{U_o} + \frac{1}{\zeta_i\omega_i}\frac{W_o}{U_o}$$

Since $[SNR_T(N+1)T]^{-1}$ multiplies parameter error covariance elements in Tables 5-4a and 5-4b, we see that these errors are proportional to both measurement and process noise, as illustrated by the solid line in Figure 5-7. For $\bar{\sigma}^2(G_i(j\omega_i))W_o/R_o \ll 1$, the effects of process noise are negligible, so parameter errors with or without the Kalman filter are identical and depend only on measurement noise. For $\bar{\sigma}^2(G_i(j\omega_i))W_o/R_o \gg 1$, the effects of measurement noise no longer dominate, so parameter errors grow linearly with process noise. Finally, for $\bar{\sigma}^2(G_i(j\omega_i))W_o/R_o \gg (1/2\zeta_i)^2$, stochastic errors are dominated by process noise. Those for identification without the filter remain linear in process noise, whereas those with the filter grow at a rate less than linear in process noise. For this latter case least-squares estimation offers some potential for improved performance. Independent analysis of the least-squares estimation errors shows that the potential for improvement at the variance level is at most a factor of 2 for ω_i^2, 4 for $2\zeta_i\omega_i$, and $1/\zeta_i\omega_i T$ for $b_{i\ell}$ and c_{im}. Thus significant reductions in estimation error with least-squares estimation are possible only for the influence coefficients. Exact analytical results of these analyses, comparing identification errors with and without the filter, are summarized in Table 5-5 for the SISO case. These comparisons, however, apply only for identifying a single parameter at a time.

Approximate Identification Accuracy Analysis Program

An approximate identification accuracy analysis program was developed to incorporate these simplifications due to light damping. In essence, it evaluates the appropriate simplified analytical expressions for identification accuracy and tabulates both absolute and relative errors for each parameter at each mode. The program accommodates MIMO systems for both the ILAS and non-ILAS case and it includes the effects of both process and measurement noise. Comparison of results between the exact and approximate programs shows virtually exact agreement for all lightly damped modes.

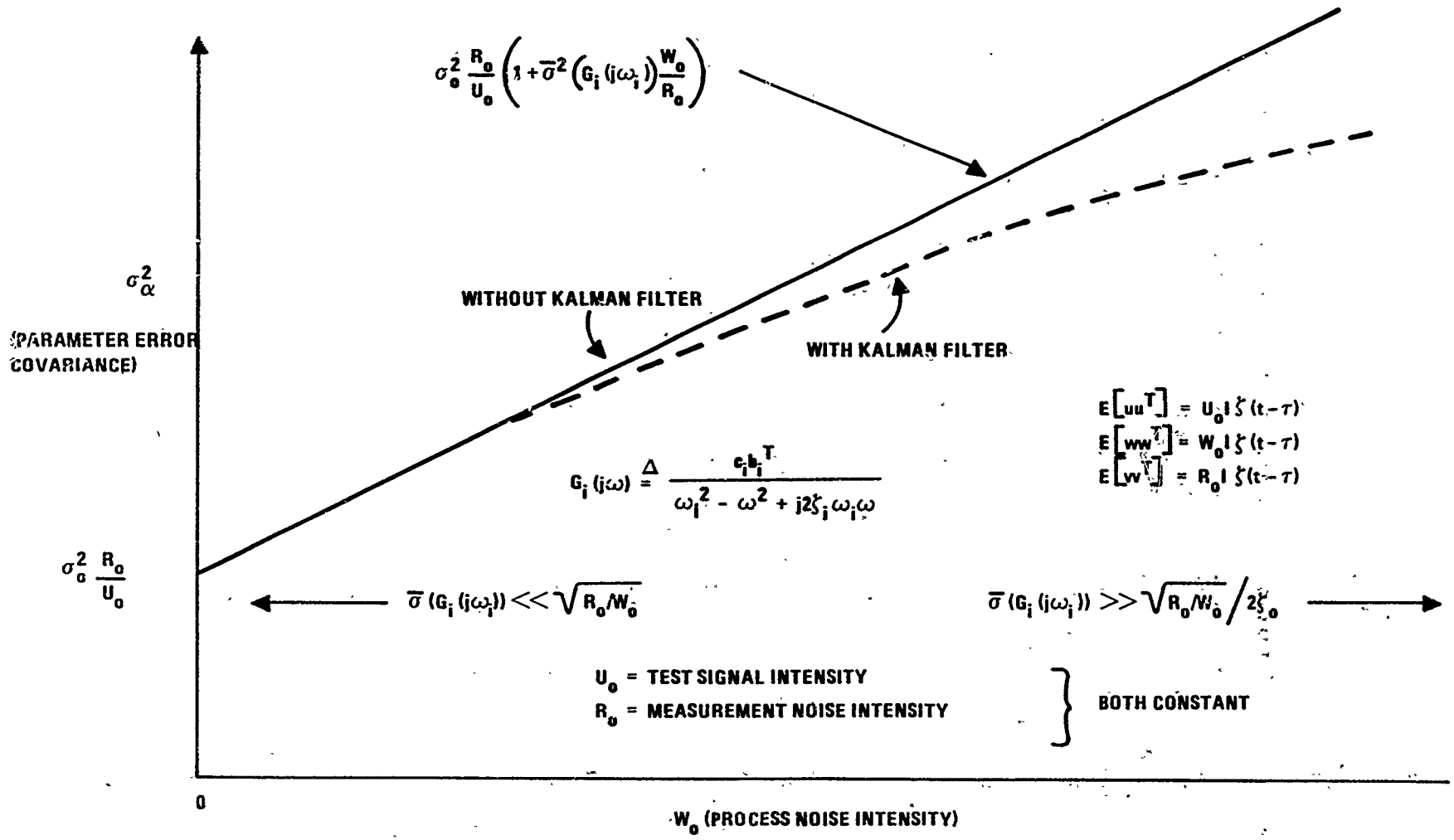

Figure 5-7. Stochastic Error with Process and Measurement Noise

TABLE 5-5. STOCHASTIC ERROR DEPENDENCE ON PROCESS NOISE

Assumptions: SISO one-mode true system and model
Test signal covariance = U, measurement noise covariance = R
Process noise covariance = W, sample time = T
Number of measurements = N

Parameter	Without Kalman Filter $\omega T \ll 1$, $\zeta \ll 1$	With Kalman Filter (least-squares estimation) $b^4WT/4\zeta\omega^3R \gg 1$
b	$\sigma_b^2 \simeq \frac{1}{(N+1)} \left[\frac{\zeta\omega^3 R}{b^2 UT} + \frac{b^2 W}{8\zeta\omega UT} \right]$	$\sigma_b^2 \simeq \frac{b^2 W}{4(N+1)U}$
$2\zeta\omega$	$\sigma_{2\zeta\omega}^2 \simeq \frac{1}{(N+1)} \frac{32\omega^5\zeta^3 R}{b^4 UT} + \frac{12\omega\zeta}{T} \frac{W}{U}$	$\sigma_{2\zeta\omega}^2 \simeq \frac{4\zeta\omega W}{(N+1)T(U+W)}$
ω^2		$\sigma_{\omega^2}^2 \simeq \frac{4\zeta\omega^3 W}{(N+1)T(U+W)}$

Rate and Acceleration Measurements--Test Signal 2

Results just described once again apply only for position measurements with Test Signal 1. For rate measurements, we find that the condition for validity of single-mode-at-a-time identification again reduces to (5-40). Moreover, assuming that $\zeta_i^2 \ll 1$, it can be shown that the Hessian matrix for rate measurements differs in form from that for position measurements given in Figure 5-6 by simple multiplication by ω_i^2. Thus, we may simply replace $R_o = R_1$ by $R_o = R_2/\omega_i^2$ for the signal-to-measurement noise ratio, SNR_R. Stochastic parameter errors due to rate measurement noise in Table 5-4 are therefore effectively multiplied by $R_2/R_1\omega_i^2$, which yields improved performance for mode frequencies above $\omega_i = \sqrt{R_2/R_i}$ = 5 r/s. Stochastic errors due to process noise, however, remain unchanged.

For acceleration measurements, assuming $4\zeta_i << \omega_i T << 1$, it can be shown that the Hessian matrix differs in form from that for position measurements by multiplication by ω_i^4. Thus, we may replace $R_o = R_1$ by $R_o = R_2/\omega_i^4$, so that stochastic parameter errors due to acceleration measurement noise are effectively multiplied by $R_3/R_1\omega_i^4$. This yields improved performance over the position measurement case for mode frequencies above $\omega_i = \sqrt[4]{R_3/R_1} = 0.707$ r/s and improved performance over the rate measurement case for mode frequencies above $\omega_i = \sqrt{R_3/R_2} = 0.1$ r/s. Stochastic errors due to process noise are again unchanged.

Results for position and rate measurements with Test Signal 2 can be obtained by replacing $U_o = U_1$ and $W_o = W_1$ by $U_o = U_2\omega_i^2$ and $W_o = W_2\omega_i^2$, assuming $4\zeta_i << \omega_i T << 1$. These same substitutions apply also for acceleration measurements, provided $\sqrt[3]{4\zeta_i/3\pi} << \omega_i T << 1$, which ensures that test signal variance measured at the acceleration level is dominated by the area under the PSD curve near resonance.

Frequency Domain Interpretation

Recall from Section 3 that to ensure stability of the closed-loop control system an approximate upper bound on allowable modal parameter error deviations of the true system from the design model for the i^{th} mode was given by (3-21)', which we repeat here (dropping the o subscript) as

$$\frac{1}{2\zeta_i}\cdot\frac{|\Delta\omega_i^2|}{\omega_i^2} + \frac{|\Delta 2\zeta_i\omega_i|}{2\zeta_i\omega_i} + \frac{|\Delta b_i|}{|b_i|} + \frac{|\Delta c_i|}{|c_i|} < 1 \qquad (5\text{-}49)$$

Approximate Transfer Function Relative Error - For convenience, we now assume that modal parameter errors in (5-49) are unbiased and independent. Technically, the correlation between parameter errors makes this a conservative assumption. Thus, we can combine error sources by simple RSS addition to get (assuming $1-\sigma$ errors)

$$TF_{re} \simeq \frac{1}{(2\zeta_i)^2}\cdot\frac{E\left\{|\Delta\omega_i|^2\right\}}{(\omega_i^2)^2} + \frac{E\left\{|\Delta 2\zeta_i\omega_i|^2\right\}}{(2\zeta_i\omega_i)^2} + \frac{E\left\{|\Delta b_i|^2\right\}}{|b_i|^2} + \frac{E\left\{|\Delta c_i|^2\right\}}{|c_i|^2}^{1/2} \qquad (5\text{-}50)$$

Letting

$$T_{ID} \triangleq (N + 1)T \simeq NT \tag{5-51}$$

denote the identification time, we see from Table 5-4b that the first two expectations are given by (assuming $\zeta_i << 1$)

$$[SNR_T\ T_{ID}]\ E\left\{\left|\Delta\omega_i\right|^2\right\} = 8\zeta_i\omega_i^4 \tag{5-52a}$$

$$[SNR_T\ T_{ID}]\ E\left\{\left|\Delta 2\zeta_i\omega_i\right|^2\right\} = 16\zeta_i\omega_i^4 \tag{5-52b}$$

To evaluate the second two expectations, it is necessary to account for the element among the b_i and c_i vectors that was eliminated for identification. We consider two cases.

Case 1: Element of b_i eliminated.

Let $\tilde{b}_i, \Delta\tilde{b}_i$ denote the reduced $b_i, \Delta b_i$ vectors. Then recognizing that

$$E\{|x|^2\} = E\{x^Tx\} = E\{Tr[xx^T]\} = Tr[E\{xx^T\}] \tag{5-53}$$

we get (from Table 5-4b)

$$[SNR_T\ T_{ID}]\ E\left\{\left|\Delta\tilde{b}_i\right|^2\right\} \tag{5-54a}$$

$$= (n_i - 1)\left|b_i\right|^2 + \rho^{-1}\left|\tilde{b}_i\right|^2$$

$$= (n_i - 1)\left|b_i\right|^2 + \rho^{-1}(1 - \rho)\left|b_i\right|^2$$

$$= \left(n_i - 2 + \rho^{-1}\right)\left|b_i\right|^2$$

$$[SNR_T\ T_{ID}]\ E\left\{\left|\Delta c_i\right|^2\right\}$$

$$= \left(n_o + \rho^{-1}\right)\left|c_i\right|^2 \tag{5-54b}$$

Case 2: Element of c_i eliminated.

Since covariances for Δb_i and Δc_i in Table 5-4b are identical for small damping, by reversing the roles of b_i and c_i in case 1 we get

$$[SNR_T\ T_{ID}]\ E\left\{\left|\Delta b_i\right|^2\right\} = (n_i + \rho^{-1})\left|b_i\right|^2 \tag{5-55a}$$

$$[SNR_T\ T_{ID}]\ E\left\{\left|\Delta \tilde{c}_i\right|^2\right\} = (n_o - 2 + \rho^{-1})\left|c_i\right|^2 \tag{5-55b}$$

Now summing up the individual terms in (5-50) gives (in either case)

$$TF_{re} \simeq \left\{(2 + 4 + n_i + n_o + 2\rho^{-1} - 2)\ (SNR_T\ T_{ID})^{-1}\right\}^{1/2} \tag{5-56a}$$

Corresponding results for the ILAS case, in which $c_i = b_i$, do not require eliminating a parameter and are easily shown to be

$$TF_{re} \simeq \left\{(2 + 4 + 2(1/2)n_i)\ (SNR_T\ T_{ID})^{-1}\right\}^{1/2} \tag{5-56b}$$

Therefore, in general, the relative transfer function error due to parameter errors in the i^{th} mode is given approximately by

$$TF_{re} \simeq \sqrt{c(SNR_T\ T_{ID})^{-1}} = \sqrt{\frac{cR_o/U_o}{\zeta_i \omega_i T_{ID}}}\left\{\frac{1}{\bar{\sigma}^2(G_i(j\omega_i)} + \frac{W_o}{R_o}\right\}^{1/2} \tag{5-57}$$

where

$$c \triangleq \begin{cases} 2 + 4 + n_i & \text{ILAS} \qquad (5\text{-}58a) \\ 2 + 4 + n_i + n_o + 2\rho^{-1} - 2 & \text{Non-ILAS} \qquad (5\text{-}59b) \end{cases}$$

Since the parameter elimination scheme used for the non-ILAS case ensures that (from 5-43a)

$$\rho^{-1} \leq \max\{n_o, n_i\}$$

the coefficient (c) for the two concepts works out to be

$$c = \begin{cases} 9 & \text{Baseline concept } (n_i = 3) \qquad (5\text{-}60a) \\ 16 & \text{Advanced concept } (n_o = n_i = 3) \qquad (5\text{-}60b) \end{cases}$$

Note that we could have taken $n_i = 1$ for the baseline concept to allow for independent identification of modal parameters for each axis, in which case

c = 7. Note also that relative transfer function error may be further approximated for two process-to-measurement noise extremes to give

$$TF_{re} \cong \begin{cases} \ell_a^o(\omega_i)/\bar{\sigma}(G_i(j\omega_i)) & \bar{\sigma}(G_i(j\omega_i)) << \sqrt{R_o/W_o} \quad (5\text{-}61a) \\ \ell_r^o(\omega_i) & \bar{\sigma}(G_i(j\omega_i)) >> \sqrt{R_o/W_o} \quad (5\text{-}61b) \end{cases}$$

where

$$\ell_a^o(\omega_i) \triangleq \sqrt{\frac{cR_o/U_o}{\zeta_i\omega_i T_{ID}}} \quad (5\text{-}62a)$$

$$\ell_r^o(\omega_i) \triangleq \sqrt{\frac{cW_o/U_o}{\zeta_i\omega_i T_{ID}}} \quad (5\text{-}62b)$$

may be interpreted as "absolute" and "relative" transfer function errors that apply for the two extremes. The latter quantity defines a lower bound on relative error and will normally be much less than one since identification time must be much longer than the modal time constant, that is,

$$T_{ID} >> 1/\zeta_i\omega_i \quad (5\text{-}63a)$$

and

$$cW_o/U_o = 0.01c << 1 \quad (5\text{-}63b)$$

for both concepts. Thus it is clear that relative transfer function error will be less than one whenever

$$\bar{\sigma}(G_i(j\omega_i)) > \ell_a^o(\omega_i) \quad (5\text{-}64a)$$

and approaches a lower bound of $\ell_r^o(\omega_i)$ whenever

$$\bar{\sigma}(G_i(j\omega_i)) > \sqrt{R_o/W_o} \quad (5\text{-}64b)$$

Graphical Results--These relationships are displayed on singular-value plots of $G(j\omega)$ for the various measurement test signal combinations for the baseline concept in Figures 5-8 through 5-10, and for the advanced concept in Figures 5-11 through 5-13 for an assumed identification time of T_{ID} = 300 sec (5 min), which

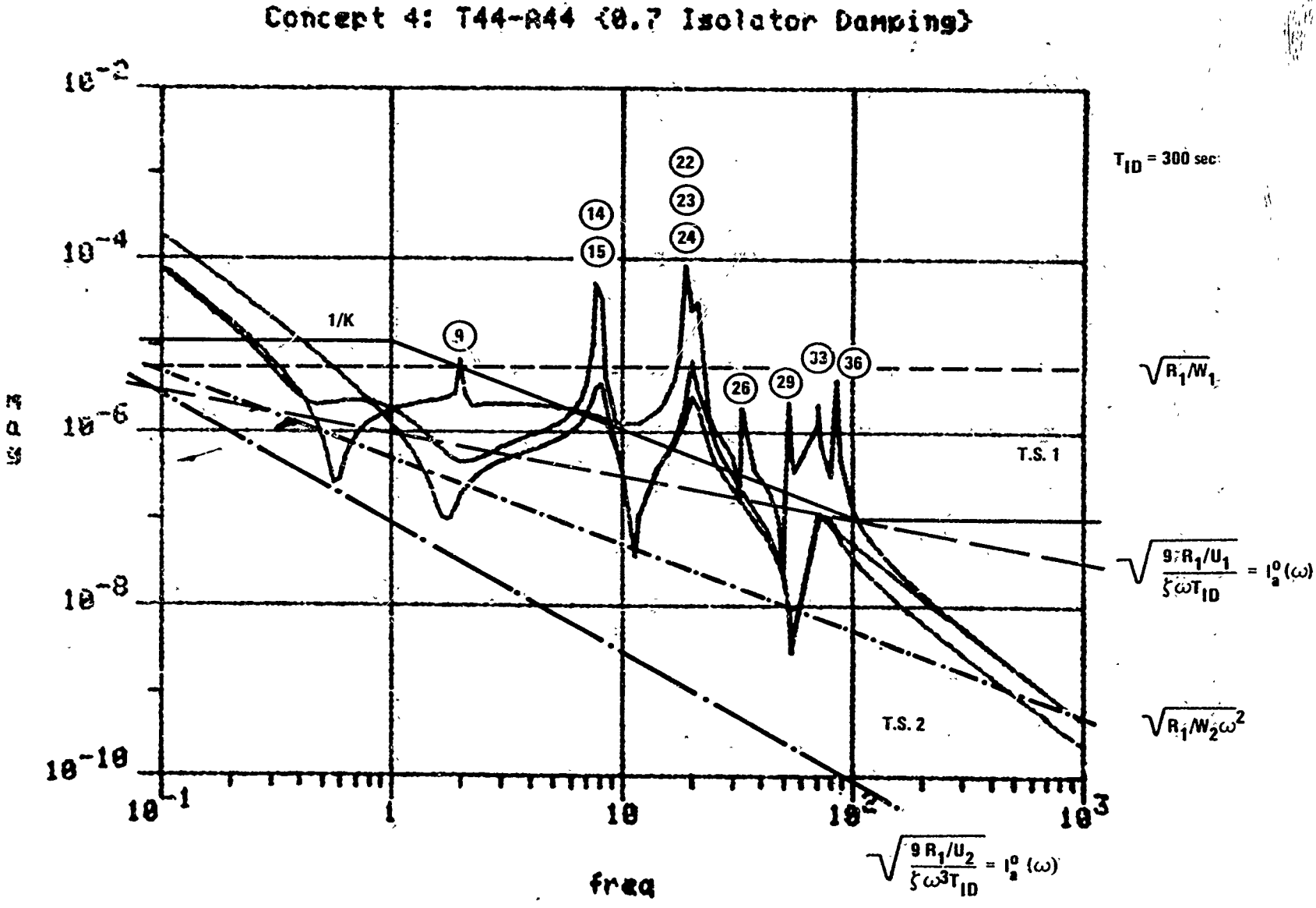

Figure 5-8. Approximate Identification Results for Baseline Concept: Position Measurements

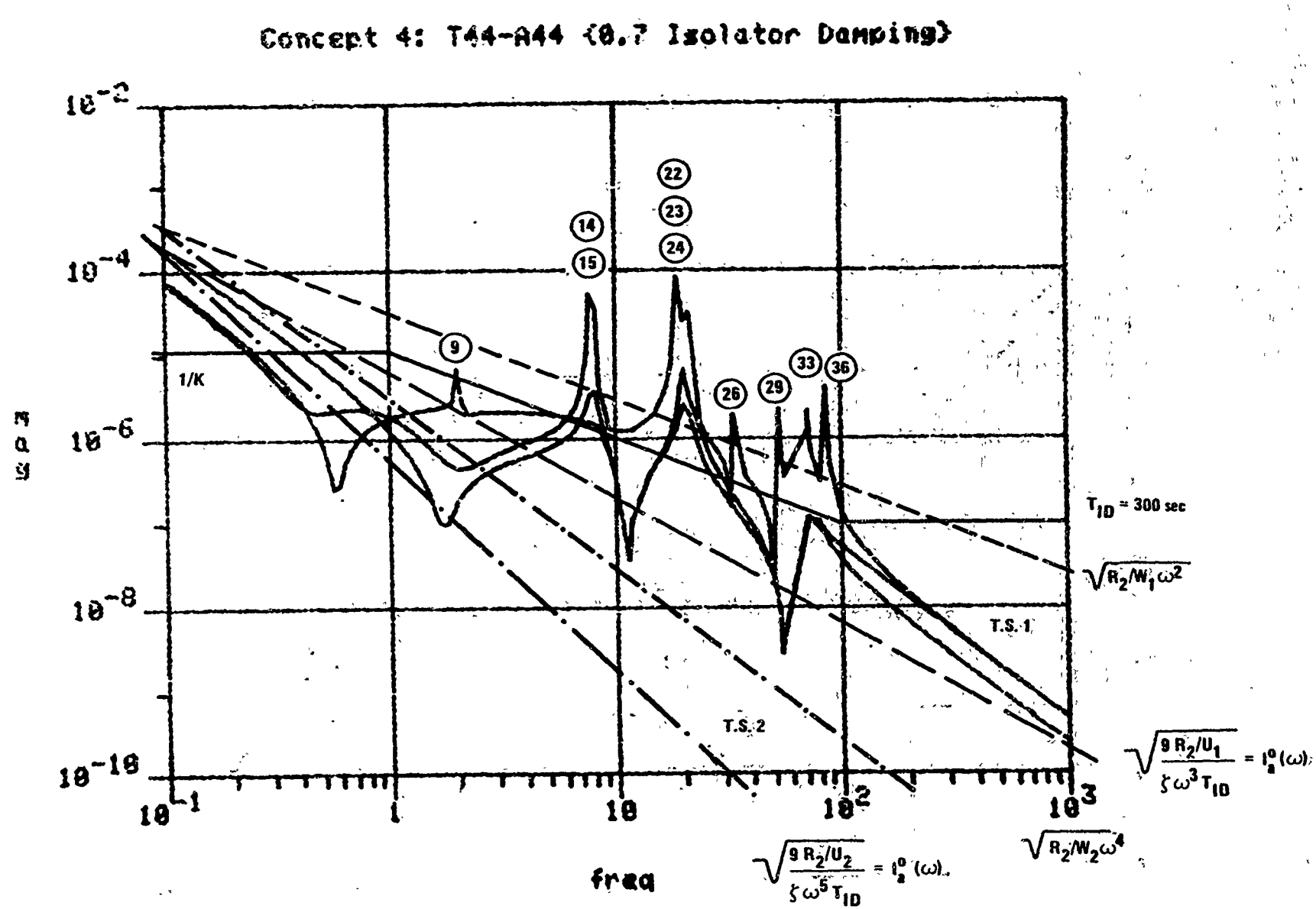

Figure 5-9. Approximate Identification Results for Baseline Concept: Rate Measurements

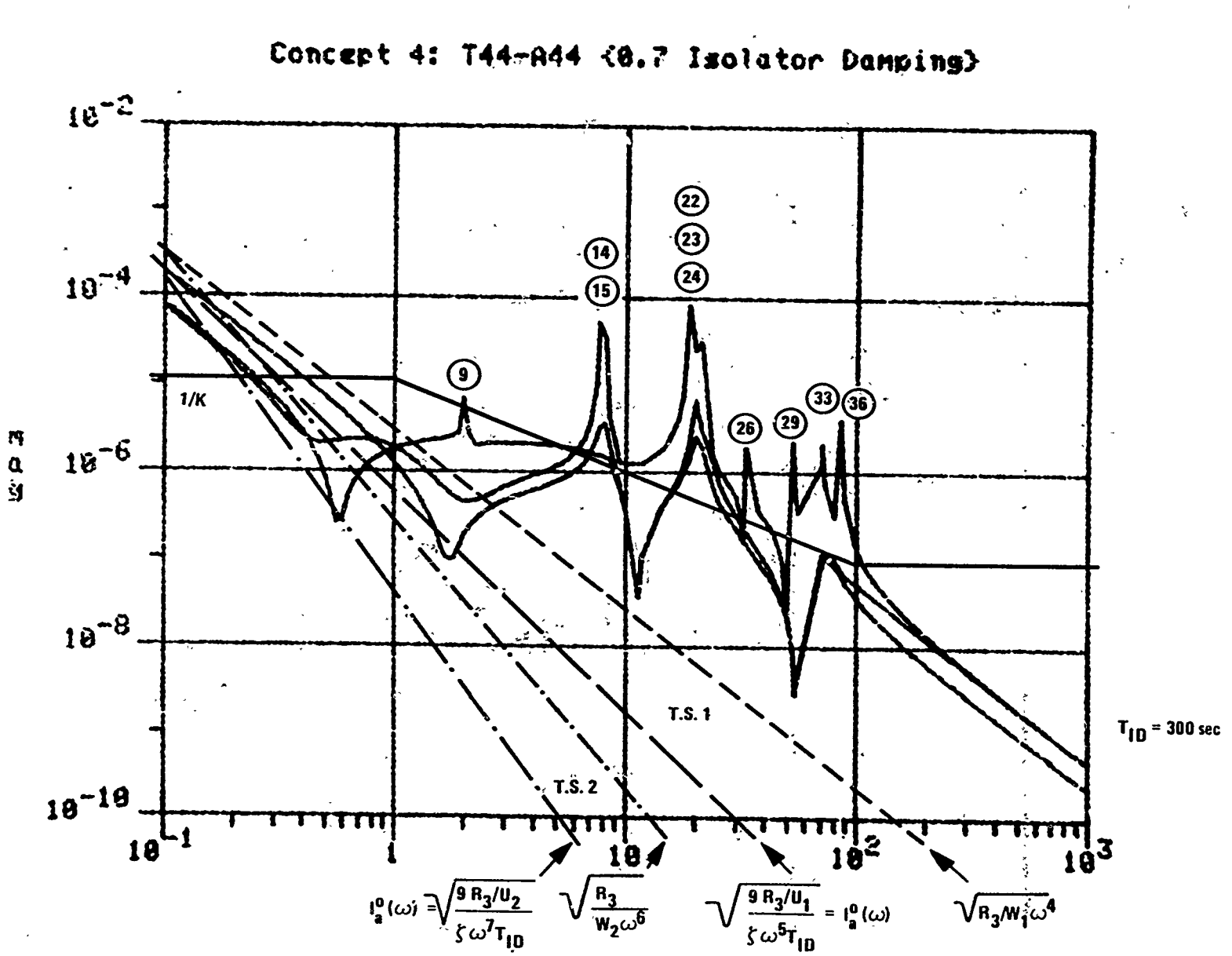

Figure 5-10. Approximate Identification Results for Baseline Concept: Acceleration Measurements

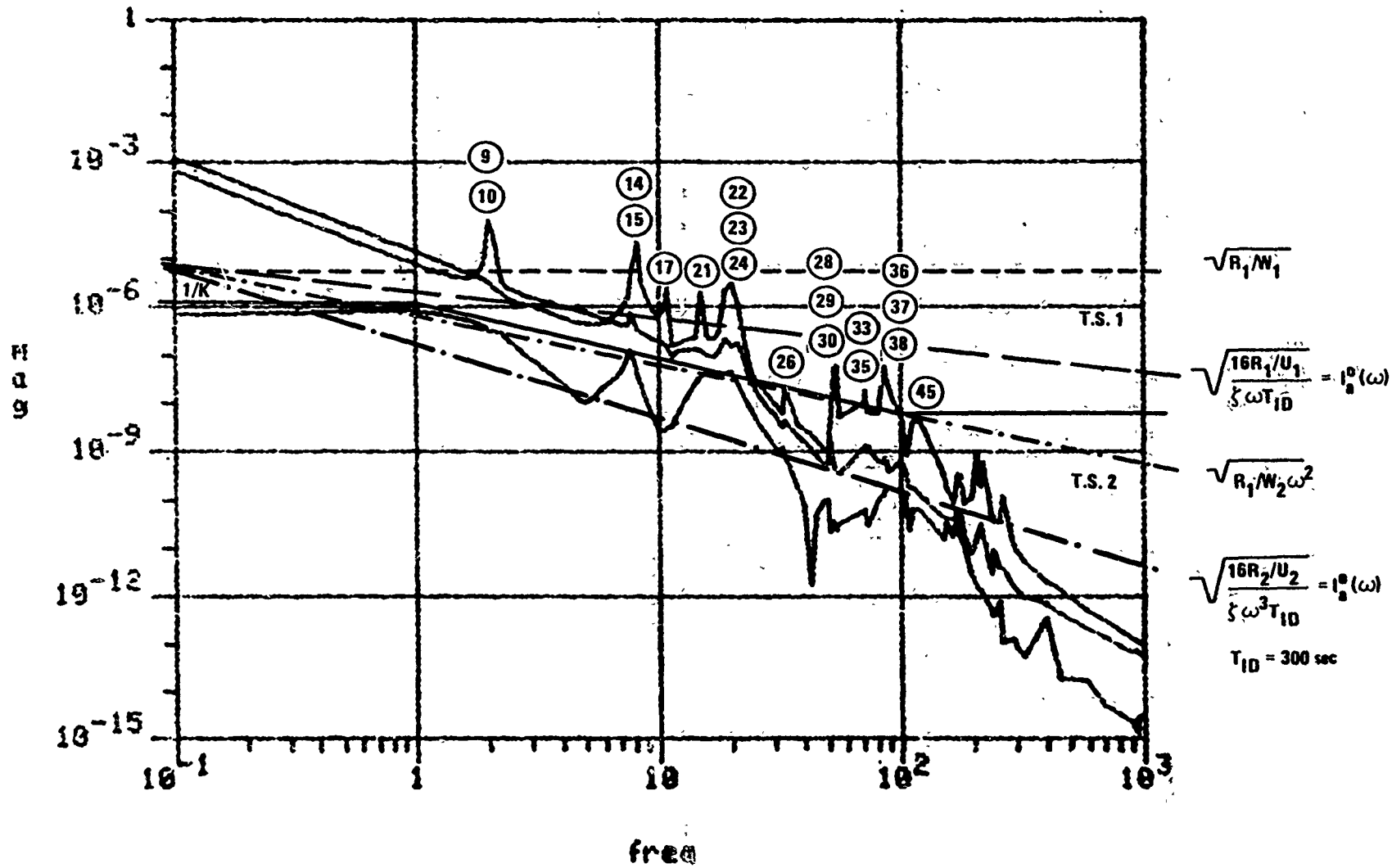

Figure 5-11. Approximate Identification Results for Advanced Concept: Position Measurements

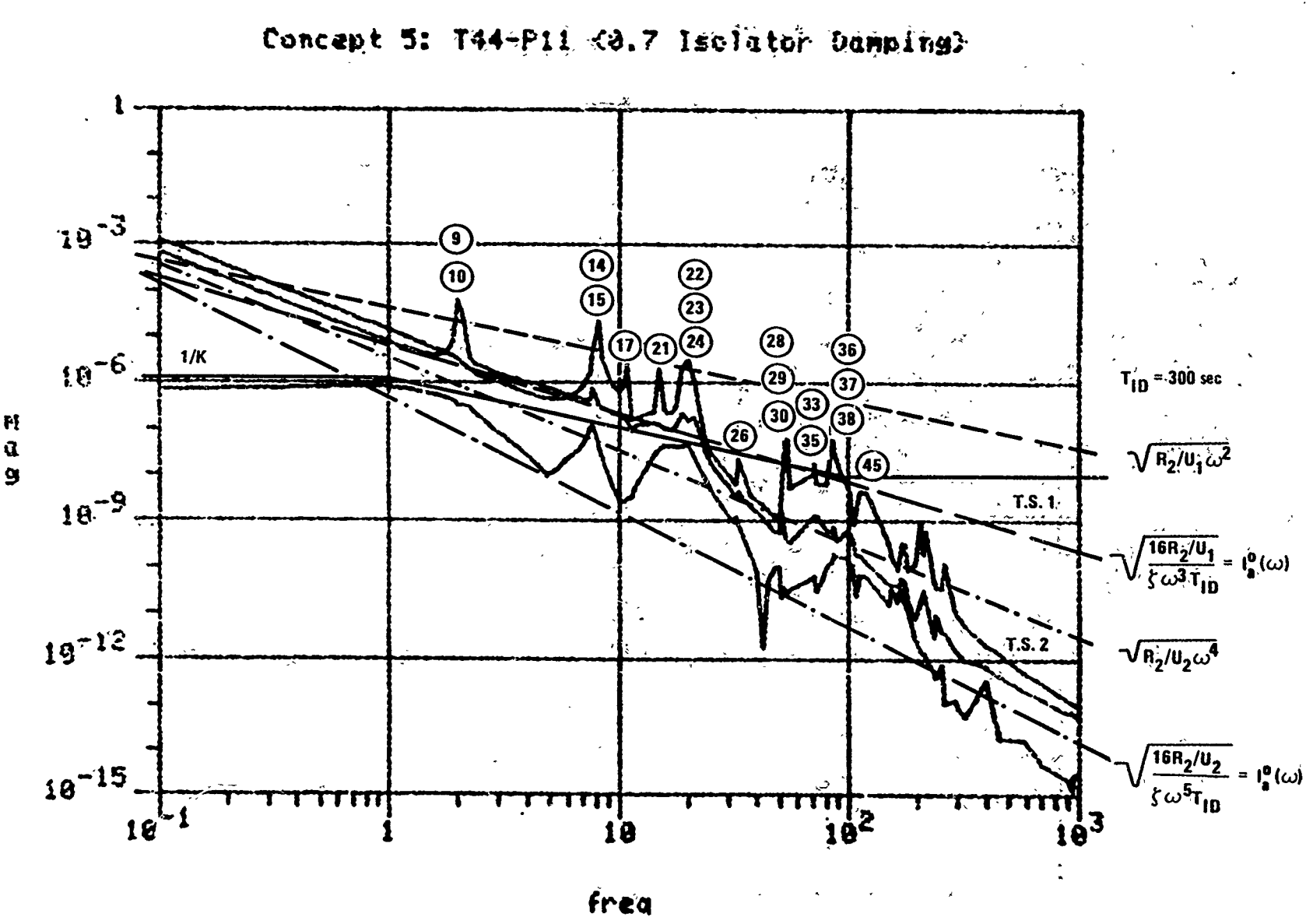

Figure 5-12. Approximate Identification Results for Advanced Concept: Rate Measurements

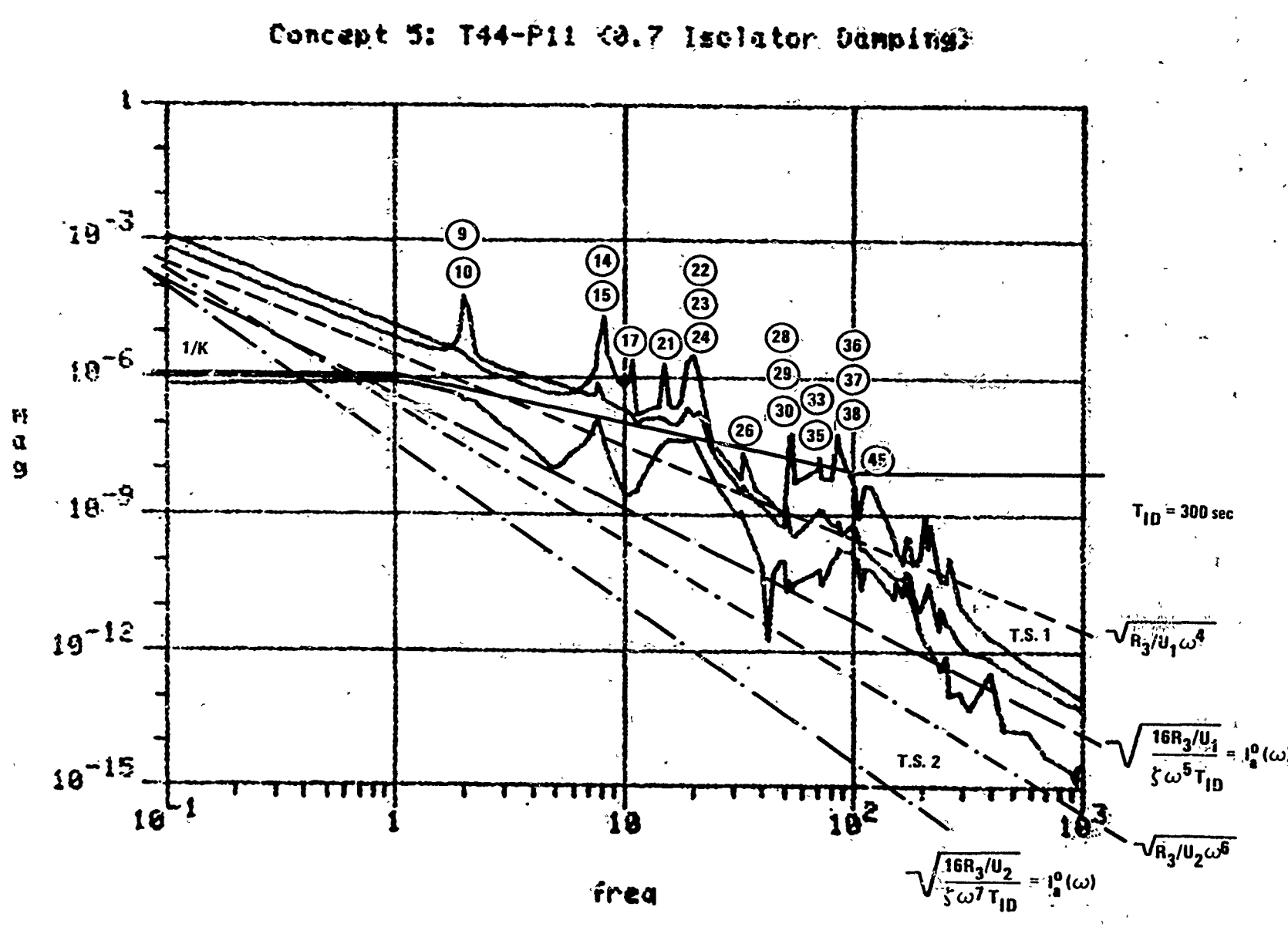

Figure 5-13. Approximate Identification Results for Advanced Concept: Acceleration Measurements

is about three times the longest modal time constant. In each case we plot lower and upper constraints (ℓ_a^o and $\sqrt{R_o/W_o}$) for G as a continuous function of frequency ω. Technically those constraints apply only at each mode frequency (ω_i). Dashed lines are used for Test Signal 1; broken (—·—) lines are used for Test Signal 2. Similarly, heavy lines are used for the lower bound and fine lines are used for the upper bound.

Mode peaks, $\bar{\sigma}(G_i(j\omega_i))$, that lie within these bounds produce essentially constant absolute transfer function errors for which the relative error is less than one. Mode peaks that fall below the lower bound, ℓ_a^o, also produce constant absolute transfer function errors for which the relative error is greater than one. Mode peaks that exceed the upper bound, $\sqrt{R_o/W_o}$, produce constant relative errors with $\ell_r^o(\omega) = \sqrt{0.05/\omega} < 1$. This defines a point of diminishing returns for identification.

The nominal control designs (1/k) are also shown superimposed on the plots for $\sigma_k(G(j\omega))$. Because the lower bound, $\ell_a^o(\omega)$, represents an upper bound on absolute errors in $G(j\omega)$ it also defines a lower bound on inverse control gain; that is,

$$k(\omega) \triangleq \bar{\sigma}(K(j\omega)) < 1/\ell_a^o(\omega)$$

Baseline Concept--As evident from Figures 5-8 through 5-10, the nominal control design for the baseline concept meets these constraints over most of the critical gain crossover frequency range (0.2 to 100 r/s) for each of the six measurement/test signal combinations. Because the upper bound, $\sqrt{R_o/W_o}$, defines a point of diminishing returns for identification, there is little reason to favor any one combination over another. The relative error ℓ_r in each case is limited to ~22% at ω = 1 r/s and ~2.2% at ω = 100 r/s. Both position measurement cases do, however, offer some advantage at low frequencies.

If control gain were, however, increased (1/k decreased) by a factor of 10, which is roughly the gain needed to meet the "ideal" control requirements, identification time would have to be increased by a factor of 100 to meet stability requirements for position measurements with Test Signal 1. The corresponding identification time interval for this case (8.33 hrs) is unacceptable. Furthermore, we would like

to exceed these minimum stability requirements by some margin (say a factor of 3 for 3-σ parameter errors). Required identification times for this case increase by a factor of $3^2 = 9$ to become 0.75 hours for the nominal design and 75 hours for the ideal design. The latter number is clearly ridiculous. Since these bounds apply for the entire gain crossover region, position measurements with Test Signal 2 define the only practical alternative. This choice is consistent with preliminary recommendations made in Section 3. An identification time interval of 5 to 10 minutes should suffice for this case.

Advanced Concept--Nominal control designs for the advanced concept shown in Figures 5-11 through 5-13 fail to meet identification constraints for Test Signal 1 with position and rate measurement. Results for the corresponding cases with Test Signal 2 are about equal. The former does offer a slight advantage at low frequency; the latter is identical to results for acceleration measurements with Test Signal 1. Results for acceleration measurements with Test Signal 2 offer no practical advantage over any of these three.

All four cases would allow an increase in control gain by a factor of 10 at $\omega = 100$ r/s. Again, this is roughly the control gain required to meet ideal control requirements, assuming little or no increase at $\omega = 1$ r/s. It should be recognized that increasing the gain calls for higher order control design and identification models. Some increase in stochastic error would result for position measurements with Test Signal 1, but no significant change in accuracy would occur for the other three cases. Moreover, the latter all provide a substantial margin for additional model errors, with no increase in identification time. Thus, our earlier recommended choice, rate measurements with Test Signal 2; or its ideal twin, acceleration measurements with Test Signal 1; remains the best alternative. An identification time interval of 5 to 10 minutes should also suffice for this case.

Closed-Loop Stability Verification

Critical Assumptions--The analyses and interpretation of the previous subsection depend on two critical assumptions used in Section 3 to reduce relative transfer function error (3-21) to the simpler forms (3-21)' or (5-50). The first assumption, that for "good" control designs

$$\left| 1 + \frac{1}{g_i(j\omega) b_i^T K(j\omega) c_i} \right| > r' \simeq 1 \qquad (5\text{-}65)$$

for $\omega \simeq \omega_i$ is a reasonable one since modern LQG-based control design methods using robustness recovery (Ref. 2) produce return and inverse-return differences which, in theory, can approach the ideal LQ state feedback guarantees of

$$\underline{\sigma}(I + KG(j\omega)) > 1 \qquad (5\text{-}66a)$$

$$\underline{\sigma}[I + (KG(j\omega))^{-1}] > 1/2 \qquad (5\text{-}66b)$$

for all $\omega \geq 0$. Note that the latter quantity is a lower bound for the lefthand side of (5-65). Thus, the first assumption is a reasonable approximation for our purpose.

The second assumption, that for "good" control designs

$$\cos_{1i}(\omega) \triangleq b_i^T K(j\omega) c_i / |K(j\omega) c_i| |b_i| \simeq 1 \qquad (5\text{-}67a)$$

$$\cos_{2i}(\omega) \triangleq b_i^T K(j\omega) c_i / |K^T(j\omega) b_i| |c_i| \simeq 1 \qquad (5\text{-}67b)$$

for $\omega \simeq \omega_i$ is not as easily dismissed. Clearly it is a desirable property, since from (3-21) it maximizes stability robustness to errors in b_i and c_i, particularly to those producing a change in direction. Whether it is achievable for all controlled modes is an open question. For our LQG-based control design of Section 6, we have verified that the above approximations are good for some modes but not for all modes. Values observed for a few selected modes ranged from roughly 0.1 to 1.0.

Failure of either assumption to hold is of course no guarantee of instability--only a potential for instability. Thus, it is necessary to verify stability robustness to parameter uncertainty for any particular control design. Such verifications, for example, might consist of testing condition (3-21) over all frequencies $\omega \geq 0$ for all modes identified. But even this test is conservative for it fails to consider the correlations between parameter errors. Condition (3-20) is far less conservative, but impossible to apply since MLE identifiability

analysis provides only an estimate of parameter error variance and not raw parameter errors. Thus, it is essential to develop more refined estimates for transfer function errors.

Transfer Function Error

We begin by developing an estimate for the error in $\Delta G_i(j\omega)$, which was defined in Section 3 as (3-18b) and is rewritten here for convenience as

$$\Delta G_i(j\omega) \triangleq g_i\left(\beta_i^T \Delta\alpha_i c_i b_i^T + c_i \Delta b_i^T + \Delta c_i b_i^T\right) \tag{5-69a}$$

where

$$\Delta\alpha_i^T \triangleq \left(\Delta\omega_i^2 \quad \Delta 2\zeta_i\omega_i\right) \tag{5-69b}$$

$$\beta_i^T \triangleq -g_i(j\omega)\,(1 \quad j\omega) \tag{5-69c}$$

We now let

$$\bar{\sigma}_{rms}(\Delta G_i) \triangleq \max_k \lambda_k^{1/2} \quad E\left[\left\{\Delta\bar{G}_i^T \Delta G_i\right\}\right] \tag{5-70}$$

define the maximum rms singular value of the transfer function $\Delta G_i(j\omega)$. The above expectation is given by

$$E\left\{\Delta\bar{G}_i^T \Delta G_i\right\} \tag{5-71}$$

$$= |g_i|^2 E\left\{\left(\bar{\beta}_i^T \Delta\alpha_i b_i c_i^T + \Delta b_i c_i^T + b_i \Delta c_i^T\right)\left(\Delta\alpha_i^T \beta_i c_i^T b_i + c_i \Delta b_i^T + \Delta c_i^T b_i\right)\right\}$$

$$= |g_i|^2 \left\{ |c_i|^2 \bar{\beta}_i^T P_{\alpha\alpha}^i \beta_i b_i b_i^T + |c_i|^2 P_{bb}^i + Tr\left(P_{cc}^i\right) b_i b_i^T \right\}$$

$$+ |g_i|^2 \left\{ |c_i|^2 \left(b_i \bar{\beta}_i^T P_{\alpha b}^i + P_{b\alpha}^i \beta_i b_i^T\right) \right.$$

$$\left. + \left(b_i \bar{\beta}_i^T P_{\alpha c}^i c_i b_i^T + b_i c_i^T P_{c\alpha}^i \beta_i b_i^T\right)\right\}$$

$$+ |g_i|^2 \left\{ P_{bc}^i c_i b_i^T + b_i c_i^T P_{cb}^i \right\}$$

where P^i_{xy} denotes the cross-covariance between the vectors x and y for the i^{th} mode. Note that this expression applies for all frequencies.

Since the trace of a matrix is equal to the sum of its eigenvalues, that is,

$$Tr(A) = \sum_{k=1}^{n} \lambda_k(A) \tag{5-72a}$$

and since

$$\left(Tr \sum_i x_i \bar{y}_i^T\right) = \sum_i Tr\left(x_i \bar{y}_i^T\right) = \sum_i \bar{y}_i^T x_i \tag{5-72b}$$

an upper bound for $\bar{\sigma}_{rms}(\Delta G_i)$ is given by

$$\begin{aligned}\bar{\sigma}^2_{rms} \leq\ & |g_i|^2\left\{|c_i|^2 |b_i|^2 \bar{\beta}_i^T P^i_{\alpha\alpha} \beta_i + |c_i|^2 Tr\left(P^i_{bb}\right) + |b_i|^2 Tr\left(P^i_{cc}\right)\right\} \\ & + |g_i|^2\left\{2|c_i|^2 \beta_{ri}^T P^i_{\alpha b} b_i + 2|b_i|^2 \beta_{ri}^T P^i_{\alpha c} c_i + 2c_i^T P^i_{cb} b_i\right\}\end{aligned} \tag{5-73}$$

where

$$\beta_{ri}^T \triangleq Re\left\{\beta_i^T\right\} = -(Re(g_i) \quad \omega Im(g_i)) \tag{5-74}$$

Now evaluating at the modal resonance frequency ($\omega = \omega_i$), where it reaches its maximum, using covariances from Table 5-4b as well as cross-covariances not shown in the table gives (assuming an element of c_i has been eliminated)

$$\begin{aligned}&\bar{\sigma}_{rms}(\Delta G_i(j\omega_i)) \\ &\leq \left\{(2+4) + (n_i + \rho^{-1}) + (n_o - 2 + \rho^{-1}) - 2(2) - 2(0) - 2(\rho^{-1} - 1)\right\}^{1/2} \\ &\times \{SNR_T\ T_{ID}\}^{1/2} \quad \bar{\sigma}(G_i(j\omega_i)) \\ &= \{2 + n_i + n_o\}^{1/2} \quad \{SNR_T\ T_{ID}\}^{1/2} \quad \bar{\sigma}\ (G_i(j\omega_i))\end{aligned} \tag{5-75}$$

This result is particularly pleasing for two reasons. First, it is independent of ρ^{-1}, which is a measure of the degree of difficulty in identifying the elements of b_i and c_i. This is consistent with the fact that a transfer function should be independent of its state space realization. Second, the final result (5-75) can be shown to hold for the ILAS case as well by letting $n_o = n_i$ and $c_i = b_i$ and making the appropriate substitutions. Associating $n_o + n_i + 2 = 8$ with the coefficient c (used in the previous subsection) shows that earlier estimates for transfer function absolute error were a bit conservative. Since this estimate is itself conservative, the true additive error in ΔG_i could be as much as a factor $\sqrt{\min(n_o, n_i)}$ smaller yet.

Loop Transfer Function Errors

Since the total error in the transfer function consists of the sum of the contributions due to all modes, that is,

$$\Delta G = \sum_{i=1}^{n} \Delta G_i \tag{5-76}$$

and since the correlations of parameter errors between modes is negligible for light damping, the total rms additive error in the transfer function ΔG is given by

$$\bar{\sigma}_{rms}(\Delta G) \simeq \max_k g_k^{1/2} \left[\sum_{i=1}^{n} E\left\{ \Delta \bar{G}_i^T \Delta G_i \right\} \right] \tag{5-77}$$

Similarly, the additive error in the loop transfer function $K\Delta G$ is given by

$$\bar{\sigma}_{rms}(K\Delta G) \simeq \max_k g_k^{1/2} \left[\sum_{i-1}^{n} E\{ (\overline{K\Delta G})^T K \Delta G \} \right] \tag{5-78}$$

while the corresponding multiplicative error is identical in form with K replaced by $(KG)^{-1}K$. These quantities may be computed by replacing c_i and Δc_i in (5-71) by Kc_i and $K\Delta c_i$ or $(KG)^{-1}Kc_i$ and $(KG)^{-1}K\Delta c_i$, recognizing that these multipliers may be factored out of all expectations.

Closed-loop stability for the true system in the face of parameter identification errors in the model may then be verified by either of the following tests:

$$\bar{\sigma}_{rms}(K\Delta G(j\omega)) < \underline{\sigma}(I + KG(j\omega)) \tag{5-79a}$$

or

$$\bar{\sigma}_{rms}[(KG(j\omega))^{-1}K\Delta G(j\omega)] < \underline{\sigma}[I + (KG(j\omega))^{-1}] \tag{5-79b}$$

for all $\omega \geq 0$.

SECTION 6

IDENTIFIABILITY ANALYSIS AND CONTROL DESIGNS

This section presents detailed identifiability analysis results and control designs for the two concepts examined in this study. Identification results for both concepts are limited to Test Signal 1 with position measurements since this was the only case examined with our detailed identifiability analysis software. Results for the other test signal/measurement noise combinations can be expected to closely follow earlier presented analytical predictions. Control designs employ simple rate-feedback for the baseline (ILAS) concept and linear-quadratic-gaussian (LQG) methods with robustness recovery (Ref. 2) for the advanced (non-ILAS) concept.

BASELINE CONCEPT

Identifiability Analysis

Because the light damping criterion (5-40) is satisfied for all critical modes in the baseline concept, both exact and approximate identifiability analysis give virtually identical results. Only results for the latter approximate analysis are presented since they include the stochastic parameter error contribution due to both measurement and process noise. Parameter biases, which are available only with the exact analysis, are negligible for this concept. Since there is essentially no coupling between axes, single-axis and multi-axis identification should be identical. Both were examined and are presented for purposes of illustration.

The following numerical results tabulate both absolute and relative parameter errors at the standard deviation level for each mode identified, using the approximate formulas described in Table 5-4a. Error source designations R, W, and T correspond to measurement noise, process noise, and their root-sum-squared total, respectively. Test signal, process noise, and measurement noise intensities assumed were those defined in Table 3-2 for Test Signal 1 and position (attitude) measurements.

All results are stated in terms of accumulated error at the end of an identification time of one second. To determine errors for a sample length of T_{ID} seconds, simply divide stated results by $\sqrt{T_{ID}}$.

Only those modes for which

$$\frac{1}{2\zeta_i}\bar{\sigma}\left(c_i b_i^T\right) = \frac{|c_i||b_i|}{2\zeta_i} > \underline{\sigma}\left(\sum_{j=1}^{i-1} c_j b_j^T\right) \qquad (6\text{-}1)$$

were assumed to be identified. This is an approximation to condition (3-17a), which neglects the effects of resonances near the i^{th} mode and ignores all modes beyond the i^{th} mode.

Roll Axis--Approximate identification errors for the roll axis of the baseline ILAS concept are summarized in Table 6-1a. For each mode, nominal frequency (W) and damping (Z) are shown, along with the ratio (RATIO) of the LHS to the RHS in condition (6-1). Results are tabulated only for those seven modes for which this ratio is greater than 1. Following the nominal values for each parameter are the absolute and relative errors for each error source described above.

It should be observed that these approximate results for errors due to measurement noise closely match the exact results for all modes except the well-damped isolator modes (11 and 16). Whereas mode 11 could easily be eliminated with little loss in model fidelity, mode 16 is evidently important for its asymptotic contribution to the transfer function model at high frequencies. Because of their heavy damping, both could be eliminated from the model for control design purposes.

The results of Table 6-1a show that errors due to measurement noise dominate those due to process noise, except for mode 9 where the two error contributions are about equal. As is obvious from the expression of Table 5-4a (for the SISO case) and supported by the results of Table 6-1a, the largest relative error for each mode occurs for the damping factor parameter ($2\zeta\omega$), while the smallest errors occur for frequency squared (ω^2). Worst-case identification errors occur for mode 10, where a total relative damping error of $\sigma_{2\zeta\omega}/2\zeta\omega = \sigma_\zeta/\zeta = 7.03$ remains after one second. To reduce relative transfer function error (5-50) below 1 would require an identification time of

TABLE 6-1a. APPROXIMATE IDENTIFICATION ERRORS FOR BASELINE CONCEPT: ROLL AXIS (X)

MODE 9 ; W = 1.9936 R/S ; ZETA = 0.0050 ; RATIO = 25.9495

PARAMETER	W**2	2*Z*W	B 4
NOM VALUE	3.9744E 00	1.9936E-02	4.7579E-04
ABS ERR-R	4.9421E-02	3.5059E-02	2.9583E-04
REL ERR-R	0.0124	1.7586	0.6218
ABS ERR-W	5.6297E-02	3.9937E-02	3.3699E-04
REL ERR-W	0.0142	2.0033	0.7083
ABS ERR-T	7.4912E-02	5.3142E-02	4.4841E-04
REL ERR-T	0.0188	2.6656	0.9425

MODE 10 ; W = 2.0916 R/S ; ZETA = 0.0050 ; RATIO = 5.7657

PARAMETER	W**2	2*Z*W	B 4
NOM VALUE	4.3748E 00	2.0916E-02	2.5169E-04
ABS ERR-R	2.0890E-01	1.4125E-01	6.0096E-04
REL ERR-R	0.0478	6.7532	2.3877
ABS ERR-W	6.0499E-02	4.0907E-02	1.7404E-04
REL ERR-W	0.0138	1.9558	0.6915
ABS ERR-T	2.1749E-01	1.4705E-01	6.2565E-04
REL ERR-T	0.0497	7.0307	2.4858

TABLE 6-1a. APPROXIMATE IDENTIFICATION ERRORS FOR BASELINE CONCEPT: ROLL AXIS (X) (continued)

MODE 11 ; W = 2.7847 R/S ; ZETA = 0.7000 ; RATIO = 1.3397

PARAMETER	W**2	2*Z*W	B 4
NOM VALUE	7.7547E 00	3.8986E 00	-1.4763E-03
ABS ERR-R	2.7388E 01	1.9572E 01	3.2038E-03
REL ERR-R	3.5318	5.0202	2.1701
ABS ERR-W	1.0997E 00	7.8584E-01	1.2864E-04
REL ERR-W	0.1418	0.2016	0.0871
ABS ERR-T	2.7410E 01	1.9587E 01	3.2064E-03
REL ERR-T	3.5347	5.0242	2.1719

MODE 16 ; W = 8.4669 R/S ; ZETA = 0.7000 ; RATIO = 16.4746

PARAMETER	W**2	2*Z*W	B 4
NOM VALUE	7.1688E 01	1.1854E 01	-9.8451E-03
ABS ERR-R	3.0185E 01	7.0943E 00	2.5471E-03
REL ERR-R	0.4211	0.5985	0.2587
ABS ERR-W	5.8301E 00	1.3703E 00	4.9197E-04
REL ERR-W	0.0813	0.1156	0.0500
ABS ERR-T	3.0743E 01	7.2255E 00	2.5942E-03
REL ERR-T	0.4288	0.6096	0.2635

TABLE 6-1a. APPROXIMATE IDENTIFICATION ERRORS FOR BASELINE CONCEPT: ROLL AXIS (X) (continued)

MODE 22 ; W = 18.7836 R/S ; ZETA = 0.0050 ; RATIO = 290.8431

PARAMETER	W**2	2*Z*W	B 4
NOM VALUE	3.5282E 02	1.8784E-01	-1.7150E-02
ABS ERR-R	9.7656E-02	7.3526E-03	2.3735E-04
REL ERR-R	0.0003	0.0391	0.0138
ABS ERR-W	1.6282E 00	1.2259E-01	3.9573E-03
REL ERR-W	0.0046	0.6526	0.2307
ABS ERR-T	1.6311E 00	1.2281E-01	3.9644E-03
REL ERR-T	0.0046	0.6538	0.2312

MODE 26 ; W = 33.0515 R/S ; ZETA = 0.0050 ; RATIO = 5.0104

PARAMETER	W**2	2*Z*W	B 4
NOM VALUE	1.0924E 03	3.3052E-01	-4.4501E-03
ABS ERR-R	1.0481E 01	4.4849E-01	2.1350E-03
REL ERR-R	0.0096	1.3570	0.4798
ABS ERR-W	3.0003E 00	1.6261E-01	7.7411E-04
REL ERR-W	0.0035	0.4920	0.1740
ABS ERR-T	1.1149E 01	4.7706E-01	2.2710E-03
REL ERR-T	0.0102	1.4434	0.5103

TABLE 6-1a. APPROXIMATE IDENTIFICATION ERRORS FOR BASELINE CONCEPT: ROLL AXIS (X) (concluded)

MODE 29 ; W = 52.5275 R/S ; ZETA = 0.0050 ; RATIO = 14.7208

PARAMETER	W**2	2*Z*W	B 4
NOM VALUE	2.7591E 03	5.2528E-01	-7.8166E-03
ABS ERR-R	1.7192E 01	4.6287E-01	2.4353E-03
REL ERR-R	0.0062	0.8812	0.3116
ABS ERR-W	7.6140E 00	2.0500E-01	1.0786E-03
REL ERR-W	0.0028	0.3903	0.1380
ABS ERR-T	1.8802E 01	5.0623E-01	2.6635E-03
REL ERR-T	0.0068	0.9637	0.3407

$$T_{ID} = \frac{1}{(2\zeta)^2}\left(\frac{\sigma_{\omega^2}}{\omega^2}\right)^2 + \left(\frac{\sigma_{2\zeta\omega}}{2\zeta\omega}\right)^2 + 2\left(\frac{\sigma_{|b|}}{|b|}\right)^2 \qquad (6\text{-}2)$$

$$= (0.05/0.01)^2 + 7.03^2 + 2(2.5)^2$$

$$\approx 87 \text{ sec}$$

To reduce this error below 0.1 (or 10%) would require $87 \times 10^2 = 8700$ sec, or roughly 2.4 hours. As evident by its absence from Figure 5-8, however, this mode is probably not critical for a nominal control gain crossover below $\omega_c = 100$ r/s.

Results for mode 9, the next most difficult mode to identify (not counting isolator mode 11), indicate that identification times of roughly 12 sec and 1200 sec (1/3 hour) would be needed to achieve relative transfer function errors of 100% and 10%, respectively. To provide such margins of safety, it is evident that either larger test signal intensity or smaller measurement errors are desirable to reduce required identification time. The need for higher bandwidth control laws leads to similar conclusions.

Pitch Axis--Approximate identification errors for the pitch axis of the baseline ILAS concept are summarized in Table 6-1b for four modes. The first mode (7) is an isolator mode and is included only for its (small) asymptotic contribution to the transfer function model at high frequencies. Worst-case identification errors occur for mode 14, where a relative damping error of 1.02 remains after one second. Thus, identification time may be somewhat shorter for the pitch axis to achieve relative accuracies comparable to those obtained for the roll axis.

Yaw Axis--Approximate identification errors for the yaw axis of the baseline ILAS concept are summarized in Table 6-1c for three modes. Isolator modes 7, 8, and 13 were not identified since their impact on the transfer function model is negligible. Worst-case identification errors occur for mode 15, where a relative damping error of 1.00 remains after one second. Here again, identification times may be somewhat shorter than for the roll axis to achieve comparable accuracy.

All Axes Combined--Approximate identification errors assuming simultaneous identification of all three axes are summarized in Table 6-2 for the total set of 14 modes included in the three single-axis cases just described. This MIMO identification assumes that all three influence coefficients (b_4, b_5, b_6) for the three input/output pairs are identified for each mode, rather than the single nonzero coefficient identified for each mode in the three SISO cases. Thus relative errors for coefficients which are nominally near zero are not particularly meaningful. Normalization for identification errors in the b and c vectors by the nominal vector magnitudes, $|b|$ and $|c|$, respectively, as was done in Table 5-4a, is clearly more meaningful here.

Comparison of identification results for the three-axis case with those for the three single-axis cases reveals that identification errors for ω^2, $2\zeta\omega$, and the dominant b parameter are virtually identical for all modes. This is, of course, to be expected since the three axes are virtually uncoupled. Thus, worst-case identification errors occur again for mode 10, which is a roll-axis mode. When significant coupling exists between axes, however, MIMO identification should offer significant performance improvement over independent identification of each input/output pair.

TABLE 6-1b. APPROXIMATE IDENTIFICATION ERRORS FOR BASELINE CONCEPT: PITCH AXIS (Y)

MODE 7 ; W = 0.9144 R/S ; ZETA = 0.7000 ; RATIO = 2.0856

PARAMETER	W**2	2*Z*W	B 5
NOM VALUE	8.3617E-01	1.2802E 00	1.5443E-03
ABS ERR-R	5.0786E-01	1.1052E 00	5.7633E-04
REL ERR-R	0.6074	0.8633	0.3732
ABS ERR-W	2.0693E-01	4.5031E-01	2.3482E-04
REL ERR-W	0.2475	0.3518	0.1521
ABS ERR-T	5.4840E-01	1.1934E 00	6.2233E-04
REL ERR-T	0.6558	0.9322	0.4030

MODE 14 ; W = 7.6891 R/S ; ZETA = 0.0050 ; RATIO = 952.2576

PARAMETER	W**2	2*Z*W	B 5
NOM VALUE	5.9122E 01	7.6891E-02	5.5364E-03
ABS ERR-R	4.1125E-02	7.5640E-03	1.9256E-04
REL ERR-R	0.0007	0.0984	0.0348
ABS ERR-W	4.2642E-01	7.8432E-02	1.9967E-03
REL ERR-W	0.0072	1.0200	0.3606
ABS ERR-T	4.2840E-01	7.8796E-02	2.0060E-03
REL ERR-T	0.0072	1.0248	0.3623

TABLE 6-1b. APPROXIMATE IDENTIFICATION ERRORS FOR BASELINE CONCEPT: PITCH AXIS (Y) (concluded)

MODE 24 ; W = 21.2828 R/S ; ZETA = 0.0050 ; RATIO = 423.6492

PARAMETER	W**2	2*Z*W	B 5
NOM VALUE	4.5296E 02	2.1283E-01	-1.1993E-02
ABS ERR-R	3.0921E-01	2.0547E-02	4.0936E-04
REL ERR-R	0.0007	0.0965	0.0341
ABS ERR-W	1.9637E 00	1.3049E-01	2.5998E-03
REL ERR-W	0.0043	0.6131	0.2168
ABS ERR-T	1.9879E 00	1.3210E-01	2.6318E-03
REL ERR-T	0.0044	0.6207	0.2194

MODE 36 ; W = 85.3456 R/S ; ZETA = 0.0050 ; RATIO = 166.9703

PARAMETER	W**2	2*Z*W	B 5
NOM VALUE	7.2839E 03	8.5346E-01	1.7229E-02
ABS ERR-R	1.9347E 01	3.2059E-01	2.2882E-03
REL ERR-R	0.0027	0.3756	0.1328
ABS ERR-W	1.5769E 01	2.6130E-01	1.8651E-03
REL ERR-W	0.0022	0.3062	0.1083
ABS ERR-T	2.4959E 01	4.1359E-01	2.9520E-03
REL ERR-T	0.0034	0.4846	0.1713

TABLE 6-1c. APPROXIMATE IDENTIFICATION ERRORS FOR BASELINE CONCEPT: YAW AXIS (Z)

MODE 15 ; W = 8.1696 R/S ; ZETA = 0.0050 ; RATIO = 914.7297

PARAMETER	W**2	2*Z*W	B 6
NOM VALUE	6.6742E 01	8.1696E-02	-4.8091E-03
ABS ERR-R	6.7388E-02	1.1666E-02	2.4279E-04
REL ERR-R	0.0010	0.1428	0.0505
ABS ERR-W	4.6702E-01	8.0846E-02	1.6826E-03
REL ERR-W	0.0070	0.9896	0.3499
ABS ERR-T	4.7185E-01	8.1683E-02	1.7000E-03
REL ERR-T	0.0071	0.9998	0.3535

MODE 23 ; W = 19.9551 R/S ; ZETA = 0.0050 ; RATIO = 411.4595

PARAMETER	W**2	2*Z*W	B 6
NOM VALUE	3.9820E 02	1.9955E-01	1.0291E-02
ABS ERR-R	3.3520E-01	2.3756E-02	4.3314E-04
REL ERR-R	0.0008	0.1190	0.0421
ABS ERR-W	1.7828E 00	1.2635E-01	2.3037E-03
REL ERR-W	0.0045	0.6332	0.2239
ABS ERR-T	1.8141E 00	1.2857E-01	2.3441E-03
REL ERR-T	0.0046	0.6443	0.2278

TABLE 6-1c. APPROXIMATE IDENTIFICATION ERRORS FOR BASELINE CONCEPT: YAW AXIS (Z) (concluded)

MODE 33 ; W = 71.2905 R/S ; ZETA = 0.0050 ; RATIO = 80.8774

PARAMETER	W**2	2*Z*W	B 6
NOM VALUE	5.0823E 03	7.1290E-01	1.0318E-02
ABS ERR-R	2.8735E 01	5.7005E-01	2.9170E-03
REL ERR-R	0.0057	0.7996	0.2827
ABS ERR-W	1.2039E 01	2.3882E-01	1.2221E-03
REL ERR-W	0.0024	0.3350	0.1184
ABS ERR-T	3.1155E 01	6.1805E-01	3.1627E-03
REL ERR-T	0.0061	0.8670	0.3065

Identification time necessary to reduce relative transfer function errors for mode 10 below one for this case is now given by

$$T_{ID} = (0.05/0.01)^2 + 7.03^2 + 2(2.5)^2 + 2(2.5)^2 + 2(2.5)^2$$

$$\approx 112 \text{ sec}$$

Similarly, for a fixed T_{ID} the assumption of possible coupling between axes seems to increase relative transfer function error over the single-axis (uncoupled) case. This characteristic is believed to be due to the conservative assumption of independent errors used to derive (5-50). It believed that when all correlations between error sources are considered, such differences must disappear.

Control Design

We have noted earlier (Section 2) that to accomplish disturbance attenuation using the vibration control structure of Figure 2-3, loop gains for each of the three vibration control loops should be greater than 1 over the frequency range of the

TABLE 6-2. APPROXIMATE IDENTIFICATION RESULTS
FOR BASELINE CONCEPT: ALL AXES

MODE 7 ; W = 0.9144 R/S ; ZETA = 0.7000 ; RATIO = 2.1216

PARAMETER	W**2	2*Z*W	B 4	B 5	B 6
NOM VALUE	8.3617E-01	1.2802E 00	2.8304E-08	1.5443E-03	-3.1183E-05
ABS ERR-R	5.0620E-01	1.1016E 00	3.3444E-04	5.7476E-04	3.3351E-04
REL ERR-R	0.6054	0.8605	0.2162	0.3716	0.2169
ABS ERR-W	2.0693E-01	4.5031E-01	1.3671E-04	2.3495E-04	1.3715E-04
REL ERR-W	0.2475	0.3518	0.0884	0.1519	0.0887
ABS ERR-T	5.4686E-01	1.1901E 00	3.6130E-04	6.2093E-04	3.6246E-04
REL ERR-T	0.6540	0.9296	0.2336	0.4014	0.2343

MODE 9 ; W = 1.9936 R/S ; ZETA = 0.0050 ; RATIO = 23.9495

PARAMETER	W**2	2*Z*W	B 4	B 5	B 6
NOM VALUE	3.9744E 00	1.9936E-02	4.7579E-04	-1.0394E-11	-5.4119E-11
ABS ERR-R	4.9421E-02	3.5059E-02	2.9583E-04	2.9581E-04	2.9581E-04
REL ERR-R	0.0124	1.7586	0.6218	0.6217	0.6217
ABS ERR-W	5.6297E-02	3.9937E-02	3.3699E-04	3.3697E-04	3.3697E-04
REL ERR-W	0.0142	2.0033	0.7083	0.7082	0.7082
ABS ERR-T	7.4912E-02	5.3142E-02	4.4841E-04	4.4839E-04	4.4839E-04
REL ERR-T	0.0188	2.6656	0.9425	0.9424	0.9424

TABLE 6-2. APPROXIMATE IDENTIFICATION RESULTS
FOR BASELINE CONCEPT: ALL AXES (continued)

MODE 10 ; W = 2.0916 R/S ; ZETA = 0.0050 ; RATIO = 5.7657

PARAMETER	W**2	2*Z*W	B 4	B 5	B 6
NOM VALUE	4.3748E 00	2.0916E-02	2.5169E-04	1.3324E-09	5.6571E-09
ABS ERR-R	2.0890E-01	1.4125E-01	6.0096E-04	6.0093E-04	6.0093E-04
REL ERR-R	0.0478	6.7532	2.3877	2.3875	2.3875
ABS ERR-W	6.0499E-02	4.0907E-02	1.7404E-04	1.7403E-04	1.7403E-04
REL ERR-W	0.0138	1.9558	0.6915	0.6914	0.6914
ABS ERR-T	2.1749E-01	1.4705E-01	6.2565E-04	6.2562E-04	6.2562E-04
REL ERR-T	0.0497	7.0307	2.4858	2.4857	2.4857

MODE 11 ; W = 2.7847 R/S ; ZETA = 0.7000 ; RATIO = 1.3397

PARAMETER	W**2	2*Z*W	B 4	B 5	B 6
NOM VALUE	7.7547E 00	3.8986E 00	-1.4763E-03	-7.9941E-10	-3.3207E-09
ABS ERR-R	2.7388E 01	1.9572E 01	3.2038E-03	1.8622E-03	1.8622E-03
REL ERR-R	3.5318	5.0202	2.1701	1.2614	1.2614
ABS ERR-W	1.0997E 00	7.8584E-01	1.2864E-04	7.4770E-05	7.4770E-05
REL ERR-W	0.1418	0.2016	0.0871	0.0506	0.0506
ABS ERR-T	2.7410E 01	1.9587E 01	3.2064E-03	1.8637E-03	1.8637E-03
REL ERR-T	3.5347	5.0242	2.1719	1.2624	1.2624

TABLE 6-2. APPROXIMATE IDENTIFICATION RESULTS
FOR BASELINE CONCEPT: ALL AXES (continued)

MODE 14 ; W = 7.6891 R/S ; ZETA = 0.0050 ; RATIO = 1219.4851

PARAMETER	W**2	2*Z*W	B 4	B 5	B 6
NOM VALUE	5.9122E 01	7.6891E-02	-3.0726E-08	5.5364E-03	7.6977E-05
ABS ERR-R	4.1117E-02	7.5626E-03	1.9254E-04	1.9254E-04	1.9254E-04
REL ERR-R	0.0007	0.0984	0.0348	0.0348	0.0348
ABS ERR-W	4.2642E-01	7.8432E-02	1.9968E-03	1.9969E-03	1.9968E-03
REL ERR-W	0.0072	1.0200	0.3606	0.3606	0.3606
ABS ERR-T	4.2840E-01	7.8796E-02	2.0061E-03	2.0062E-03	2.0061E-03
REL ERR-T	0.0072	1.0248	0.3623	0.3623	0.3623

MODE 15 ; W = 8.1696 R/S ; ZETA = 0.0050 ; RATIO = 916.3227

PARAMETER	W**2	2*Z*W	B 4	B 5	B 6
NOM VALUE	6.6742E 01	8.1696E-02	2.1435E-06	6.7892E-05	-4.8091E-03
ABS ERR-R	6.7375E-02	1.1663E-02	2.4276E-04	2.4276E-04	2.4277E-04
REL ERR-R	0.0010	0.1428	0.0505	0.0505	0.0505
ABS ERR-W	4.6702E-01	8.0846E-02	1.6827E-03	1.6827E-03	1.6828E-03
REL ERR-W	0.0070	0.9896	0.3499	0.3499	0.3499
ABS ERR-T	4.7185E-01	8.1683E-02	1.7001E-03	1.7001E-03	1.7002E-03
REL ERR-T	0.0071	0.9998	0.3535	0.3535	0.3535

TABLE 6-2. APPROXIMATE IDENTIFICATION RESULTS
FOR BASELINE CONCEPT: ALL AXES (continued)

MODE 16 ; W = 8.4669 R/S ; ZETA = 0.7000 ; RATIO = 16.4747

PARAMETER	W**2	2*Z*W	B 4	B 5	B 6
NOM VALUE	7.1688E 01	1.1854E 01	-9.8451E-03	6.0526E-09	-9.7898E-07
ABS ERR-R	3.0185E 01	7.0943E 00	2.5471E-03	1.4805E-03	1.4805E-03
REL ERR-R	0.4211	0.5985	0.2587	0.1504	0.1504
ABS ERR-W	5.8301E 00	1.3703E 00	4.9197E-04	2.8595E-04	2.8595E-04
REL ERR-W	0.0813	0.1156	0.0500	0.0290	0.0290
ABS ERR-T	3.0743E 01	7.2255E 00	2.5942E-03	1.5078E-03	1.5078E-03
REL ERR-T	0.4288	0.6096	0.2635	0.1532	0.1532

MODE 22 ; W = 18.7836 R/S ; ZETA = 0.0050 ; RATIO = 1142.8687

PARAMETER	W**2	2*Z*W	B 4	B 5	B 6
NOM VALUE	3.5282E 02	1.8784E-01	-1.7150E-02	-3.7565E-08	-4.9650E-08
ABS ERR-R	9.7656E-02	7.3526E-03	2.3735E-04	2.3734E-04	2.3734E-04
REL ERR-R	0.0003	0.0391	0.0138	0.0138	0.0138
ABS ERR-W	1.6282E 00	1.2259E-01	3.9573E-03	3.9571E-03	3.9571E-03
REL ERR-W	0.0046	0.6526	0.2307	0.2307	0.2307
ABS ERR-T	1.6311E 00	1.2281E-01	3.9644E-03	3.9642E-03	3.9642E-03
REL ERR-T	0.0046	0.6538	0.2312	0.2311	0.2311

TABLE 6-2. APPROXIMATE IDENTIFICATION RESULTS
FOR BASELINE CONCEPT: ALL AXES (continued)

MODE 23 ; W = 19.9551 R/S ; ZETA = 0.0050 ; RATIO = 411.4819

PARAMETER	W**2	2*Z*W	B 4	B 5	B 6
NOM VALUE	3.9820E 02	1.9955E-01	-5.2503E-08	-4.1569E-05	1.0291E-02
ABS ERR-R	3.3520E-01	2.3756E-02	4.3312E-04	4.3312E-04	4.3314E-04
REL ERR-R	0.0008	0.1190	0.0421	0.0421	0.0421
ABS ERR-W	1.7828E 00	1.2635E-01	2.3036E-03	2.3036E-03	2.3038E-03
REL ERR-W	0.0045	0.6332	0.2239	0.2239	0.2239
ABS ERR-T	1.8141E 00	1.2857E-01	2.3440E-03	2.3440E-03	2.3441E-03
REL ERR-T	0.0046	0.6443	0.2278	0.2278	0.2278

MODE 24 ; W = 21.2828 R/S ; ZETA = 0.0050 ; RATIO = 423.6661

PARAMETER	W**2	2*Z*W	B 4	B 5	B 6
NOM VALUE	4.5296E 02	2.1233E-01	5.6825E-08	-1.1993E-02	-2.8140E-05
ABS ERR-R	3.0921E-01	2.0547E-02	4.0934E-04	4.0936E-04	4.0934E-04
REL ERR-R	0.0007	0.0965	0.0341	0.0341	0.0341
ABS ERR-W	1.9637E 00	1.3049E-01	2.5996E-03	2.5998E-03	2.5996E-03
REL ERR-W	0.0043	0.6131	0.2168	0.2168	0.2168
ABS ERR-T	1.9879E 00	1.3210E-01	2.6317E-03	2.6318E-03	2.6317E-03
REL ERR-T	0.0044	0.6207	0.2194	0.2194	0.2194

TABLE 6-2. APPROXIMATE IDENTIFICATION RESULTS
FOR BASELINE CONCEPT: ALL AXES (continued)

MODE 26 ; W = 33.0515 R/S ; ZETA = 0.0050 ; RATIO = 15.0447

PARAMETER	W**2	2*Z*W	B 4	B 5	B 6
NOM VALUE	1.0924E 03	3.3052E-01	-4.4501E-03	1.6294E-09	-7.4501E-10
ABS ERR-R	1.0481E 01	4.4849E-01	2.1350E-03	2.1349E-03	2.1349E-03
REL ERR-R	0.0096	1.3570	0.4798	0.4797	0.4797
ABS ERR-W	3.8003E 00	1.6261E-01	7.7411E-04	7.7407E-04	7.7407E-04
REL ERR-W	0.0035	0.4920	0.1740	0.1739	0.1739
ABS ERR-T	1.1149E 01	4.7706E-01	2.2710E-03	2.2709E-03	2.2709E-03
REL ERR-T	0.0102	1.4434	0.5103	0.5103	0.5103

MODE 29 ; W = 52.5275 R/S ; ZETA = 0.0050 ; RATIO = 46.4166

PARAMETER	W**2	2*Z*W	B 4	B 5	B 6
NOM VALUE	2.7591E 03	5.2528E-01	-7.8166E-03	-3.7546E-10	2.2738E-09
ABS ERR-R	1.7192E 01	4.6287E-01	2.4353E-03	2.4352E-03	2.4352E-03
REL ERR-R	0.0062	0.8812	0.3116	0.3115	0.3115
ABS ERR-W	7.6140E 00	2.0500E-01	1.0786E-03	1.0785E-03	1.0785E-03
REL ERR-W	0.0028	0.3903	0.1380	0.1380	0.1380
ABS ERR-T	1.8802E 01	5.0623E-01	2.6635E-03	2.6633E-03	2.6633E-03

TABLE 6-2. APPROXIMATE IDENTIFICATION RESULTS
FOR BASELINE CONCEPT: ALL AXES (concluded)

MODE 33 ; W = 71.2905 R/S ; ZETA = 0.0050 ; RATIO = 80.8774

PARAMETER	W**2	2*Z*W	B 4	B 5	B 6
NOM VALUE	5.0823E 03	7.1290E-01	1.6504E-08	-5.9175E-08	1.0318E-02
ABS ERR-R	2.8735E 01	5.7005E-01	2.9169E-03	2.9169E-03	2.9170E-03
REL ERR-R	0.0057	0.7996	0.2827	0.2827	0.2827
ABS ERR-W	1.2039E 01	2.3882E-01	1.2220E-03	1.2220E-03	1.2221E-03
REL ERR-W	0.0024	0.3350	0.1184	0.1184	0.1184
ABS ERR-T	3.1155E 01	6.1805E-01	3.1625E-03	3.1625E-03	3.1627E-03
REL ERR-T	0.0061	0.8670	0.3065	0.3065	0.3065

MODE 36 ; W = 85.3456 R/S ; ZETA = 0.0050 ; RATIO = 166.9703

PARAMETER	W**2	2*Z*W	B 4	B 5	B 6
NOM VALUE	7.2839E 03	8.5346E-01	2.7185E-07	1.7229E-02	-1.5168E-07
ABS ERR-R	1.9347E 01	3.2059E-01	2.2881E-03	2.2882E-03	2.2881E-03
REL ERR-R	0.0027	0.3756	0.1328	0.1328	0.1328
ABS ERR-W	1.5769E 01	2.6130E-01	1.8650E-03	1.8651E-03	1.8650E-03
REL ERR-W	0.0022	0.3062	0.1082	0.1083	0.1082
ABS ERR-T	2.4959E 01	4.1359E-01	2.9519E-03	2.9520E-03	2.9519E-03
REL ERR-T	0.0034	0.4846	0.1713	0.1713	0.1713

disturbance, 10 r/s $\leq \omega \leq$ 100 r/s. That is, their bandwidths should be greater than 100 r/s. Since our models are not reliable beyond 100 r/s, however, we have opted to relax this requirement to ensure that loop gains do not exceed 1 for frequencies above 100 r/s.

A control design consistent with this constraint is shown in Figure 6-1. Angular rate feedback was assumed here with a control gain of $K = 1 \times 10^5$ in each axis. Damping for isolator modes was assumed to 0.005 for this design. These loop transmissions agree with our earlier assessment that all modes apparent in these plots lie within the critical region described in Section 3. They should be included in the identification model since they are all close to the critical zero dB line. However, due to the favorable phase characteristics of these loops (-90 deg $\leq \phi \leq$ 90 deg), no instabilities would occur if the smallest two or three of these were neglected. Technically, ILAS control loops require only a lower bound on mode damping to guarantee stability and are relatively insensitive to the assumed mode frequencies. Practically, however, it is impossible to identify damping without knowing frequency. Thus, both frequency and damping of all relevant modes should be identified. This "positive real" control design exhibits theoretical stability margins of $\pm\infty$ dB gain margin and ±90 deg phase margin. After accounting for sensor and actuator dynamics and sampling of the digital control system, practical margins of ±6 dB and ±35 deg should be easily achievable. Though this design assumes rate feedback, substantially the same results could be obtained with attitude measurements from rate-integrating gyros using the lead-lag compensator

$$K(s) \triangleq 1 \times 10^7 \quad \frac{s + 1}{s + 100}$$

Though the control design of Figure 6-1 pushes the bandwidth limit for model validity, it fails to meet performance requirements at all frequencies in the range 10 r/s $\leq \omega \leq$ 100 r/s. The disturbance to LOS transmissions for the closed vibration-control loop just defined are compared with the open loop in Figure 6-2. The DEFOCUS response is omitted since it meets specification as open loop. As expected, this design fails to attenuate disturbances at certain mode frequencies that are not controllable and observable (e.g., 22, 24, 26, 29, and 36). Between these frequencies it provides little if any attenuation. It does, however, come

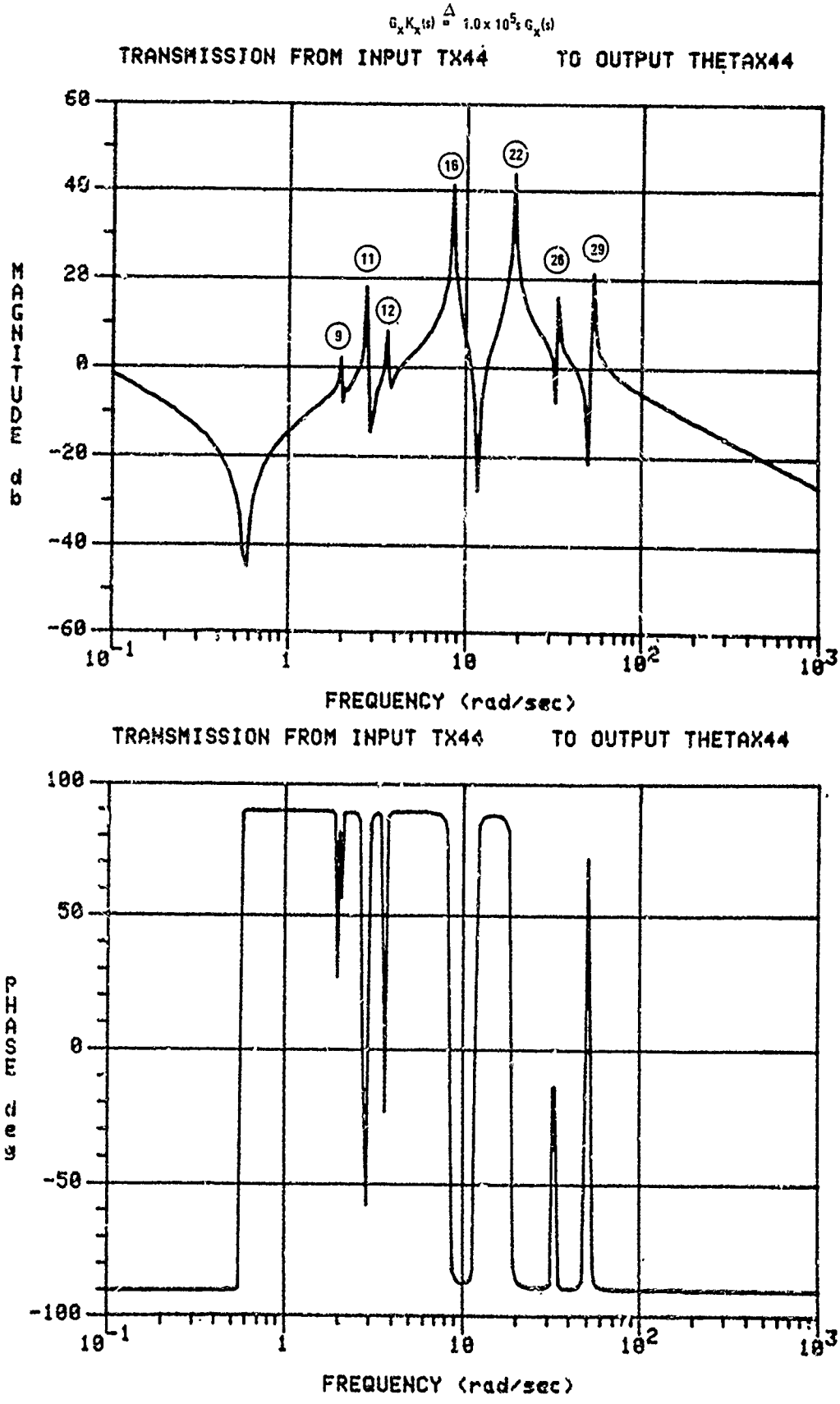

Figure 6-1a. Control Design for Baseline Concept: Roll Axis (X)

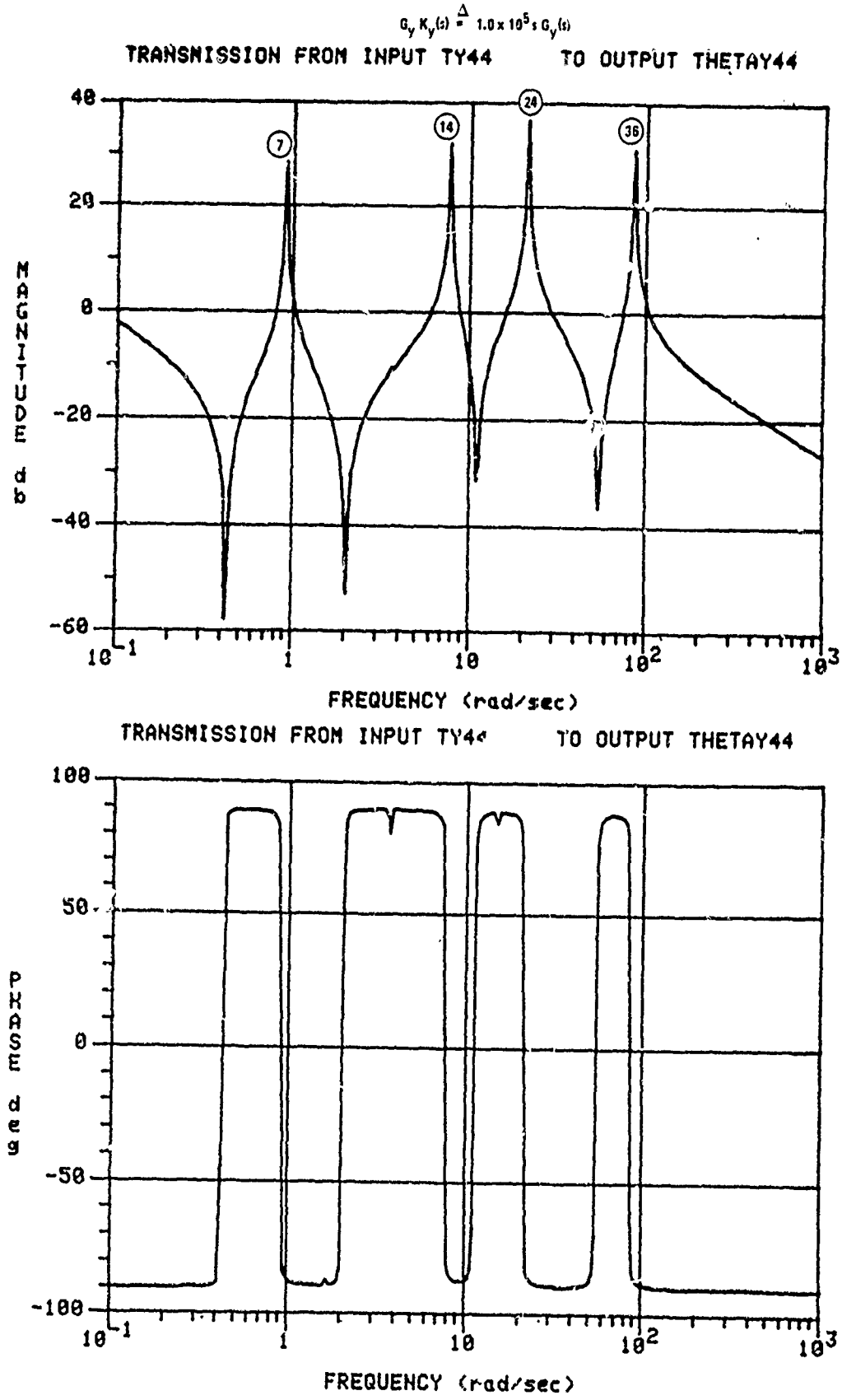

Figure 6-1b. Control Design for Baseline Concept: Pitch Axis (Y)

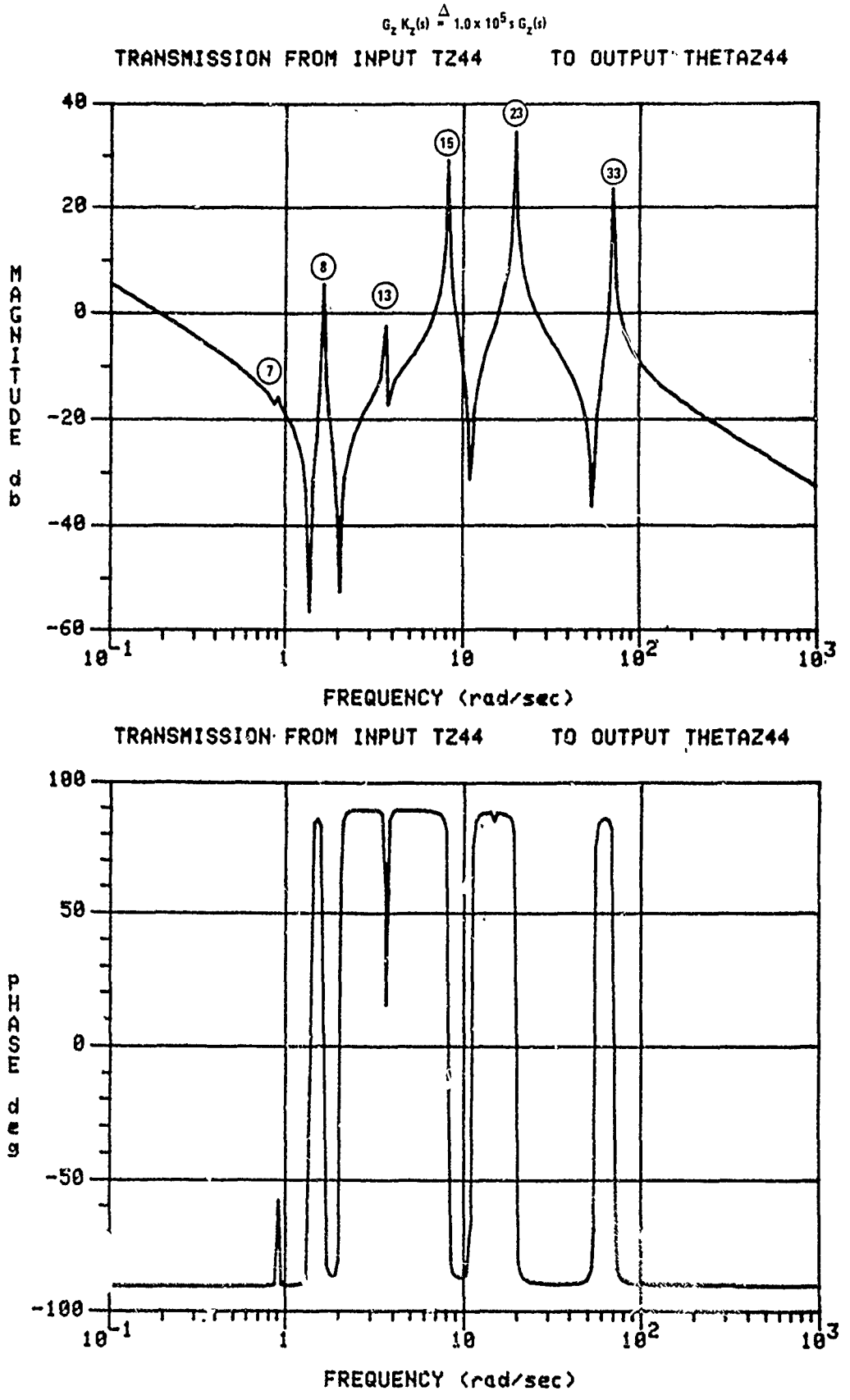

Figure 6-1c. Control Design for Baseline Concept: Yaw Axis (Z)

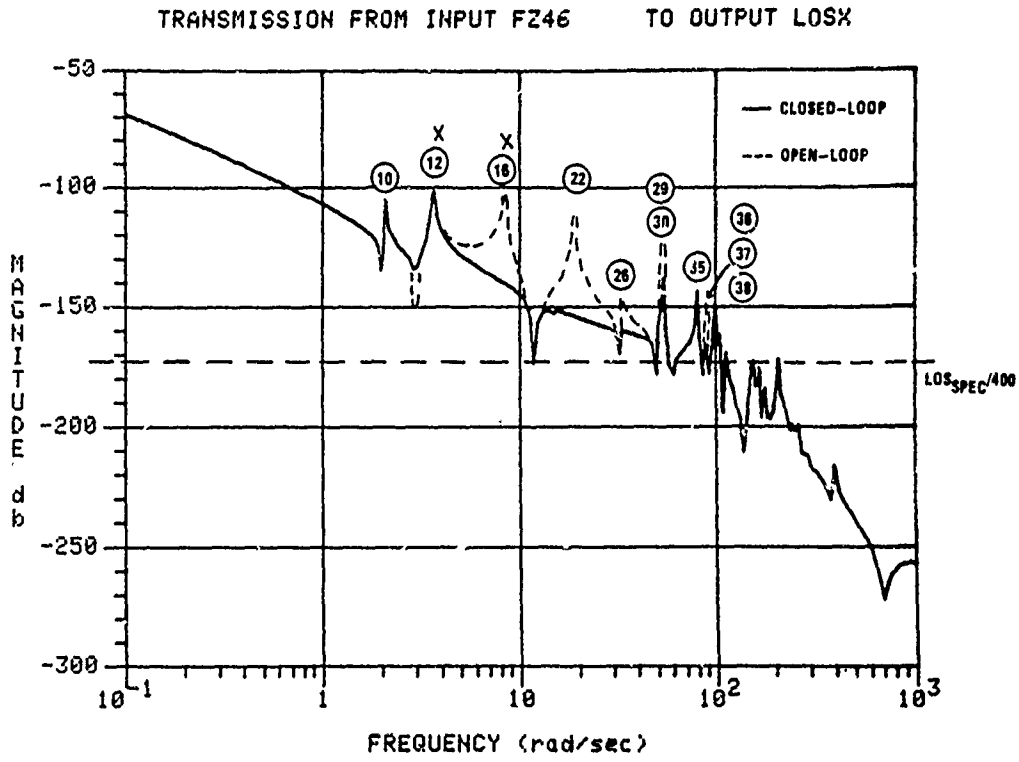

Figure 6-2a. Disturbance to LOS_X Transmission: Closed-Loop vs Open-Loop

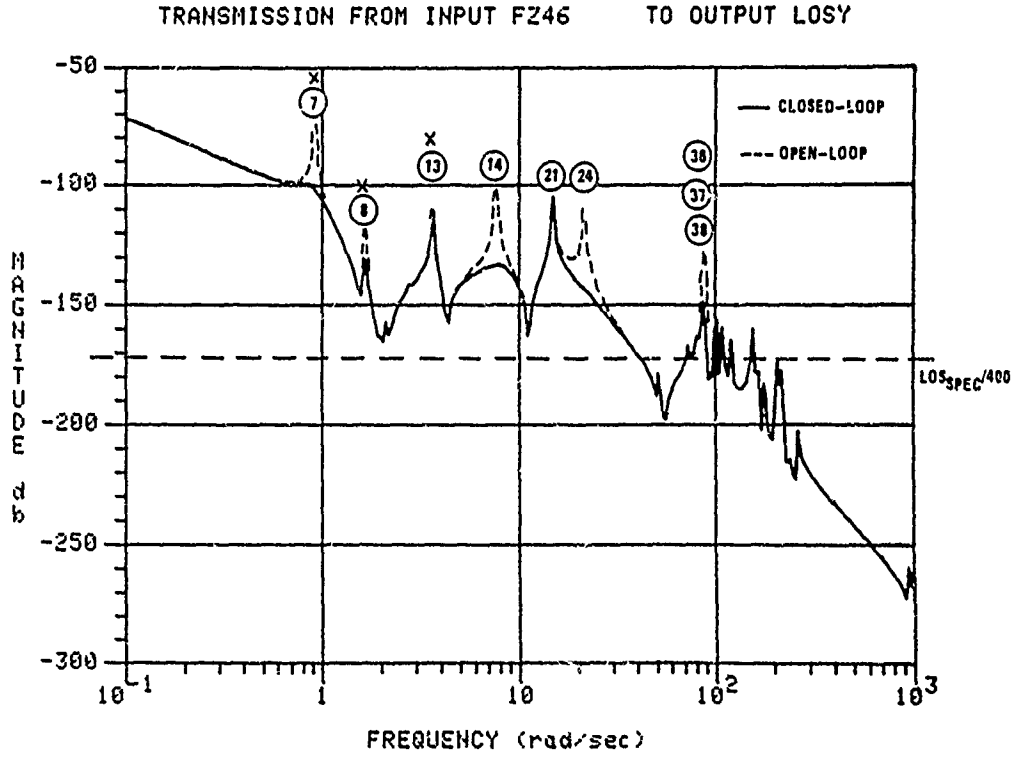

Figure 6-2b. Disturbance to LOS_Y Transmission: Closed-Loop vs Open-Loop

within a factor of 4 (12 dB) of meeting the LOS specification at ω = 31.4 r/s (near mode 26), which was the disturbance frequency assumed by Draper (Ref. 1).

As evident from Figures 6-1 and 6-2 and equation (2-7a), higher control-loop gain (or control bandwidth) will not improve disturbance attenuation performance for this concept. Rather, performance is limited by uncontrollable/unobservable modes, so that "ideal" control requirements are unachievable with this concept for any control design. The presence of uncontrollable/unobservable modes, therefore, imposes a fundamental limitation on control performance. For the advanced concept, which we examine next, all critical modes are controllable and observable so that performance is largely limited by control bandwidth.

ADVANCED CONCEPT

Specific numerical results for the advanced concept identifiability analysis and control design will be discussed in this subsection. The advanced concept, in sharp contrast to the baseline concept, presents a much more difficult (non-ILAS and strongly coupled MIMO dynamics) identification and control problem. But it has the advantage that all critical modes are strongly controllable and observable.

Actuators and sensors were assumed to be the same for both identification and control. This assumption was based on the philosophy that it is only necessary to identify dynamics that affect the control design. Other purposes for doing identification, which are likely to require different actuators and sensors, were not addressed in this study. As discussed in Section 2, actuators for the advanced concept were chosen to be paired shakers to give a torque input about the x, y, z axes at node 44. The sensors were chosen to be accelerometers about the x, y, z axes at node 11. These sensors and actuators produce an extreme case of non-ILAS. That is, not only are the sensors and actuators not at the same location, but they are on different parts of the spacecraft, which are separated by the isolators. In addition, the actuator and sensor types are inconsistent (i.e., torques and linear position). The finite-element model for the structure, which was treated as the true system, had 84 second-order modes modeled. Of these 84 modes, 6 are rigid-body free-free modes, 6 are isolator modes, and the remaining 72 are flexible modes of the spacecraft. The damping coupling due to

the isolators was ignored and was assumed to give the six isolator modes a damping ratio of 0.7; the inherent structural damping was assumed to give all the other modes a damping ratio of 0.005.

Identifiability Analysis

Identifiability analysis was carried out using both the exact and approximate identification analysis software. Both of these computer programs assumed that Test Signal 1 and position output were used.

The numerical results obtained were consistent with each other and with the frequency domain interpretation discussed in Section 5. The frequency domain interpretation was used to make recommendations for test signal sizing and shaping, type of measurement to use, and minimum time for identification. The detailed numerical results for Test Signal 1 and position output will be discussed next. It should be noted that, although results of Section 5 favor the use of Test Signal 2 and rate measurements, these recommendations were actually made after all identifiability analyses of this section were complete.

Stochastic Parameter Error--Recall from Section 4 that stochastic error is the error in the parameter estimates due to random effects. The contributions to stochastic error from measurement noise and process noise were considered for MLE identification without the Kalman filter. Specifically, the stochastic error was defined as

$$\text{Stochastic error:} \quad \Sigma_{\alpha_N} = E\left[(\alpha_N - \hat{\alpha})(\alpha_N - \hat{\alpha})^T\right] \tag{6-3}$$

where α_N is the parameter estimate at the N^{th} sample time and $\hat{\alpha}$ is the limit of α_N as N goes to infinity (i.e., $\hat{\alpha}$ is the expected value of the parameter estimate). For MLE identification in general, stochastic error decreases linearly with increasing measurement time, and increases nonlinearly with decreasing test signal intensity and increasing process noise and measurement noise intensities. For MLE without the Kalman filter, these nonlinear relationships become linear. These statements can be expressed as

$$\Sigma_{\alpha_N} = \frac{1}{(N+1)T}\,\frac{1}{U_o}\left[R_o\Sigma_R + W_o\Sigma_W\right] \qquad (6\text{-}4)$$

where T is the sample time and Σ_R and Σ_W are the sensitivities of stochastic error to measurement and process noise, respectively. The test signal, process noise, and measurement noise intensities are assumed to be given by

Test signal intensity: $U = U_o I$

Process noise intensity: $W = W_o I$

Measurement noise intensity: $R = R_o I$

where U_o, W_o, and R_o are scalars and I is an identity matrix.

The sensitivity to measurement noise was computed exactly for true systems and model systems of the same order using the exact identifiability analysis software. An approximation to it was also computed using the approximate identifiability analysis software, where one-mode true and model systems are assumed. The sensitivity to process noise is exceedingly difficult to compute exactly and was not implemented in the exact identifiability analysis software. An upper bound to this sensitivity was, however, computed as a part of the approximate identifiability analysis software.

Typically, only the diagonal elements of $\Sigma_{\alpha N}$ are of interest, since they are proportional to the square of the standard deviations of the parameters. Also of interest is the relative or normalized error. The relative errors are dimensionless and are easily related to identification accuracy required for control design. The relative errors for a specific mode were defined as

$$\omega^2 \text{ relative error} = \frac{\sigma_{\omega^2}}{\omega_*^2}$$

$$2\zeta\omega \text{ relative error} = \frac{\sigma_{2\zeta\omega}}{2\zeta_*\omega_*}$$

$$b_\ell \text{ relative error} = \frac{b_\ell}{|b_*|} \qquad \ell = 1,2,3$$

$$c_m \text{ relative error} = \frac{c_m}{|c_*|} \qquad m = 1,2,3$$

where the star (*) subscript indicates the true or nominal parameter value. The symbols b_ℓ and c_m stand for the ℓ^{th} and m^{th} element of the parameter vectors b and c, respectively.

Numerical results for 21 flexible modes (147 parameters) in the frequency range 1 to 100 r/sec are shown in Table 6-3 for the approximate identification analysis software and in Table 6-4 for the exact identification analysis software for the following values:

$$T_{ID} = (N + 1)T = 1 \text{ sec}$$

$$U_o = 4 \times 10^{-2}(N-m)^2/Hz \qquad \text{(Test Signal 1)}$$

$$R_o = 10^{-14} r^2/Hz \qquad \text{(position output)}$$

$$W_o = 0.01 U_o$$

As expected, relative errors for damping are the largest parameter errors for each mode. It can be seen that the higher frequency modes are the hardest to identify. This is again consistent with the frequency domain interpretation regarding Test Signal 1 and position output. For comparison, worst-case results for Test Signal 1 with position output and Test Signal 2 with rate output are shown in Table 6-5 for a 300 sec identification time interval. Thus, while identification time intervals would be unreasonable for Test Signal 1 with position output, a 5 min identification time interval with Test Signal 2 and rate output would be sufficient to reduce all relative errors to less than unity.

Worst-case results for stochastic error due to process noise are shown in Table 6-6 for a 300 sec identification time interval. These results are independent of test signal since process noise intensity was assumed proportional to test signal intensity. It is evident that all relative errors are sufficiently small.

It should be observed that approximate and exact results for stochastic error due to measurement noise are essentially the same. Worst-case discrepancies are shown in Table 6-7. These discrepancies are due to "close" modal frequencies, which make the one-mode-at-a-time assumption break down (i.e., $\Delta\omega/\omega \leq 2\zeta$).

TABLE 6-3. APPROXIMATE IDENTIFICATION ANALYSIS STOCHASTIC ERROR RESULTS FOR ADVANCED CONCEPT

MODE 9 ; W = 1.9936 R/S ; ZETA = 0.0050 ; RATIO = 28.4092

PARAMETER	W**2	2*Z*W	B 4	B 5	B 6	C 1	C 2	C 3
NOM VALUE	3.9744E 00	1.9936E-02	4.7579E-04	-1.0394E-11	-5.4119E-11	2.3927E-06	-2.5322E-04	-5.1421E-03
ABS ERR-R	4.5468E-03	3.2397E-03	0.	3.8657E-05	3.8657E-05	4.1834E-04	4.1889E-04	5.9127E-04
REL ERR-R	0.0011	0.1625	0.	0.0812	0.0812	0.0812	0.0814	0.1148
ABS ERR-W	5.6207E-02	3.9937E-02	0.	4.7655E-04	4.7655E-04	5.1571E-03	5.1638E-03	7.2888E-03
REL ERR-W	0.0142	2.0033	0.	1.0016	1.0016	1.0016	1.0029	1.4156
ABS ERR-T	5.6482E-02	4.0168E-02	0.	4.7811E-04	4.7811E-04	5.1740E-03	5.1808E-03	7.3128E-03
REL ERR-T	0.0142	2.0098	0.	1.0049	1.0049	1.0049	1.0062	1.4203

MODE 10 ; W = 2.0916 R/S ; ZETA = 0.0050 ; RATIO = 15.0073

PARAMETER	W**2	2*Z*W	B 4	B 5	B 6	C 1	C 2	C 3
NOM VALUE	4.3748E 00	2.0916E-02	2.5169E-04	1.3324E-09	5.6571E-09	-9.8898E-07	4.9347E-03	7.8374E-04
ABS ERR-R	1.0523E-02	7.1152E-03	0.	4.2809E-05	4.2809E-05	8.4984E-04	1.1945E-03	8.6023E-04
REL ERR-R	0.0024	0.3402	0.	0.1701	0.1701	0.1701	0.2391	0.1722
ABS ERR-W	6.0499E-02	4.0907E-02	0.	2.4612E-04	2.4612E-04	4.8859E-03	6.8674E-03	4.9457E-03
REL ERR-W	0.0138	1.9558	0.	0.9779	0.9779	0.9779	1.3744	0.9898
ABS ERR-T	6.1408E-02	4.1521E-02	0.	2.4981E-04	2.4981E-04	4.9593E-03	6.9706E-03	5.0199E-03
REL ERR-T	0.0140	1.9851	0.	0.9925	0.9925	0.9925	1.3951	1.0047

MODE 14 ; W = 7.6891 R/S ; ZETA = 0.0050 ; RATIO = 12.5233

PARAMETER	W**2	2*Z*W	B 4	B 5	B 6	C 1	C 2	C 3
NOM VALUE	5.9122E 01	7.6891E-02	-3.0726E-08	5.5364E-03	7.6977E-05	4.8514E-04	6.0668E-05	-8.1447E-05
ABS ERR-R	4.5931E-01	8.4482E-02	3.0417E-03	0.	3.0420E-03	3.8104E-04	2.7432E-04	2.7594E-04
REL ERR-R	0.0078	1.0987	0.5493	0.	0.5494	0.7688	0.5535	0.5567
ABS ERR-W	4.2642E-01	7.8432E-02	2.8239E-03	0.	2.8242E-03	3.5376E-04	2.5467E-04	2.5618E-04
REL ERR-W	0.0072	1.0200	0.5100	0.	0.5101	0.7137	0.5138	0.5169
ABS ERR-T	6.2674E-01	1.1528E-01	4.1505E-03	0.	4.1509E-03	5.1994E-04	3.7431E-04	3.7652E-04
REL ERR-T	0.0106	1.4992	0.7496	0.	0.7497	1.0490	0.7552	0.7597

TABLE 6-3. APPROXIMATE IDENTIFICATION ANALYSIS STOCHASTIC ERROR RESULTS FOR ADVANCED CONCEPT (continued)

MODE 15 ; W = 1.1696 R/S ; ZETA = 0.0050 ; RATIO = 68.6431

PARAMETER	W**2	2*Z*W	B 4	B 5	B 6	C 1	C 2	C 3
NOM VALUE	6.8342E 01	8.1696E-02	2.1435E-06	6.7892E-05	-4.8091E-03	2.9030E-03	-1.0413E-03	-5.8811E-04
ABS ERR-R	1.0321E-01	1.7966E-02	5.2590E-04	5.2595E-04	0.	4.6761E-04	3.6170E-04	3.4928E-04
REL ERR-R	0.0015	0.2187	0.1093	0.1094	0.	0.1489	0.1152	0.1112
ABS ERR-W	4.6702E-01	8.0946E-02	2.3797E-03	2.3799E-03	0.	2.1159E-03	1.6367E-03	1.5805E-03
REL ERR-W	0.0070	0.9896	0.4848	0.4848	0.	0.6739	0.5213	0.5034
ABS ERR-T	4.7828E-01	8.2796E-02	2.4371E-03	2.4373E-03	0.	2.1670E-03	1.6762E-03	1.6186E-03
REL ERR-T	0.0072	1.0135	0.5067	0.5068	0.	0.6902	0.5339	0.5155

MODE 17 ; W = 10.8130 R/S ; ZETA = 0.0050 ; RATIO = 16.8035

PARAMETER	W**2	2*Z*W	B 4	B 5	B 6	C 1	C 2	C 3
NOM VALUE	1.1692E 02	1.0813E-01	-3.9589E-07	-8.2180E-07	1.4074E-04	1.5048E-02	-1.0072E-02	-6.2419E-03
ABS ERR-R	1.5422E 00	2.0170E-01	1.3127E-04	1.3127E-04	0.	2.2718E-02	2.0183E-02	1.8788E-02
REL ERR-R	0.0132	1.8654	0.9427	0.9427	0.	1.1861	1.0538	0.9809
ABS ERR-W	7.1113E-01	9.3010E-02	6.0532E-05	6.0532E-05	0.	1.0476E-02	9.3071E-03	8.6639E-03
REL ERR-W	0.0061	0.8602	0.4301	0.4301	0.	0.5470	0.4859	0.4523
ABS ERR-T	1.6982E 00	2.2211E-01	1.4455E-04	1.4455E-04	0.	2.5017E-02	2.2226E-02	2.0690E-02
REL ERR-T	0.0145	2.0541	1.0270	1.0271	0.	1.3062	1.1604	1.0802

MODE 21 ; W = 14.8503 R/S ; ZETA = 0.0050 ; RATIO = 31.7335

PARAMETER	W**2	2*Z*W	B 4	B 5	B 6	C 1	C 2	C 3
NOM VALUE	2.2053E 02	1.4850E-01	1.5491E-07	-2.7118E-04	-2.4793E-04	-2.0781E-03	-3.6152E-03	1.1057E-02
ABS ERR-R	2.9066E 00	2.7680E-01	3.4243E-04	4.3615E-04	4.2219E-04	1.1206E-02	1.1587E-02	0.
REL ERR-R	0.0132	1.8640	0.9320	1.1870	1.1490	0.9483	0.9805	0.
ABS ERR-W	1.1445E 00	1.0900E-01	1.3484E-04	1.7175E-04	1.6625E-04	4.4127E-03	4.5627E-03	0.
REL ERR-W	0.0052	0.7340	0.3670	0.4674	0.4525	0.3734	0.3861	0.
ABS ERR-T	3.1238E 00	2.9749E-01	3.6802E-04	4.6875E-04	4.5375E-04	1.2043E-02	1.2453E-02	0.
REL ERR-T	0.0142	2.0033	1.0016	1.2757	1.2349	1.0191	1.0538	0.

TABLE 6-3. APPROXIMATE IDENTIFICATION ANALYSIS STOCHASTIC ERROR RESULTS FOR ADVANCED CONCEPT (continued)

MODE 22 : W = 17.7836 R/S ; ZETA = 0.0050 ; RATIO = 56.8853

PARAMETER	w**2	2*Z*W	B 4	B 5	B 6	C 1	C 2	C 3
NOM VALUE	3.5282E 02	1.8784E-01	-1.7150E-02	-3.7565E-08	-4.9650E-08	-2.0396E-05	4.0528E-04	-2.2701E-04
ABS ERR-R	3.6819E 00	2.7119E-01	0.	1.2380E-02	1.2380E-02	3.3597E-04	4.4528E-04	3.7353E-04
REL ERR-R	0.0102	1.4438	0.	0.7219	0.7219	0.7226	0.9576	0.8033
ABS ERR-W	1.6282E 00	1.2259E-01	0.	5.5962E-03	5.5962E-03	1.5187E-04	2.0128E-04	1.6884E-04
REL ERR-W	0.0046	0.6526	0.	0.3263	0.3263	0.3266	0.4329	0.3631
ABS ERR-T	3.9528E 00	2.9761E-01	0.	1.3586E-02	1.3586E-02	3.6871E-04	4.8865E-04	4.0991E-04
REL ERR-T	0.0112	1.5844	0.	0.7922	0.7922	0.7930	1.0509	0.8816

MODE 23 : W = 18.9551 R/S ; ZETA = 0.0050 ; RATIO = 93.1679

PARAMETER	w**2	2*Z*W	B 4	B 5	B 6	C 1	C 2	C 3
NOM VALUE	3.9620E 02	1.9955E-01	-5.2503E-08	-4.1569E-05	1.0291E-02	6.8976E-04	-9.1464E-04	-7.1273E-05
ABS ERR-R	3.0052E 00	2.1299E-01	5.4916E-03	5.4917E-03	0.	7.1464E-04	7.8325E-04	6.1370E-04
REL ERR-R	0.0075	1.0673	0.5337	0.5337	0.	0.6226	0.6824	0.5347
ABS ERR-W	1.7828E 00	1.2635E-01	3.2579E-03	3.2579E-03	0.	4.2395E-04	4.6465E-04	3.6407E-04
REL ERR-W	0.0045	0.6332	0.3166	0.3166	0.	0.3694	0.4048	0.3172
ABS ERR-T	3.4943E 00	2.4785E-01	6.3853E-03	6.3853E-03	0.	8.3093E-04	9.1070E-04	7.1357E-04
REL ERR-T	0.0088	1.2410	0.6205	0.6205	0.	0.7239	0.7934	0.6217

MODE 24 : W = 21.2828 R/S ; ZETA = 0.0050 ; RATIO = 90.8078

PARAMETER	w**2	2*Z*W	B 4	B 5	B 6	C 1	C 2	C 3
NOM VALUE	4.5296E 02	2.1283E-01	5.6825E-08	-1.1993E-02	-2.8140E-05	-5.2388E-05	1.1939E-04	-3.8048E-04
ABS ERR-R	9.2200E 00	6.1267E-01	1.7262E-02	0.	1.7262E-02	5.8379E-04	6.0387E-04	7.9693E-04
REL ERR-R	0.0204	2.8787	1.4393	0.	1.4393	1.4515	1.5014	1.9814
ABS ERR-W	1.9437E 00	1.3049E-01	3.6764E-03	0.	3.6764E-03	1.2434E-04	1.2861E-04	1.6973E-04
REL ERR-W	0.0043	0.6131	0.3065	0.	0.3046	0.3091	0.3198	0.4220
ABS ERR-T	9.4248E 00	6.2642E-01	1.7649E-02	0.	1.7649E-02	5.9688E-04	6.1741E-04	8.1480E-04
REL ERR-T	0.0208	2.9433	1.4716	0.	1.4716	1.4840	1.5351	2.0259

TABLE 6-3. APPROXIMATE IDENTIFICATION ANALYSIS STOCHASTIC ERROR RESULTS FOR ADVANCED CONCEPT (continued)

MODE 26 ; W = 33.0515 R/S ; ZETA = 0.0050 ; RATIO = 12.4843

PARAMETER	W**2	2*Z*W	B 4	B 5	B 6	C 1	C 2	C 3
NOM VALUE	1.0924E 03	3.3052E-01	-4.4501E-03	1.6294E-09	-7.4501E-10	-5.4634E-06	3.3179E-05	-3.5396E-05
ABS ERR-R	9.5540E 02	4.0881E 01	0.	2.7521E-01	2.7521E-01	3.0381E-03	3.6506E-03	3.7294E-03
REL ERR-R	0.8746	123.6881	0.	61.8425	61.8425	62.2286	74.7741	76.3884
ABS ERR-W	3.8003E 00	1.6261E-01	0.	1.0947E-03	1.0947E-03	1.2085E-05	1.4521E-05	1.4834E-05
REL ERR-W	0.0035	0.4920	0.	0.2460	0.2460	0.2475	0.2974	0.3039
ABS ERR-T	9.5541E 02	4.0881E 01	0.	2.7521E-01	2.7521E-01	3.0381E-03	3.6506E-03	3.7294E-03
REL ERR-T	0.8746	123.6891	0.	61.8430	61.8430	62.2291	74.7747	76.3890

MODE 28 ; W = 50.9991 R/S ; ZETA = 0.0050 ; RATIO = 3.8127

PARAMETER	W**2	2*Z*W	B 4	B 5	B 6	C 1	C 2	C 3
NOM VALUE	2.6009E 03	5.0999E-01	-9.9076E-07	3.2542E-06	-7.6340E-06	-4.0058E-03	1.2803E-03	7.3376E-03
ABS ERR-R	1.3402E 04	3.7164E 02	3.0706E-03	3.3102E-03	0.	3.4711E 00	3.1234E 00	4.2501E 00
REL ERR-R	5.1527	728.7195	367.4063	396.0729	0.	410.4296	369.3211	502.5335
ABS ERR-W	7.2841E 00	2.0199E-01	1.6689E-06	1.7992E-06	0.	1.8866E-03	1.6977E-03	2.3100E-03
REL ERR-W	0.0028	0.3961	0.1997	0.2153	0.	0.2231	0.2007	0.2731
ABS ERR-T	1.3402E 04	3.7164E 02	3.0706E-03	3.3102E-03	0.	3.4711E 00	3.1234E 00	4.2501E 00
REL ERR-T	5.1527	728.7196	367.4064	396.0729	0.	410.4296	369.3212	502.5336

MODE 29 ; W = 52.5275 R/S ; ZETA = 0.0050 ; RATIO = 64.5197

PARAMETER	W**2	2*Z*W	B 4	B 5	B 6	C 1	C 2	C 3
NOM VALUE	2.7591E 03	5.2528E-01	-7.8166E-03	-3.7546E-10	2.2738E-09	-8.0694E-06	-4.7428E-05	-1.9354E-04
ABS ERR-R	6.7382E 02	1.8142E 01	0.	1.3498E-01	1.3498E-01	3.4467E-03	3.5399E-03	4.7992E-03
REL ERR-R	0.2442	34.5301	0.	17.2686	17.2686	17.2828	17.7503	24.0648
ABS ERR-W	7.6140E 00	2.0500E-01	0.	1.5252E-03	1.5252E-03	3.8946E-05	4.0000E-05	5.4229E-05
REL ERR-W	0.0028	0.3903	0.	0.1951	0.1951	0.1953	0.2006	0.2719
ABS ERR-T	6.7387E 02	1.8143E 01	0.	1.3499E-01	1.3499E-01	3.4469E-03	3.5402E-03	4.7995E-03
REL ERR-T	0.2442	34.5403	0.	17.2697	17.2697	17.2839	17.7515	24.0663

TABLE 6-3. APPROXIMATE IDENTIFICATION ANALYSIS STOCHASTIC ERROR RESULTS FOR ADVANCED CONCEPT (continued)

MODE 30 ; W = 53.9508 R/S ; ZETA = 0.0050 ; RATIO = 52.4435

PARAMETER	W**2	2*Z*W	B 4	B 5	B 6	C 1	C 2	C 3
NOM VALUE	2.8309E 03	5.3851E-01	1.3943E-04	-1.8262E-09	3.2560E-09	4.9001E-05	-5.9715E-03	-1.1164E-07
ABS ERR-P	6.4326E 02	1.7025E 01	0.	2.2039E-03	2.2039E-03	2.0041E-01	2.2153E-01	2.6726E-01
REL ERR-P	0.2235	31.6146	0.	15.8069	15.8069	15.8070	17.4727	21.0791
ABS ERR-W	7.9335E 00	2.0756E-01	0.	2.6870E-05	2.6870E-05	2.4434E-03	2.7009E-03	3.2584E-03
REL ERR-W	0.0027	0.3854	0.	0.1927	0.1927	0.1927	0.2130	0.2570
ABS ERR-T	6.4330E 02	1.7026E 01	0.	2.2041E-03	2.2041E-03	2.0043E-01	2.2155E-01	2.6728E-01
REL ERR-T	0.2236	31.6170	0.	15.8081	15.8081	15.8082	17.4740	21.0806

MODE 33 ; W = 71.2905 R/S ; ZETA = 0.0050 ; RATIO = 49.4160

PARAMETER	W**2	2*Z*W	B 4	B 5	B 6	C 1	C 2	C 3
NOM VALUE	5.0823E 03	7.1290E-01	1.6504E-08	-5.9175E-08	1.0318E-02	4.3431E-05	-5.8691E-05	-5.1668E-05
ABS ERR-R	3.3148E 03	6.5758E 01	4.7586E-01	4.7586E-01	0.	4.5858E-03	4.9340E-03	4.7640E-03
REL ERR-R	0.6522	92.2400	46.1188	46.1188	0.	51.2690	55.1623	53.2618
ABS ERR-W	1.2039E 01	2.3882E-01	1.7282E-03	1.7282E-03	0.	1.6655E-05	1.7919E-05	1.7302E-05
REL ERR-W	0.0024	0.3350	0.1675	0.1675	0.	0.1862	0.2003	0.1934
ABS ERR-T	3.3148E 03	6.5759E 01	4.7586E-01	4.7586E-01	0.	4.5858E-03	4.9340E-03	4.7640E-03
REL ERR-T	0.6522	92.2406	46.1191	46.1191	0.	51.2694	55.1627	53.2621

MODE 34 ; W = 72.2430 R/S ; ZETA = 0.0050 ; RATIO = 3.2513

PARAMETER	W**2	2*Z*W	B 4	B 5	B 6	C 1	C 2	C 3
NOM VALUE	5.2190E 03	7.2243E-01	1.7226E-05	7.8978E-07	-9.0542E-06	5.0133E-04	3.4317E-04	-3.1113E-03
ABS ERR-R	5.1904E 04	1.0161E 03	1.8438E-02	1.3708E-02	1.5156E-02	2.2580E 00	2.2428E 00	0.
REL ERR-R	9.9452	1406.4938	946.6831	703.8294	778.1365	712.3001	707.4941	0.
ABS ERR-W	1.2281E 01	2.4041E-01	4.3626E-06	3.2435E-06	3.5859E-06	5.3425E-04	5.3065E-04	0.
REL ERR-W	0.0024	0.3328	0.2540	0.1665	0.1841	0.1685	0.1674	0.
ABS ERR-T	5.1904E 04	1.0161E 03	1.8438E-02	1.3708E-02	1.5156E-02	2.2580E 00	2.2428E 00	0.
REL ERR-T	9.9452	1406.4938	946.6831	703.8294	778.1365	712.3001	707.4941	0.

TABLE 6-3. APPROXIMATE IDENTIFICATION ANALYSIS STOCHASTIC ERROR RESULTS FOR ADVANCED CONCEPT (continued)

MODE 35 ; W = 74.9584 R/S ; ZETA = 0.0050 ; RATIO = 20.9308

PARAMETER	**2	2*Z*W	B 4	B 5	B 6	C 1	C 2	C 3
NOM VALUE	5.3433E 03	7.9958E-01	-8.8576E-05	6.8362E-07	-1.7934E-06	-6.9326E-04	4.0320E-04	4.2904E-03
ABS ERR-R	1.1521E 04	2.0908E 02	0.	1.1584E-02	1.1586E-02	5.7780E-01	5.7307E-01	8.0030E-01
REL ERR-R	1.8490	261.4878	0.	130.7444	130.7673	132.3805	131.2976	183.3579
ABS ERR-W	1.4300E 01	2.5292E-01	0.	1.4012E-05	1.4015E-05	6.9896E-04	6.9324E-04	9.6811E-04
REL ERR-W	0.0022	0.3163	0.	0.1582	0.1582	0.1601	0.1588	0.2218
ABS ERR-T	1.1521E 04	2.0908E 02	0.	1.1584E-02	1.1586E-02	5.7780E-01	5.7307E-01	8.0030E-01
REL ERR-T	1.8490	261.4878	0.	130.7445	130.7674	132.3806	131.2976	183.3581

MODE 36 ; W = 85.3456 R/S ; ZETA = 0.0050 ; RATIO = 298.5829

PARAMETER	**2	2*Z*W	B 4	B 5	B 6	C 1	C 2	C 3
NOM VALUE	7.2839E 03	8.5346E-01	2.7185E-07	1.7229E-02	-1.5168E-07	1.4179E-05	7.9660E-05	2.5561E-04
ABS ERR-R	1.2432E 03	2.0601E 01	2.0794E-01	0.	2.0794E-01	3.2404E-03	3.3757E-03	4.4711E-03
REL ERR-R	0.1707	24.1388	12.0491	0.	12.0491	12.0860	12.5907	16.6760
ABS ERR-W	1.5769E 01	2.6130E-01	2.6375E-03	0.	2.6375E-03	4.1101E-05	4.2817E-05	5.6710E-05
REL ERR-W	0.0022	0.3062	0.1531	0.	0.1531	0.1533	0.1597	0.2115
ABS ERR-T	1.2433E 03	2.0603E 01	2.0795E-01	0.	2.0796E-01	3.2407E-03	3.3760E-03	4.4714E-03
REL ERR-T	0.1707	24.1408	12.0701	0.	12.0701	12.0870	12.5917	16.6773

MODE 37 ; W = 86.1685 R/S ; ZETA = 0.0050 ; RATIO = 61.0834

PARAMETER	**2	2*Z*W	B 4	B 5	B 6	C 1	C 2	C 3
NOM VALUE	7.4260E 03	8.6169E-01	6.1448E-06	-1.2412E-03	-4.8017E-06	1.1188E-04	1.5601E-03	1.6176E-03
ABS ERR-R	2.1265E 03	3.4901E 01	2.5135E-02	0.	2.5136E-02	4.5625E-02	5.5453E-02	5.6175E-02
REL ERR-R	0.2864	40.5037	20.2516	0.	20.2515	20.2764	24.6438	24.9423
ABS ERR-W	1.5908E 01	2.6256E-01	1.8910E-04	0.	1.8910E-04	3.4324E-04	4.1717E-04	4.2222E-04
REL ERR-W	0.0022	0.3047	0.1524	0.	0.1524	0.1525	0.1854	0.1876
ABS ERR-T	2.1266E 03	3.4902E 01	2.5137E-02	0.	2.5137E-02	4.5627E-02	5.5454E-02	5.6126E-02
REL ERR-T	0.2864	40.5048	20.2522	0.	20.2521	20.2769	24.6445	24.9430

TABLE 6-3. APPROXIMATE IDENTIFICATION ANALYSIS STOCHASTIC ERROR RESULTS FOR ADVANCED CONCEPT (concluded)

MODE 39 : W = 87.9727 R/S ; ZETA = 0.0050 ; RATIO = 65.0530

PARAMETER	W**2	2*Z*W	B 4	B 5	B 6	C 1	C 2	C 3
NOM VALUE	7.9161E 03	8.8973E-01	2.1882E-05	1.4894E-04	-1.1227E-05	-1.1347E-03	2.1758E-03	-1.3161E [illegible]
ABS ERR-R	3.8513E 03	6.1218E 01	5.2488E-03	0.	5.2078E-03	3.9510E-01	4.0037E-01	5.[illegible]185E-01
REL ERR-R	0.4865	68.8049	34.7709	0.	34.4992	34.5754	35.0364	[illegible].4084
ABS ERR-W	1.6785E 01	2.6680E-01	2.2876E-05	0.	2.2497E-05	1.7219E-03	1.7449E-03	2.4109E-03
REL ERR-W	0.0021	0.2999	0.1515	0.	0.1504	0.1507	0.1527	0.2110
ABS ERR-T	3.8513E 03	6.1218E 01	5.2489E-03	0.	5.2079E-03	3.9511E-01	4.0038E-01	5.5318E-01
REL ERR-T	0.4865	68.8055	34.7712	0.	34.4995	34.5757	35.0367	48.4088

MODE 39 : W = 98.3460 R/S ; ZETA = 0.0050 ; RATIO = 39.2356

PARAMETER	W**2	2*Z*W	B 4	B 5	B 6	C 1	C 2	C 3
NOM VALUE	9.6719E 03	9.8346E-01	5.4278E-05	1.6224E-04	1.2676E-06	-8.8208E-04	1.4911E-03	-9.6114E-03
ABS ERR-R	1.7782E 04	2.5571E 02	0.	7.0646E-03	7.0633E-03	1.2748E 00	1.2844E 00	1.7821E 00
REL ERR-R	1.8385	260.0121	0.	130.0609	130.0383	130.5329	131.5119	182.4731
ABS ERR-W	1.9506E 01	2.8050E-01	0.	7.7494E-06	7.7481E-06	1.3984E-03	1.4089E-03	1.9548E-03
REL ERR-W	0.0020	0.2852	0.	0.1427	0.1426	0.1432	0.1443	0.2002
ABS ERR-T	1.7782E 04	2.5571E 02	0.	7.0646E-03	7.0633E-03	1.2748E 00	1.2844E 00	1.7821E 00
REL ERR-T	1.8385	260.0123	0.	130.0610	130.0383	130.5329	131.5119	182.4732

MODE 40 : W = 100.0860 R/S ; ZETA = 0.0050 ; RATIO = 47.1944

PARAMETER	W**2	2*Z*W	B 4	B 5	B 6	C 1	C 2	C 3
NOM VALUE	1.0198E 04	1.0099E 00	-2.8500E-06	5.7720E-05	-2.1964E-06	4.3494E-03	1.7099E-03	-5.7912E-03
ABS ERR-R	2.4048E 04	3.3677E 02	9.6546E-03	0.	9.6498E-03	1.4580E 00	1.2733E 00	1.5735E 00
REL ERR-R	2.3580	333.4857	166.9418	0.	166.8594	193.2295	171.1009	211.4417
ABS ERR-W	2.0207E 01	2.8424E-01	8.1486E-06	0.	8.1445E-06	1.2136E-03	1.0747E-03	1.3280E-03
REL ERR-W	0.0020	0.2815	0.1409	0.	0.1408	0.1631	0.1444	0.1785
ABS ERR-T	2.4048E 04	3.3677E 02	9.6546E-03	0.	9.6498E-03	1.4580E 00	1.2733E 00	1.5735E 00
REL ERR-T	2.3580	333.4858	166.9419	0.	166.8594	193.2295	171.1010	211.4418

Table 6-4. EXACT IDENTIFICATION ANALYSIS SOFTWARE STOCHASTIC ERROR RESULTS FOR THE ADVANCED CONCEPT

MODE 9 : W = 1.9936 ; ZETA = 0.0050 ; BMAG= 4.7579E-04 ; CMAG= 5.1488E-03

PARAMETER	W**2	2*Z*W	B 1	B 2	B 3	C 1	C 2	C 3
NOM VALUE	3.9744E 00	1.9936E-02	4.7579E-04	-1.0394E-11	-5.4119E-11	2.3927E-06	-2.6322E-04	-5.1471E-03
ABS ERR-R	4.5672E-03	3.2506E-03	0.	3.8659E-05	3.8659E-05	4.1870E-04	4.2066E-04	5.9361E-04
REL ERR-R	1.1491E-03	1.6305E-01	0.	8.1252E-02	8.1252E-02	8.1426E-02	8.1807E-02	1.1544E-01

MODE 10 : W = 2.0916 ; ZETA = 0.0050 ; BMAG= 2.5169E-04 ; CMAG= 4.9966E-03

PARAMETER	W**2	2*Z*W	B 1	B 2	B 3	C 1	C 2	C 3
NOM VALUE	4.3748E 00	2.0916E-02	2.5169E-04	1.3324E-09	5.4571E-09	-9.8898E-07	4.9347E-03	7.8374E-04
ABS ERR-R	1.0524E-02	7.1403E-03	0.	4.2810E-05	4.2810E-05	8.5057E-04	1.1992E-03	8.6402E-04
REL ERR-R	2.4055E-03	3.4138E-01	0.	1.7009E-01	1.7009E-01	1.0853E 00	1.5300E 00	1.1024E 00

MODE 14 : W = 7.6891 ; ZETA = 0.0050 ; BMAG= 5.5369E-03 ; CMAG= 4.9565E-04

PARAMETER	W**2	2*Z*W	B 1	B 2	B 3	C 1	C 2	C 3
NOM VALUE	5.9122E 01	7.6891E-02	-3.0726E-08	5.5364E-03	7.4977E-05	4.8514E-04	6.0668E-05	-8.1447E-05
ABS ERR-R	4.5932E-01	8.4569E-02	3.0426E-03	0.	3.0465E-03	3.8151E-04	2.7432E-04	2.7396E-04
REL ERR-R	7.7691E-03	1.0999E 00	5.4950E-01	0.	5.4021E-01	4.6841E 00	3.3681E 00	3.3882E 00

MODE 15 : W = 8.1696 ; ZETA = 0.0050 ; BMAG= 4.8095E-03 ; CMAG= 3.1397E-03

PARAMETER	W**2	2*Z*W	B 1	B 2	B 3	C 1	C 2	C 3
NOM VALUE	6.6742E 01	8.1696E-02	2.1435E-06	6.7892E-05	-4.8091E-03	2.9030E-03	-1.0413E-03	-5.8811E-04
ABS ERR-R	1.0321E-01	1.7886E-02	5.2604E-04	5.2669E-04	0.	4.6822E-04	3.6173E-04	3.4931E-04
REL ERR-R	1.5464E-03	2.1894E-01	1.0938E-01	1.0951E-01	0.	7.9615E-01	6.1508E-01	5.9396E-01

MODE 17 : W = 10.8130 ; ZETA = 0.0050 ; BMAG= 1.4075E-04 ; CMAG= 1.9153E-02

PARAMETER	W**2	2*Z*W	B 1	B 2	B 3	C 1	C 2	C 3
NOM VALUE	1.1692E 02	1.0815E 01	-3.9589E-07	-8.2180E-07	1.4074E-04	1.5048E-02	-1.0072E-02	-6.2419E-03
ABS ERR-R	1.5422E 00	2.0170E-01	1.3127E-04	1.3127E-04	0.	2.2719E-02	2.0184E-02	1.8789E-02
REL ERR-R	1.3190E-02	1.8654E 00	9.3266E-01	9.3267E-01	0.	3.6397E 00	3.2335E 00	3.0101E 00

MODE 21 : W = 14.8503 ; ZETA = 0.0050 ; BMAG= 3.6743E-04 ; CMAG= 1.1817E-02

PARAMETER	W**2	2*Z*W	B 1	B 2	B 3	C 1	C 2	C 3
NOM VALUE	2.2053E 02	1.4850E-01	1.5491E-07	-2.7118E-04	-2.4793E-04	-2.0781E-03	-3.6152E-03	1.1057E-02
ABS ERR-R	2.9066E 00	2.7680E-01	3.4243E-04	4.3615E-04	4.2220E-04	1.1206E-02	1.1587E-02	0.
REL ERR-R	1.3180E-02	1.8640E 00	9.3196E-01	1.1870E 00	1.1491E 00	1.0135E 00	1.0479E 00	0.

MODE 22 : W = 18.7836 ; ZETA = 0.0050 ; BMAG= 1.7150E-02 ; CMAG= 4.6498E-04

PARAMETER	W**2	2*Z*W	B 1	B 2	B 3	C 1	C 2	C 3
NOM VALUE	3.5282E 02	1.8784E-01	-1.7150E-02	-3.7565E-08	-4.9650E-08	-2.0396E-05	4.0528E-04	-2.2701E-04
ABS ERR-R	3.6019E 00	2.7137E-01	0.	1.2383E-02	1.2393E-02	3.3603E-04	4.4563E-04	3.7358E-04
REL ERR-R	1.0209E-02	1.4447E 00	0.	7.2203E-01	7.2251E-01	1.4802E 00	1.9630E 00	1.6457E 00

MODE 23 : W = 19.9551 ; ZETA = 0.0050 ; BMAG= 1.0291E-02 ; CMAG= 1.1478E-03

PARAMETER	W**2	2*Z*W	B 1	B 2	B 3	C 1	C 2	C 3
NOM VALUE	3.9820E 02	1.9955E-01	-5.2503E-08	-4.1569E-05	1.0291E-02	6.8976E-04	-9.1464E-04	-7.1273E-05
ABS ERR-R	3.0053E 00	2.1714E-01	5.4971E-03	5.4945E-03	0.	7.1480E-04	7.8396E-04	6.1388E-04
REL ERR-R	7.5471E-03	1.0681E 00	5.3419E-01	5.3393E-01	0.	1.0029E 01	1.0999E 01	8.6131E 00

MODE 24 : W = 31.2828 ; ZETA = 0.0050 ; BMAG= 1.1993E-02 ; CMAG= 4.0220E-04

PARAMETER	W**2	2*Z*W	B 1	B 2	B 3	C 1	C 2	C 3
NOM VALUE	4.5296E 02	2.1283E-01	5.6825E-08	-1.1993E-02	-2.8140E-05	-5.2388E-05	1.1939E-04	-3.8048E-04
ABS ERR-R	9.2200E 00	6.1275E-01	1.7263E-02	0.	1.7268E-02	5.8386E-04	6.0402E-04	7.9698E-04
REL ERR-R	2.0355E-02	2.8791E 00	1.4394E 00	0.	1.4398E 00	1.5345E 00	1.5875E 00	2.0947E 00

MODE 26 : W = 33.0515 ; ZETA = 0.0050 ; BMAG= 4.4501E-03 ; CMAG= 4.8821E-05

PARAMETER	W**2	2*Z*W	B 1	B 2	B 3	C 1	C 2	C 3
NOM VALUE	1.0924E 03	3.3052E-01	-4.4501E-03	1.6294E-09	-7.4531E-10	-5.4634E-06	3.3179E-05	-3.5396E-05
ABS ERR-R	9.5540E 02	4.0881E 01	0.	2.7521E-01	2.7521E-01	3.0381E-03	3.6506E-03	3.7294E-03
REL ERR-R	8.7459E-01	1.2369E 02	0.	6.1843E 01	6.1843E 01	8.5832E 01	1.0314E 02	1.0536E 02

Table 6-4. EXACT IDENTIFICATION ANALYSIS SOFTWARE STOCHASTIC ERROR RESULTS FOR THE ADVANCED CONCEPT (concluded)

MODE 28 ; W = 50.9991 ; ZETA = 0.0050 ; BMAG= 8.3575E-04 ; CMAG= 8.4573E-03

PARAMETER	W**2	2*Z*W	B 1	B 2	B 3	C 1	C 2	C 3
NOM VALUE	2.6009E 03	5.0999E-01	-9.9076E-07	3.2542E-06	-7.4340E-06	-4.0058E-03	1.2803E-03	7.3376E-03
ABS ERR_R	1.3413E 04	3.7672E 02	3.1303E-03	3.3236F-03	0.	3.4793E 00	3.1279E 00	4.3189E 00
REL ERR_R	5.1569F 00	7.3868E 02	3.7455E 02	3.9768E 02	0.	4.7418E 02	4.2629E 02	5.8860F 02

MODE 29 ; W = 52.5275 ; ZETA = 0.0050 ; BMAG= 7.8166E-03 ; CMAG= 1.9943E-04

PARAMETER	W**2	2*Z*W	B 1	B 2	B 3	C 1	C 2	C 3
NOM VALUE	2.7591E 03	5.2528E-01	-7.8166E-03	-3.7546E-10	2.2738E-09	-8.0694E-06	-4.7428E-05	-1.9354E-04
ABS ERR_R	6.8113E 02	1.9752E 01	0.	1.3701E-01	1.3832E-01	3.4841E-03	3.6609E-03	5.4075E-03
REL ERR_R	2.4686E-01	3.7603E 01	0.	1.7528E 01	1.7695E 01	1.8003E 01	1.8916E 01	2.7940E 01

MODE 30 ; W = 53.8508 ; ZETA = 0.0050 ; BMAG= 1.3943E-04 ; CMAG= 1.2679E-02

PARAMETER	W**2	2*Z*W	B 1	B 2	B 3	C 1	C 2	C 3
NOM VALUE	2.8999E 03	5.3851E-01	1.3943E-04	-1.8262E-09	3.2560E-08	4.9001E-05	-5.9715E-03	-1.1184E-02
ABS ERR_R	6.5464F 02	1.8310E 01	0.	2.2246E-03	2.2255E-03	2.0240E-01	2.3007E-01	2.9735E-01
REL ERR_R	2.2575E-01	3.4001E 01	0.	1.5956E 01	1.5962E 01	1.8097E 01	2.0571E 01	2.6587F 01

MODE 33 ; W = 71.2905 ; ZETA = 0.0050 ; BMAG= 1.0318E-02 ; CMAG= 8.9445E-05

PARAMETER	W**2	2*Z*W	B 1	B 2	B 3	C 1	C 2	C 3
NOM VALUE	5.0823E 03	7.1290E-01	1.6504E-08	-5.9173E-08	1.0318E-02	4.3431E-05	-5.8691E-05	-5.1668E-05
ABS ERR_R	3.3958E 03	7.0524E 01	5.3143E-01	4.8654E-01	0.	4.8022E-03	5.1395E-03	5.6044F-03
REL ERR_R	6.6816E-01	9.8925E 01	5.1505E 01	4.7154E 01	0.	9.2943E 01	9.9470E 01	1.0847F 02

MODE 34 ; W = 72.2430 ; ZETA = 0.0050 ; BMAG= 1.9477E-05 ; CMAG= 3.1700E-03

PARAMETER	W**2	2*Z*W	B 1	B 2	B 3	C 1	C 2	C 3
NOM VALUE	5.2190E 03	7.2243E-01	1.7226E-05	7.8978E-07	-9.0542E-06	5.0133E-04	3.4317E-04	-3.1113E-03
ABS ERR_R	5.3145F 04	1.0006E 03	1.9902E-02	1.4017E-02	1.7961E-02	2.3290E 00	2.4024E 00	0.
REL ERR_R	1.0183E 01	1.5096E 03	1.0218E 03	7.1968E 02	9.2218E 02	7.4858F 02	7.7218E 02	0.

MODE 35 ; W = 79.9584 ; ZETA = 0.0050 ; BMAG= 8.8597E-05 ; CMAG= 4.3647E-03

PARAMETER	W**2	2*Z*W	B 1	B 2	B 3	C 1	C 2	C 3
NOM VALUE	6.3933E 03	7.9958E-01	-8.8576E-05	6.8362E-07	-1.7934E-06	-5.9326E-04	4.0320E-04	4.2904E-03
ABS ERR_R	1.1821E 04	2.0940E 02	0.	1.1604F-02	1.1590E-02	5.7785E-01	5.7317E-01	8.0176F-01
REL ERR_R	1.8490E 00	2.6189E 02	0.	1.3097F 02	1.3082E 02	1.3469E 02	1.3359E 02	1.8687F 02

MODE 36 ; W = 85.3456 ; ZETA = 0.0050 ; BMAG= 1.7229E-02 ; CMAG= 2.6811E-04

PARAMETER	W**2	2*Z*W	B 1	B 2	B 3	C 1	C 2	C 3
NOM VALUE	7.2839E 03	8.5346E-01	2.7185E-07	1.7229E-02	-1.5168E-07	1.4179E-05	7.9660E-05	2.5561F-04
ABS ERR_R	1.8699E 03	3.1950E 01	2.1522E-01	0.	2.3507E-01	3.8360E-03	6.4073E-03	1.0605E-02
REL ERR_R	2.5672F-01	3.7437E 01	1.3653E 01	0.	1.3644E 01	1.5007E 01	2.5419E 01	4.1487E 01

MODE 37 ; W = 86.1685 ; ZETA = 0.0050 ; BMAG= 1.2412E-03 ; CMAG= 2.2502E-03

PARAMETER	W**2	2*Z*W	B 1	B 2	B 3	C 1	C 2	C 3
NOM VALUE	7.4250E 03	8.6169E-01	6.1448E-06	-1.2412E-03	-4.8017E-06	1.1188E-04	1.5601E-03	1.6176E-03
ABS ERR_R	3.1881E 03	5.5247E 01	2.8421E-02	0.	2.8416E-02	5.4147E-02	1.0438E-01	1.4198E-01
REL ERR_R	4.2937E-01	6.4115E 01	2.2898E 01	0.	2.2894E 01	3.3473E 01	6.4526E 01	8.7769F 01

MODE 38 ; W = 88.9727 ; ZETA = 0.0050 ; BMAG= 1.5096E-04 ; CMAG= 1.1427E-02

PARAMETER	W**2	2*Z*W	B 1	B 2	B 3	C 1	C 2	C 3
NOM VALUE	7.9161E 03	8.8973E-01	2.1882E-05	1.4894E-04	-1.1227E-05	-1.1347E-03	2.1758E-03	-1.1161F-02
ABS ERR_R	3.8577E 03	6.2703E 01	5.2607E-03	0.	5.2173E-03	3.9688E-01	4.0500E-01	5.7411E-01
REL ERR_R	4.8732E-01	7.0475E 01	3.4849E 01	0.	3.4562E 01	3.5560E 01	3.6288E 01	5.1440F 01

MODE 39 ; W = 98.3460 ; ZETA = 0.0050 ; BMAG= 5.4317E-05 ; CMAG= 9.7663E-03

PARAMETER	W**2	2*Z*W	B 1	B 2	B 3	C 1	C 2	C 3
NOM VALUE	9.6719E 03	9.8346E-01	5.4278E-05	1.6224E-06	1.2676E-06	-8.8208E-04	1.4911E-03	-9.6114F-03
ABS ERR_R	1.7800E 04	2.5929E 02	0.	7.2281F-03	7.0949E-03	1.2771E 00	1.2863E 00	1.8138F 00
REL ERR_R	1.8404E 00	2.6365E 02	0.	1.3307E 02	1.3062E 02	1.3287E 02	1.3383E 02	1.8871E 02

MODE 40 ; W = 100.9860 ; ZETA = 0.0050 ; BMAG= 5.7832E-05 ; CMAG= 7.4417E-03

PARAMETER	W**2	2*Z*W	B 1	B 2	B 3	C 1	C 2	C 3
NOM VALUE	1.0190E 04	1.0099E 00	-2.8500E-06	5.7720E-05	-2.1954E-06	4.3494E-03	1.7099E-03	-5.7912F-03
ABS ERR_R	2.4071E 04	3.4155E 02	9.8730E-03	0.	9.6923E-03	1.4421F 00	1.2754E 00	1.6056E 00
REL ERR_R	2.3603F 00	3.3822E 02	1.7072E 02	0.	1.4759E 02	2.4901F 02	2.2023E 02	2.7724F 02

TABLE 6-5. WORST-CASE RESULTS FOR STOCHASTIC ERROR DUE TO MEASUREMENT NOISE: T_{ID} = 300 sec

Mode	$\frac{\sigma_{\omega^2}}{\omega^2}$	$\frac{\sigma_{2\zeta\omega}}{2\zeta\omega}$	$\frac{\sigma_{b1}}{b1}$	$\frac{\sigma_{b2}}{b2}$	$\frac{\sigma_{b3}}{b3}$	$\frac{\sigma_{c1}}{ci}$	$\frac{\sigma_{c2}}{c2}$	$\frac{\sigma_{c3}}{c3}$	Test Signal	Measurement
34	5.88×10^{-1}	8.72×10^{1}	5.90×10^{1}	4.16×10^{1}	5.32×10^{1}	4.32×10^{1}	4.46×10^{1}	---	TS1	Position
10	1.59×10^{-5}	2.25×10^{-3}	---	1.12×10^{-3}	1.12×10^{-3}	7.16×10^{-3}	1.01×10^{-2}	7.27×10^{-3}	TS2	Rate

TABLE 6-6. WORST-CASE RESULTS FOR STOCHASTIC ERROR DUE TO PROCESS NOISE: T_{ID} = 300 sec and W = 0.01U

Mode	$\frac{\sigma_{\omega^2}}{\omega^2}$	$\frac{\sigma_{2\zeta\omega}}{2\zeta\omega}$	$\frac{\sigma_{b1}}{b1}$	$\frac{\sigma_{b2}}{b2}$	$\frac{\sigma_{b3}}{b3}$	$\frac{\sigma_{c1}}{c1}$	$\frac{\sigma_{c2}}{c2}$	$\frac{\sigma_{c3}}{c3}$
9	8.20×10^{-4}	1.16×10^{-1}	---	5.78×10^{-2}	5.78×10^{-2}	5.78×10^{-2}	5.79×10^{-2}	8.17×10^{-2}

TABLE 6-7. PERCENT INCREASE IN STOCHASTIC ERROR DUE TO "CLOSE" MODAL FREQUENCIES*

Mode	$\frac{\Delta\omega}{\omega}$	ω^2	$2\zeta\omega$	b1	b2	b3	c1	c2	c3
29	0.025	1.1	8.9	---	1.5	2.5	1.1	3.4	12.7
30		1.0	7.5	---	0.9	1.0	1.0	3.9	11.3
33	0.013	2.4	7.2	11.7	2.2	---	4.7	4.2	17.6
34		2.4	7.3	7.9	2.3	18.5	3.1	7.1	---
36	0.010	50.4	55.1	13.1	---	13.0	18.4	92.5	137.2
37		49.9	58.3	13.1	---	13.0	18.7	88.2	153.0

Note: Expect a discrepancy when $\frac{\Delta\omega}{\omega} \approx 2\zeta = 0.010$

Systematic Parameter Error--The systematic parameter errors or parameter biases were also computed for the 21 flexible modes considered significant for the advanced concept. Parameter biases are defined as

$$\alpha_{bias} = \hat{\alpha} - \alpha_*$$

where α_* is the true parameter vector. Parameter biases are only possible when the identification model is not capable of being the same as the true system model (i.e., a model mismatch).

Examples of model mismatches include 1) MLE without the Kalman filter with finite process noise, and 2) MLE with the true system model order different than the identification model order. As already discussed, the former only produces biases when process noise and test signal are correlated. The latter gives rise to parameter biases even when these quantities are uncorrelated.

Model order mismatch is, in practice, always present for identification of LSSs. The true system model is of infinite order and the identification model is of finite order. For this part of the study the true system model was taken to be

the 78 flexible modes, and parameter biases were computed for an identification model with 21 modes.

Relative parameter biases are also of interest for the same reason that relative stochastic errors are important. The relative parameter biases for a specific mode were defined as

$$\omega^2 \text{ relative bias} = \frac{\hat{\omega}^2_{bias} - \omega^2_*}{\omega^2_*}$$

$$2\zeta\omega \text{ relative bias} = \frac{\widehat{2\zeta\omega} - 2\zeta_*\omega_*}{2\zeta_*\omega_*}$$

$$b_\ell \text{ relative bias} = \frac{\hat{b}_\ell - b_{\ell_*}}{|b|} \qquad \ell = 1,2,3$$

$$c_m \text{ relative bias} = \frac{\hat{c}_m - c_{m_*}}{|c|} \qquad m = 1,2,3$$

Parameter biases differ from stochastic error in that they cannot be made smaller by increasing measurement time, as is the case for stochastic errors. The biases can be made smaller only by changing the identification model.

The expected value of the parameter estimate was found by numerically minimizing the expected value of the negative log likelihood function with the NR update method described earlier. Satisfactory convergence was obtained after three iterations with starting values equal to the true values. These are not time updates; rather, minimization updates of the expected value of the negative log likelihood function. Note that the parameter value that produces the minimum is slightly different than the true parameter value because of the model order mismatch.

The absolute and relative biases for the 21 modes (147 parameters) considered significant for the advanced concept are shown in Table 6-8. The biases are due to model order mismatch (21-mode ID model and 78-mode truth model). All the relative errors can be seen to be less than unity. Worst-case results are shown in Table 6-9.

TABLE 6-8. EXACT IDENTIFICATION ANALYSIS SOFTWARE SYSTEMATIC ERROR RESULTS FOR THE ADVANCED CONCEPT

BIAS RESULTS

MODE 9 : W = 1.9936 ; ZETA = 0.0050 ; BMAG= 4.7579E-04 ; CMAG= 5.1488E-03

PARAMETER	W	ZETA	B 1	B 2	B 3	C 1	C 2	C 3
NOM VALUE	1.9936E 00	5.0000E-03	4.7579E-04	-1.0394E-11	-5.4119E-11	2.3927E-06	-2.5322E-04	-5.1421E-03
ID VALUE	1.9936E 00	5.3221E-03	4.7579E-04	-5.3979E-06	-2.5288E-06	1.0243E-06	-1.6594E-04	-5.4799E-03
ABS BIAS	-1.2210E-06	3.2214E-04	0.	-5.3979E-06	-2.5287E-04	-1.3685E-06	9.7282E-05	-3.3777E-04
REL BIAS	-6.1291E-07	6.4427E-02	0.	-1.1345E-02	-5.3148E-03	-2.6578E-04	1.8894E-02	-6.5601E-02

MODE 10 : W = 2.0916 ; ZETA = 0.0050 ; BMAG= 2.5169E-04 ; CMAG= 4.9966E-03

PARAMETER	W	ZETA	B 1	B 2	B 3	C 1	C 2	C 3
NOM VALUE	2.0916E 00	5.0000E-03	2.5169E-04	1.3324E-09	5.4571E-09	-9.8898E-07	4.9347E-03	7.8374E-04
ID VALUE	2.0916E 00	5.4388E-03	2.5169E-04	-2.3277E-07	-7.7558E-06	-1.5018E-05	5.3971E-03	4.9961E-04
ABS BIAS	1.2547E-05	4.3881E-04	0.	-2.3410E-07	-7.7625E-06	-1.4029E-05	4.6241E-04	-3.1413E-04
REL BIAS	5.9984E-06	8.7763E-02	0.	-9.3017E-04	-3.0841E-02	-2.8078E-03	9.2547E-02	-6.2870E-02

MODE 14 : W = 7.6891 ; ZETA = 0.0050 ; BMAG= 5.5369E-03 ; CMAG= 4.9565E-04

PARAMETER	W	ZETA	B 1	B 2	B 3	C 1	C 2	C 3
NOM VALUE	7.6891E 00	5.0000E-03	-3.0726E-08	5.5364E-03	7.6977E-05	4.8514E-04	6.0668E-05	-8.1447E-05
ID VALUE	7.6891E 00	4.9702E-03	1.4259E-05	5.5364E-03	3.2581E-04	4.8092E-04	5.9894E-05	-8.0251E-05
ABS BIAS	1.6093E-06	-2.9814E-05	1.4289E-05	0.	2.4984E-04	-4.2150E-06	-7.7450E-07	1.1958E-06
REL BIAS	2.0930E-07	-5.9626E-03	2.5808E-03	0.	4.4941E-02	-8.5040E-03	-1.5626E-03	2.4125E-03

MODE 15 : W = 8.1696 ; ZETA = 0.0050 ; BMAG= 4.8095E-03 ; CMAG= 3.1397E-03

PARAMETER	W	ZETA	B 1	B 2	B 3	C 1	C 2	C 3
NOM VALUE	8.1696E 00	5.0000E-03	2.1435E-06	6.7892E-05	-4.8091E-03	2.9030E-03	-1.0413E-03	-5.8811E-04
ID VALUE	8.1696E 00	4.9228E-03	3.6080E-06	6.4088E-05	-4.8091E-03	2.8540E-03	-1.0307E-03	-5.8866E-04
ABS BIAS	3.4571E-06	-7.7224E-05	1.5644E-06	-3.8040E-06	0.	-4.8961E-05	1.0615E-05	-5.5267E-07
REL BIAS	4.2314E-07	-1.5445E-02	3.2112E-04	-7.9093E-04	0.	-1.5594E-02	3.3808E-03	-1.7603E-04

MODE 17 : W = 10.8130 ; ZETA = 0.0050 ; BMAG= 1.4075E-04 ; CMAG= 1.9153E-02

PARAMETER	W	ZETA	B 1	B 2	B 3	C 1	C 2	C 3
NOM VALUE	1.0813E 01	5.0000E-03	-3.9589E-07	-8.2180E-07	1.4074E-04	1.5048E-02	-1.0072E-02	-6.2419E-03
ID VALUE	1.0813E 01	5.3324E-03	1.3548E-06	-1.3067E-06	1.4074E-04	1.6304E-02	-1.0468E-02	-6.2959E-03
ABS BIAS	-3.3379E-05	3.3245E-04	1.7507E-06	-4.8487E-07	0.	1.2561E-03	-3.9631E-04	-5.3996E-05
REL BIAS	-3.0863E-06	6.6489E-02	1.2439E-02	-3.4450E-03	0.	6.5582E-02	-2.0691E-02	-2.8191E-03

MODE 21 : W = 14.8503 ; ZETA = 0.0050 ; BMAG= 3.6743E-04 ; CMAG= 1.1717E-02

PARAMETER	W	ZETA	B 1	B 2	B 3	C 1	C 2	C 3
NOM VALUE	1.4850E 01	5.0000E-03	1.5491E-07	-2.7118E-04	-2.4793E-04	-2.0781E-03	-3.6152E-03	1.1057E-02
ID VALUE	1.4850E 01	4.9927E-03	4.7602E-06	-2.7018E-04	-2.4717E-04	-2.7038E-03	-3.6136E-03	1.1057E-02
ABS BIAS	9.5367E-07	-7.2564E-04	4.6142E-06	1.0000E-06	7.7528E-07	-1.2575E-04	1.6253E-06	0.
REL BIAS	6.4213E-08	-1.4513E-01	1.2550E-02	2.7216E-03	2.0933E-03	-1.0642E-02	1.3754E-04	0.

MODE 22 : W = 11.7836 ; ZETA = 0.0050 ; BMAG= 1.7150E-02 ; CMAG= 4.6498E-04

PARAMETER	W	ZETA	B 1	B 2	B 3	C 1	C 2	C 3
NOM VALUE	1.1784E 01	5.0000E-03	-1.7150E-02	-3.7565E-08	-4.3650E-08	-2.0396E-05	4.0578E-04	-2.2701E-04
ID VALUE	1.1784E 01	5.0985E-03	-1.7150E-02	-2.0976E-06	-2.3827E-05	-2.0642E-05	4.1390E-04	-2.3081E-04
ABS BIAS	-2.1457E-05	9.8493E-05	0.	-2.0600E-06	-2.3778E-05	-2.4610E-07	8.6185E-06	-3.8015E-06
REL BIAS	-1.1424E-06	1.9699E-02	0.	-1.2012E-04	-1.3865E-03	-5.7923E-04	1.8535E-02	-8.1757E-03

TABLE 6-8. EXACT IDENTIFICATION ANALYSIS SOFTWARE SYSTEMATIC ERROR RESULTS FOR THE ADVANCED CONCEPT (continued)

MODE 23 : W = 14.9541 ; ZETA = 0.0050 ; BMAG= 1.0291E-02 ; CMAG= 1.1478E-03

PARAMETER	W	ZETA	B 1	B 2	B 3	C 1	C 2	C 3
NOM VALUE	1.9955E 01	5.0000E-03	-5.2503E-08	-4.1569E-05	1.0291E-02	4.8976E-04	-9.1464E-04	-7.1273E-05
ID VALUE	1.9955E 01	5.0348E-03	4.7686E-05	-4.4438E-05	1.0291E-02	5.9772E-04	-9.1828E-04	-7.0519E-05
ABS BIAS	-5.7229E-06	3.4780E-05	4.7736E-05	-2.8695E-06	0.	7.9550E-04	-3.6383E-06	7.5382E-07
REL BIAS	-2.8679E-07	6.9559E-03	4.6314E-03	-2.8857E-04	0.	6.9307E-03	-3.1698E-03	6.5676E-04

MODE 24 : W = 21.2928 ; ZETA = 0.0050 ; BMAG= 1.1993E-02 ; CMAG= 4.0220E-04

PARAMETER	W	ZETA	B 1	B 2	B 3	C 1	C 2	C 3
NOM VALUE	2.1283E 01	5.0000E-03	5.6825E-08	-1.1993E-02	-2.8140E-05	-5.2388E-05	1.1939E-04	-3.8048E-04
ID VALUE	2.1283E 01	5.0036E-03	-1.9752E-04	-1.1993E-02	-4.9730E-05	-5.1907E-05	1.1953E-04	-3.8049E-04
ABS BIAS	-2.3842E-06	3.5504E-05	-2.0575E-04	0.	-2.1590E-05	4.8154E-07	1.4526E-07	-2.0135E-07
REL BIAS	-1.1202E-08	7.1008E-04	-3.9792E-03	0.	-3.4575E-03	1.1973E-03	3.6115E-04	-5.2892E-04

MODE 26 : W = 33.0515 ; ZETA = 0.0050 ; BMAG= 4.4501E-03 ; CMAG= 4.8821E-05

PARAMETER	W	ZETA	B 1	B 2	B 3	C 1	C 2	C 3
NOM VALUE	3.3052E 01	5.0000E-03	-4.4501E-03	1.4294E-09	-7.4501E-10	-5.4634E-06	3.3179E-05	-3.5396E-05
ID VALUE	3.3050E 01	6.0503E-03	-4.4501E-03	-1.2048E-05	-2.1904E-04	-7.3914E-06	5.4212E-05	-4.7300E-05
ABS BIAS	-1.3974E-03	-1.0503E-03	0.	-1.2050E-05	-2.1904E-04	-1.9280E-06	2.1033E-05	-1.1905E-05
REL BIAS	-4.2286E-05	2.1005E-01	0.	-2.7077E-03	-4.9220E-02	-3.9491E-02	4.3082E-01	-2.4384E-01

MODE 28 : W = 51.9991 ; ZETA = 0.0050 ; BMAG= 8.3575E-04 ; CMAG= 8.4573E-03

PARAMETER	W	ZETA	B 1	B 2	B 3	C 1	C 2	C 3
NOM VALUE	5.0999E 01	5.0000E-03	-9.9076E-07	3.2542E-06	-7.4340E-06	-4.0058E-03	1.2803E-03	7.3376E-03
ID VALUE	5.0999E 01	6.0500E-03	-7.2739E-07	2.6481E-06	-7.4340E-06	-9.9740E-03	2.6261E-03	9.2321E-03
ABS BIAS	-1.3447E-04	1.0500E-03	2.6337E-07	-6.0611E-07	0.	-5.9682E-03	1.3459E-03	1.8945E-03
REL BIAS	-2.6367E-06	2.1000E-01	3.1513E-02	-7.2523E-02	0.	-7.0569E-01	1.5914E-01	2.2401E-01

MODE 29 : W = 52.5275 ; ZETA = 0.0050 ; BMAG= 7.8166E-03 ; CMAG= 1.9943E-04

PARAMETER	W	ZETA	B 1	B 2	B 3	C 1	C 2	C 3
NOM VALUE	5.2528E 01	5.0000E-03	-7.8166E-03	-3.7546E-10	2.2738E-09	-8.0694E-06	-4.7428E-05	-1.9354E-04
ID VALUE	5.2528E 01	5.0169E-03	-7.8166E-03	1.3164E-06	-3.4759E-05	-8.0953E-06	-4.4178E-05	-1.9519E-04
ABS BIAS	1.0443E-04	1.6937E-05	0.	1.3168E-06	-3.5767E-05	-2.5969E-08	3.2497E-06	-1.6543E-06
REL BIAS	1.9887E-06	3.3875E-03	0.	1.6846E-04	-4.7030E-03	-1.3022E-04	1.6295E-02	-8.2952E-03

MODE 30 : W = 54.8508 ; ZETA = 0.0050 ; BMAG= 1.3943E-04 ; CMAG= 1.2679E-02

PARAMETER	W	ZETA	B 1	B 2	B 3	C 1	C 2	C 3
NOM VALUE	5.3851E 01	5.0000E-03	1.3943E-04	-1.8262E-09	3.2550E-08	4.9001E-05	-5.9715E-03	-1.1184E-02
ID VALUE	5.3851E 01	5.0378E-03	1.3943E-04	-1.3898E-08	-1.8596E-07	5.1372E-05	-6.1808E-03	-1.1172E-02
ABS BIAS	-2.7451E-05	3.7787E-05	0.	-1.2071E-08	-2.1852E-07	2.3709E-06	-2.0932E-04	1.2465E-05
REL BIAS	-5.1354E-07	7.5574E-03	0.	-8.6578E-05	-1.5673E-03	1.8699E-04	-1.4509E-02	9.8315E-04

MODE 33 : W = 71.2905 ; ZETA = 0.0050 ; BMAG= 1.0318E-02 ; CMAG= 8.9445E-05

PARAMETER	W	ZETA	B 1	B 2	B 3	C 1	C 2	C 3
NOM VALUE	7.1290E 01	5.0000E-03	1.4504E-08	-5.9175E-08	1.0318E-02	4.3431E-05	-5.9691E-05	-5.1668E-05
ID VALUE	7.1291E 01	5.1591E-03	1.1717E-04	-1.1489E-05	1.0318E-02	4.5805E-05	-6.0131E-05	-5.2246E-05
ABS BIAS	9.7561E-04	1.5911E-04	1.1715E-04	-1.1430E-05	0.	2.3738E-06	-1.4407E-06	-5.7919E-07
REL BIAS	1.3684E-05	3.1821E-02	1.1354E-02	-1.1077E-03	0.	2.4539E-02	-1.6108E-02	-6.4754E-03

TABLE 6-8. EXACT IDENTIFICATION ANALYSIS SOFTWARE SYSTEMATIC ERROR RESULTS FOR THE ADVANCED CONCEPT (concluded)

MODE 34 : W = 72.2430 ; ZETA = 0.0050 ; BMAG= 1.9477E-05 ; CMAG= 3.1700E-03

PARAMETER	W	ZETA	B 1	B 2	B 3	C 1	C 2	C 3
NOM VALUE	7.2243E 01	5.0000E-03	1.7226E-05	7.8978E-07	-9.0542E-06	5.0133E-04	3.4317E-04	-3.1113E-03
ID VALUE	7.2248E 01	4.6578E-03	1.4048E-05	4.2724E-07	-1.0256E-05	2.0413E-04	-6.3480E-04	-3.1113E-03
ABS BIAS	4.6014E-03	-3.4217E-04	-3.1783E-06	-1.6256E-07	-1.2015E-06	-2.9720E-04	-9.7797E-04	0.
REL BIAS	6.3694E-05	-6.8433E-02	-1.6319E-01	-8.3456E-03	-6.1691E-02	-9.3752E-02	-3.0851E-01	0.

MODE 35 : W = 79.9584 ; ZETA = 0.0050 ; BMAG= 8.8597E-05 ; CMAG= 4.3647E-03

PARAMETER	W	ZETA	B 1	B 2	B 3	C 1	C 2	C 3
NOM VALUE	7.9958E 01	5.0000E-03	-8.8576E-05	6.8362E-07	-1.7934E-06	-6.9326E-04	4.0320E-04	4.2904E-03
ID VALUE	7.9959E 01	4.9701E-03	-8.8576E-05	8.3792E-07	-1.7549E-06	-6.9925E-04	6.1909E-04	4.2110E-03
ABS BIAS	9.2504E-05	-2.9890E-05	0.	1.5430E-07	3.8454E-08	-5.9857E-06	2.1589E-04	-7.9387E-05
REL BIAS	1.1569E-06	-5.9780E-03	0.	1.7416E-03	4.3403E-04	-1.3714E-03	4.9469E-02	-1.8190E-02

MODE 36 : W = 85.3456 ; ZETA = 0.0050 ; BMAG= 1.7229E-02 ; CMAG= 2.6811E-04

PARAMETER	W	ZETA	B 1	B 2	B 3	C 1	C 2	C 3
NOM VALUE	8.5346E 01	5.0000E-03	2.7195E-07	1.7229E-02	-1.5158E-07	1.4179E-05	7.9660E-05	2.5561E-04
ID VALUE	8.5346E 01	5.0031E-03	1.6145E-05	1.7229E-02	1.0549E-05	1.4128E-05	7.9667E-05	2.5572E-04
ABS BIAS	3.7193E-05	3.0798E-06	1.5873E-05	0.	1.0701E-05	-5.1244E-08	6.4865E-09	1.0681E-07
REL BIAS	4.3580E-07	6.1597E-04	5.2131E-04	0.	6.2110E-04	-1.9113E-04	2.4193E-05	3.9838E-04

MODE 37 : W = 86.1685 ; ZETA = 0.0050 ; BMAG= 1.2412E-03 ; CMAG= 2.2502E-03

PARAMETER	W	ZETA	B 1	B 2	B 3	C 1	C 2	C 3
NOM VALUE	8.6169E 01	5.0000E-03	6.1448E-06	-1.2412E-03	-4.8017E-06	1.1188E-04	1.5601E-03	1.6176E-03
ID VALUE	8.6169E 01	4.9968E-03	1.2728E-06	-1.2412E-03	-4.6661E-06	1.1242E-04	1.5596E-03	1.6177E-03
ABS BIAS	-1.7164E-05	-3.1742E-06	-4.8720E-06	0.	1.3568E-07	5.3603E-07	-5.1539E-07	6.5018E-08
REL BIAS	-1.9922E-07	-6.3485E-04	-3.9252E-03	0.	1.0931E-04	2.3822E-04	-2.2904E-04	2.8895E-05

MODE 38 : W = 88.9727 ; ZETA = 0.0050 ; BMAG= 1.5096E-04 ; CMAG= 1.1427E-02

PARAMETER	W	ZETA	B 1	B 2	B 3	C 1	C 2	C 3
NOM VALUE	8.8973E 01	5.0000E-03	2.1882E-05	1.4894E-04	-1.1227E-05	-1.1347E-03	2.1758E-03	-1.1161E-02
ID VALUE	8.8973E 01	4.9915E-03	2.1169E-05	1.4894E-04	-1.1615E-05	-1.1494E-03	2.1590E-03	-1.1151E-02
ABS BIAS	-4.7684E-06	-8.5401E-06	-7.1246E-07	0.	-3.8777E-07	-1.4768E-05	-1.6754E-05	1.0194E-05
REL BIAS	-5.3594E-08	-1.7080E-03	-4.7197E-03	0.	-2.5688E-03	-1.2924E-03	-1.4662E-03	8.9211E-04

MODE 39 : W = 98.3460 ; ZETA = 0.0050 ; BMAG= 5.4311E-05 ; CMAG= 9.7663E-03

PARAMETER	W	ZETA	B 1	B 2	B 3	C 1	C 2	C 3
NOM VALUE	9.8346E 01	5.0000E-03	5.4278E-05	1.6224E-06	1.2676E-06	-8.8208E-04	1.4911E-03	-9.6114E-03
ID VALUE	9.8347E 01	5.0439E-03	5.4279E-05	1.6332E-06	7.7620E-07	-8.7371E-04	1.7520E-03	-9.6303E-03
ABS BIAS	9.3079E-04	4.3923E-05	0.	1.0798E-08	-4.8944E-07	8.3641E-06	-2.3915E-04	-1.8861E-05
REL BIAS	9.4644E-06	8.7845E-03	0.	1.9870E-04	-9.0108E-03	8.5642E-04	-2.4487E-02	-1.9312E-03

MODE 40 : W = 100.9860 ; ZETA = 0.0050 ; BMAG= 5.7832E-05 ; CMAG= 7.4417E-03

PARAMETER	W	ZETA	B 1	B 2	B 3	C 1	C 2	C 3
NOM VALUE	1.0099E 02	5.0000E-03	-2.8500E-06	5.7720E-05	-2.1354E-06	-.3494E-03	1.7099E-03	-5.7912E-03
ID VALUE	1.0098E 02	4.7280E-03	-2.4857E-06	5.7720E-05	-1.5017E-06	4.1902E-03	1.6614E-03	-5.5149E-03
ABS BIAS	-3.4723E-03	-2.7195E-04	3.6436E-07	0.	6.3473E-07	-1.5920E-04	-4.8463E-05	2.7626E-04
REL BIAS	-3.4384E-05	-5.4390E-02	5.3003E-03	0.	1.2013E-02	-2.1393E-02	-6.5123E-03	3.7123E-02

TABLE 6-9. WORST-CASE RESULTS FOR BIAS ERROR FOR 21 ID MODES AND 78 TRUE SYSTEM MODES

Mode	ω^2	$2\zeta\omega$	b1	b2	b3	c1	c2	c3
28	≈0	21%	3%	-7%	--	-7i%	16%	22%

The numbers listed for frequency squared are considered to be larger than the true parameter bias. This is true because all computations were done in single precision on the computer so that smaller numbers than those listed are not significant. Thus, earlier analytical results for frequency bias are consistent with these numerical results.

Add One Mode at a Time--Another simplification to the MLE identification method, called add one mode at a time, was tried for the advanced concept. A step-by-step procedure for identifying the parameters corresponding to one mode at a time is

Step 1: Estimate the parameters for a one-mode ID model

Step 2: Increase the number of ID model modes by one

Step 3: Estimate only the parameters of the new mode

Step 4: If more modes are desired go to step 2; otherwise, quit

The procedure gave essentially the same results as all modes at the same time for up to 10 modes. The success of this procedure is due to the light damping of the modes. In some cases it is expected that maybe two or three modes would have to be added at one time. The benefit of this procedure is that the total number of parameters being identified at one time is considerably smaller than when identifying them all at once.

The expected value of the negative log likelihood function, I^*, decreases as another mode is added to the ID model, as indicated in Figure 6-3. The modes added one at a time from low frequency to high frequency are the first 10 in the subset of true system modes discussed earlier. The leveling off of the plot with ID model order is due to the missing isolator modes that were not identified.

Identifiability Analysis Conclusions--Though the number of parameters to identify is enormous (147 for 21 modes) for the advanced concept, the identifiability analysis shows that identification of all the parameters is a practical possibility. Many simplifications to the general MLE algorithm were employed, such as eliminating the Kalman filter and the one-mode-at-a-time results for light damping. The achievable accuracy was found to be sufficient for control design for an identification time interval of 5 min, if the recommended test signal and measurement are used.

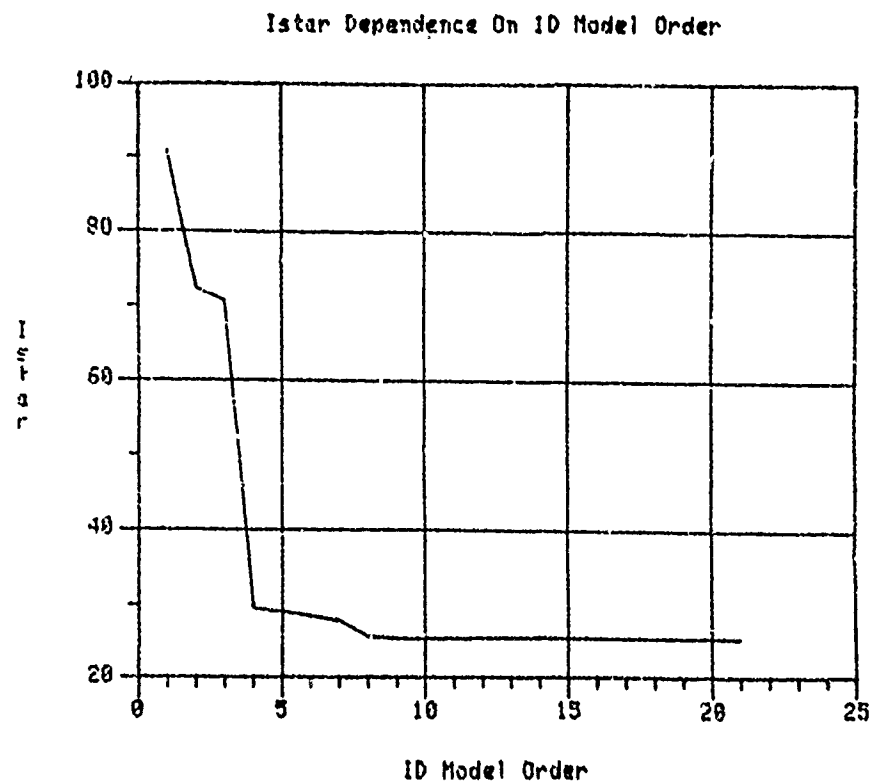

Figure 6-3. Expected Value of the Negative Log Likelihood Function (I^*): Dependence on ID Model Order

Control Design

Recall from Section 2 that the objective of the control design is to control LOS response to a force disturbance at node 46 by measuring the position of node 11 and applying control torques about node 44.

Open- and closed-loop transfer function relations are given by

Open-loop response:

$$\begin{bmatrix} \ell \\ y \end{bmatrix} = \begin{bmatrix} G_{\ell d} & G_{\ell u} \\ G_{yd} & G_{yu} \end{bmatrix} \begin{bmatrix} d \\ u \end{bmatrix} \qquad \begin{aligned} d &= FZ46 \\ u^T &= [T44X \quad T44Y \quad T44Z] \end{aligned} \tag{6-5a}$$

$$\ell^T = [LOS_x \quad LOS_y \quad DEFOCUS_z] \tag{6-5b}$$

$$y^T = [Pll_x \quad Pll_y \quad Pll_z] \tag{6-5c}$$

Closed-loop response:

$$\ell = \left[G_{\ell d} - G_{\ell u}K(I + G_{yu}K)^{-1}G_{yd}\right] d \tag{6-6}$$

where $\mu = -Ky$ and the Laplace variable s has been suppressed for convenience. The control design means constructing a compensator matrix K(s) to meet the above objective.

Sensor and Actuator Placement--Ideally, to meet the objective of the design, the control actuators should be as close to the disturbance as possible in both type (force and torque) and placement, and the output to be controlled should be measured. Neither of these is satisfied exactly for the advanced concept. For frequencies of interest, nowever, the actuators and ensors were chosen such that the following approximate relations were satisfied:

$$G_{\ell u} \approx G_{yu}$$

$$G_{yd} \approx G_{\ell d}$$

In other words, these relations imply that the critical modes that affect disturbance to LOS transmission should also dominate the actuator-to-sensor transmissions. Under these conditions large loop gains imply small closed-loop disturbance to LOS transmissions.

Control Law Design Procedure--As already mentioned, the sensors and actuators are not collocated. The design of the compensation matrix for this non-ILAS problem was carried out with the following step-by-step procedure. For convenience let $G(s) = G_{yu}(s)$; the steps are:

Step 1: Choose bandwidth and loop gain needed to meet specification.

Step 2: Find state space realization of reduced-order model (ROM) of $G(s)$, that is, find $\{A,B,C\}$ such that $\hat{G}(s) = C(sI - A)^{-1}B \simeq G(s)$.

Step 3: Compute magnitude of the multiplicative perturbation for this ROM, that is, $\bar{\sigma}[L] = \bar{\sigma}[\hat{G}^{-1}G - I]$. If $\bar{\sigma}[L] > 1$ for ω less than desired bandwidth, go back to step 2.

Step 4: Find H such that $H(sI - A)^{-1}B$ has desired bandwidth and loop gain of step 1.

Step 5: Compute full state feedback gain matrix, K_c, to minimize

$$J = \int_0^\infty \left[x^T H^T H x + u^T u \right] dt \quad \text{where } \dot{x} = Ax + Bu.$$

Step 6: Compute Kalman filter gain matrix, K_f, for process noise intensity $q^2 BB^T$, where q is a scalar. Here measurement noise intensity is I.

Step 7: Compute $K(s) = K_c(sI - A + BK_c + K_f C)^{-1}K_f$.

Step 8: If $K(s)\hat{G}(s)$ has desired bandwidth and loop gain, quit. Otherwise, increase q and go to step 6.

The design was achieved by making use of the frequency domain properties of the LQG feedback synthesis technique. These design steps have evolved over the years at Honeywell Systems and Research Center and are described in more detail in Ref. 2. It was necessary to add the model reduction steps to make the order of the matrices involved manageable. The parameters of this ROM would in practice be determined by identification. Each of the steps will be discussed in more detail in the following pages.

Desired Loop Gain and Bandwidth

The open-loop disturbance to LOS_x, LOS_y, and DEFOCUS frequency response were presented in Section 2 and are repeated in Figures 6-4a,b,c. Also shown is the LOS specification divided by the 400 N disturbance force to show the amount of attenuation required. The frequency range of interest is 10 r/s to 100 r/s. In this range it can be seen that as much as 70 dB attenuation, or a factor of over 3000, is required to meet the imposed LOS specification. The DEFOCUS plot shows that no additional attenuation is required (i.e., it meets specification open-loop). These plots are of interest for sizing the amount of loop gain needed to satisfy the control objectives. Fundamentals of feedback dictate that to attenuate the disturbance to LOS response by a factor of 3000 at some frequency requires a loop gain of approximately 3000 at that frequency.

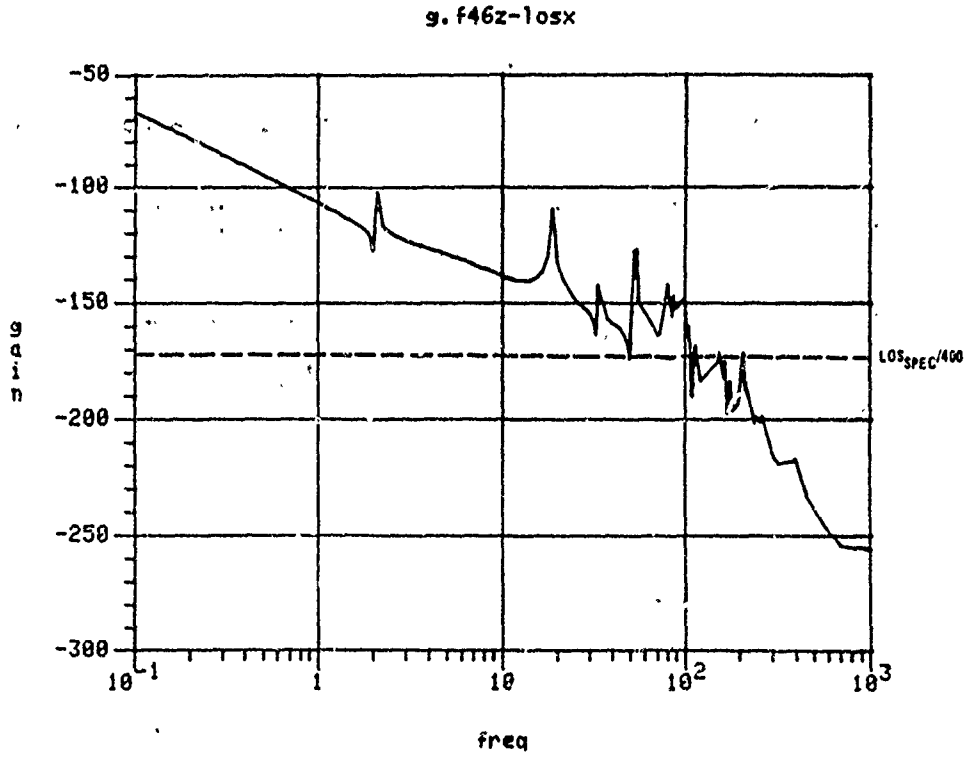

Figure 6-4a. Open-Loop Frequency Response for Disturbance to LOS_x

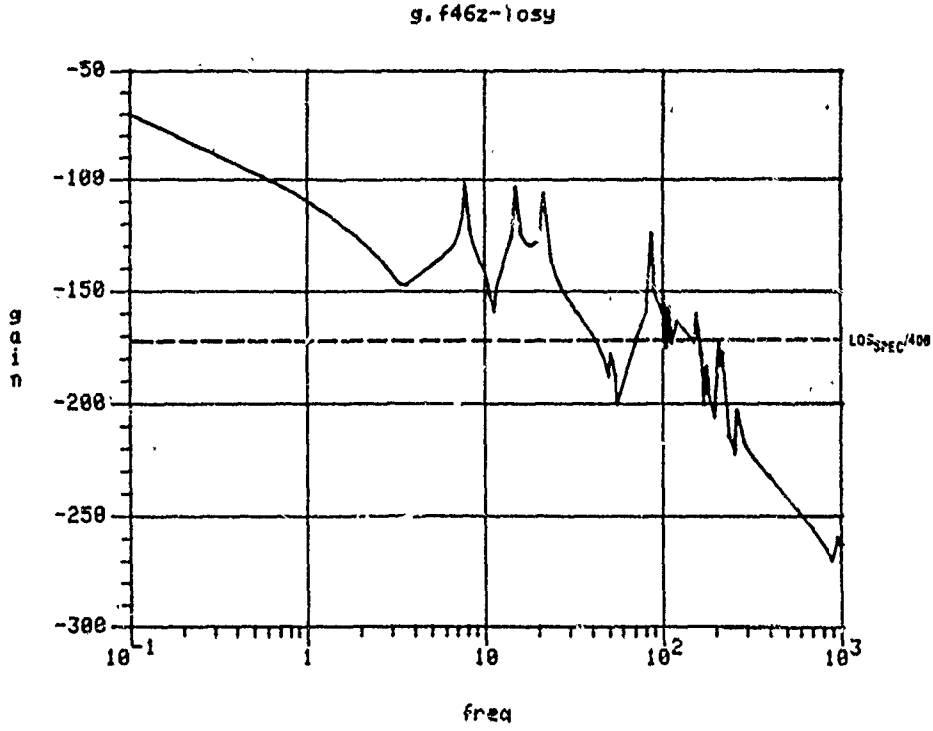

Figure 6-4b. Open-Loop Frequency Response for Disturbance to LOS_y

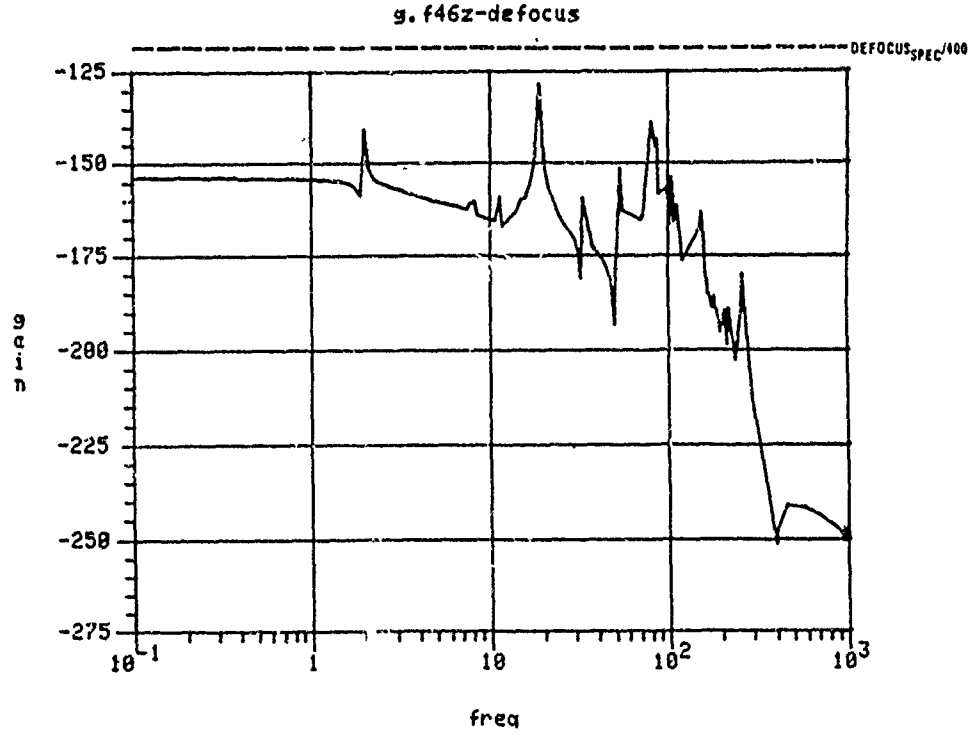

Figure 6-4c. Open-Loop Frequency Response for Disturbance to DEFOCUS

The singular values of the open-loop true system $G_t(s)$ were also shown in Section 2, and are repeated in Figure 6-5 for the torque actuator at node 44 and the position sensors at node 11. This response is of interest in determining the bandwidth sufficient to provide the loop gain needed to attenuate the disturbance to LOS transmission. By roughly sizing the gain of just the lead portion of the compensator, and performing the multiplication $\hat{KG}$ to obtain the loop gain, a bandwidth requirement of roughly 1300 r/s would be necessary to meet specification. This required bandwidth was considered to be higher than would be practical for the control design and identification model. A bandwidth of 30 r/s was deemed practical and the design proceeded, recognizing that it would not meet the imposed specification but should attenuate disturbances in the frequency range of 10 to 30 r/s.

Elimination of Uncontrollable or Unobservable Rigid-Body Modes--A minimal state-space realization was desired for the control-law computations. Therefore all uncontrollable and unobservable modes were eliminated. Of the six free-free

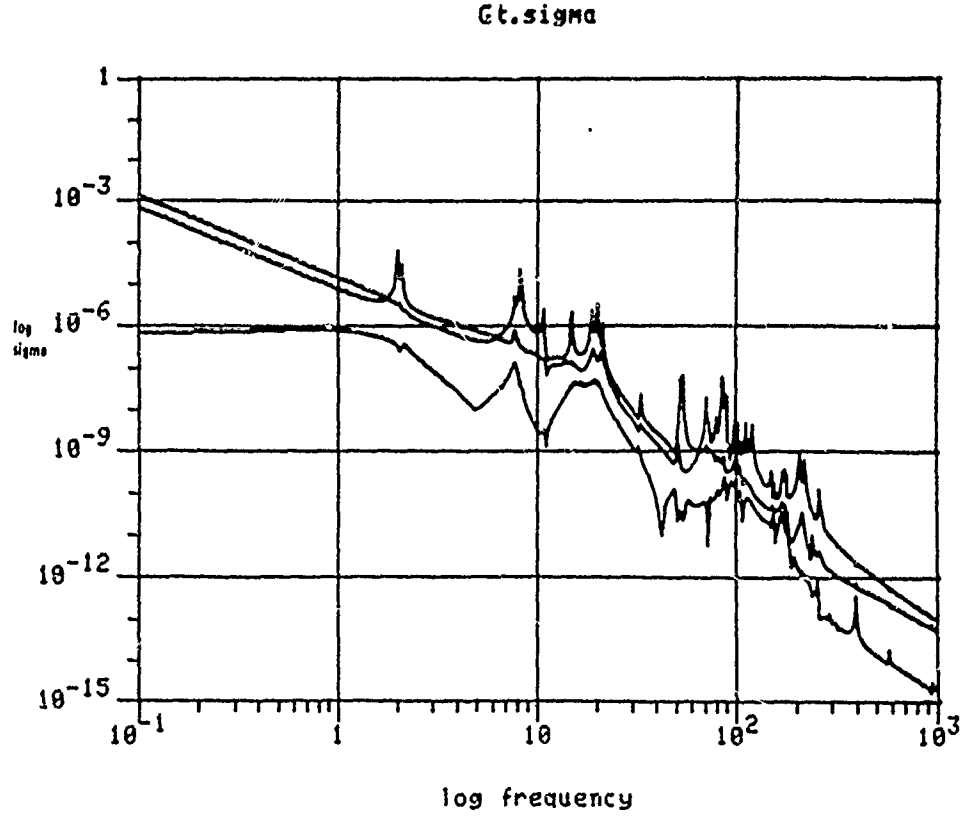

Figure 6-5. Open-Loop Frequency Response (Singular Values of G_t) for True System: Actuator Inputs to Sensor Outputs

rigid-body modes, only two were both controllable and observable. Specifically, the three translation modes are uncontrollable due to torque inputs. Also, position outputs at node 11 imply that the rotation mode in the direction of the line connecting node 11 and the spacecraft center of mass is unobservable. This also explains why the minimum singular value of G_t (Figure 6-5) flattens out at low frequency, whereas the other two have the familiar $1/s^2$ behavior.

Reduced-Order Model--The ROM was obtained by truncating the full-order model past 100 r/s and some of the nearly uncontrollable/unobservable modes below 100 r/s. No optimal model reduction procedure was attempted. The resulting ROM had 24 second-order modes, including two rigid-body modes. The frequency response for the ROM, $\hat{G}(s)$, is shown in Figure 6-6. The singular values of the multiplicative perturbation $L = \hat{G}^{-1}G - I$ are shown in Figure 6-7 and can be seen to be less than 1 for frequencies less than the desired bandwidth of 30 r/s. Note, however, that they are larger than 1 past 40 r/s due to truncation. This plot indicates that the ROM should be satisfactory for design of a 30 r/s bandwidth control law.

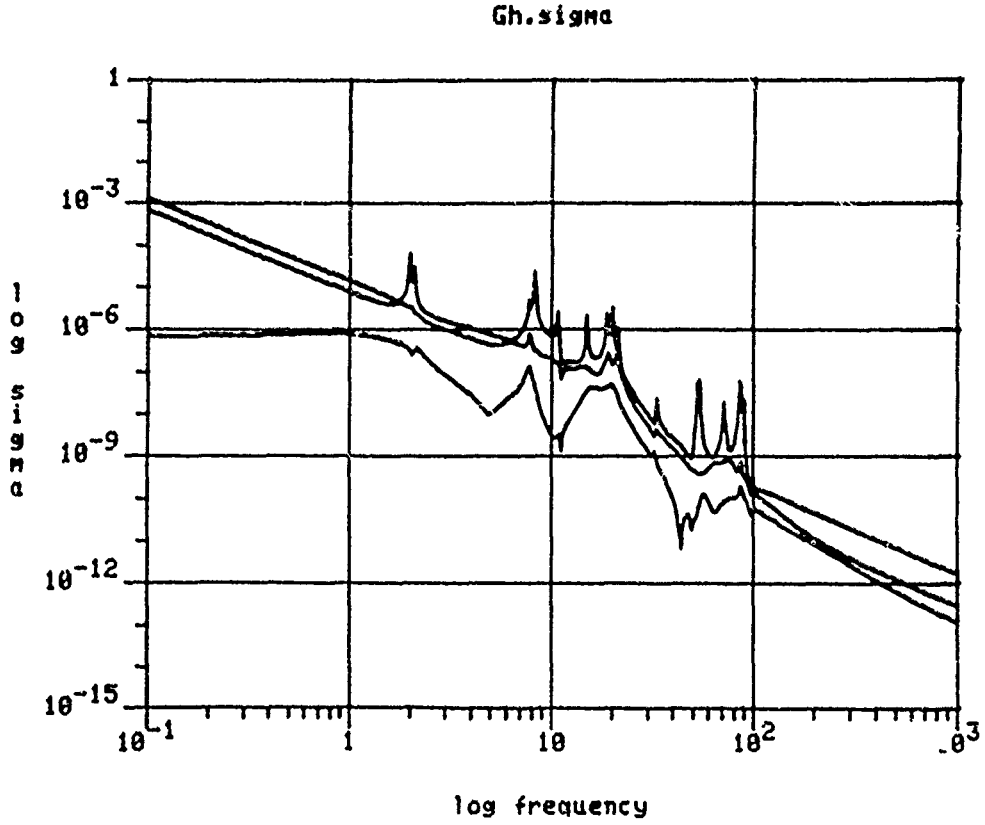

Figure 6-6. Open-Loop Frequency Response (Singular Values of $\hat{G}$) for ROM: Actuator Inputs to Sensor Outputs

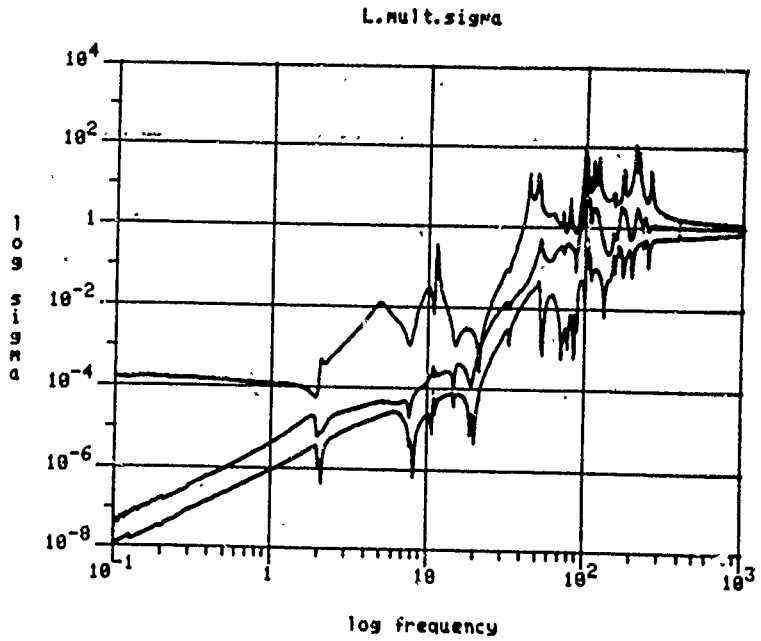

Figure 6-7. Singular Values of the Multiplicative Perturbation Implied by the ROM

Linear Quadratic Gaussian (LQG) Design--The H matrix was chosen to be a scalar times the C matrix. The scalar was chosen such that the bandwidth of the loop would be 30 r/s. The singular values of $H(j\omega I - A)^{-1} B$ vs ω are shown in Figure 6-8. The idea is that this will be the approximate shape of the eventual LQG loop that will be the final design. The fact that the minimum singular value is less than 1 below the desired bandwidth is undesirable, but the design was continued in the interest of time.

The full-state feedback LQ loop, $K_c(sI - A)^{-1}B$, is shown in Figure 6-9. It can be seen to be approximately the same as the desired loop below 30 r/s and to have the guaranteed 1/s rolloff above 30 r/s.

After iterating up to $q = 10^9$, the loop gain for the LQG compensator is shown in Figure 6-10. The loop gain of the LQG loop has not quite reached the loop gain of the LQ loop. This could be theoretically improved by increasing q, but numerical difficulties prevented increasing q any further. The final plot (Figure 6-11) is the same as Figure 6-10 (i.e., K(s) G(s), the loop gain of the final design) but with more frequency resolution and a larger frequency range.

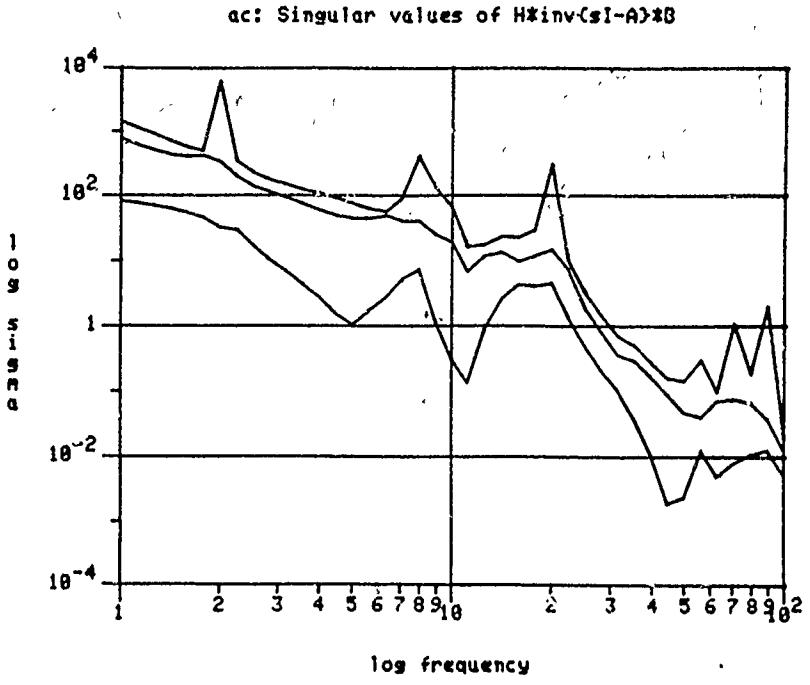

Figure 6-8. Singular Values of Desired Loop Transfer Function

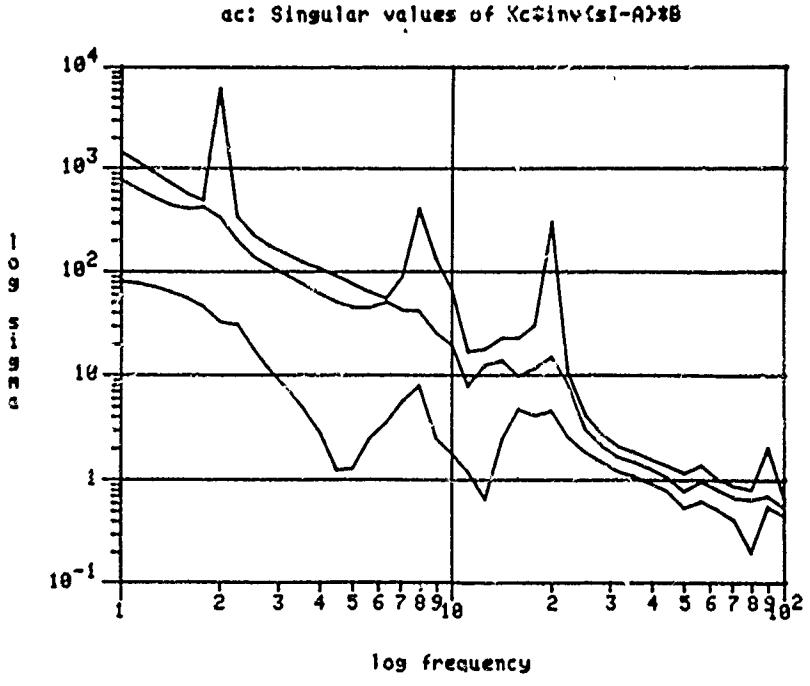

Figure 6-9. Singular Values of Full-State Feedback Loop LQ Design

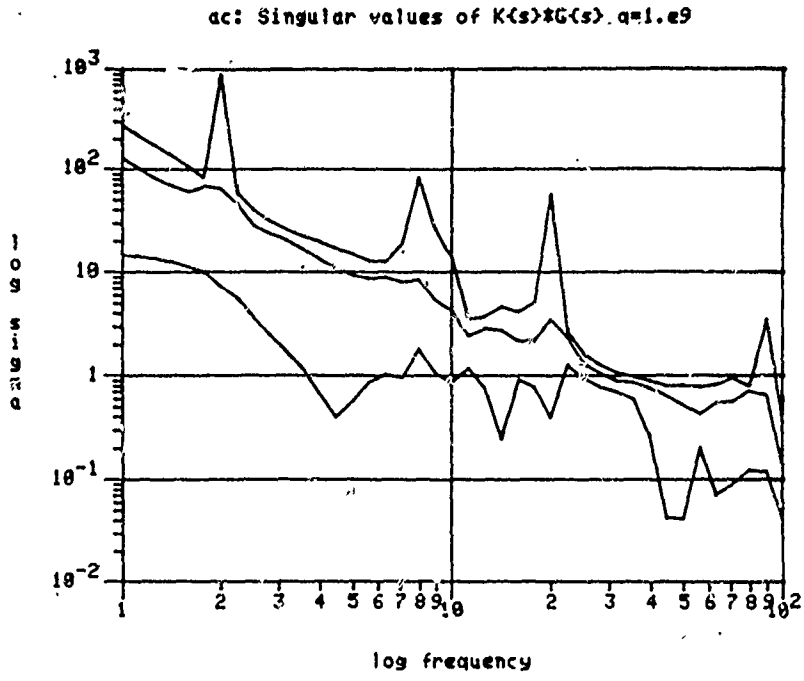

Figure 6-10. Singular Values of LQG Loop (Final design)

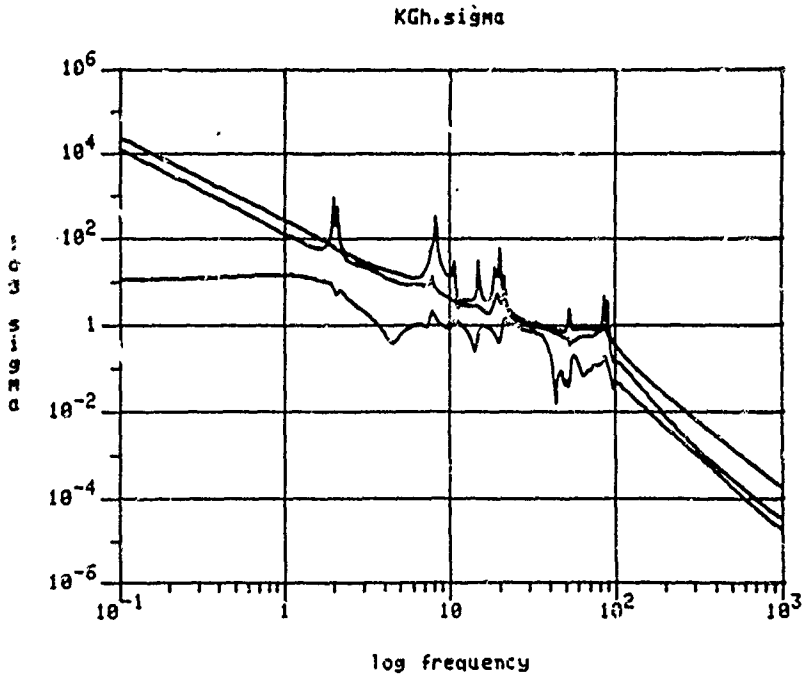

Figure 6-11. Singular Values of LQG Loop (Final design with finer frequency resolution and larger frequency range)

Evaluation of the Control Design--After completing the design of K(s), we investigated its performance and stability with the true system. LQG guarantees stability of the closed-loop system when there are no modeling errors. Since the design was carried out using a ROM, closed-loop stability with the true system must be verified. Finally, the closed-loop disturbance to LOS frequency responses were compared to the corresponding open-loop frequency responses.

Poles and Zeros--A subset of the open-loop poles is plotted in the s-plane in Figure 6-12. The flexible modes are all lightly damped ($\zeta = 0.005$) except for the six isolator modes ($\zeta = 0.7$). There are also four poles at the origin that are not indicated.

Transmission zeros are defined to be the values of s such that

$$\det \begin{bmatrix} sI - A & B \\ -C & 0 \end{bmatrix} = 0$$

A subset of these open-loop transmission zeros is plotted in the s-plane in Figure 6-13. They correspond to the control inputs and measurement outputs for the advanced concept. The zeros of interest are the ones in the right half-plane. These nonminimum phase zeros limit performance of the feedback system.

Also plotted are the regulator and estimator closed-loop poles in Figures 6-14 and 6-15 for the ROM. They are, of course, all stable as the LQG design method guarantees. A theorem of the LQ recovery procedure says that the estimator closed-loop poles asymptotically approach the transmission zeros as q goes to infinity, or their left half-plane mirror images for nonminimum phase zeros. This can be verified by comparing the two plots (Figures 6-13 and 6-15).

Verification of Stability of Closed-Loop System--The control law consists of a compensator with order equal to the order of the ROM, so it has 24 x 2 = 48 states. The true system has 84 x 2 = 168 states. The closed-loop system thus has 168 + 48 = 216 states whose eigenvalues must lie in the left half-plane in order for the closed-loop system to be stable. The eigenvalue routines available were not considered reliable for computing such a large number of eigenvalues. The frequency response of the true system could, however, be computed very efficiently

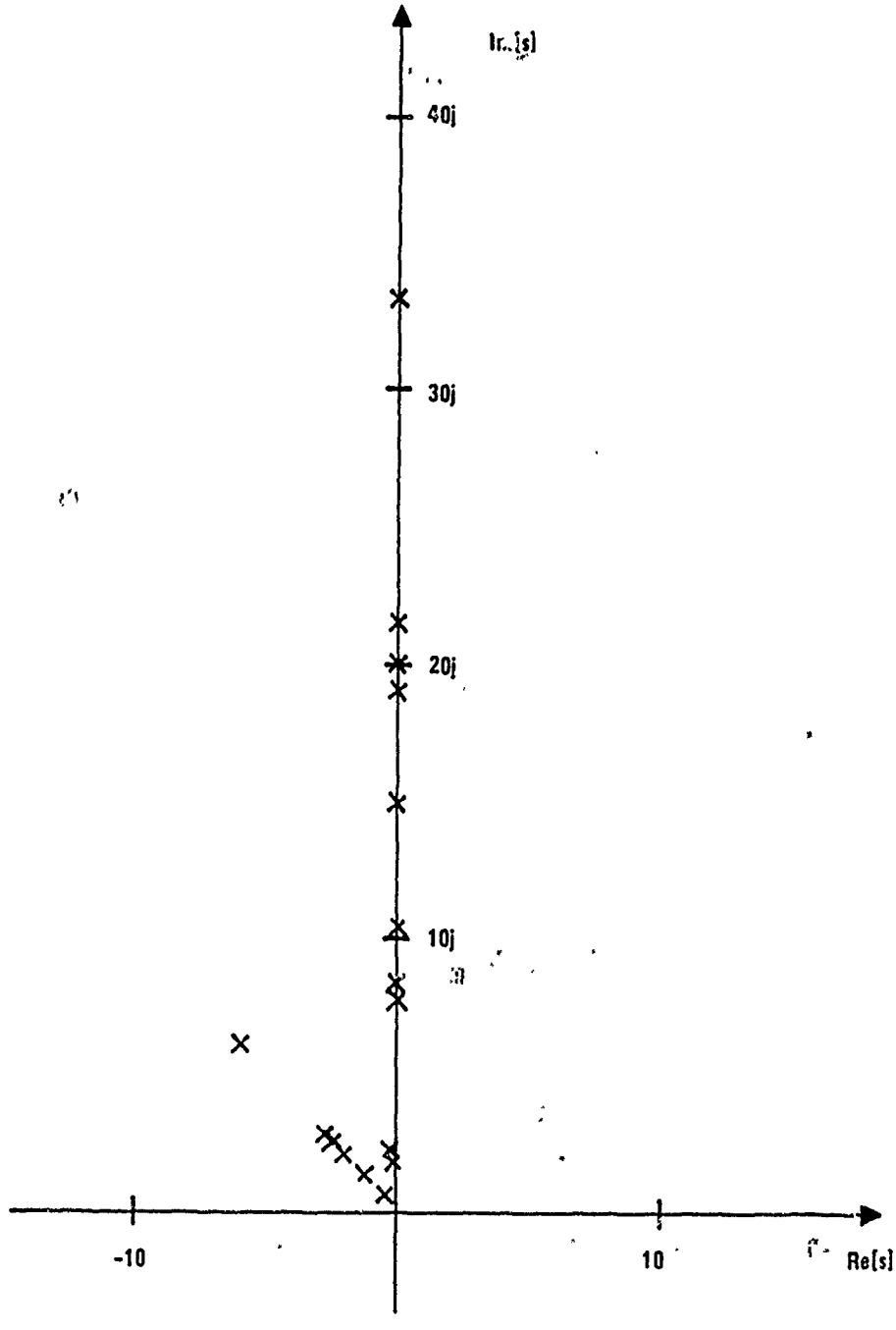

Figure 6-12. Open-Loop Poles of the Plant with Smallest Magnitude

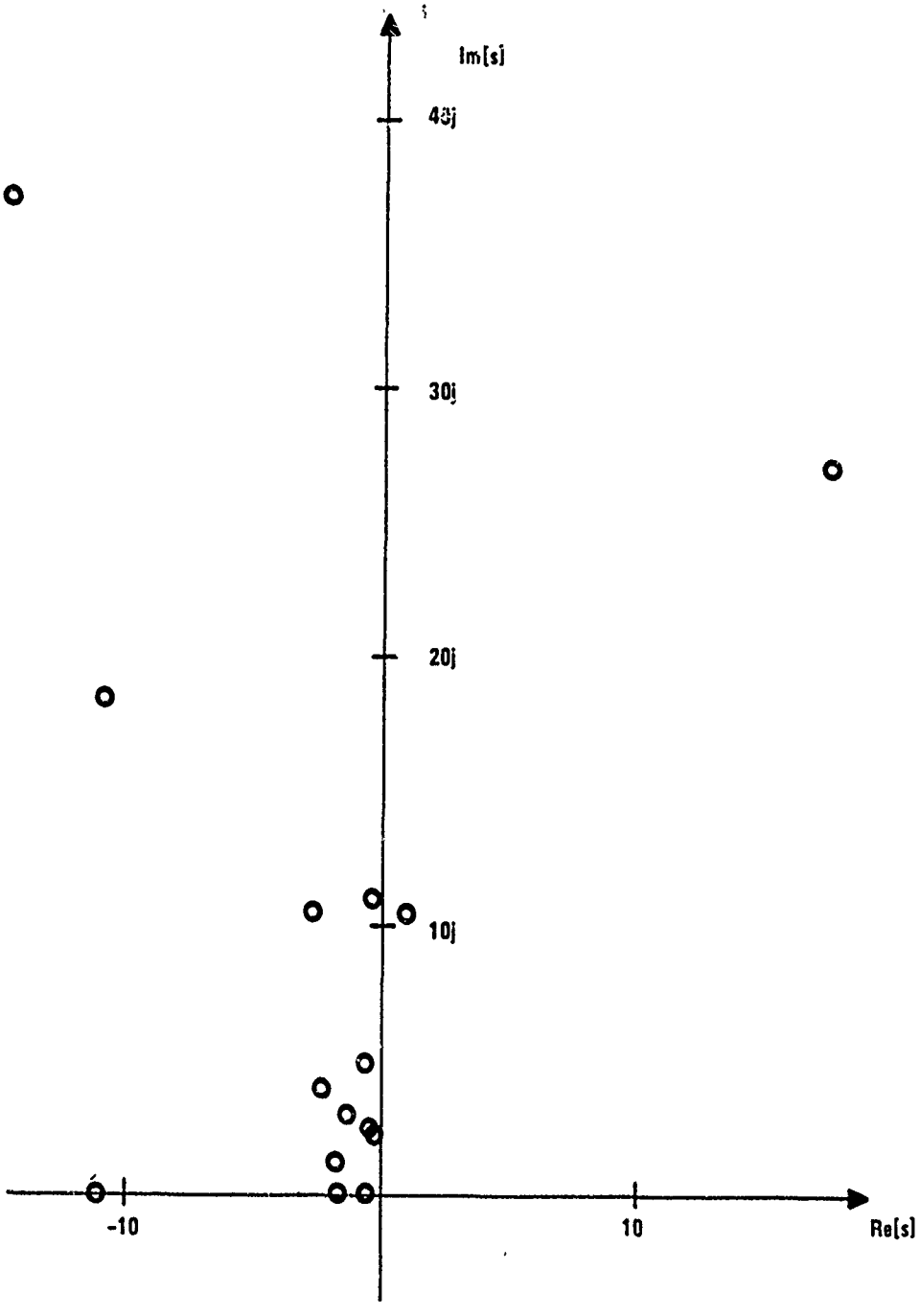

Figure 6-13. Open-Loop Transmission Zeros of the Plant with Smallest Magnitude

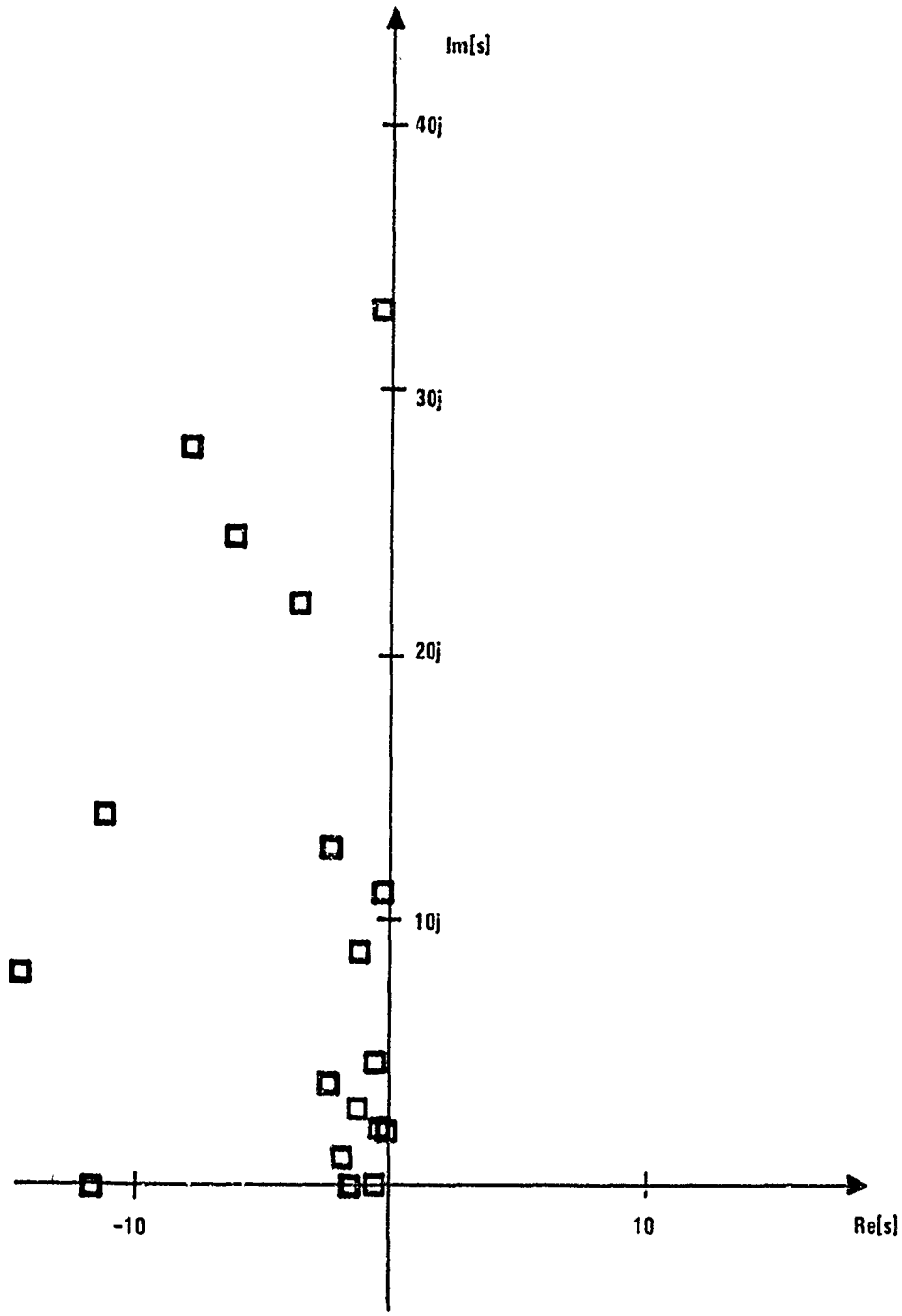

Figure 6-14. Closed-Loop System Regulator Poles with Smallest Magnitude

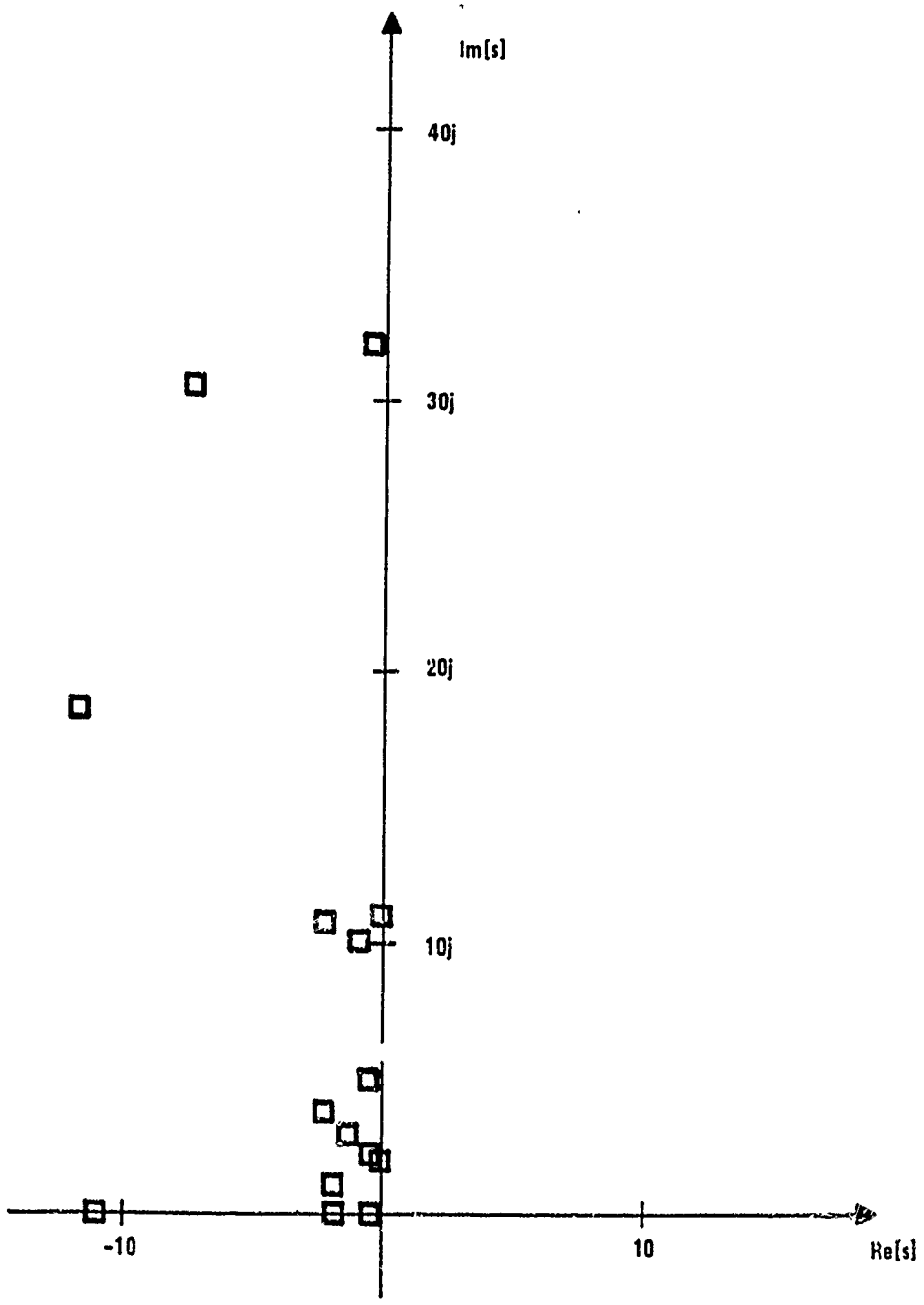

Figure 6-15. Closed-Loop System Estimator Poles with Smallest Magnitude

and accurately as the sum of the contributions of each of the 84 second-order modes. Likewise, the frequency response of the 48th-order compensator could be computed accurately. These two frequency response evaluations allow the assessment of closed-loop stability of the control law with the true system using the multivariable Nyquist Theorem.

Nyquist Theorem: The closed-loop system is stable if and only if the number of counterclockwise encirclements of the origin obtained by mapping the Nyquist D contour by det[I + KG] is equal to the number of unstable poles of G.

A computer program was written to count encirclements and check for enough frequency resolution of the data computed. The result, indicated qualitatively in Figure 6-16, was that the det[I + KG] showed one counterclockwise encirclement for $j0^+ < j\omega < \infty$, which implies two counterclockwise encirclements for the part of the Nyquist D contour from $j0^+$ to $j0^-$. The indentation around the origin of the D contour, required because of the rigid-body poles of the true system, was

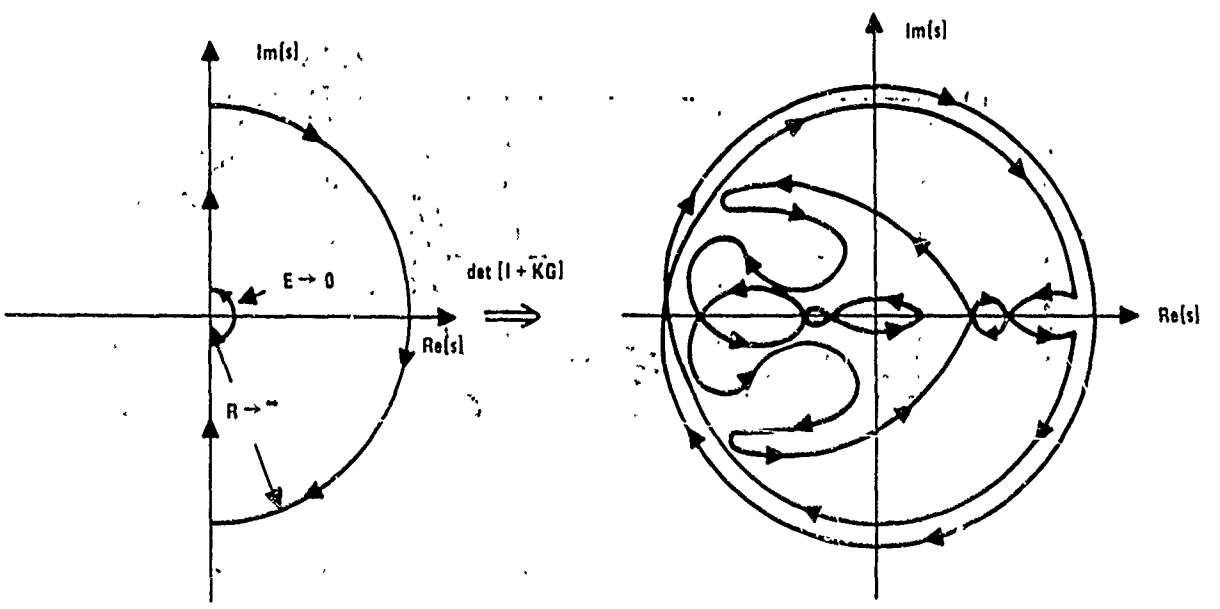

Figure 6-16. Qualitative Plot of the Image of the Nyquist D Contour By the det[I + KG] Map, Indicating Closed-Loop Stability

handled separately. The det[I + KG] showed two clockwise encirclements for the indentation part of the D contour. There were thus no net encirclements, so the control law is closed-loop stable with the true system.

Compensator Frequency Response--A plot of the three singular values of compensator, K(jω), is shown in Figure 6-17. The compensator exhibits the familiar lead characteristic in the crossover region, that is, ω ≈ 30 r/s. Notch filters are very evident in the minimum singular-value plot. These notches are likely to be very sensitive to the parameters of the design model of the true system that was used to design the compensator. This indicates the need for very accurate identification of parameters for non-ILAS control system design. Another item of interest is the dramatic rate of change of gain with frequency near ω = 10 r/s and ω = 30 r/s. This is especially interesting since the nonminimum phase zeros have magnitudes of 10 r/s and 30 r/s. Although no MIMO results are available to explain these peculiarities, they are consistent with intuition from SISO Bode gain-phase relations.

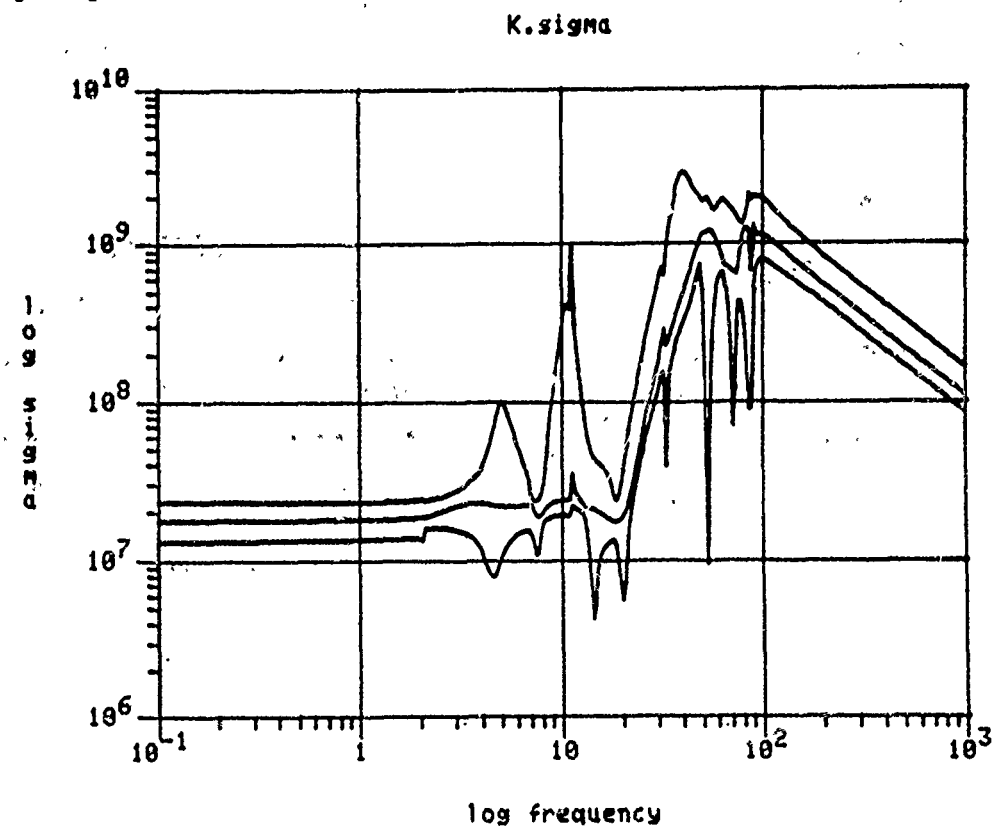

Figure 6-17. Singular Values of the Compensator Matrix Transfer Function

Return Difference Frequency Response--Singular values of $I + K\hat{G}$, the return difference, are plotted vs frequency in Figure 6-18. Fundamentals of feedback require that the return difference be large in the frequency range of interest to achieve the benefits of feedback (i.e., disturbance rejection). The plot indicates that disturbance rejection is achieved for two directions in the input/output space for frequencies less than 20 r/s. However, directions in input-output space corresponding to the minimum singular value do not share these benefits. In fact, the return difference is less than unity, which means that feedback actually amplifies disturbances in these directions. This poor performance is a fundamental limitation of using feedback to control a nonminimum phase plant.

Multivariable Stability Margins--The plot of the singular values of $I + (K\hat{G})^{-1}$ vs ω in Figure 6-19 is an indication of multivariable stability margins with respect to multiplicative perturbations. When the maximum singular value of a multiplicative perturbation to $\hat{G}$ is less than the minimum singular value of

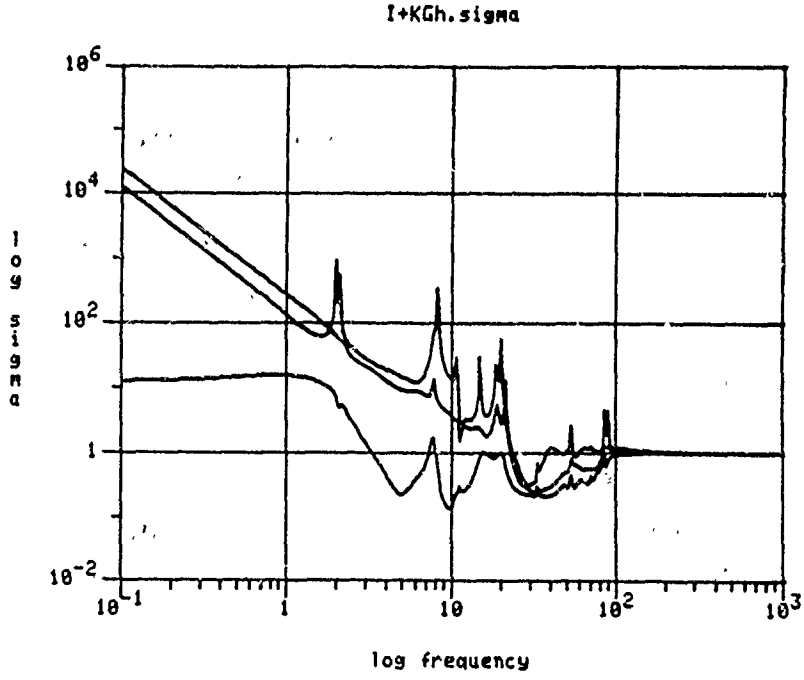

Figure 6-18. Singular Values of the Return Difference: $I + K\hat{G}$

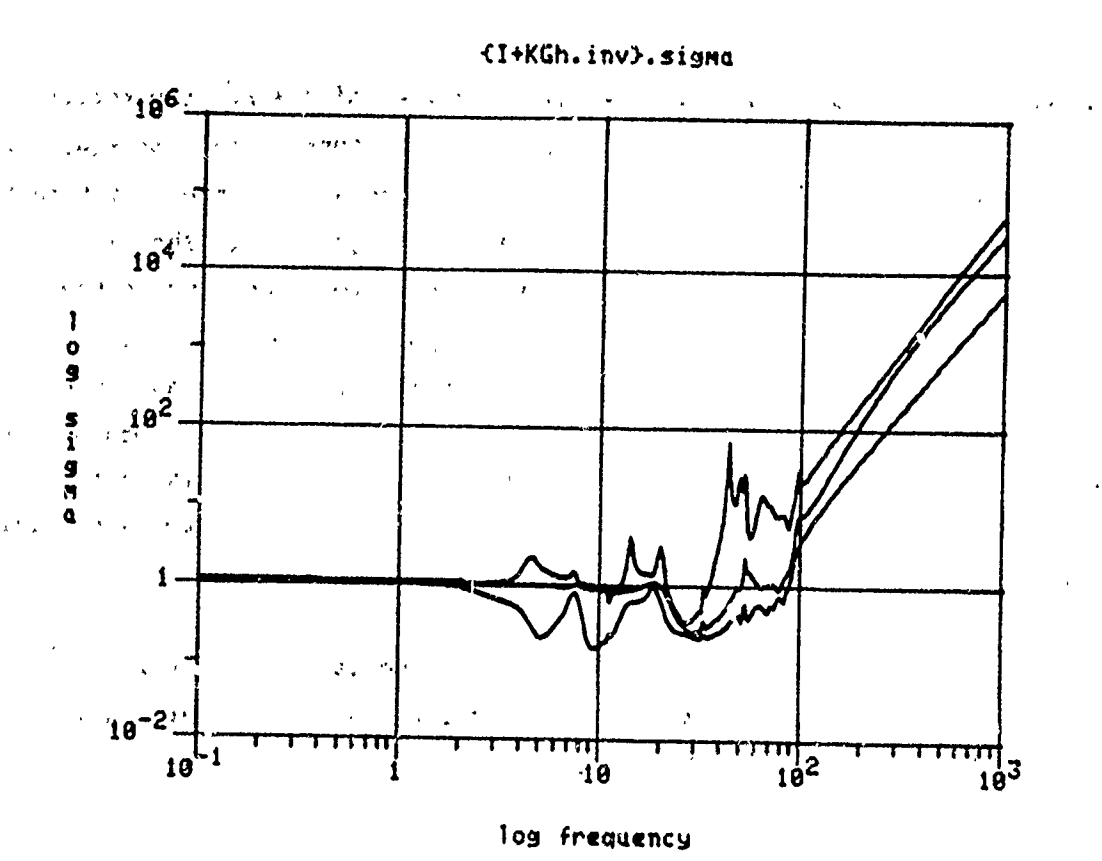

Figure 6-19. Singular Values of $I + (K\hat{G})^{-1}$

$I + (K\hat{G})^{-1}$, the closed-loop system is guaranteed to be stable in the face of the perturbation. This condition is sufficient for stability, but is not necessary. Thus it is conservative in some cases. It is especially conservative for application to the multiplicative perturbation ($I_{mult} = \hat{G}^{-1}G - I$) implied by the ROM. Comparing the two plots (Figures 6-7 and 6-19), it can be seen that the sufficient condition for stability is violated for 10 r/s < ω < 250 r/s. However, the closed-loop system was earlier shown to be stable in the face of this specific perturbation. For perturbations that are unstructured but bounded, unlike the highly structured perturbation implied by the ROM, the condition is not conservative. From the plot in Figure 6-19 of $I + (K\hat{G})^{-1}$, it can be seen that the stability of the closed-loop system is guaranteed for unstructured multiplicative perturbations of less than 15% below 30 r/s. More robustness woul be required for a practical implementation of this controller.

Closed-Loop Disturbance Attenuation Performance--Final evaluation of closed-loop performance is made by comparing the frequency response of the closed-loop system and open-loop system for disturbance to LOS. The disturbance has a frequency between 10 r/s and 100 r/s so only this range of frequencies need be compared. LOS_x and LOS_y (Figures 6-20a,b) are the only plots of interest since DEFOCUS (Figure 6-20c) meets the specification both open- and closed-loop. The plots in Figures 6-20a,b show that performance was improved for the modes 22 in the LOS_x response and 21 and 24 in the LOS_y response; all these have frequencies in the range 10 to 30 r/s.

At the outset of the design it was recognized that to meet specifications, a bandwidth of roughly 1300 r/s was required. This was considered impractical for the model of the spacecraft available and performance was compromised for the sake of a practical bandwidth. Sensor and actuator placement were based on critical mode controllability and observability in the frequency range 10 r/s to 100 r/s. Loop gain greater than unity was achieved for frequencies less than the bandwidth, 30 r/s. Considering these factors, we expect performance improvement in the frequency range 10 r/s to 30 r/s.

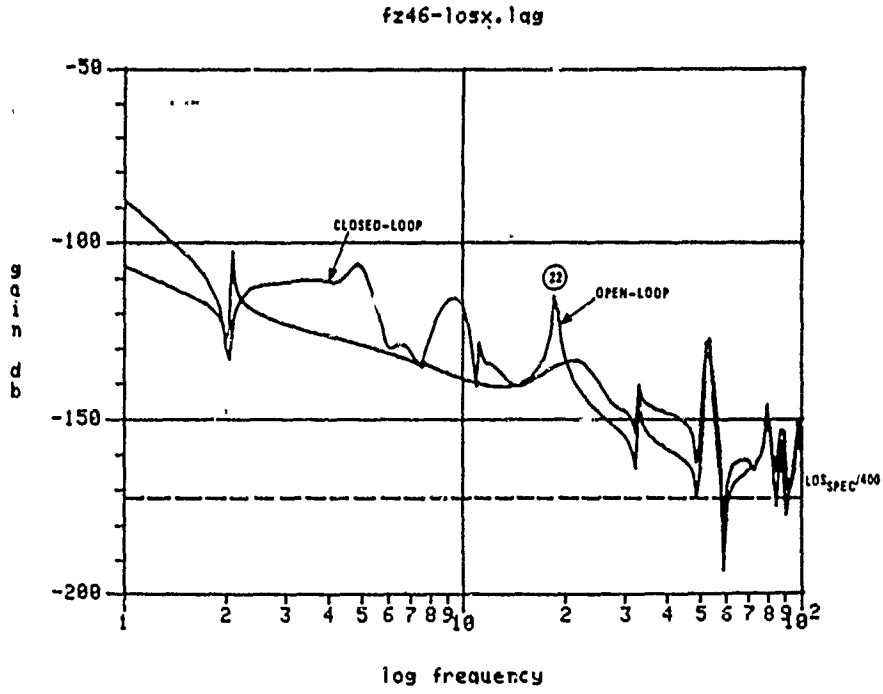

Figure 6-20a. Open- and Closed-Loop Frequency Response for Disturbance to LOS_x

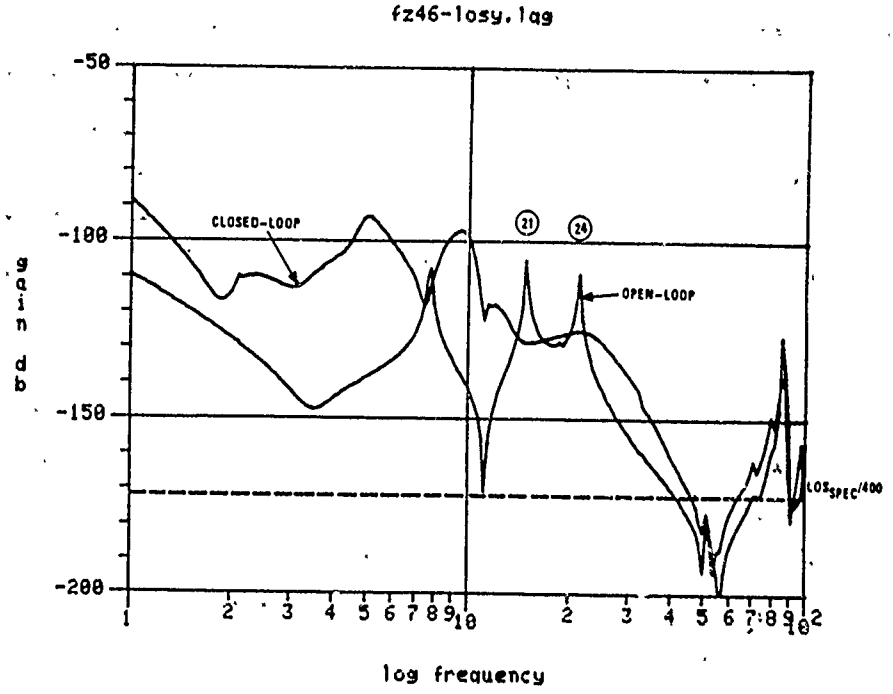

Figure 6-20b. Open- and Closed-Loop Frequency Response for Disturbance to LOS_y

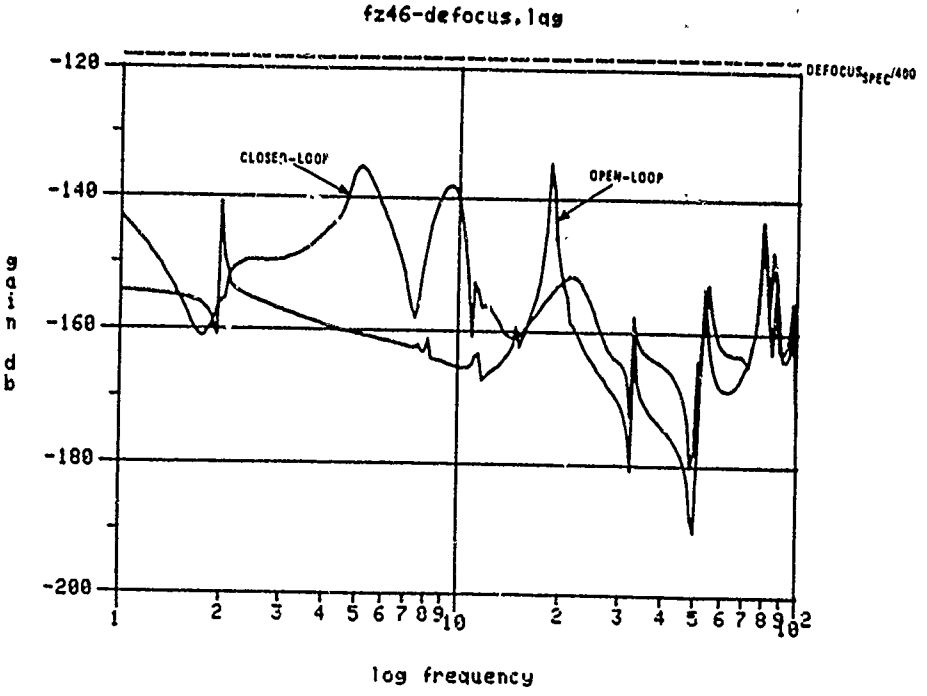

Figure 6-20c. Open- and Closed-Loop Frequency Response for Disturbance to DEFOCUS

Control Design Conclusions--A compensator matrix for the advanced concept was designed and found to be stable with the true system and to provide some performance improvement. The performance improvement is not enough to meet the LOS pointing specification, but it was not expected to do so. Control performance was compromised for the sake of a practical controller bandwidth. The nonminimum phase zeros of the plant impose fundamental limits to performance, as was observed in the return difference magnitude plots.

Although the closed-loop system was stable with the true system, it is not very robust to modeling errors of the unstructured type. The multivariable stability margins were found to be less than adequate for a practical design. This sensitivity is in large part due to the limitations of controlling such an extremely non-ILAS plant.

Further iterations on the design would have to be carried out to achieve a more practical control law, but were not possible in the limited time available. It is evident that the advanced concept is a good example of a very difficult control problem, because of the tight performance specification required for a non-ILAS, nonminimum phase plant with highly coupled MIMO dynamics. Though it is believed that the tools of modern control theory are capable of dealing with such difficult problems, ultimate performance will always be limited by nonminimum phase zeros.

REFERENCES

1. Strunce, R.R., et al., "Active Control of Space Structures," C.S. Draper Laboratory Interim Report Rk-1404, Contract No. F30602-80-C-0096, September 1980.

2. Doyle, J.C. and Stein, G., "Multivariable Feedback Design: Concepts for a Classical/Modern Synthesis," IEEE Transactions on Automatic Control, February 1981.

3. Lehtomaki, N.A., et al., "Robustness Results in Linear-Quadratic-Gaussian Based Multivariable Control Designs," IEEE Transactions on Automatic Control, February 1981.

4. Barrett, M.F., "Conservatism with Robustness Tests for Linear Feedback Control Systems," IEEE 1980 CDC Proceedings, December 1980.

5. Schweppe, F., Uncertain Dynamical Systems. Englewood Cliffs, New Jersey: Prentice-Hall, 1973.

6. Gelb, A. (Ed.), Applied Optimal Estimation. Cambridge, Massachusetts: MIT Press, 1974.

7. Yared, K., "On Maximum Likelihood Identification on Linear State Space Models," LIDS-TH-920, Labaratory for Information and Decision Systems, MIT, Cambridge, Massachusetts, July 1979.

8. Stein, G., et al., "Adaptive Control Laws for the F-8 Flight Test, IEEE Transactions on Automatic Control, Vol. AC-22, No. 5, 1977, pp. 758-768.

9. Hartmann, G.L. and Stein, G., "Digital Adaptive Control Laws for VTOL Aircraft," 17th Conference on Decision and Control, San Diego, California, January 1979.

10. Harvey, C.A., Stein, G. and Felt, L.R., "Adaptive Control of Wing/Store Flutter--A Feasibility Study," AIAA 79-0789, Proceedings of 20th Structures, Structural Dynamics and Materials Conference, St. Louis, Missouri.

11. Hartmann, G.L., Stein, G. and Gay, T.A., "An Adaptive Riser Angle Reference System for Dynamic Positioning," Joint Automatic Control Conference, San Francisco, California, August 1980.

12. Mueller, C.E. and Stein, G., "Calibration of High Precision Navigators with Maximum Likelihood Estimation," ONR Conference on Control Theory and Naval Applications, Monterey, California, 1975.

13. Pope, R.E., "A Users Manual for Program ID, A Parameter Identification Computer Program," AFDL-FGC-TM-73-34, 1973.

14. Green, C.S. and Barrett, M.F., "Identification and Control for Flexible Vehicles," Final Report for NASA Langley Contract No. NAS1-16524, March 1982.

15. Stein, G. and Greene, C.S., "Inherent Damping, Solvability Conditions, and Solutions for Structural Vibration Control," 1979 IEEE CDC Conference Proceedings, December 1979.

R. Carman RADC/OCSE	5	
RADC/TSLD GRIFFISS AFB NY 13441	1	2
RADC/DAP GRIFFISS AFB NY 13441	2	3
ADMINISTRATOR DEF TECH INF CTR ATTN: DTIC-DDA CAMERON STA BG 5 ALEXANDRIA VA 22314	12	5
Honeywell Systems & Research Center 2600 Ridgway Parkway Minneapolis, MN 54413	5	3
Charles Stark Draper Labs 555 Technology Square Cambridge, MA 02139	5	4
Charles Stark Draper Lab Attn: Dr. Keto Soosar 555 Technology Square M.S. -95 Cambridge, MA 02139	1	5
Charles Stark Draper Lab Attn: Dr. J.B. Linn 555 Technology Square Cambridge, MA 02139	1	6
Charles Stark Draper Lab Attn: Mr. R. Strunce 555 Technology Square M.S.-60 Cambridge, MA 02139	1	7

Charles Stark Draper Lab Attn: Dr. Daniel R. Hegg 555 Technology Square M.S. -60 Cambridge, MA 02139	1	8
ARPA/MIS 1400 Wilson Blvd Arlington, VA 22209	1	9
ARPA/STO Attn: Lt Col A. Herzberg 1400 Wilson Blvd Arlington, VA 22209	1	10
ARPA/STO Attn: Maj E. Dietz 1400 Wilson Blvd Arlington, VA 22209	1	11
Riverside Research Institute Attn. Dr. R. Kappesser Attn. Mr. A. DeVilliers 1701 N. Ft. Myer Drive Suite 711 Arlington, VA 22209	3	12
Riverside Research Attn: HALO Library, Mr. Bob Passut 1701 N.Ft. Myer Drive Arlington, VA 22209	1	13
Itek Corp Optical Systems Division 10 Maguire Rd. Lexington, MA 02173	1	14
Perkin Elmer Corp Attn: Mr. H. Levenstein Electro Optical Division Main Avenue Norwalk, CT 06856	1	15
Hughes Aircraft Company Attn: Mr. George Speak M.S. B 156 Culver City, CA 09230	1	16

Hughes Aircraft Company
Attn: Mr. Ken Beale
Centinela Teale Sts
Culver City, CA 90230

Air Force Flight Dynamics Lab
Attn+ Dr. Lynn Rogers
Wright Patterson AFB, OH 45433 — 1 — 18

AFWL/FIBG
Attn: Mr. Jerome Pearson
Wright Patterson AFB, OH 45433 — 1 — 19

Air Force Wright Aero Lab. FIEE
Attn: Capt Paul Wren
Wright Patterson AFB, OH 45433 — 1 — 20

Air Force Institute of Technology
Attn: Prof. R. Calico/ENY
Wright Patterson AFB, OH 45433 — 1 — 21

Aerospace Corp.
Attn: Dr. G.T. Tseng
2350 E. El Segundo Blvd
El Segundo, CA 90245 — 2 — 22

Aerospace Corp.
Attn: Mr. J. Mosich
2350 E. El Segundo Blvd
El Segundo, CA 90245 — 1 — 23

Aerospace Corp/Bldg 125/1054
Attn: Mr. Steve Burrin
Advanced Systems Tech Div.
2400 E El Segundo Blvd
El Segundo, CA 90245 — 1 — 24

SD/SD/YLVS
Attn: Mr. Lawrence Weeks
P.O. Box 92960
Worldway Postal Center
Los Angeles CA 90009 — 1 — 25

SD/YCD
Attn: YCPT/Capt Gajewski
P.O. Box 92960
Worldway Postal Center
Los Angelel, CA 90009

1 26

Grumman Aerospace Corp
Attn: Dr. A. Mendelson
South Oyster Bay Road
Bethpage, NY 11714

1 27

OUSDR&E/DS
Attn. Mr. A. Bertapelli
Room 3D136
Pentagon, Washington, DC 20301

1 28

Jet Propulsion Laboratory
Attn: Mr. D.B. Schaechter
4800 Oak Grove Drive
Pasadena, CA 91103

2 29

MIT/Lincoln Laboratory
Attn: S. Wright
P.O. Box 73
Lexington, MA 02173

1 30

MIT/Lincoln Laboratory
Attn: Dr. D. Hyland
P.O. Box 73
Lexington, MA 02173

11 31

MIT/Lincoln Laboratory
Attn: Dr. N. Smith
P.O. Box 73
Lexington, MA 02173

11 32

Control Dynamics Co.
Attn: Dr. Sherman Seltzer
221 East Side Square, Suite 1B
Huntsville, Al 35801

1 33

Lockheed Space Missile Corp. Attn: A. A. Woods, Jr., 0/62-E6 p.O. Box 504 Sunnyvale, California 94088-3504	5	34
Lockheed Missiles Space Co. Attn: Mr. Paul Williamson 3251 Hanover St. Palo Alto, CA 94304	1	35
General Dynamics Attn: Ray Halstenberg Convair Division 5001 Keary Villa Rd San Diego, CA 92123	1	36
STI Attn: Mr. R.C. Stroud 20065 Stevens Creek Blvd. Cupertiono, CA 95014	1	37
NASA Langley Research Ctr Dr. Earle K. Huckins III Attn: Dr. Card Langley Station Bldg 1293B M/s 230 Hampton, VA 23665	2	38
NASA Johnson Space Center Attn: Robert Piland Ms. EA Houston, TX 77058	1	39
McDonald Douglas Corp Attn: Mr. Read Johnson Douglas Missile Space Systems Div 5301 Bulsa Ave Huntington Beach, CA 92607	1	40
Integrated Systems Inc. Attn: Dr.N. K. Gupta and M.G. Lyons 151 University Avenue, Suite 400 Palo Alto, California 94301	2	41
Boeing Aerospace Company Attn: Mr. Leo Cline P.O. Box 3999 Seattle, WA 98124 MS 8 W-23	1	42

TRW Defense Space Sys Group Inc. Attn: Ralph Iwens Bldg 82/2054 One Space Park Redondo Beach, CA 90278	1	43
TRW Attn: Mr. Len Pincus Bldg R-5, Room 2031 Redondo Beach, CA 90278	1	44
Department of the navy Attn: Dr. K.T. Alfriend Naval Research Laboratory Code 7920 Washington, DC 20375	1	45
Airesearch Manuf. Co. of Calif. Attn: Mr. Oscar Buchmann 2525 West 190th St. Torrance, CA 90509	1	46
Analytic Decisions, Inc. Attn: Mr. Gary Glaser 1401 Wilson Blv. Arlington, VA 22209	1	47
Ford Aerospace & Communications Corp. Drs. I. P. Leliakov and P. Barba, MS/G80 3939 Fabian way Palo Alto, California 94304	1	48
Center for Analysis Attn: Mr. jim Justice 13 Corporate Plaza Newport Beach, CA 92660	1	49
General Research Crop. Attn: Mr. G. R. Curry P.O. Box 3587 Santa Barbara, CA 93105	1	50
General Research Corp Attn: Mr. Thomas Zakrzewski 7655 Old Springhouse Road McLean, VA 22101	1	51

Attn: Dr. Hans Wolfhard 400 Army Navy Drive Arlington, VA 22202		
Karman Sciences Corp. Attn: Dr. Walter E. Ware 1500 Garden of the Gods Road P.O. Box 7463 Colorado Springs, CO 80933	1	53
MRJ, Inc. 10400 Eaton Place Suite 300 Fairfax, VA 22030	1	54
Photon Research Associates Attn: mr. Jim Myer P.O. Box 1318 La Jolla, CA 92038	1	55
Rockwell International Attn: Russell Loftman (Space Systems Group) (Mail Code - SL56) 12214 Lakewood Blvd. Downey, CA 90241	1	56
Science Applications, Inc. Attn: Mr. Richard Ryan 3 Preston Court Bedford, MA 01730	1	57
U.S. Army Missile Command Attn: DRSMI-RAS/Mr. Fred Haak Redstone Arsenal, AL	1	58
Naval Electronic Systems Command Attn: Mr. Charles Good PME 106-4 National Center I Washington, DC 20360	1	59
Lockheed Palo Alto Research Laboratory Attn: Dr. J. N. Aubrun, O/52-56 3251 Hanover Street Palo Alto, California 94304-1187	2	60

Attn: Mr. Bernie Chasnov AMC Bldg 5001 Eisenhower Ave Alexandria, VA 22333		
Defense Documentation Center Cameron Station Alexandria, VA 22314	1	62
Honeywell Inc. Attn: Dr. Thomas B. Cunningham Attn: Dr. Michael F. Barrett 2600 Ridgway Parkway MN 17-2375 Minneapolis, MN 55413	2	63
NASA Marshal Space Flight Center Attn. Dr. J. C. Blair, ED01 Henry B. Waites Marshal Space Flight Center, AL 35812	2	64
TRW Attn: Robert Benhabib Bldg 82/2024 One Space Park Redondo Beach, CA 90278	1	65

MISSION
of
Rome Air Development Center

RADC plans and executes research, development, test and selected acquisition programs in support of Command, Control Communications and Intelligence (C^3I) activities. Technical and engineering support within areas of technical competence is provided to ESD Program Offices (POs) and other ESD elements. The principal technical mission areas are communications, electromagnetic guidance and control, surveillance of ground and aerospace objects, intelligence data collection and handling, information system technology, ionospheric propagation, solid state sciences, microwave physics and electronic reliability, maintainability and compatibility.